DOT/FAA/AR-05/30

Office of Aviation Research
Washington, D.C. 20591

Inspection Development for Titanium Billet—Engine Titanium Consortium Phase II

September 2005

Final Report

This document is available to the U.S. public
through the National Technical Information Service (NTIS),
Springfield, VA 22161.

U.S. Department of Transportation
Federal Aviation Administration

NOTICE

This document is disseminated under the sponsorship of the U.S. Department of Transportation in the interest of information exchange. The United States Government assumes no liability for the contents or use thereof. The United States Government does not endorse products or manufacturers. Trade or manufacturers names appear herein solely because they are considered essential to the objective of this report. This document does not constitute FAA certification policy. Consult your local FAA aircraft certification office as to its use.

This report is available at the Federal Aviation Administration William J. Hughes Technical Center's Full-Text Technical Reports page: actlibrary.tc.faa.gov in Adobe Acrobat portable document format (PDF).

Technical Report Documentation Page

1. Report No.	2. Government Accession No.	3. Recipient's Catalog No.
DOT/FAA/AR-05/30		

4. Title and Subtitle	5. Report Date
INSPECTION DEVELOPMENT FOR TITANIUM BILLET—ENGINE TITANIUM CONSORTIUM PHASE II	September 2005
	6. Performing Organization Code
7. Author(s)	8. Performing Organization Report No.
Mike Keller[1], Thadd Patton[1], Andrei Degtyar[2], Jeff Umbach[2], Waled Hassan[3], Andy Kinney[3], Ron Roberts[4], Frank Margetan[4], and Lisa Brasche[4]	
9. Performing Organization Name and Address	10. Work Unit No. (TRAIS)
[1]General Electric Company Cincinnati, Ohio 45215 [3]Honeywell Engines, Systems & Services Phoenix, AZ [2]Pratt & Whitney East Hartford, CT [4]Iowa State University Ames, IA	11. Contract or Grant No. DTFA0398FIA029
12. Sponsoring Agency Name and Address	13. Type of Report and Period Covered
U.S. Department of Transportation Federal Aviation Administration Office of Aviation Research Washington, DC 20591	Final Report
	14. Sponsoring Agency Code ANE-110

15. Supplementary Notes

The FAA William J. Hughes Technical Center Technical Monitors were Rick Micklos and Cu Nguyen.

16. Abstract

The Engine Titanium Consortium (ETC) is comprised of Iowa State University; General Electric; Honeywell Engines, Systems & Services; and Pratt & Whitney. The ETC Phase I program began in 1993 with a focus on improved inspection of titanium billet used in the production of jet engines. The Phase I program completed in 1998 included the development and evaluation of two zoned approaches to billet inspection, namely, multizone and phased array inspections. The Phase II program began in 1999 and focused on further sensitivity improvements to titanium billet using the multizone approach. The goal of the Phase II effort was to achieve a #1 flat-bottom hole sensitivity for 10″ diameter billet and assess the impact of attenuation compensation procedures. This report documents the results for 5″, 10″, and 14″ diameter billets using calibration standards in a laboratory setting.

17. Key Words	18. Distribution Statement
Titanium billet, Ultrasonic inspection, Probability of detection	This document is available to the public through the National Technical Information Service (NTIS) Springfield, Virginia 22161.

19. Security Classif. (of this report)	20. Security Classif. (of this page)	21. No. of Pages	22. Price
Unclassified	Unclassified	151	

Form DOT F1700.7 (8-72) Reproduction of completed page authorized

TABLE OF CONTENTS

		Page
EXECUTIVE SUMMARY		xiii
1.	INTRODUCTION	1
1.1	Purpose	1
1.2	Background	1
1.3	Program Objectives	4
2.	APPROACH	4
3.	DISCUSSION OF RESULTS	5
3.1	Validation and Use of Transducer Design Models	5
3.2	Transducer Design and Procurement	8
3.2.1	Transducer Manufacturing Parameter Tolerance Analysis	12
3.2.2	Transducer Characterization	12
3.3	Transducer Evaluations	24
3.3.1	Evaluation of F/10 Transducers	24
3.3.2	Pulse Volume Calculations	28
3.3.3	Phased Array Evaluation	28
3.3.4	Evaluation of F/8 Transducers	31
3.3.5	Explanation for Zones 6a and 6b	36
3.3.6	Sensitivity Curves	38
3.4	Summary of Laboratory Evaluation for 10″ Diameter Billet	41
3.5	Attenuation Compensation Procedures	41
3.6	Banding Phenomena and UT Property Variations	45
3.6.1	Attenuation Compensation Research Plan	48
3.6.2	Current Billet Compensation Procedures	50
3.6.3	Test Billet and Transducer Selection	51
3.6.4	Back-Wall Variations and Near-OD FBH Placements	53
3.6.5	Correlation Between Back-Wall and Near-OD FBH Amplitude Variations	56
3.6.6	Straw Man Procedures for Global Attenuation Compensation	67

3.6.7 Proposed Straw Man Global Attenuation Compensation Procedure 67

3.7 Fabrication of a Test Specimen Containing Near-Center FBHs 69

3.7.1 Tests of the Global Attenuation Compensation Straw Man Procedure 73

3.7.2 Local Attenuation Adjustments and Their Computation 79

3.8 Summary and Recommendations for Attenuation Compensation 98
3.9 Assessment of Large-Diameter Billet 102

3.9.1 Chord Block Fabrication 103
3.9.2 Baseline CV Inspection 104
3.9.3 Transducer Design 106
3.9.4 Transducer Characterization 112
3.9.5 Chord Block Measurements 118

3.10 Summary of 14″ Chord Block Evaluation 120

4. SUMMARY AND CONCLUSIONS 121

5. REFERENCES 122

APPENDICES

A—Major Accomplishments of the ETC Phase 1 Program
B—Description of Multizone Inspection for Billet

LIST OF FIGURES

Figure		Page
1	Summary of Transducer Performance Measurements on Billet Standard	7
2	Results of Sensitivity Analysis for Zone 4 F/10 Transducer Design	12
3	Voltage Response V(z) for Manufacturer B Curved Element Transducer	13
4	(a) Billet Inspection Geometry Showing the Beam Coordinate System and (b) The Four Parameters Used to Characterize the Focal Properties of a Transducer	14
5	Three Measurement Geometries for Acquiring Data for Transducer Characterization	15
6	Function That is Minimized to Determine the Best Fit Transducer Characteristics	16
7	Measurement of the Time Offset (0.81 μsec) for the UT System Used for the BMIW Method	17
8	The BMIW Method (a) Water Paths Used For 2D Scans and (b-d) Comparison of Fitted and Measured Beam Profiles for Three of the Water Paths	18
9	The BMIW Method Fitted and Measured Beam Profiles at 5.08 MHz for Each of the Ten Water Paths	18
10	The BMIS Method (a) Data Acquisition Details and (b-e) Fitted and Measured Beam Profiles at 5.08 MHz for Each of the Four FBHs	19
11	V(z) Method (a) Data Acquisition Details and (b) Measured and Fitted Amplitude Profiles at 5.08 MHz	19
12	Deduced Focal Parameters for Each Method When all Four Parameters are Allowed to Vary	21
13	Comparison of V(z) Curves Calculated Using Two Different Beam Models	23
14	Percentage Error Resulting From Using The Paraxial MGB Model Rather Than the Green's Function Formalism to Deduce Probe Focal Parameters From Synthetic V(z) Data	24
15	C-Scan of Targets in ETC 10″ Diameter Calibration Standard Using the Zone 2 Transducer	25
16	Noise and Target Amplitude Responses, Zone 2 Transducer	27
17	Noise and Target Amplitude Responses, Zone 4 Transducer	27

18	Comparison of Modeled Beam Diameters for the F/8 and F/10 Transducer Designs	29
19	Results of Phased Array Evaluation of the ETC Calibration Standard on the 3.15″ Deep Calibration Target	30
20	Comparison of the Measured and Projected Peak Noise Levels vs the sqrt pv for the F/10, Phased Array, and Projected F/8 Transducers	31
21	F/8, Elliptical Elements, 7.5 MHz, Zones 5 and 6 Transducers	31
22	Zone Sensitivity Model Predictions for the F/8 Transducers	32
23	Set of Six F/8 7.5-MHz Transducers and Table of Dimensions	33
24	Comparison of Pulse Volumes as Determined by the ISU Model and the Pulse Volumes of the Delivered Transducers	35
25	Zone 6 Divided Into Two Zones, 6a and 6b, to Improve SNR	36
26	Comparison of Sensitivity Variation Throughout the Inspection Zone for the F/10 and F/8 Transducer Designs	36
27	Pulse Volume Calculations for the Zone 6 Transducer	37
28	Percent Noise Peak vs the sqrt pv Original Curve Based on F/10 Zone 4 Results	38
29	C-Scan of ETC Calibration Standard Showing the Five FBHs for Zones 6a and 6b	38
30	Sensitivity Graph Using the ETC 10″ Diameter Calibration Standards	39
31	Sensitivity Graph Using the RDB 10″ Diameter Specimen	39
32	#1 FBH Inspection Sensitivity for Zones 1-3 on the ETC Calibration Standard	40
33	Zone 2 #1 FBH Sensitivity on the RDB	40
34	Billets Awaiting Inspection	42
35	Conventional and MZ Billet Inspections Use Calibration Standards Containing FBH Reflectors	42
36	Calibration Standard for an MZ Inspection of a 6″ Diameter Billet	43
37	Ultrasonic Billet Inspection (Idealized at Depth Z)	43
38	The Standard Method for Attenuation Compensation Makes Use of Average Back-Wall Amplitudes	44

39	Banding Patterns Seen During the Inspection of a 14″ Diameter Ti-6-4 Billet Specimen	46
40	Noise Banding and UT Property Variations Seen in a 6″ Diameter Ti-6-4 Billet	47
41	Correlation Between Backscattered Noise FOM and Attenuation for Six Coupons From a 6″ Diameter Ti-6-4 Billet	48
42	Areas Typically Scanned to Acquire Back-Wall Amplitude Data for Attenuation Compensation	51
43	Model Calculations of Beam Properties for Two 5-MHz MZ Transducers	52
44	Five-MHz Phased Array Transducer, Operated in Standard Focusing Mode to Simulate Inspections With Fixed-Focus Probes	53
45	Back-Wall C-Scan Images of 6″ Diameter CBS Billet (B2W1A) Acquired Using Two MZ Transducers	54
46	Back-Wall Amplitude Statistics for Four Regions of the 15″ Long Billet Section	54
47	Possible Schemes for Positioning Near-OD FBHs Relative to the Back-Wall Amplitude Pattern	55
48	(a) 6″ Diameter Ti-6-4 Test Specimen Containing Near-OD #4 FBHs and (b) C-Scan Image Showing the FBH Enumeration Scheme	56
49	Measurements on a Ti-6-4 Billet Segment Using a 5-MHz, 6″ MZ Probe Focused Near the Billet Center	58
50	Measurements on a Ti-6-4 Billet Segment Using a 5-MHz, 13″ MZ Probe Focused Near the Billet Back Wall	59
51	Measurements on a Ti-6-4 Billet Segment Using a 5-MHz Phased Array Transducer Focused Near the Billet Center	60
52	Measurements on a Ti-6-4 Billet Segment Using a 5-MHz Phased Array Transducer Focused Near the Billet Back Wall	61
53	Measurements on a Ti-6-4 Billet Segment Using a Phased Array Transducer Focused Near the Billet Center	62
54	Measurements on a Ti-6-4 Billet Segment Using a Phased Array Transducer Focused Near the Billet Back Wall	63
55	Normalized FBH Amplitudes and Nearby Back-Wall Amplitudes Seen in the Six Measurement Trials	64

56 Flat-Bottom Holes and (Nearby) Back-Wall Amplitude Fluctuations Seen in Six Measurement Trials Using a 15″ Long Ti-6-4 Billet Containing 13 Near-OD FBHs 65

57 Correlation Between Back-Wall and FBH Amplitudes as a Function of Beam Size at the FBH Depth 66

58 Fabrication of Specimens to Test Straw Man Procedures for Attenuation Compensation 69

59 Back-Wall C-Scans of the Candidate Billet for the Straw Man Test 69

60 Mean, Maximum, and Minimum Back-Wall Amplitudes for Various Regions of the C-Scan Images Shown in Figure 59 70

61 Comparison of Mean Amplitudes of Back-Wall Echoes for the Six Regions Indicated in Figures 59 and 60 70

62 Six-in.-Diameter, 18-in.-Long Ti-6-4 Test Specimen Showing How #2 FBHs Were Drilled at a Depth of 3.5″ From the Inspection Surface 71

63 Six-in.-Diameter, 18-in.-Long Ti-6-4 Test Billet Showing Drilled and Plugged Holes 71

64 Numbering Scheme for FBH Locations in all C-Scans of the 18″ Long Test Billet 72

65 (a) Layout of the Deep-Zone (Zone 4) Portion of the 6″ Diameter MZ Calibration Standard and (b) C-Scan of the Deep-Zone Region of the Calibration Standard 72

66 Back-Wall C-Scans of the Calibration Standard and Test Billet Acquired With the Beam Focused Near the 6″ Diameter Billet Centerline (Zone 4) 73

67 Back-Wall C-Scans of the Calibration Standard and Test Billet Acquired With the Beam Focused Near the 13″ Diameter Billet Back Wall (Zone 7) 74

68 Example Attenuation Compensation Calculation 74

69 (a) C-Scan Images From Zone 4 Inspections of the Calibration Standard and Test Billet and (b) Raw Peak Amplitudes of the 17 #2 FBHs in the Test Billet 76

70 Peak Amplitudes of the 17 #2 FBHs in the Test Billet When no Attenuation Compensation is Used 77

71 (a) Output Generated When Automatic S/N Software Was Applied to the As-Run Zone 4 C-Scan of the Test Billet and (b) As-Run Peak Amplitudes of the 17 #2 FBH Defects With S/N Ranges Indicated 78

72 Peak Amplitudes of the 17 #2 FBHs in the Test Billet Using the Standard Compensation Procedure and no Attenuation Compensation 80

73	Results of Applying Three Global Attenuation Compensation Procedures to the Test Billet Containing 17 #2 FBH Defects, Zone 4	81
74	Results of Applying Three Global Attenuation Compensation Procedures to the Test Billet Containing 17 #2 FBH Defects, Zone 7	82
75	Summary of FBH Amplitude Statistics for the Six Global Compensation Procedures	84
76	Zone 3 C-Scan of the 18″ Long Test Billet Showing Analysis Boxes for the Computation of Noise Statistics	86
77	Noise Statistics at the Axial and Hoop Locations of the 17 FBH Defects	87
78	Raw and Normalized Average Gated-Peak Noise Amplitudes Seen in the MZ Inspection of the Ti-6-4 Test Billet	87
79	(a) Methods of Choosing the Analysis Region Used to Compute the Average Back-Wall Amplitude in the Vicinity of Each Defect and (b) Analysis Regions for the Back-Wall C-Scan of the Test Billet Made With the Beam Focused Near the Billet Back-Wall	88
80	Raw Average Back-Wall Amplitudes in the Vicinities of the 17 FBH Defects in the Test Billet	89
81	Comparison of Measured and Predicted FBH Amplitudes of the 17 #2 FBH Defects in the Test Billet	91
82	Correlation Between Predicted and Measured FBH Amplitudes in the Ti-6-4 Test Billet	92
83	Results of Applying Local Attenuation Compensation Procedures to FBH Amplitudes in the Ti-6-4 Test Billet	93
84	Results of Applying Local Attenuation Compensation Procedures to FBH Amplitudes in the Ti-6-4 Test Billet, Standard Global Compensation	94
85	Results of Applying Local Attenuation Compensation Procedures to FBH Amplitudes in the Ti-6-4 Test Billet, Semiconservative—Global Compensation	95
86	Combinations of Global and Local Attenuation Compensation Procedures Considered in This Report	96
87	Chord Block Schematic	103
88	Noise Scan of the Billet From Which Chord Block Was Made	104
89	Scans of the Chord Block With a Transducer Used in a CV Inspection	105

90	Scans of the Chord Block With an MZ Transducer Designed for the Inspection of the Central Zone of 13″ Diameter Billet	106
91	Schematic of an Elliptical Element, Bicylindrically Focused Transducer	107
92	Model-Predicted on-Axis (Radial Direction) Response Within Center Zone of 14″ Diameter Ti Billet for Various Transducer Designs	109
93	Model-Predicted Beam Size Within Center Zone of 14″ Diameter Ti Billet for Various Transducer Designs	110
94	Predicted Beam Area Within the Central Zone of 14″ Diameter Billet for Transducers 1 and 2	111
95	Transducer 2	112
96	V(z) Method for Transducer Characterization	113
97	Waveforms Around the First Focus of Transducer 1	113
98	V(z) at (a) 4.69 MHz and (b) 6.08 MHz for Transducer 1	114
99	V(z) at (a) 4.69 MHz and (b) 6.08 MHz for Transducer 2	114
100	Reconstruction Results for GFL in (a) Circumferential, F_x, and (b) Axial, F_y, Directions at Various Frequencies for Transducer 1	115
101	Reconstruction Results for GFL in (a) Circumferential, F_x, and (b) Axial, F_y, Directions at Various Frequencies for Transducer 2	116
102	Measured and Simulated C-Scans of 5/16″ Diameter Steel Ball Target in Water for Transducer 1	117
103	Measured and Simulated C-Scans of 5/16″ Diameter Steel Ball Target in Water for Transducer 2	117
104	Scans of the Chord Block With Different Water Paths	118
105	Analysis of One of the Chord Block Scans (Water Path = 2.5″) Using Automatic SNR Calculation Feature of GE-Multizone Software	119
106	Waveforms With Responses From #2 FBHs in Chord Block Water Path = 2.7″	120

LIST OF TABLES

Table		Page
1	First-Generation Transducer Design Parameters	9
2	Designs for F/8 and F/10 Transducers for 10″ Diameter Billet	10
3	Predicted Beam Diameters and Signal-to-Noise Improvement of Proposed Transducer Designs	11
4	Values of Effective Diameters and GFL Deduced Using Various Fitting Methods	22
5	Preliminary Evaluation Results for Zone 2 Transducer	24
6	Preliminary Evaluation Results for Zone 4 Transducer	25
7	Frequency Measurements for Zone 2 Transducer	26
8	Frequency Measurements for Zone 4 Transducer	26
9	Details of the Beam Dimensions and the Resultant Signal-to-Noise Values for One Set of Parameters	30
10	Summary of the Transducer Beam Characteristics for Pulse Volume Calculations and Results of the Noise Statistics for the ETC and Random Defect Billets	35
11	Computed Attenuation Compensation Values in dB/inch of Depth in the Test Billet	75
12	Flat-Bottom Hole Amplitudes for the Ti-6-4 Test Billet After Adjustment	83
13	Local Attenuation Adjustment Factors at the 17 FBH Sites Determined From Local Back-Wall and Grain Noise Amplitudes	90
14	Statistics of Adjusted FBH Amplitude Variations in the 18″ Long Test Billet for Each of the Attenuation Compensation Procedures Considered	97
15	Zoning Scheme for MZ Inspection of 14″ Diameter Billets	103
16	Specifications of Transducers 1 (F/10) and 2 (F/7) Intended for the Inspection of the Central Zone of 14″ Diameter Ti Billet as Well as F/8 Design and Existing Transducer Intended for Inspection of Center Zone of 13″ Diameter Billet	109
17	Results of V(z) Reconstruction for Transducers 1 and 2	116

LIST OF ACRONYMS

2D	Two-dimensional
BMIS	Beam mapping in solid
BMIW	Beam mapping in water
BTBI	Billet to be inspected
CBS	Contaminated Billet Study
CV	Conventional
DAC	Distance-amplitude correction
GEAE	General Electric Aircraft Engines
ETC	Engine Titanium Consortium
FAA	Federal Aviation Administration
FBH	Flat-bottom hole
FOM	Figure of merit
FSH	Full screen height
GE	General electric
GFL	Geometrical focal length
ID	Inside diameter
ISU	Iowa State University
MGB	Multi-Gaussian Beam
MZ	Multizone
Ni	Nickel
OD	Outside diameter
OEM	Original Equipment Manufacturer
PoD	Probability of Detection
POP	Pulse-on-position
RAM	Random access memory
RDB	Random defect billet
ROI	Region of interest
SNR	Signal-to-Noise ratio
TRCRT	Titanium Rotating Components Review Team
UT	Ultrasonic
WORM	Write-once-read-many

EXECUTIVE SUMMARY

A critical element in ensuring overall flight safety is the performance of the propulsion system, in particular, the safe operation of the rotating components. In data analysis performed by the Federal Aviation Administration (FAA) and industry in the 1990s, the need for reduction in engine incidents caused by failure of disks was identified. In response to this need, the Engine Titanium Consortium (ETC) carried out several efforts to improve inspection of jet engine components and the materials used in their manufacture. Much of the effort has focused on the detection of hard alpha, a melt-related defect that can occur in the manufacture of titanium (Ti) ingots and inspection of billets and forging. This report, however, is limited to details of the Ti billet inspection activity.

The objective of this research was to evaluate means to improve the ultrasonic inspection sensitivity for Ti cylindrical billet. The specific goals were:

- To achieve #1 flat-bottom hole (FBH) sensitivity in Ti billet up to 10 inches in diameter.

- To improve means of accounting for attenuation in the billet, thus making the inspection more uniform.

- To assess the inspection capability in billet diameters greater than 10 inches in diameter.

Highlights of each are provided here with full details in the report:

- Achieving #1 FBH Sensitivity: Multizone technology is currently used to inspect a 10-inch-diameter billet to 7/8 of a #2 FBH sensitivity, with the reject amplitude set at 87.5% of calibration. Setting a goal of #1 FBH would improve this sensitivity by 4 times over the calibration sensitivity. To meet this goal, an inspection was designed based on extensive use of model calculations to design improved transducers. Not all of the 7.5-MHz, F/8 transducers in the new set meet ETC specifications. In spite of this problem, the #1 FBH goal was nearly achieved or exceeded in 100% of the material volume, FBH sensitivities varying between #0.9 FBH and #1.1 FBH in the most difficult to inspect (3″ to 5″ depth) center zones. Sensitivities in the shallower zones (to ~3″ depth) varied between #0.6 FBH and #0.8 FBH, thus exceeding the program goal. Current transducer manufacturing limitations prevented achievement of this goal at the deeper sections of the billet but did demonstrate improved inspection sensitivity by 2.7 times over existing sensitivity levels.

- Attenuation Compensation Procedures: Several means of accounting for sound attenuation in the billet were evaluated, ranging from less to more conservative. These can be applied globally to the inspection data to enhance sensitivity in the areas of highest attenuation. Alternate postinspection evaluation of attenuation using the C-scan images is another possibility. This approach would apply compensation locally in the billet and might reduce the areas of overinspection, unlike the global applied procedure. Impacts of these compensation procedures have not been fully evaluated in a production environment and could have substantial effects on the billet inspection.

- Assessment of Large Diameter Billet: Inspection sensitivity improvements were assessed for billets up to 14″ in diameter. Research showed that inspection sensitivity could be improved by use of focused multizone transducers in place of the conventional transducers. It was demonstrated, using 14″ diameter chord blocks in the laboratory, that a #2 FBH sensitivity could be achieved at the center of the billet using the multizone inspection system. This represents more than a 2 times improvement in sensitivity through application of the multizone system.

1. INTRODUCTION.

1.1 PURPOSE.

Titanium (Ti) alloys were selected for jet engine applications because of their strength-to-weight ratio and ability to operate in harsh environments. The performance demands for Ti jet engine components can be quite stringent which, in turn, necessitates high-sensitivity inspection of the product forms that lead to the final engine component. Typical Ti material used in production of commercial jet engine disks underwent ultrasonic (UT) inspection at the billet and forging stages. The Engine Titanium Consortium (ETC) focused much of its Phase I work on Ti billet inspection.

The goal of this research was to build on the Phase I progress to improve Ti billet inspection and to evaluate further multizone (MZ) improvements that could lead to improvements in sensitivity of 10″ diameter billets and explore potential sensitivity improvements that could be realized through the application of MZ techniques on larger (14″) diameter billets. Improvements in sensitivity should lead to enhanced detection of deleterious defects such as hard alpha, reducing the risk of catastrophic failure and improving flight safety. An evaluation was also performed on the 5″ diameter nickel (Ni) and Ti billet. Those results are reported in the Ni billet inspection report [1].

1.2 BACKGROUND.

In 1989, an in-flight separation of a Ti fan disk led to substantial loss of an aircraft and 111 lives in Sioux City, Iowa. The failure was attributed to the occurrence of hard alpha in the Ti-6Al-4V disk, a material defect caused by localized concentrations of interstitial impurities, such as nitrogen, oxygen, or carbon. The Federal Aviation Administration (FAA) established the Titanium Rotating Components Review Team (TRCRT), which was chartered to review the design, manufacturing, inspection, and life management procedures of rotating parts used in all types of commercial aircraft turbine engines and to make recommendations for improvement of their structural integrity [2]. While the occurrence and consequences of the Sioux City crash are tragic, they have served as catalysts in shoring up the safety of the commercial aviation engine community.

The FAA is working with the materials, lifing, and inspection communities to address recommendations for the TRCRT. The ETC was established in 1993 to address the inspection recommendations of the FAA TRCRT report [2] and has as its objective to provide reliable and cost-effective new methods and improvements in mature methods for detecting cracks, inclusions, and imperfections in materials or components used in engine applications. Starting in 1992, working with the FAA William J. Hughes Technical Center and New England Directorate staff; Iowa State University (ISU); General Electric Aircraft Engines (GEAE); Honeywell Engines, Systems & Services (formerly AlliedSignal); and Pratt & Whitney have addressed high-priority inspection issues related to critical rotating components. Other efforts related to lifing and design issues are being addressed by the Rotor Integrity Subcommittee and FAA-funded efforts as part of the Turbine Rotor Materials Design program at Southwest Research Institute. The Jet Engine Titanium Quality Committee and Special Metals Processing Consortium are addressing issues related to melt quality.

The conventional rotor life management methodology used in the commercial industry is known as “safe life,” where components are designed and substantiated to have a specified service life, which is stated in operating cycles and operation hours, during which no detectable cracks will occur. Continued safe operation, up to the stated life limit, is not contingent upon interim inspections, and when a component reaches the published life limit, it is retired from service. Under the safe-life concept, 100 percent of the units are expected to be capable of reaching the published life limit. Under nominal conditions, the methodology provides a structured process for the design and life management of high-energy rotors, which results in assurance of structural integrity throughout the life of the rotor. Because the safe-life approach was founded on a database of nominal material and manufacturing conditions, the approach does not address the occurrence of material and manufacturing anomalies that can potentially degrade structural integrity, e.g., hard alpha in Ti. Undetectable material and manufacturing anomalies, therefore, represent a departure from the assumed conditions and necessitate a potential change in the maintenance, inspection, and operation of engine components.

As a result of the Sioux City crash in 1989, the FAA requested through the Aerospace Industries Association that the industry review available techniques to determine if a damage tolerance approach to engine life management could be introduced and thereby reduce the rate of uncontained rotor events [3]. Note that engine uncontained rotor events, in their own right, should not result in catastrophic accidents, but have occasionally done so in conjunction with other adverse circumstances. Advisory material has been published that presents a generic damage tolerance approach that can be readily integrated with the existing safe-life process for high-energy rotors to produce an Enhanced Life Management Process [4]. In response to an FAA request for prioritization, the industry working group focused its efforts on subsurface defects in Ti materials. As efforts were completed on subsurface defects in Ti, focus was turned to other alloy systems, i.e., Ni, and surface-related anomalies. It should also be noted that there was no intention of using these changes to extend the life of existing engines, but rather the intention was to reduce the risk within the existing safe-life approach. Given the focus of these industry and regulatory efforts on subsurface flaw detection, the ETC undertook efforts to improve the inspection of Ti billets and forgings.

Many of the recommendations of the TRCRT report addressed the need for improvements in the inspection of Ti. Phase I of the ETC Production Inspection Task concentrated on improved inspection of Ti billet. Two approaches to zoned inspection, MZ [5] and phased array [6], were evaluated and improved with an objective of providing uniform sensitivity inspection at all depths. Model-based approaches developed at ISU were used to enhance the inspection, including transducer design optimization for both MZ and phased array. Phased array and MZ systems were demonstrated to the Ti melters using facilities at RMI Titanium in Niles, Ohio. Currently, five MZ systems are operating in a production environment. Phased array systems are also being used in evaluation of billet finds by some melters. In a related effort, a program that made use of extensive naturally occurring hard alpha defects was completed as part of the ETC Phase I and Phase II programs. The program known as the Contaminated Billet Study (CBS) provided an unprecedented amount of data in the public domain on the morphology of hard alpha and the changes it undergoes throughout the processing and service life of Ti components. Acoustic, metallographic, and chemical analysis were completed on ten representative hard alpha defects, and the results were provided to the Ti community [7]. Significant improvements were

made in inspection sensitivity with a thorough, quantitative assessment occurring in the reliability and CBS programs of ETC. A list of the ETC Phase I accomplishments are provided in appendix A.

Progress made in Phase I on transducer design modeling [8] and transducer characterization established a foundation for increasing the sensitivity significantly beyond that achieved by current MZ and phased array systems. An extensive fundamental understanding was developed for inspection properties of billets and led to identification of significant limitations in the methods currently used to measure and compensate for attenuation [9]. Improved methods for attenuation compensation were developed in Phase II and are reported in section 3.5 of this report.

The TRCRT report recommended that engine manufacturers should require billets to be inspected to the highest standard (smallest flat-bottom hole (FBH) or equivalent) practicable in the industry for the size of the part being inspected. The report stated that the levels considered to be practicable were a #2 FBH from 6″ to 10″ diameter billet and #3 FBH for diameters greater than 10″. Phase I met or exceeded the practicable FBH sensitivities for all diameters, demonstrating approximately a four-fold increase in sensitivity. The lifing community requested that further improvements be made in inspection sensitivity, particularly for larger diameter billets. A goal of #1 FBH sensitivity was established for billets up to and including 10″ in diameter, with an additional need to improve and quantify the inspection sensitivity for >10″ to 14″ diameter billet, all without significant reduction in productivity. ETC Phase I provided improved transducer design models, transducer parameters, signal processing approaches, and calibration standards with potential to further improve the sensitivity through the application of these results.

The results of Phase I indicated that a sensitivity improvement of 4-6 dB is needed to achieve #1 FBH sensitivity in billets up to 10″ in diameter, with the largest improvement needed in the center region of the billet. Several potential approaches were identified, though none individually was expected to provide the required improvement in isolation. The potential approaches were as follows:

- Improved specification of transducer parameters through improved, model-based design and manufacturing, applying techniques developed in Phase I are expected to yield 2 dB sensitivity improvement.

- The use of electronic distance-amplitude correction (DAC), which is not part of the current MZ systems and should provide a 1 to 2 dB sensitivity gain.

- Material processing approaches to yield lower-noise Ti billets are being pursued outside the ETC program and are expected to yield significant sensitivity improvements on the order of 2 dB.

Other approaches considered were use of denser sampling (not pursued because it would reduce productivity) and signal processing (not pursued because of concern over production readiness). Larger-diameter (13″ and 14″) billets cannot be inspected to as high a sensitivity because of

coarser material structure (due to less thermomechanical work) and because of the increased difficulty of producing well-focused sound beams through a greater thickness of material. The same approaches described above for 10″ diameter billet were expected to yield significant improvement in sensitivity for larger-diameter billets as well, but there may be a falloff in sensitivity with increasing diameter.

Models developed in Phase I were valuable in improving the design and performance of fixed-focus transducers and in understanding the operation of phased arrays. However, even with the use of design models, it appeared that transducers were not achieving the performance for which they were theoretically capable. An assessment of the discrepancies between the predicted and actual performance was completed.

Measurement of, and compensation for, attenuation differences between billet and calibration standards were a source of potential variation between true inspection sensitivity and the FBH sensitivity assumed from the calibration standard. This problem has received very little attention in the past, so the magnitude of errors due to attenuation compensation is largely unknown. Initial approaches to this problem were considered in Phase I and further developed in Phase II.

1.3 PROGRAM OBJECTIVES.

The following were the specific program objectives:

- To demonstrate the UT equipment and techniques required to inspect Ti alloy billets to #1 FBH sensitivity for 10″ diameter and smaller billet.
- To suggest procedures to account for attenuation effects so that the variation between calibration and inspection sensitivity is minimized.
- To provide an initial assessment of sensitivity at diameters greater that 10″.

2. APPROACH.

The approach for this research effort included the following steps.

Transducer design models and characterization tools were developed and used to optimize bicylindrically focused transducers. A comparison of predicted to actual performance for several transducers revealed manufacturing variabilities.

- Laboratory Demonstration on 10″ Diameter Billet: The results from the Phase I measurements (at 2.25″ and 4.05″ depths) were used to identify the best combination of focal spot diameter and frequency, and this information was used to design a complete set of transducers [10]. Phase I work indicated that frequency and bandwidth should be increased from the current production transducers, which are 5 MHz frequency and approximately 50% bandwidth. Transducer evaluations were performed on the ETC 10″ diameter standards. The FBH amplitudes, noise, and signal-to-noise ratios (SNR) were evaluated. A determination was made of whether the sensitivity level met the #1 FBH goal in all regions of the billet.

- Small-Diameter Billet Assessment: Honeywell also performed a sensitivity assessment on smaller 5″ diameter billets. Technology developed in Phase II for larger Ti billet was applied to improve Ti billet inspection of interest to small engine manufacturers. A feasibility demonstration was conducted in the laboratory environment with small Ti alloy billet using MZ transducers developed for the smallest of the large-diameter billets. The ETC also chose to evaluate phased array for the small-diameter billets. A sensitivity analysis (#FBH) was conducted for the 5″ billets and a comparison was made with the conventional spherical focus approach.

- Assessment of Large-Diameter Billet (>10″ diameter): Assessment of the sensitivity at larger billet diameters used 14″ chord blocks. Existing 13″ calibration standards were used, and a 14″ chord block standard with near-centerline targets was designed and built. Initial assessments were compared to baseline conventional (CV) inspection sensitivity using transducers borrowed from suppliers.

- Attenuation Compensation Procedures: The current procedures used to measure and compensate for material attenuation were evaluated and improved. The current procedure for the MZ inspection uses a preinspection of four short sections (1″ long) of the billet to obtain an average back-wall echo amplitude. This is compared with an average back-wall amplitude measured on the calibration standard, and the difference is used to calculate an attenuation compensation factor in decibels per inch. A transducer focused at the billet center is used to make the measurements. The drawback of this method is that it ignores the effects of distortion of the UT beam during propagation through the metal microstructure. Phase I work has shown that beam distortion can be a major contributor to the response from flaws and back walls. Even when beam distortion effects are minor and energy loss dominates, the material attenuation is found to vary significantly with position in a given billet in conjunction with noise banding. The effects of noise banding and nonuniform attenuation can lead to an incorrect measurement of flaw response, and a true inspection sensitivity different from that assumed from calibration. The current attenuation compensation technique was evaluated by drilling a number of FBHs into several billet sections and comparing the measured amplitudes of those holes to those expected from the attenuation analysis. Improvements focused on selecting a transducer that minimized the effects of beam distortion and provide an attenuation estimate, which enables good prediction of the hole echo amplitudes.

3. DISCUSSION OF RESULTS.

3.1 VALIDATION AND USE OF TRANSDUCER DESIGN MODELS.

Computer models were developed at ISU in ETC Phase I and transitioned to the original equipment manufacturers (OEM) for use as a design aid to optimize transducer performance, which could lead to time and money savings in transducer procurement. At the close of the Phase I program, the models were used in procurement of several transducers. Discrepancies were found between the predicted and actual performance. The first task of Phase II was to identify and resolve any existing discrepancy between experimentally observed and

model-predicted transducer performance. In the Phase I work, it was observed that transducers fabricated according to the specifications generated from the models were consistently focusing short of the model prediction. The purpose of this task was to establish whether or not such a discrepancy existed with the computer models at their present stage of development. If so, a careful examination of the various physical assumptions underlying the present computer models would occur to determine where the discrepancy lies and enable necessary modifications to the code.

The approach taken to test the model was to specify a transducer design using the computer codes, have the transducer fabricated by a manufacturer, and then perform a comparison of model predictions and measured performance to determine if a significant discrepancy existed. Should a significant discrepancy be observed, the study would then turn to an examination of the functioning of the various components of the transducer to determine which of the components were being improperly modeled.

Procurement specifications for the transducers were established using computer models employed in the ETC work, which are based on the Gauss-Hermite beam transmission model [1]. A different computer model was used in the Phase I procurement activity based on the Green's function transmission model [11]. However, ISU experience to date indicated that, in the case of billet geometry, the two computer models yielded nearly identical predictions. To test this observation, a current version of the Green's function transmission model was transferred to General Electric (GE) from ISU, and GE personnel performed a model comparison. This comparison confirmed past observations that no appreciable difference was observed in model predictions. However, in performing this comparison, it was determined that the version of the Green's function model software code used in the Phase I procurement did not include provisions to account for acoustic attenuation. This was a provision that was added at later stages of the Phase I activity. It is well understood at this point in time that neglect of attenuation will indeed result in an erroneous prediction of focal depth, possibly accounting for the consistent discrepancy observed in the Phase I activity.

ETC was able to take advantage of an ongoing, internal GE-funded program to procure MZ transducers for 10″ diameter billets from three transducer suppliers. Under this activity, purchase orders were placed with three transducer manufacturers requiring each to make two identical transducers according to the current design provided by the Gauss-Hermit model. All transducers were built to the same design goal (focus at 3.1″ depth in 10″ diameter billet). Two of the manufacturers produced transducers having lens configurations, and one transducer manufacturer provided transducers to their own design using a Fermat transducer surface without a lens. Upon receipt of the sets of transducers, a careful comparison of model predictions and measured performance of the transducers was made.

The comparisons showed that one manufacturer produced transducers that focused short of the model predictions. A second manufacturer produced transducers that focused slightly deeper than the model predictions. A third manufacturer produced a transducer that was in close agreement with model predictions. Figure 1 summarizes some performance measurements from the three pairs of transducers.

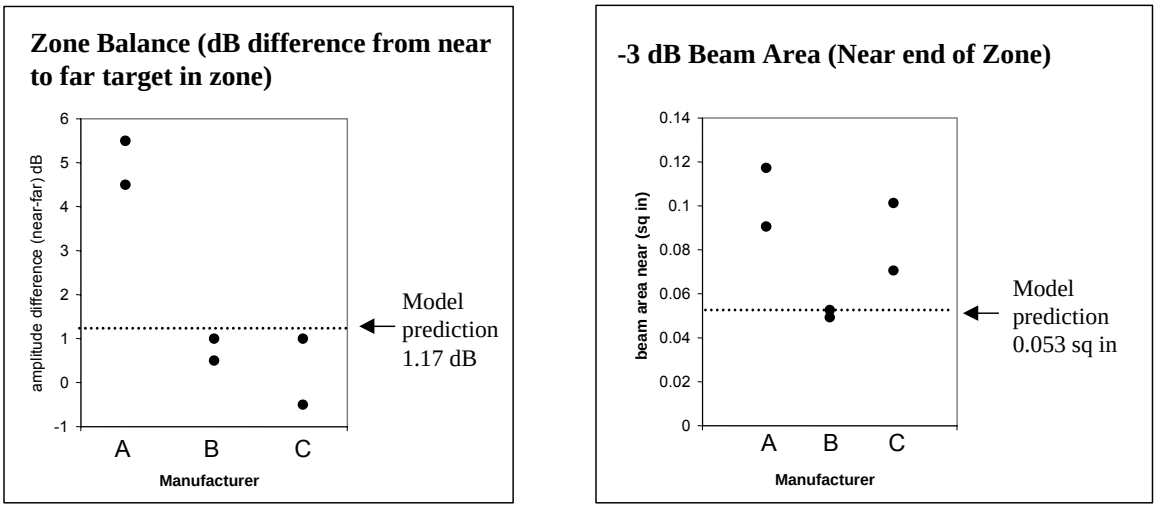

(a) (b)

FIGURE 1. SUMMARY OF TRANSDUCER PERFORMANCE MEASUREMENTS ON BILLET STANDARD

The model predictions were made using the Gauss-Hermite model and the specified design parameters. Manufacturer B used the curved element approach and designed the transducers using an alternative model. Comparison of the alternative model with the Gauss-Hermite design showed no significant difference in element surface profile. It can be seen that performance of Manufacturer B transducers is very close to the model prediction and that their two transducers perform almost identically. This confirms the expectation that curved element transducers will perform more predictably because the variations associated with lens manufacture are eliminated.

Manufacturers A and C used a lens-focused design with a flat, piezoelectric element. In each case, the pair of transducers from each manufacturer did not perform consistently with each other. This was not unexpected, as the addition of a lens introduces potential variation in lens velocity and possible variation in element flatness, which is not measurable because of the added lens. Figure 1 also shows that performance of the lens-focused transducers does not agree as well with the model.

To accelerate the transducer evaluation, it was agreed by the ETC team to participate in a series of face-to-face meetings to formulate approaches to accommodate variability in manufacturing when determining procurement specifications. At the first meeting, follow-on action items were identified and preliminary conclusions were drawn as follows:

- There can be significant variation in performance between transducers made by the same manufacturer.

- Lens-focused transducers showed variation within and between manufacturers as well as variation from the model predictions.

- The curved element transducers with Fermat surface had good consistency within manufacturers and good agreement with model predictions.

A second transducer meeting was held and included presentation of additional data, which supported the idea that manufacturing variation is the source of performance/model disagreement. The consensus of the ETC team members was that the discrepancy that exists in transducer performance was not a result of the design model but rather inconsistencies in the transducer manufacturing process. Some sources of the inconsistencies included variation in lens velocity, curvature variations, element flatness, and frequency variation. With the action to resolve model discrepancies completed, there was the confidence to proceed with the design of the transducers for the #1 FBH sensitivity inspection of the 10″ diameter billet using the ISU models. The work did point out the need for additional transducer studies to further improve their manufacturing processes.

3.2 TRANSDUCER DESIGN AND PROCUREMENT.

The plan to design the first prototype transducer included the following steps:

- Design using a similar design approach to the one used by GE in 1993 for the original 5 MHz transducers.

- Team review of assumptions and resulting first design.

- Use Gauss-Hermite model and iterative procedure to calculate lens radii and predict performance.

- Team review of model results.

- Finalize the design and procure transducers.

As a first step, prior experience in designing MZ transducers was used in the first transducer design. The general framework for the design was reported by Howard, Copley, and Gilmore [12]. The following parameters were considered:

- Frequency: SNR improves with increasing frequency and with decreasing beam diameter. Experimental data supported the original design approach developed by GE of maximizing SNR by minimizing the pulse volume. Experience indicates that 7.5 MHz is the highest useful frequency for a 10″ billet. Higher frequencies up to 10 MHz would have too much attenuation and would not have enough signal to the billet center.

- Zones: Continue with the current zones of 0.8″ to 0.9″. This is consistent with using an eight-channel system for billets up to 13″ in diameter. Current hardware is limited to an eight-channel system. The 14″ diameter billet would require the zones be increased to 1.1 inches.

- Depth-of-Field: The original transducer design was based on a 3 dB sensitivity variation within the zone. This was designed for instrumentation without DAC. DAC was to be

operational for the next generation of MZ and for evaluation of the new transducers. The decision was made to purchase two sets of transducers, one set of transducers to meet similar criteria (3 dB depth of field at 0.8″) and another more highly focused set with a shorter depth of field. The final selection was based on model predictions of beam cross section at the ends of the zone.

- Shape of Element: Utilize elliptical element that most accurately accounts for billet curvature. The same F number will be maintained.

- Calculations: Approximate formulae used for the original design were as follows:

  – Depth of field = $4\lambda\ (F/D)^2$
  – Beam diameter = $1.03\lambda\ (F/D)$

  Where F is the frequency, D is the transducer diameter, and λ is the wavelength.

- Designs: Approximate calculations from the above formulae were completed for two F numbers and resulted in the designs listed in table 1.

TABLE 1. FIRST-GENERATION TRANSDUCER DESIGN PARAMETERS

Series	Frequency (MHz)	F/D	Cone Half Angle (degrees)	Beam diameter (in.)	Depth-of-Field (in.)
1	7.5	10	11.6	0.080	0.75
2	7.5	8	14.6	0.064	0.48

With the general guidelines described above, two series of elliptical element transducers were designed using the iterative design model incorporating the Gauss-Hermite algorithm. Both sets of transducers were 7.5 MHz frequency and were based on the current zoning scheme with six zones to cover from 0.2″ to 5.5″ in depth. One set has an F/8 aperture, producing a focal spot diameter around 0.065″, and approximately 6 dB sensitivity variation within the zone. The other set, with a smaller aperture of F/10, was predicted to give 3 dB sensitivity variation within the zone and a focal spot diameter around 0.085″. Table 2 lists the transducer design parameters. The zone 1 transducers were spherically focused rather than the bicyclindrical design used for the other zones to address potential near-surface resolution issues.

Calculations were made to estimate whether the proposed transducer would improve signal-to-noise levels enough to achieve the #1 FBH sensitivity goal. An improvement of 4 to 6 dB (equal to a factor of 1.6 to 2.0) is needed in SNR. The calculation was made for zone 4 transducers using the current production design as a baseline and used the rule-of-thumb that SNR is inversely proportional to the square root of the pulse volume. Table 3 shows the estimated relative improvement in SNR for the new design transducers, both in the focal plane and at the extremes of the inspection zone. These estimated improvements vary from 1.67 times to 2.4 times, which compares favorably with the 1.6 to 2.0 times improvement required to achieve the #1 FBH sensitivity.

TABLE 2. DESIGNS FOR F/8 AND F/10 TRANSDUCERS FOR 10″ DIAMETER BILLET

Series 1, F/8 design

Zone	Focus Depth	Diameter x	Diameter y	Radius of Curvature x	Radius of Curvature y
1	0.5	Spherical Focus to be Calculated			
2	1.3	1.33	1.03	6.273	8.773
3	2.2	2.00	1.49	6.939	12.846
4	3.1	2.67	1.95	7.427	16.501
5	4.0	3.34	2.41	7.774	20.125
6	5.0	4.08	2.91	8.024	24.041

Series 2, F/10 design

Zone	Focus Depth	Diameter x	Diameter y	Radius of Curvature x	Radius of Curvature y
1	0.5	Spherical Focus to be Calculated			
2	1.3	1.08	0.83	6.519	10.483
3	2.2	1.62	1.20	7.073	14.096
4	3.1	2.16	1.57	7.535	17.440
5	4.0	2.70	1.94	7.821	21.084
6	5.0	3.30	2.36	8.115	23.923

Based on these results, the decision was made to purchase one set of transducers of each of the F/8 and F/10 configurations, with transducers for zone 2 (0.9″ to 1.8″ depth) and zone 4 (2.7″ to 3.6″ depth) to be ordered initially. It was also agreed to purchase curved element designs, which eliminates two of the critical parameters found in lens-focused designs (lens velocity and element deviation from flatness). This reduced the critical parameters to radius of curvature in the x and y directions (geometrical focal lengths (GFL)x and GFLy) and frequency.

Because the transducer price was much higher than expected, it was decided to buy only the F/10 transducers and evaluate them on the ETC 10″ diameter calibration standards. If the results indicated that the F/10 design was adequate for the #1 FBH sensitivity, then the ETC team would proceed to buy the additional four transducers to complete the set. If it appeared that the F/8 transducers were needed to achieve the sensitivity, then they were to be purchased and evaluated. There was some additional modeling effort by GE to support the purchase of the two F/10 transducers. The transducers were designed using an optimization routine based on the ISU Gauss-Hermite model. The transducer supplier also performed a design, using the CIVA [13] model, resulting in a slightly different curvature and some differences in predicted performance. Discussions with the supplier led to the conclusion that the source of the differences was that the ETC design incorporated the effects of material attenuation, whereas the supplier design did not. The predicted differences were consistent with this explanation, and the supplier was instructed to manufacture the transducers according to the ETC design.

TABLE 3. PREDICTED BEAM DIAMETERS AND SIGNAL-TO-NOISE IMPROVEMENT OF PROPOSED TRANSDUCER DESIGNS

Transducer Type	Depth	Beam Diameter x (in.)	Beam Diameter y (in.)	Beam Area (sq. in.)	Relative Pulse Length*	Relative Pulse Volume**	Relative SNR***
Current (5 MHz, 1.75″ diameter)	At focus	0.143	0.115	0.0129	1.5	1.000	1.000
Proposed 7.5 MHz F/10	Zone start	0.0803	0.08	0.0050	1	0.260	1.960
Proposed 7.5 MHz F/10	At focus	0.086	0.085	0.0057	1	0.296	1.837
Proposed 7.5 MHz F/10	Zone end	0.0929	0.095	0.0069	1	0.358	1.672
Proposed 7.5 MHz F/8	Zone start	0.072	0.07	0.0040	1	0.204	2.212
Proposed 7.5 MHz F/8	At focus	0.066	0.065	0.0034	1	0.174	2.398
Proposed 7.5 MHz F/8	Zone end	0.078	0.08	0.0049	1	0.253	1.988

*Used arbitrary values for pulse length assuming pulse length proportional to 1/frequency.
**Ratio of the pulse volume to the pulse volume of the current transducer.
***Calculated as 1/(square root of relative pulse volume)

In an attempt to get further agreement between the CIVA model and the ISU transducer design model, the UT attenuation coefficients for Ti were provided to the manufacturer for incorporation with their model. After some additional effort, the manufacturer achieved agreement in lens designs with the ISU Gauss-Hermite model.

3.2.1 Transducer Manufacturing Parameter Tolerance Analysis.

A sensitivity analysis was completed to gain a better understanding of how the element curvatures and frequency affect the transducer performance and to help define a manufacturing tolerance on these parameters. The analysis was performed for each of the proposed transducer designs. The inputs for radii of curvature were the design value and values 1% above and below the design value. The inputs for frequency were the design value (7.5 MHz) and values 0.5 MHz above and below this. For each transducer, the Gauss-Hermite model was used to predict the location of the focal point and the value of the zone balance (amplitude difference between targets at the near and far ends of the zone) for all combinations of the input parameters (a zone balance limit of 3 dB is currently used for acceptance of production transducers). The output of these calculations was used to generate a fit of predicted zone balance versus the deviation of the radii and frequency from their nominal values.

Figure 2 shows an example of fitted data for the zone 4 F/10 transducer and predicted change in zone balance (in dB) for variation of ±1% in radius of curvature normal to billet axis (DGFLX) and variation of the ±6.7% (±0.5 MHz) in frequency (DFREQ). As shown in the plot, a shift in frequency of -0.5 MHz and a shift in radius of curvature of -1% would result in a 2 dB change in the zone balance. This analysis was completed for each of the transducer designs to define tolerance limits for the purchase specification.

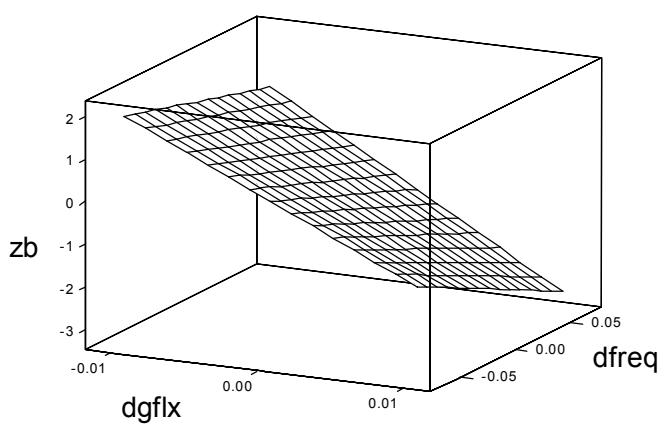

FIGURE 2. RESULTS OF SENSITIVITY ANALYSIS FOR ZONE 4 F/10 TRANSDUCER DESIGN

3.2.2 Transducer Characterization.

In addition to model validation activities, the ETC team began to look at simple ways the transducer manufacturers might have of verifying the performance of the transducers without the need for costly reference blocks. The current evaluation of billet transducers requires a

full-round billet standard and the means to rotate and scan it; this is not a practical arrangement for a transducer manufacturer. Three different approaches were considered. The approach deemed easiest to implement involved mapping the V(z) amplitude profile against a flat surface reflector [14]. The test performs a simple V(z) measurement, that is, the voltage in response to reflection from a planar surface is recorded as a function of distance, z, from the surface. A model was developed to predict the V(z) response for the billet transducers. The predicted V(z) response was compared to the measured V(z) response for three transducers. The agreement observed in these tests were consistent with the agreement previously observed when comparing performance using the FBH billet standard. Specifically, the transducer that showed good agreement in the billet standard also showed good agreement in the V(z) measurement. The other transducers displayed a discrepancy similar to that observed in the billet standard. It was noted that the V(z) measurement allows an independent check of the focal lengths in the circumferential and axial directions. Figure 3 shows this agreement for manufacturer B. The lens-focused transducers displayed a discrepancy similar to that observed in the billet standard. This observation gave further insight into the underlying cause of the anomalous performance seen in the billet standard.

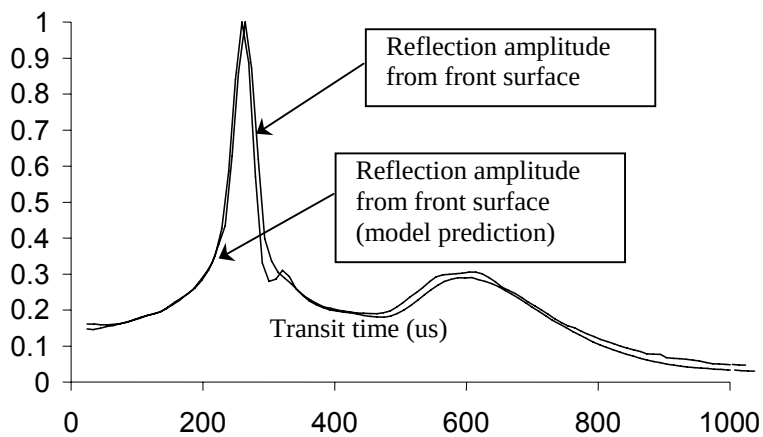

FIGURE 3. VOLTAGE RESPONSE V(z) FOR MANUFACTURER B CURVED ELEMENT TRANSDUCER

Tests and modeling were performed to show that the V(z) method is sensitive to errors in the axial and circumferential focusing radii and can predict the focusing performance in the billet. This was done by using the tolerance analysis to estimate how much perturbation would be needed in each of the design parameters in order to cause a 1 dB shift in the zone balance. These same perturbations were then used to calculate V(z) curves for the nominal and perturbed conditions. The robustness of the method was investigated relative to pulse shape and alignment of the transducer during the test. This study indicated that it was a viable transducer evaluation process that the supplier might use for an acceptance test.

MZ transducers used for billet inspections are typically bicylindrically focused to compensate for the curved sound entry surface of the billet. The two distinct focal zones in water coalesce to a single focal zone in metal after transmission through the billet surface, and the focusing of the

beam in the metal tends to improve the SNRs. Prior to certifying transducers for service, it is useful to determine how accurately their actual focal characteristics match their intended design values. The focal characteristics are also necessary inputs to inspection simulation models used by ETC to estimate the probability of detecting billet defects of various types, sizes, and locations. The term characterizing a transducer is used to mean providing a method for describing the radiation pattern broadcast by the transducer.

The radiation pattern of a transducer is determined both by its physical geometry and the manner in which it is excited. A broadband sonic pulse can always be decomposed into its Fourier (single-frequency) spectral components, and thus, it is sufficient to provide a means for describing the radiation pattern at each frequency within the transducer's operating bandwidth. As a working hypothesis, it was assumed that a given commercial transducer behaves approximately like an ideal, focused piston probe, i.e., one in which the entire face oscillates with uniform amplitude and generates (if focused) curved initial wave fronts in water. The characterization problem then reduces to determining, at each frequency of interest, the four geometrical parameters shown in figure 4(b): two diameters (Dx and Dy) defining the effective lateral size of the elliptically shaped probe cross section and two GFLs (Fx and Fy) describing the bicyclindrical curvature of the initial wave fronts in water. These four parameters are understood as being properties of the transducer alone, independent of the method in which it is excited. Different excitation methods, i.e., the use of different UT pulsers, will produce different sonic pulses with different spectral mixtures, but at a given frequency, all would have the same radiation pattern to within a constant factor.

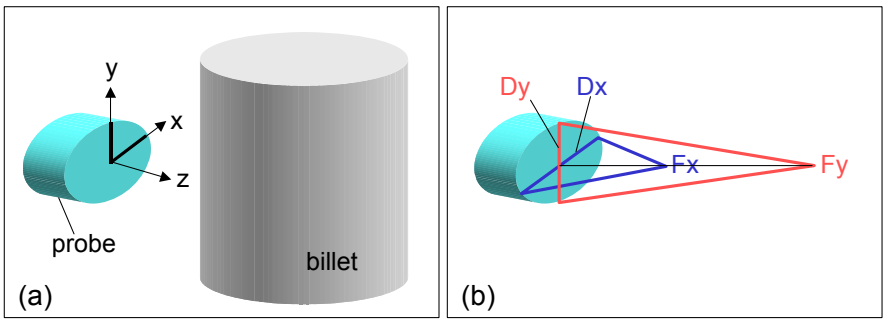

FIGURE 4. (a) BILLET INSPECTION GEOMETRY SHOWING THE BEAM COORDINATE SYSTEM AND (b) THE FOUR PARAMETERS USED TO CHARACTERIZE THE FOCAL PROPERTIES OF A TRANSDUCER

Three approaches for characterizing MZ transducers were explored prior to selecting the V(z) method. Details of all three methods are described below.

a. The three experiment geometries considered for probe characterization are shown in figure 5. In the Beam Mapping in Water (BMIW) method, echoes from a small hemispherical target are acquired as the probe is scanned in the two lateral dimensions. Several such scans are made with different water paths, bracketing the two focal lengths. Although the measurements are easy to perform, the BMIW method generally leads to single-frequency images of reflected amplitude, which are relatively complicated

interference patterns at all water paths. This is a consequence of having two, often widely separated, focal zones in water.

b. Since the probe is designed to project a single, well-defined focal zone within a billet, simpler images of reflected amplitude can be obtained using the Beam Mapping in Solid (BMIS) method. There, echoes are similarly acquired by scanning the probe above a small reflector, typically an FBH, located within a metal specimen having a cylindrically curved surface. The sound entry surface should have approximately the same radius of curvature as the billet the probe was designed to inspect. To map out different portions of the beam in metal, several FBHs located at different depths are scanned. The hole depths should bracket the focal zone in the metal. In the BMIS method, two methods of scanning the transducer above the target can be used: a simple two-dimensional (2D) planar scan (in the x y plane of figure 4(a)) or a surface-following rotational scan. There are inherent difficulties with using a rotational scan for deep-zone transducers. An FBH target located near the billet center is seen over a wide angular range, and hence, the size and shape of the amplitude image are primarily determined by the scanning geometry rather than the beam spot size. This makes it more difficult to estimate focal parameters from the FBH images. This method also requires access to standards for the range of billet diameters of interest, which presents a difficulty for the transducer manufacturer.

c. When using the V(z) method, one orients the transducer at normal incidence to a flat reflecting surface and measures the amplitude (V) of the front-wall echo as a function of water path (z). Data are acquired at 100 or so equally spaced water paths covering the two focal zones. Unlike BMIW and BMIS, the V(z) measurement does not provide direct information about transverse beam cross sections. However, it is much simpler to apply, and was found to yield accurate estimates of focal characteristics.

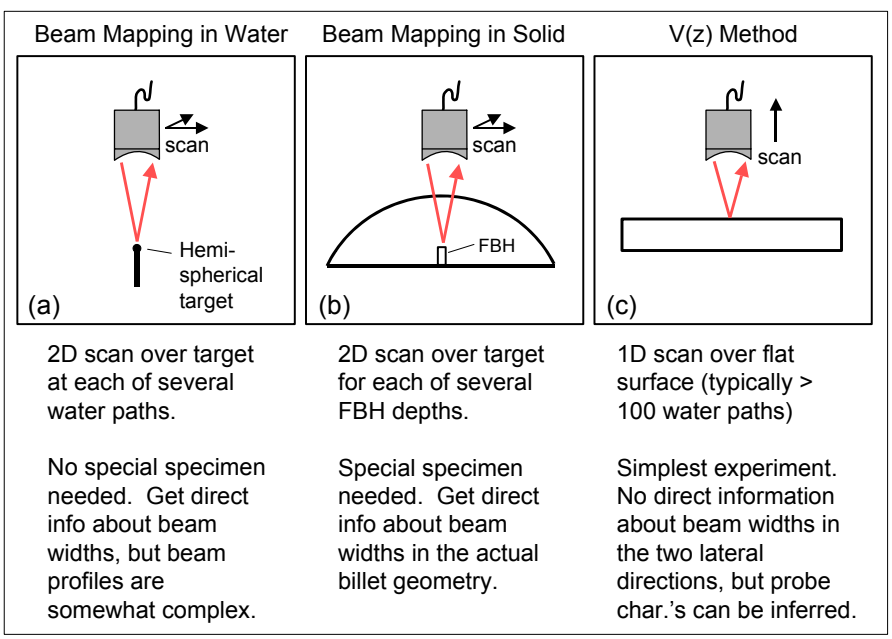

FIGURE 5. THREE MEASUREMENT GEOMETRIES FOR ACQUIRING DATA FOR TRANSDUCER CHARACTERIZATION

The estimation of focal parameters proceeds similarly for the three measurement geometries. In each case, UT A-scans are acquired and stored at each transducer position in the scan pattern. Fast Fourier transform operations are then used to produce reflected amplitude-versus-position maps at each discrete frequency of interest. These maps are a sequence of 2D images for the BMIW and BMIS methods, and a one-dimensional (1D) curve for the V(z) method. The model parameters are then adjusted to optimize the agreement between the measured and predicted maps.

There are two general philosophies for the parameter adjustment or fitting procedure. When circular, spherically focused, commercial transducers are approximated as ideal piston probes. Past studies have shown that the best choice for the effective diameter is usually very near to or slightly smaller than the nominal diameter. However, the effective focal length can be quite different than the nominal value. Thus, the effective diameter is usually not in question, but the focal length is. Assuming that this will also be the case for MZ transducers, one can choose to fix Dx and Dy near their nominal values, and then adjust only Fx and Fy. This greatly speeds and simplifies the optimization procedure and helps to limit the multiple minima problem that occurs when differing sets of {Dx, Dy, Fx, Fy} values are found for which theory and experiment are in similar agreement. Rather than fixing Dx and Dy, one can, of course, choose to simultaneously fit all four model probe parameters. Both the two- and four-parameter fits were considered in the exploratory work.

Under either fitting philosophy, the optimal probe parameters are determined by using a numerical search to minimize the function, shown in figure 6, which quantifies the difference between the measured and predicted amplitudes. For the V(z) method, the attenuation of water must be known. For BMIW and BMIS, probe characterization can be done even if the attenuation values of the water and solid media are unknown. In such cases, the fitting philosophy is to adjust the probe parameters so that the measured and predicted 2D amplitude images are as similar as possible in shape, i.e., to within an amplitude scale factor that is different for each image. Thus, amplitude differences from image to image are ignored. For BMIW and BMIS, both the with attenuation (absolute amplitude fitting) and without amplitude (profile shape fitting) approaches were considered.

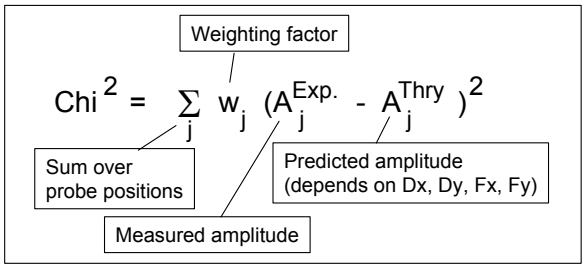

FIGURE 6. FUNCTION THAT IS MINIMIZED TO DETERMINE THE BEST FIT TRANSDUCER CHARACTERISTICS

To test the three characterization methods, they were applied in turn to a typical 5-MHz MZ transducer. This commercially manufactured probe had a curved element rather than a focusing lens. It was designed to focus 3.15″ deep in the 10″ diameter Ti alloy billet when operated at

normal incidence with a 3″ water path (i.e., zone 4 for the 10″ billet). The nominal design parameters were {Dx, Dy, Fx ,Fy}={1.75″, 1.75″, 7.5″, 18.5″}.

By chance, each of the three characterization methods was performed using a different inspection system, i.e., different pulser and scanning bridge. Since inspection water paths were inferred from sound arrival times, for each UT system, it was necessary to determine the sound speed in water (v0) and the time offset (t0). The latter appears in the equation t = t0 + 2z0/v0, which specifies the arrival time (t) of an echo from a small reflector located at a water path z0 along the beam axis. It represents the time delay between the triggering of the oscilloscope trace (when an electrical impulse is sent to the probe) and the arrival time of an echo from a target in contact with the probe. As illustrated in figure 7, t0 is determined by measuring echo arrival times for a series of known water paths and extrapolating to z = 0. To do this, a small spherical target is placed in contact with the center of the transducer face, and the water path is defined to be z = 0 for this setup. The probe is then moved away from the target, with the target remaining on the beam axis. The water path is increased until the target echo cleanly separates from the main bang, and then data acquisition commences; this occurred for a water path of about 0.13″ in figure 7. Water paths and echo arrival times are then recorded, and a linear fit yields an estimate of both the time offset and the sound speed in water. Note that when a focal length in water is deduced by any of the methods, that focal length is always measured from the center point on the face of the transducer.

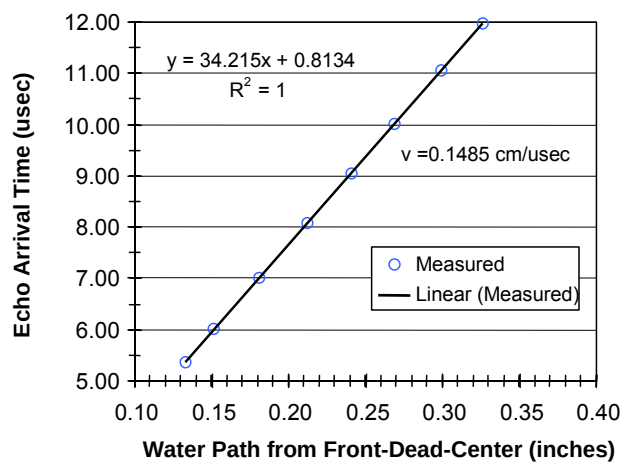

FIGURE 7. MEASUREMENT OF THE TIME OFFSET (0.81 μsec) FOR THE UT SYSTEM USED FOR THE BMIW METHOD
(The time offset is obtained by extrapolating the line to zero water path.)

Typical measured amplitude profiles are compared with their fitted model counterparts in figures 8, 9, 10, and 11. Details about the experimental setups used to acquire probe characterization data are shown in figures 8(a), 10(a), and 11(a) for the BMIW, BMIS, and V(z) methods, respectively. For the BMIW method, a 1/8″ diameter glass rod having a hemispherical cap was used as the reflector, and 2D scans were performed at ten water paths. For the BMIS method, a cylindrical chord block of fine-grained Ni alloy containing FBHs at various depths was used. The chord block was one-half of the Inconel (IN)718 10″ diameter billet calibration standard that was fabricated as part of the ETC effort in Ni billet inspection development [1]. As indicated in

figure 10(a), 2D scans were made over four of the holes, three of which lie in the depth zone that the transducer was designed to inspect. BMIS data was also acquired for a shallower hole (at 2.25″ depth), but that data from the near field of the transducer was quite distorted and deemed unusable. For both the BMIW and BMIS methods, each 2D scan typically contained about 80 by 80 probe positions with about 40 by 40 of these in the region where the reflected amplitude was at least 10% of its peak value. For the V(z) method, A-scan data was acquired at 100 equally spaced water paths, as indicated in figure 11(a). For all three methods, A-scans were digitized at a 100-MHz sampling rate.

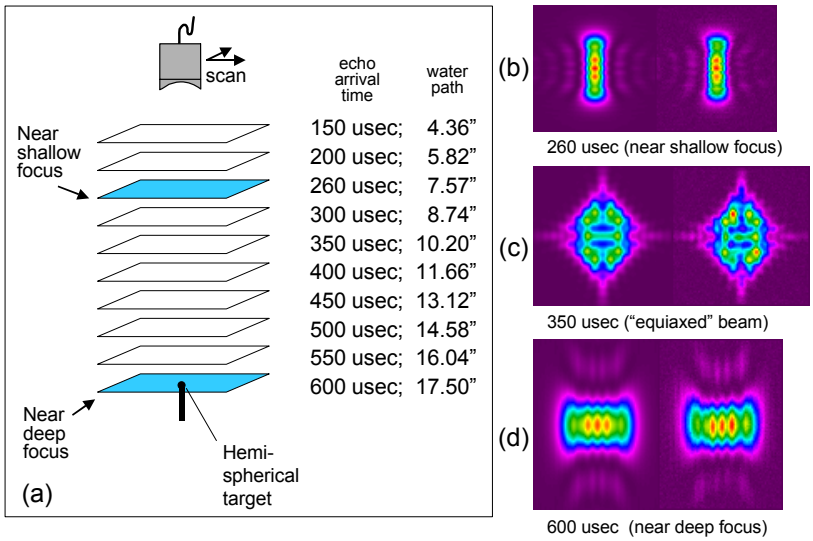

FIGURE 8. THE BMIW METHOD (a) WATER PATHS USED FOR 2D SCANS AND (b-d) COMPARISON OF FITTED (LEFT) AND MEASURED (RIGHT) BEAM PROFILES FOR THREE OF THE WATER PATHS
(Results for the 5.08-MHz spectral component are shown.)

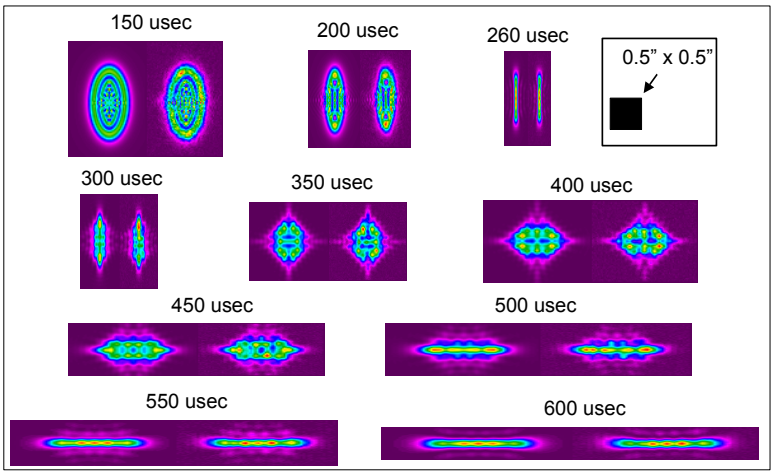

FIGURE 9. THE BMIW METHOD FITTED (LEFT) AND MEASURED (RIGHT) BEAM PROFILES AT 5.08 MHz FOR EACH OF THE TEN WATER PATHS
(Images have true aspect ratios and a common size scale, indicated at upper right.)

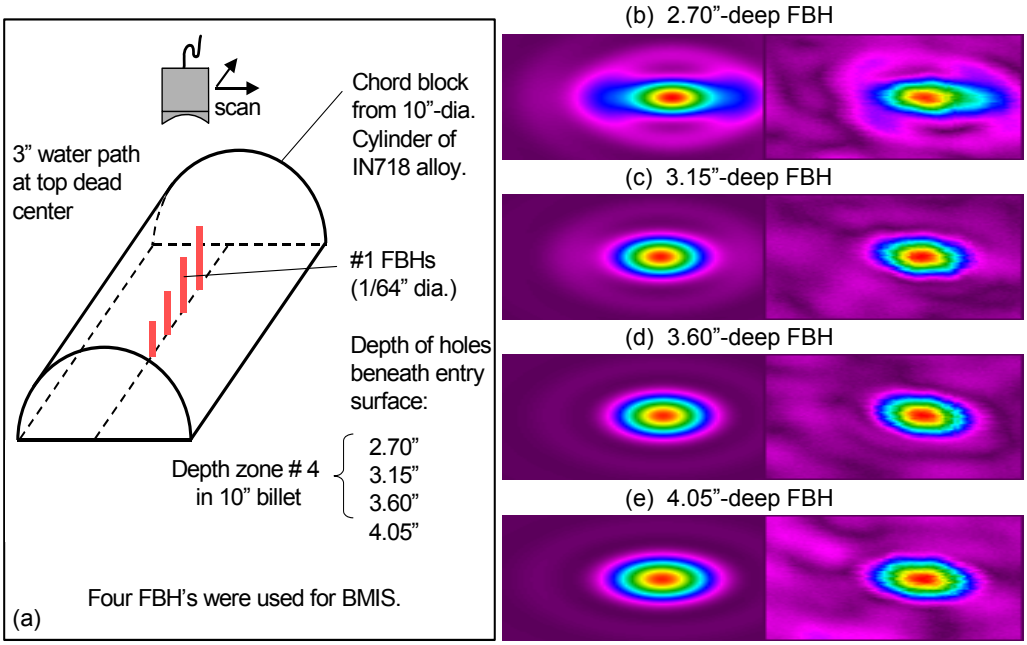

FIGURE 10. THE BMIS METHOD (a) DATA ACQUISITION DETAILS AND (b-e) FITTED (LEFT) AND MEASURED (RIGHT) BEAM PROFILES AT 5.08 MHz FOR EACH OF THE FOUR FBHs

(Images have true aspect ratios and a common size scale. Each image measured 0.20″ by 0.43″, with the long dimension parallel to the billet axis.)

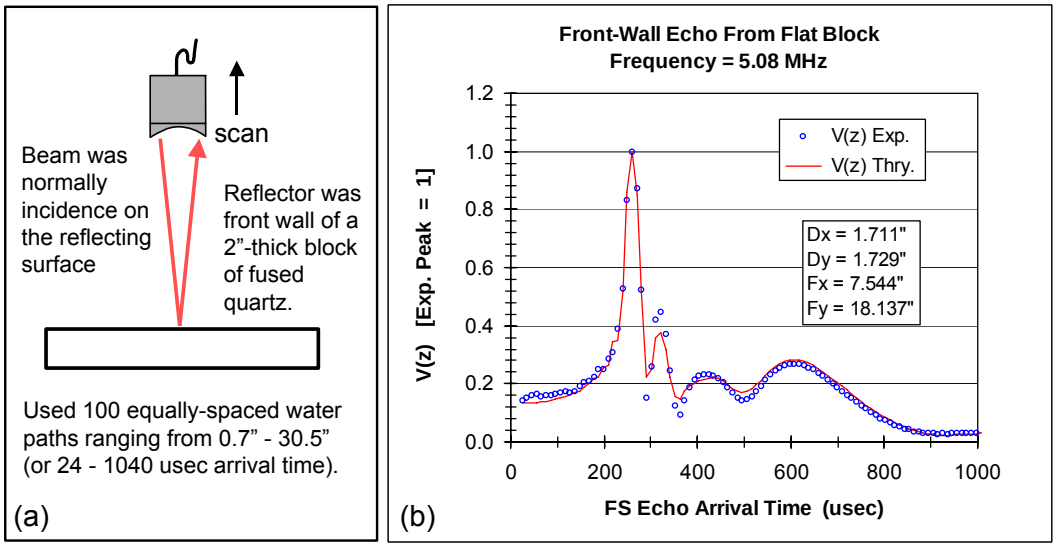

FIGURE 11. V(z) METHOD (a) DATA ACQUISITION DETAILS AND (b) MEASURED AND FITTED AMPLITUDE PROFILES AT 5.08 MHz

The good overall agreement between the measured and predicted profiles adds credibility to the ideal piston probe approximation that was used. Note the relative complexity of the BMIW images compared to those for BMIS. As pointed out earlier, this is a consequence of having a single focal zone in the metal, but two widely separated focal zones in water. Thus, for BMIW, all measurements are effectively being made in the near field of the transducer. As the frequency increases, the BMIW images tend to become more complicated, with a higher density of relative minima and maxima. The same is true for BMIS images when the reflector is positioned outside the focal zone in metal. The images shown in figure 9(b) for the BMIS method have the correct aspect ratio; the image elongation in the axial direction is primarily due to the refraction of the central ray by the curved entry surface during scanning. For a fixed transducer position, the beam cross section in the metal has a much more circular appearance. For the BMIW images shown in figure 8(b), false aspects ratios have been used to make it easier to visually compare the measured and predicted amplitude profiles. BMIW images with correct aspect ratios and relative sizes are shown in figure 9. There, one can more clearly see the focusing in the horizontal direction (x in figure 4(a)) at short water paths, and the focusing in the vertical direction y at long water paths.

For the V(z) method, the two focal points in water manifest themselves as separate maxima located at echo arrival times near 250 and 600 μsec in figure 11(b). As the frequency increases, these two principal maxima tend to sharpen, and the smaller, secondary peaks (near 300-500 μsec in figure 11(b)) tend to increase in number.

Focal parameters deduced by the fitting process when {Dx, Dy, Fx, Fy} are all simultaneously varied are shown in figure 10 as functions of frequency for each method. For BMIW, the four-parameter fits results are independent of frequency to within about ±1% in each parameter when the full complement of data is used (i.e., 2D images at ten water paths). When a much smaller subset of the BMIW data is used, the deduced focal parameters typically display a more marked dependence on frequency. As can be seen in figure 12 for BMIW, using all ten water paths led to fitted parameters with the least overall dependence on frequency. V(z) was a close second, and BMIS was a more distant third. For BMIS, the results are shown (1) using absolute amplitude data and available attenuation values and (2) using only relative amplitude data within each 2D image. The results for BMIW used only relative amplitude data.

A commercial transducer will not behave exactly like the ideal piston transducer assumed by the model. Thus, there will always be differences between the measured and predicted responses, and the precise model parameter set deemed to produce the best fit will depend to some extent on details of the fitting procedure. For example, in the BMIW and BMIS methods, an algorithm is used to align the centers of the measured and predicted amplitude images, and all measured amplitudes in an image below some cutoff value are excluded from the fit. Typical cutoff values were 10% of peak amplitude for BMIW and 30%-50% for BMIS. Modifying the alignment and cutoff choices can change the best-fit parameters, typically by several tenths of 1% in this example. In addition, different choices of the weighting factors (the wj in figure 6) can influence the results. Various methods for choosing the weighting factors were explored, and the following choices seemed to perform well:

- For V(z), all weights were chosen equal.

- For BMIW and BMIS, all weights were equal within a given 2D scan, but different weights were assigned to each scan; these weights were chosen so that each 2D scan contributed about the same amount to the chi-squared function in figure 6.

- For BMIW, neglecting the absolute amplitudes of each 2D scan and, hence, concentrating only on the shapes of the 2D profiles seem to produce the most stable fits.

- For BMIS, which had relatively few 2D scans as input, using absolute amplitude and attenuation data, seemed to improve the fits.

The metal attenuation value used in the fitting procedure was based on measurements of coupons from a different 10″ diameter IN718 billet that had been Gesellschaft fur Maschinenbau-und-Fertigungstechik (GFM)-forged like the chord block. GFM employs multiple hammers oriented at 90 degrees to one another that pound the ingot while it rotates. Those attenuation measurements were made under the ETC Ni billet fundamental studies efforts [15].

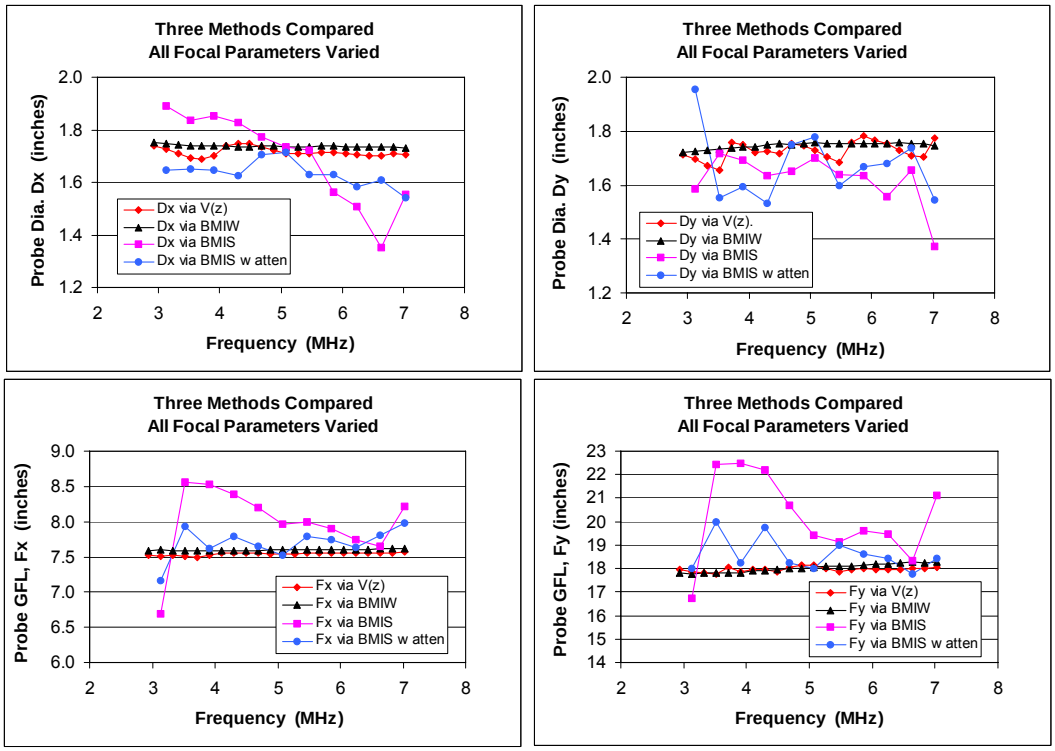

FIGURE 12. DEDUCED FOCAL PARAMETERS FOR EACH METHOD WHEN ALL FOUR PARAMETERS ARE ALLOWED TO VARY

The variation of the deduced {Dx, Dy, Fx, Fy} with frequency is one indicator of the uncertainty in the measurement procedure. The mean and standard deviation of the fitted focal parameters, computed for the 3-7 MHz frequency range, are listed in table 4 for various fitting trials. The mean and standard deviation of the single-frequency estimates are shown for the 3-7 MHz frequency range. Included are cases where Fx and Fy alone have been varied, with Dx and Dy held fixed at 99% of their common nominal value (i.e., approximately the average of the fitted

diameters for the BMIW and V(z) methods). Note that a coordinate measurement machine (CMM) was used to map out the physical surface of the transducer. Bicylindrical functions were fitted to the CMM data, with both local and global fits being made. These CMM results appear in the lower portion of table 4. CMM values for the focal lengths were obtained by fitting a bicylindrical surface to the physical transducer surface as mapped out using a coordinate measurement machine. The local CMM fit is to the central region of the probe surface only.

TABLE 4. VALUES OF EFFECTIVE DIAMETERS AND GFL DEDUCED USING VARIOUS FITTING METHODS

Method	Dx (in.)	Dy (in.)	Fx (in.)	Fy (in.)		Notes
V(z)	1.72 ±0.02	1.73 ±0.03	7.54 ±0.02	17.96 ±0.10	A	100 A-scans
V(z)	1.73 (fixed)	1.73 (fixed)	7.56 ±0.02	17.97 ±0.06	A	100 A-scans
BMIW	1.74 ±0.01	1.75 ±0.01	7.60 ±0.01	18.03 ±0.17		Scans at 10 water paths
BMIW	1.72 ±0.04	1.75 ±0.02	7.56 ±0.05	18.28 ±0.58		Scans at 3 water paths
BMIW	1.73 (fixed)	1.73 (fixed)	7.59 ±0.02	18.16 ±0.24		Scans at 10 water paths
BMIW	1.73 (fixed)	1.73 (fixed)	7.58 ±0.03	18.10 ±0.44		Scans at 3 water paths
BMIW	1.73 (fixed)	1.73 (fixed)	7.55 ±0.02	18.66 ±0.42	A	Scans at 10 water paths
BMIS	1.69 ±0.17	1.62 ±0.10	7.98 ±0.52	20.14 ±1.83		Scans of 4 FBHs
BMIS	1.63 ±0.05	1.67 ±0.13	7.70 ±0.22	18.59 ±0.71	A	Scans of 4 FBHs
BMIS	1.73 (fixed)	1.73 (fixed)	7.91 ±0.38	19.02 ±1.15		Scans of 4 FBHs
BMIS	1.73 (fixed)	1.73 (fixed)	7.57 ±0.22	18.34 ±0.53	A	Scans of 4 FBHs
Design	1.75	1.75	7.50	18.54		Design specifications
CMM			7.66	17.83		Local fit to surface
CMM			7.66	18.35		Global fit to surface

A = Absolute amplitude and attenuation data used during fitting.

For the three characterization methods, the differences in the mean values of {Dx, Dy, Fx, Fy} are typically within the listed standard deviations. Notice that the uncertainties for BMIS are much larger than for the other two methods. The BMIS method is conceptually inviting because the sonic beam is focused in the chord block in the same manner as in an actual billet inspection. In practice, however, there seem to be two shortcomings that limit its accuracy: (1) available chord blocks typically contain FBHs at only a few depths within the designed inspection zone, thus limiting the data input to the fitting algorithm and (2) alignment difficulties and the metal microstructure act to distort the FBH images, as shown in figure 10(b).

As shown in table 4, the most trustworthy of the characterization methods (BMIW and V(z)) yielded probe diameters in good agreement with the nominal 1.75″ value when all four parameters were varied. This assumes that the effective diameters of curved element MZ transducers are at or near the design diameters, and then fitting only the focal lengths. This not only speeds the fitting process, but also leads to results that are much more stable with respect to changes in the fitting process (i.e., changes in the cutoff values, weights, or profile-centering algorithm).

Of the three methods studied, V(z) was by far the quickest, both for data acquisition and for the fitting analysis. It yielded average focal length estimates in good agreement with BMIW, about midway between the design values and those estimated from the CMM data. Thus, V(z) appeared to be the leading candidate for use by OEMs and transducer manufacturers for transducer characterization.

Note that the fitting process required model calculations of the pressure fields generated by ideal piston transducers. In this work, the paraxial Multi-Gaussian Beam (MGB) model was used for such calculations, since it affords both rapid computation and reasonable accuracy. In the MGB model [16], the sonic field emitted by the transducer is represented as a summation of Gaussian beams, and in this case, a 15-Gaussian representation was used. Questions arose about the accuracy of the paraxial MGB model for calculating the front-wall echoes needed for the V(z) method. To check the accuracy, V(z) curves calculated using the MGB model were compared to those calculated using a more exact model based on a Green's function formulation [11]. Comparisons were made for four probe designs being considered for 7.5-MHz MZ inspections of 10″ billet. Good agreement was seen between the two model calculations, as illustrated in figure 13 for two typical cases. In addition, the V(z) curves generated by the exact model were used as the experimental input into the MGB-based fitting procedure. As shown in figure 14, the deduced probe parameters were in good agreement with the correct values, with the differences generally being much less than the variations between model and experiment seen when fitting actual data from a commercial transducer. The results are shown for four proposed probe designs for 7.5-MHz Ti billet inspections. Thus, errors resulting from using the MGB model to calculate V(z) curves will likely have little practical impact on the accuracy but have the advantage of being a faster calculation.

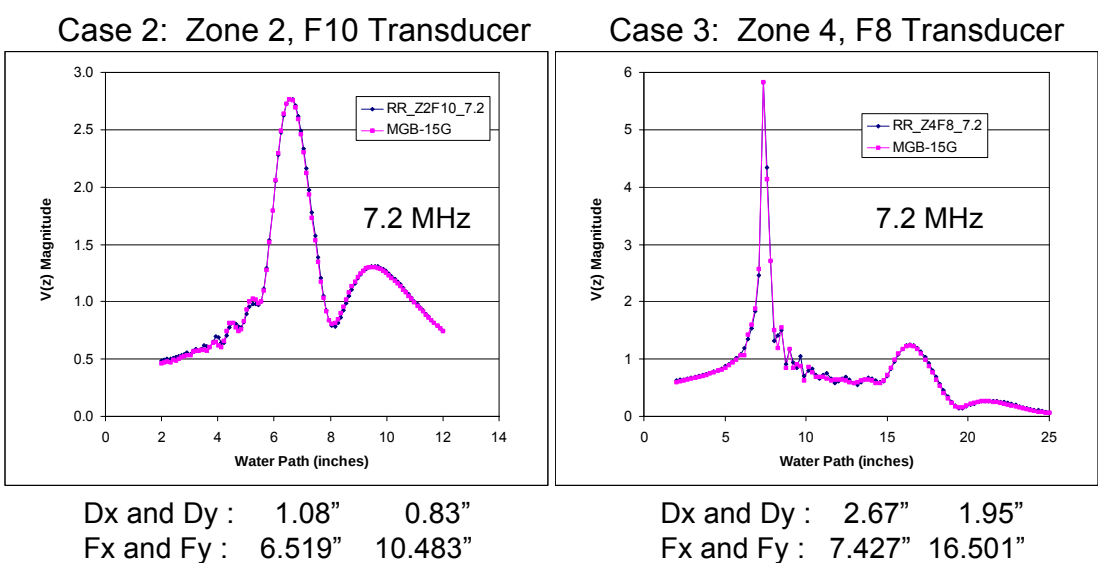

FIGURE 13. COMPARISON OF V(z) CURVES CALCULATED USING TWO DIFFERENT BEAM MODELS—THE GREEN'S FUNCTION-BASED FORMALISM AND THE PARAXIAL MULTI-GAUSSIAN BEAM MODEL

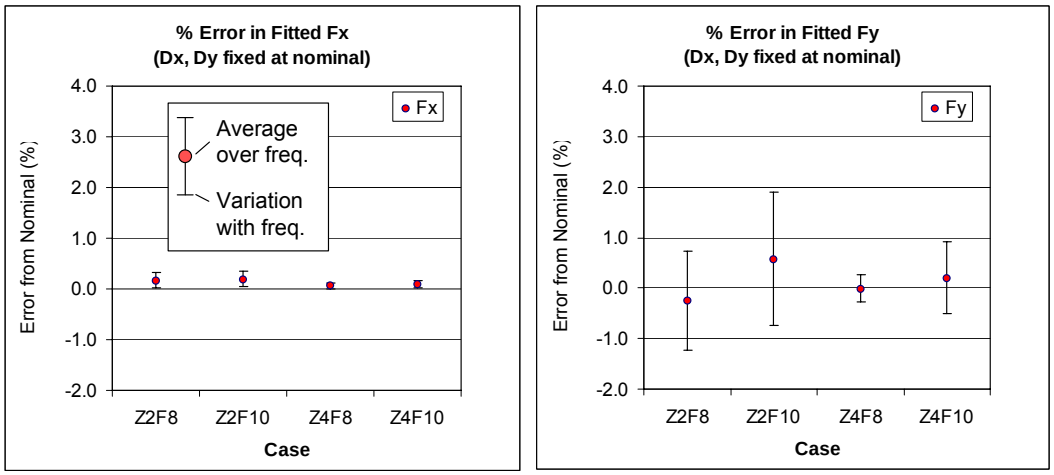

FIGURE 14. PERCENTAGE ERROR RESULTING FROM USING THE PARAXIAL MGB MODEL RATHER THAN THE GREEN'S FUNCTION FORMALISM TO DEDUCE PROBE FOCAL PARAMETERS FROM SYNTHETIC V(z) DATA

3.3 TRANSDUCER EVALUATIONS.

3.3.1 Evaluation of F/10 Transducers.

Using the model-based design approach, the first two F/10 transducers were ordered. Once the two transducers for the 10″ diameter Ti billet were received, a preliminary evaluation was performed. The evaluation consisted of measuring beam diameters and zone balance and taking scans of FBH targets in the ETC 10″ diameter standards. A summary of the results is shown in tables 5 and 6. Note that the center frequency and bandwidth measurements shown are those reported by the manufacturer. The zone balance is defined as the difference in amplitude response between targets at the near and far end of the inspection zone.

TABLE 5. PRELIMINARY EVALUATION RESULTS FOR ZONE 2 TRANSDUCER

	Center Frequency (MHz)	Bandwidth (%)	-6 dB Beam Diameter (Axial x Circular)		Zone Balance (dB)
			Zone Start (0.9″ depth)	Zone End (1.8″ depth)	
Measured	6.33	68	0.13″ x 0.10″	0.10″ x 0.11″	-5.0
Specified	7.5 ±0.5	≥ 60			
Calculated from model			0.086″ x 0.08″	0.10″ x 0.10″	0

TABLE 6. PRELIMINARY EVALUATION RESULTS FOR ZONE 4 TRANSDUCER

	Center Frequency (MHz)	Bandwidth (%)	-6 dB Beam Diameter (Axial x Circular)		Zone Balance (dB)
			Zone Start (2.7″ depth)	Zone End (3.6″ depth)	
Measured	6.02	72	0.09″ x 0.09″	0.09″ x 0.10″	-0.5
Specified	7.5 ±0.5	≥ 60			
Calculated from model			0.080″ x 0.080″	0.093″ x 0.095″ at 3.6″ depth	-0.5

The preliminary results indicated that the frequency was lower than the range specified, which was a concern. Replacements were to be requested if the performance did not fall within the specification. The beam balance and beam diameter results for the zone 2 transducer also showed significant discrepancy from the model predictions. Some C-scans were performed using these transducers on the ETC 10″ diameter Ti-6-4 calibration standards, which contain FBH targets of diameters ranging from 0.4 mm (#1) to 0.8 mm (#2) at depth locations corresponding to the start, middle, and end of each zone. Figure 15 shows the results of the scan using the zone 2 transducer, imaging FBH targets at 0.9″, 1.35″, and 1.8″ depth. All the targets, including the 0.4 mm, can be discerned in the image.

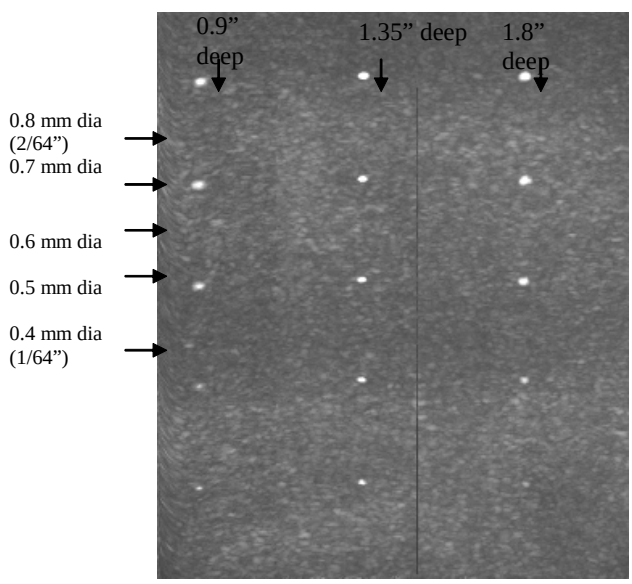

FIGURE 15. C-SCAN OF TARGETS IN ETC 10″ DIAMETER CALIBRATION STANDARD USING THE ZONE 2 TRANSDUCER

The two 7.5-MHz F/10 aperture elliptical transducers were evaluated in more detail. Frequency measurements were made using the echoes from #2 FBH targets in 10″ diameter calibration standards. Tables 7 and 8 compare these frequency measurements with those supplied by the manufacturer, which had been measured on a flat brass target, located at the near focal point, in water.

TABLE 7. FREQUENCY MEASUREMENTS FOR ZONE 2 TRANSDUCER

	Specified	Reported by Manufacturer	Measured on #2 FBH, 1.35″ Deep in IN718
Center frequency (MHz)	7.5 ±0.5	6.33	7.1
Lower—6 dB frequency (MHz)			5.4
Upper—6 dB frequency (MHz)			8.8
Bandwidth (MHz)			3.4
Bandwidth (%)	≥ 60	68	48
Pulse duration (μsec)			0.21

TABLE 8. FREQUENCY MEASUREMENTS FOR ZONE 4 TRANSDUCER

	Specified	Reported by Manufacturer	Measured on 2/64″ FBH, 3.15″ deep in IN718	Measured on 2/64″ FBH, 3.15″ deep in Ti-6-4
Center frequency (MHz)	7.5 ±0.5	6.02	6.35	6.25
Lower—6 dB frequency (MHz)			4.9	4.7
Upper—6 dB frequency (MHz)			7.8	7.8
Bandwidth (MHz)			2.9	3.1
Bandwidth (%)	≥ 60	72	46	50
Pulse duration (μsec)			0.25	0.31

To assess the performance relative to the #1 FBH sensitivity program goal, a number of scans were made using the 10″ diameter Ti-6-4 ETC calibration standards, which contain targets of various diameters down to 0.4 mm (1/64″). These scans were done as closely as possible to production inspection conditions, with the exceptions that the scan index was reduced to 0.01″ to capture the peak signals, and the gate length was reduced where necessary to avoid back surface signals in the gate. For the zone 2 transducer, targets at 0.9″, 1.35″, and 1.8″ (start, center, and end of zone) were analyzed from the C-scan data. For the zone 4 transducer, targets were at 3.15″ and 3.6″ (center and end of zone). In each case, there was some lateral banding of the noise pattern, so regions of noise in the highest and lowest bands were analyzed and are shown separately on the plots. Figures 16 and 17 show the target amplitudes and noise amplitudes for zones 2 and 4. Note that the zone 4 transducer was not capable of performing an inspection of the material in the calibration standard to a 1/64″ FBH sensitivity. The noise level in the high-noise band was marginally above the amplitude of the 0.4-mm (1/64″) target at the deep end of the zone. A 3 dB margin is required between the noise and the target amplitude to achieve the inspection sensitivity. Review of the measured frequency performance, and the manufacturer's

reported measurements also showed that the transducer had frequency significantly lower than specified (measured at 6.02, 6.25, and 6.35 MHz versus the lower specification limit of 7.0 MHz). The transducer was returned to the manufacturer.

The zone 2 transducer appeared marginally capable of meeting the required sensitivity. It showed a difference of 2.8 dB between the noise and the lowest target signal versus the 3 dB requirement. There is a concern that the measured bandwidth was lower than specified (48% versus the lower specification limit of 60%), and the manufacturers reported measurement of frequency was only 6.33 MHz.

The smaller F/10 transducers reported above were purchased with the intent of making the final decision on aperture size based on the results of their evaluation. Based on the data of figures 16 and 17, a decision was made to pursue development of transducers designed with the larger F/8 aperture.

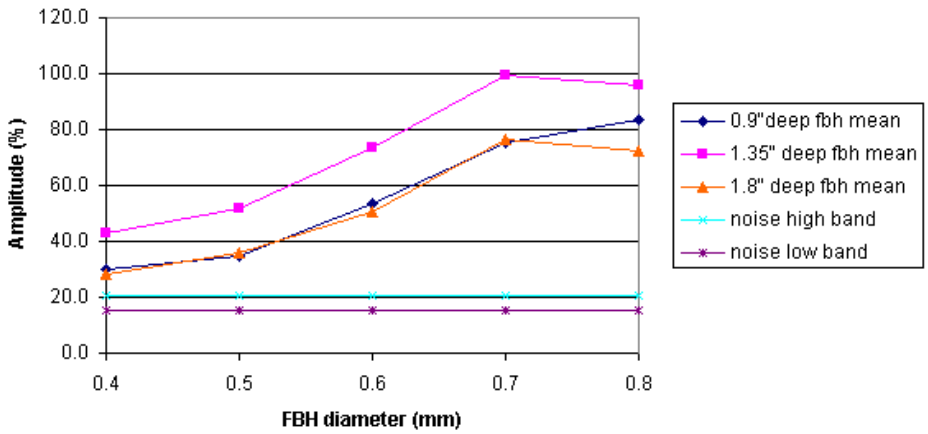

FIGURE 16. NOISE AND TARGET AMPLITUDE RESPONSES, ZONE 2 TRANSDUCER

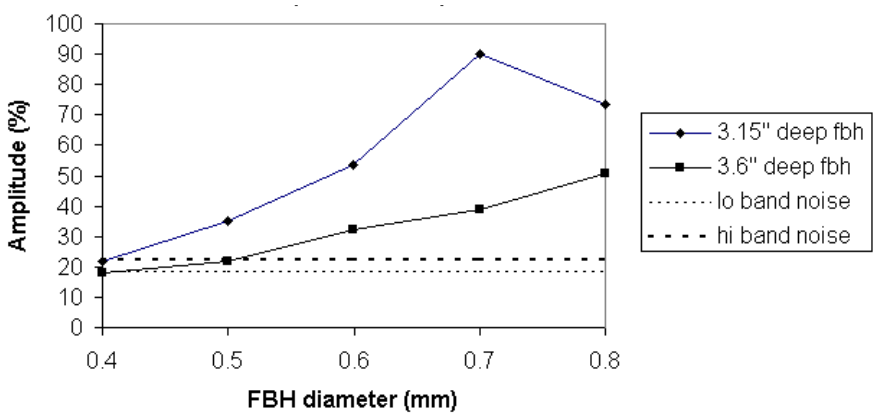

FIGURE 17. NOISE AND TARGET AMPLITUDE RESPONSES, ZONE 4 TRANSDUCER

3.3.2 Pulse Volume Calculations.

As part of the decision process to compare F/10 and F/8 transducer parameters, the pulse volume concept was used [17]. Based on ETC Phase I activities and analysis by ISU, acoustic noise was found to be roughly proportional to the square root of the UT pulse volume. The pulse volume in this case is defined as the 6 dB beam area times the 6 dB pulse width. To achieve #1 FBH sensitivity, the principle direction of the transducer development was to reduce the pulse volume in the focal zone of the transducer, thus reducing the material noise while maintaining a strong signal from the calibration target. Decreasing the pulse volume can be accomplished by several means:

- Reducing the focal diameter either by increasing the transducer frequency or increasing the aperture
- Increasing the bandwidth of the transducer, thus shortening the pulse width
- Combination of both these techniques

The elliptical design and the increase in frequency from 5 to 7.5 MHz decreases the pulse volume by a third at comparable bandwidth over the same transducer at 5 MHz. The F/10 zone 4 transducer designed to focus 3.15″ deep produced a peak noise signal in the C-scan image of 80% compared to the #1 FBH calibrated at 80%. In other words, a SNR of 1. As agreed earlier by the ETC, a minimum SNR of 1.4 or 3 dB is required to claim achievement of target inspection sensitivity. By knowing the pulse volume and using that transducer to measure the peak noise in the billet, one can project the pulse volume required to achieve a signal to noise of 3 dB. Although the zone 4 transducer was returned to the manufacturer for frequency adjustment and subsequently returned to ETC for evaluation, projections of meeting the required 1.4 SNR would not be met with the F/10 design.

The fixed-focus 7.5 MHz, F/10 elliptical element produced a pulse volume of about 360,000 $mils^3$ (600 square root pulse volume (sqrt pv)) at the transducer focal point and a pulse volume of 577,600 $mils^3$ (760 sqrt pv) at the far end of the inspection zone. The projected pulse volume for the F/8 transducer was about 250,000 $mils^3$ (500 sqrt pv) at the far end of the zone, which was projected to be very close to the 3 dB SNR requirement. These results are shown in figure 18.

3.3.3 Phased Array Evaluation.

To further determine the projected pulse volume required for achieving the #1 FBH sensitivity, the ETC 10″ diameter calibration standard #2 FBH was sent to Honeywell for phased array evaluation. The goal here was to capitalize on the phased array capability to vary the focal spot size to evaluate pulse volumes that would achieve the required sensitivity. The transducer available for this evaluation was a 7.5 MHz annular sectorial array designed for an 8″ diameter billet.

Table 9 shows the details of the beam dimensions and the resultant signal to noise values for one set of parameters. The evaluation (figures 19 and 20) of the phased array volume equal to 311,724 mils^3 (sqrt pv) of 558 produced a SNR of about 2.3, exceeding the 1.4 SNR requirement.

F/8

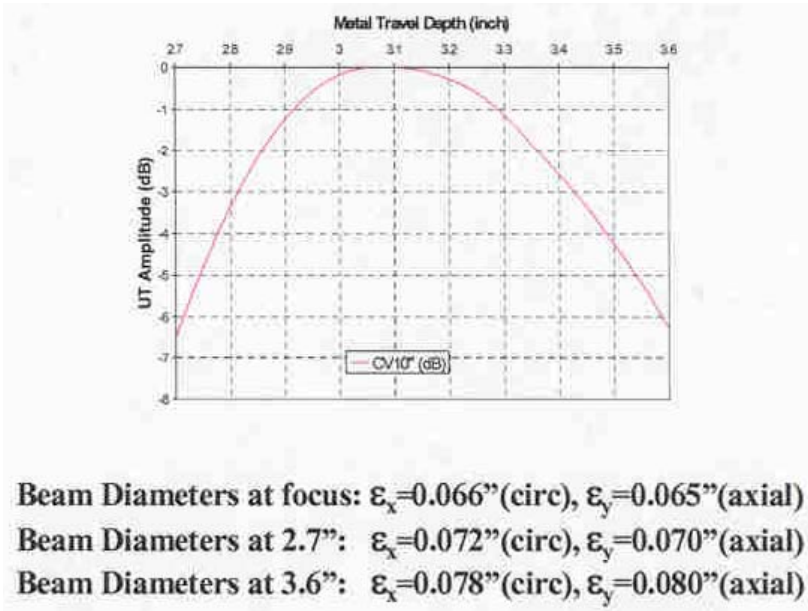

F/10

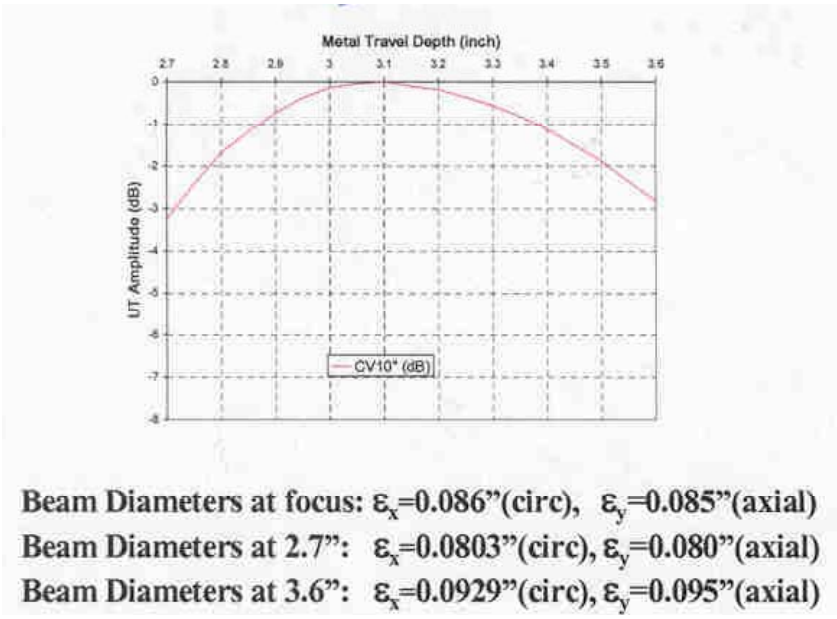

FIGURE 18. COMPARISON OF MODELED BEAM DIAMETERS FOR THE F/8 AND F/10 TRANSDUCER DESIGNS
(F/10 = 588 sqrt pv at 3.6″ depth and F/8 = 495 sqrt pv at 3.6″ depth. Pulse width at 60% bandwidth is 50 mils.)

TABLE 9. DETAILS OF THE BEAM DIMENSIONS AND THE RESULTANT SIGNAL-TO-NOISE VALUES FOR ONE SET OF PARAMETERS

Scan Parameters:	
Probe:	7.5 MHz annular-sectorial array
Focusing:	3.15″ in emission
	3.15″ in reception
Gain:	20 dB
Water path:	0.5″
Beam width:	63 mils (1.6 mm)

Defect Size (mm)	Defect Depth (in.)	Peak Signal (%FSH)	Peak Noise (%FSH)	Mean Noise (%FSH)	SNR	SNR (dB)	-6 dB Beam Width Along Scan Direction (deg)	-6 dB Beam Width Along Scan Direction (mils)	-6 dB Beam Height Along Index Direction (mils)
0.8	3.15	96.5	38.4	20.1	4.17	12.41	3.6	116	100
0.7	3.15	100	33.7	20.3	5.95	15.49	4.05	131	100
0.6	3.15	76.5	30.6	19.1	4.99	13.96	4.5	145	100
0.5	3.15	52.5	26.3	15.7	3.47	10.81	2.7	87	100
0.4	3.15	41.2	26.3	14.9	2.31	7.26	5.4	174	100

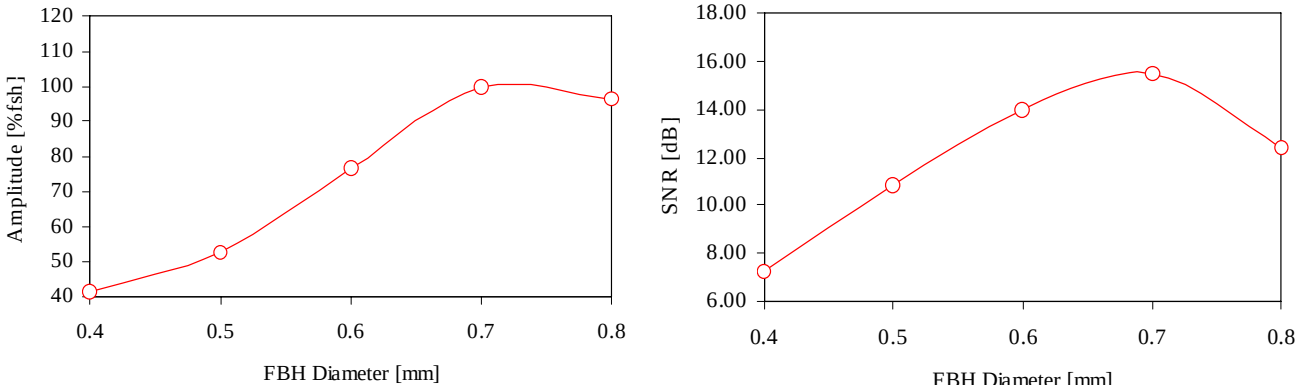

FIGURE 19. RESULTS OF PHASED ARRAY EVALUATION OF THE ETC CALIBRATION STANDARD ON THE 3.15″ DEEP CALIBRATION TARGET
(A 0.4-mm target equal to #1 FBH produced an SNR of 2.3 or 7.23 dB.)

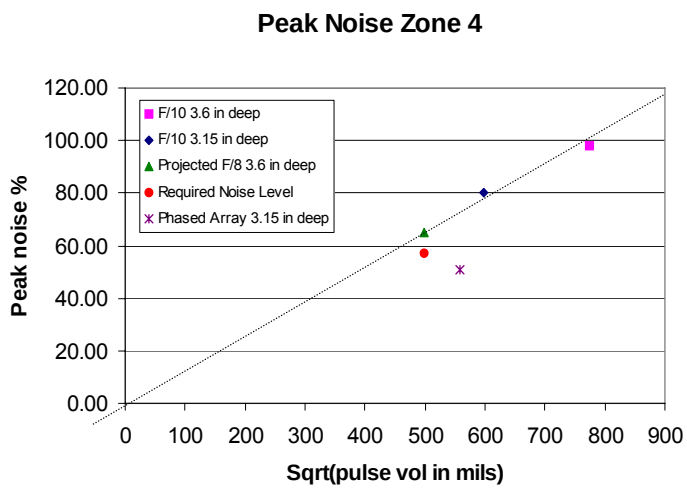

FIGURE 20. COMPARISON OF THE MEASURED AND PROJECTED PEAK NOISE LEVELS VS THE SQRT PV FOR THE F/10, PHASED ARRAY, AND PROJECTED F/8 TRANSDUCERS
(A sqrt pv of between 450 and 500 should meet the 3 dB noise limit.)

3.3.4 Evaluation of F/8 Transducers.

Based on the projected pulse volume required to meet the sensitivity requirement, an order was placed to construct two F/8 transducers for zones 5 and 6, which are the more difficult and deepest zones in the billet. In the event that these transducers met the performance specifications but failed to meet the 3 dB SNR requirement on the ETC calibration standard, other options such as phased array technology were to be explored as a contingency in the original program. Further efforts to reduce the pulse volume on fixed-focus transducers will have to be weighed carefully. Reducing the F number to less than an F/8 would necessitate more zones and is likely to have diminishing improvement on the SNR. A redesign of the calibration standard is also probable because of the increased number of zones. These actions would increase the inspection time considerably as smaller scan and pulse increments would be required.

GE received the two F/8 design transducers in November 2002. These are 7.5 MHz elliptical elements designed to focus at 4″ and 5″ deep, respectively, and are shown in figure 21.

FIGURE 21. F/8, ELLIPTICAL ELEMENTS, 7.5 MHz, ZONES 5 AND 6 TRANSDUCERS

Based on transducer modeling, it was expected that there would be about a 7 dB of sensitivity difference between the center of focus and the two extreme targets located at the zone beginning and end. This sensitivity range will require the use of an instrument that has DAC and a calibration standard that has a target positioned in the center of each zone. Figure 22 shows the model prediction for these two zones.

Model Design of Zone5 Transducer w/ Attenuation

focus depth (inches)	GFLx (in) (Circ)	GFLy (in) (Axial)	Diax (in) (Circ)	Diay (in) (Axial)	Zone		GFLx (model design)	GFLy (model design)
0.5	4.58	5.08	0.74	0.62	Zone1		5.506	5.671
1.3	5.97	8.42	1.33	1.03	Zone2		6.273	8.773
2.2	6.83	12.17	2.00	1.49	Zone3		6.939	12.846
3.1	7.36	15.92	2.67	1.95	Zone4		7.427	16.501
4.0	7.72	19.67	3.34	2.41	Zone5		7.774	20.125
5.0	8.00	23.84	4.08	2.91	Zone6		8.024	24.041

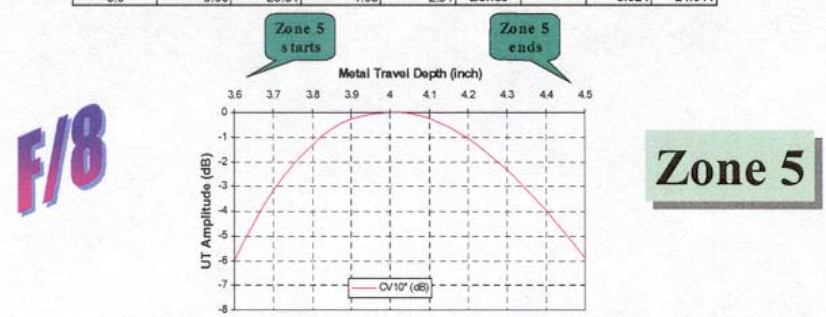

6dB Pulse-Echo Beam Diameters at focus: ε_x=0.0698"(circ), ε_y=0.07"(axial)
6dB Pulse-Echo Beam Diameters at 3.6": ε_x=0.078"(circ), ε_y=0.07"(axial)
6dB Pulse-Echo Beam Diameters at 4.5": ε_x=0.077"(circ), ε_y=0.08"(axial)

Model Design of Zone6 Transducer w/ Attenuation

focus depth (inches)	GFLx (in) (Circ)	GFLy (in) (Axial)	Diax (in) (Circ)	Diay (in) (Axial)	Zone		GFLx (model design)	GFLy (model design)
0.5	4.58	5.08	0.74	0.62	Zone1		5.506	5.671
1.3	5.97	8.42	1.33	1.03	Zone2		6.273	8.773
2.2	6.83	12.17	2.00	1.49	Zone3		6.939	12.846
3.1	7.36	15.92	2.67	1.95	Zone4		7.427	16.501
4.0	7.72	19.67	3.34	2.41	Zone5		7.774	20.125
5.0	8.00	23.84	4.08	2.91	Zone6		8.024	24.041

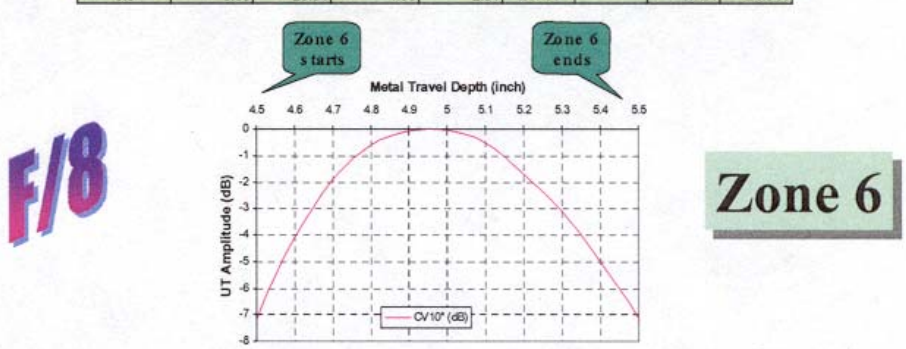

6dB Pulse-Echo Beam Diameters at focus: ε_x=???"(circ), ε_y=0.07"(axial)
6dB Pulse-Echo Beam Diameters at 4.5": ε_x=0.084"(circ), ε_y=0.075"(axial)
6dB Pulse-Echo Beam Diameters at 5.5": ε_x=0.079"(circ), ε_y=0.085"(axial)

FIGURE 22. ZONE SENSITIVITY MODEL PREDICTIONS FOR THE F/8 TRANSDUCERS

The transducer evaluation was completed using the ETC set of four 10″ diameter Ti-6-4 calibration standards, which contain a center hole in each zone that is useful in calibrating a DAC. A commercially available instrument was selected for the measurements because of its DAC capability, and it could easily be transported and adapted to the factory site for later evaluation. The gated output of the commercial instrument was modified for compatibility to the MZ data acquisition system for C-scan generation. This was necessary because the MZ hardware is not currently capable of DAC.

The F/8 transducer focal properties were measured in water and found to be well within the purchase specifications. Following some initial evaluation with the transducers on the ETC standards, an order was placed for the four remaining transducers covering zones 1 through 4 of the 10″ diameter billet. The four remaining F/8 transducers were received in June 2003.

The complete set of six 7.5-MHz F/8 transducers were evaluated on the ETC Ti-6-4 calibration standards and the random defect billet to determine sensitivity curves. Detailed beam measurements and pulse widths were taken for each transducer from which to calculate a pulse volume.

Figure 23 shows the six transducers that comprise the 10″ diameter billet set and a table of the element and lens designs for each transducer.

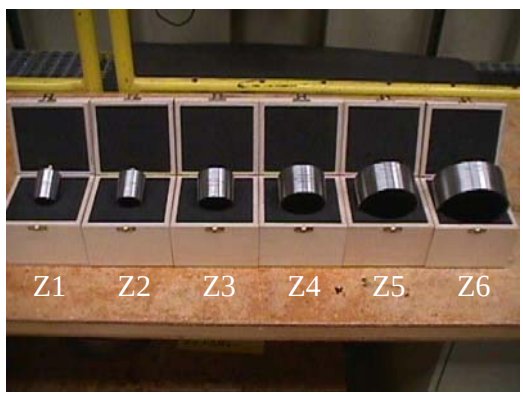

Focus Depth (in.)	GFLX (in.) (circular)	GFLY (in.) (axial)	DIAX (in.) (circular)	DIAY (in.) (axial)	Zone	GFLX (model design)	GFLY (model design)
0.5	4.58	5.08	0.74	0.62	1	5.506	5.671
1.3	5.97	8.42	1.33	1.03	2	6.273	8.773
2.2	6.83	12.17	2.00	1.49	3	6.939	12.846
3.1	7.36	15.92	2.67	1.95	4	7.427	16.501
4.0	7.72	19.67	3.34	2.41	5	7.774	20.125
5.0	8.00	23.84	4.08	2.91	6	8.024	24.041

FIGURE 23. SET OF SIX F/8 7.5-MHz TRANSDUCERS AND TABLE OF DIMENSIONS

Once the transducers were received, the following procedure was used to calibrate each zone of the ETC calibration standards:

- Initially establish a 3″ water path.
- By a combination of water path adjustment and achieving the maximum response from the target holes in each zone, the transducer to billet orientation was established. Adjust the water path within the range of ±0.5″ of 3″ to obtain the best balance between the shallowest and deepest holes for each zone.
- Record the amplitude of all three holes in the zone without DAC.
- Adjust the greatest FBH signal close to 80% full screen height (FSH), which was the center hole for each zone, then create a DAC to bring each FBH to 80%.
- Generate a C-scan of the calibration holes using a 0.020″ index, adjusting the gate during scanning so the back wall from adjacent holes is not gated.
- Record the maximum amplitude in the C-scan using the full zone gate to get a peak noise figure.
- Determine the 6 dB pulse width using the A-scan from the zone's center hole target.
- Measure the 3 and 6 dB axial and circumferential dimensions of the transducer beam on the shallow center and deep holes for each zone.
- Calculate the 6 dB pulse volume using the pulse width and beam diameters and take the square root of this figure.

Table 10 summarizes the results of these measurements for each of the six transducers.

The pulse volumes were calculated using the 6 dB beam dimensions and pulse width (the results are in cubic mils). The largest pulse volume of the three target holes in each zone were compared to the largest volume derived from a model calculation of the F/8 transducers. These comparisons along with the F/10 model predictions are shown in figure 24. The model assumes a constant 6 dB pulse width of 200 nsec or about 0.050″ of material.

Comparing the delivered large element transducers and the predicted pulse volumes highlight some of the current issues with transducer manufacturing. Although progress is being made in transducer fabrication, there are still parameters not tightly controlled, mainly the frequency and bandwidth. These two transducer characteristics have a direct impact on the desired pulse volume.

TABLE 10. SUMMARY OF THE TRANSDUCER BEAM CHARACTERISTICS FOR PULSE VOLUME CALCULATIONS AND RESULTS OF THE NOISE STATISTICS FOR THE ETC AND RANDOM DEFECT BILLETS

Transducer Beam Characteristics										ETC		Random Defect Billets	
	Water Path	FBH Depth	No DAC Amp.	Axial 6 dB (in.)	Axial 3 dB (in.)	Cir (deg.)	Cir (in.)	Pulse Width (nsec)	Sqrt 6 dB Pulse Volume	C-Scan Max.	C-Scan Mean	C-Scan Max.	C-Scan Mean
Z1	102 µsec	0.2	31	0.065		0.6	0.050		354	33	18	31	15
		0.55	80	0.04	0.029	0.5	0.039	200	244	23	10	29	9
		0.9	31	0.058		0.8	0.057		357				
Z2	105 µsec	0.9	30	0.092		1	0.072		539				
		1.35	80	0.055	0.037	0.95	0.061	230	383	41	16	54	17
		1.8	29	0.081		1.4	0.078		528				
Z3	105 µsec	1.8	30	0.087		1.05	0.059		442				
		2.25	82	0.056	0.039	1.1	0.053	200	337	42	15	43	16
		2.7	30	0.061		1.85	0.074		417				
Z4	103 µsec	2.7	30	0.097		1.6	0.064		535				
		3.15	58	0.07	0.048	1.8	0.058	240	433	62	26	72	29
		3.6	32	0.071		2.6	0.064		456				
Z5	104 µsec	3.6	36	0.098		2.75	0.067		615				
		4.05	80	0.07	0.056	5.2	0.086	300	589	64	23	71	24
		4.5	34	0.085		9.5	0.083		637				
Z6a	103 µsec	4.5	80	0.115		5.4	0.047		499	50	17	55	20
		5	80					240					
Z6b	96 µsec	5	80			8.4	0.073		475	64	27	70	29
		5.5	80	0.067				240					

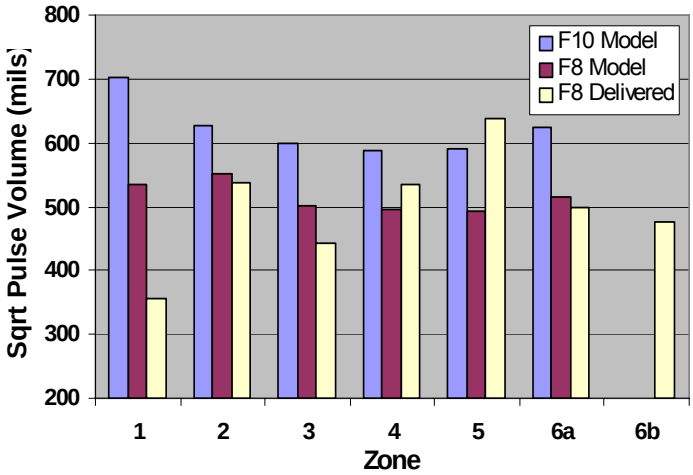

FIGURE 24. COMPARISON OF PULSE VOLUMES AS DETERMINED BY THE ISU MODEL AND THE PULSE VOLUMES OF THE DELIVERED TRANSDUCERS

3.3.5 Explanation for Zones 6a and 6b.

Following numerous attempts without success to achieve adequate signal to noise from the zone 6 transducer on the ETC calibration standard, a second approach was evaluated. This involved dividing zone 6 into two smaller zones, referred to as 6a and 6b. Zone 6a extends from 4.5″ to 5″, and zone 6b extends from 5″ to 5.5″. The goal was to decrease the maximum pulse volume by shortening the inspection zone that resulted in improved SNR. Figure 25 illustrates this principle.

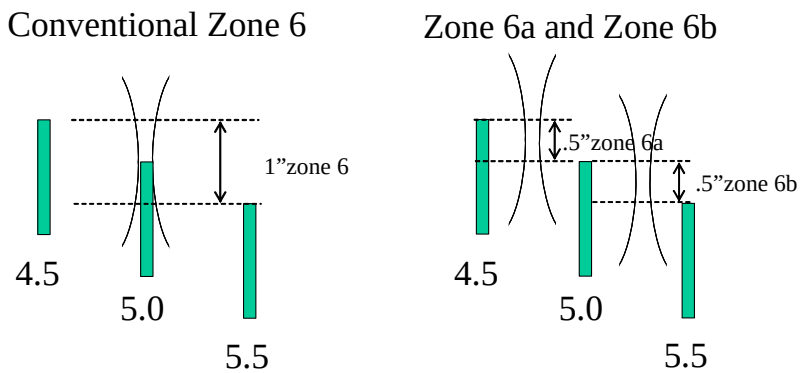

FIGURE 25. ZONE 6 DIVIDED INTO TWO ZONES, 6a AND 6b, TO IMPROVE SNR

To achieve a balance between FBH targets in each zone, the transducer water path was changed slightly. Adjusting a bicyclindrical transducer off its designed operating water path will of course distort the beam near its focus and is not as straight forward as for a spherical transducer on a flat entry surface; however, the water path adjustments are small (< 0.25″). Figure 26 shows the intended effect of shortening the inspection zone to 0.5″.

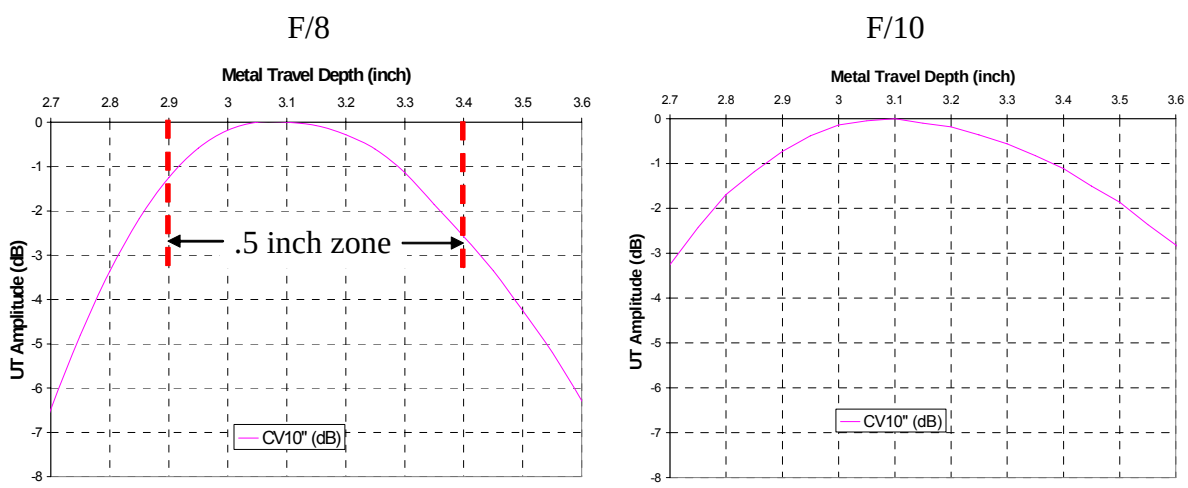

FIGURE 26. COMPARISON OF SENSITIVITY VARIATION THROUGHOUT THE INSPECTION ZONE FOR THE F/10 AND F/8 TRANSDUCER DESIGNS

The sensitivity loss across the zone drops to less than 3 dB, as highlighted by the red dashed lines in figure 26. Based on earlier measurements of the F/10 zone 4 transducer and the respective material noise from the ETC calibration standards, predictions were made of the performance of the F/8 transducers. The pulse volume predicted by the ISU models indicated that the F/8 transducers would be close to meeting the noise criteria but perhaps just short of the goal. Projections from the zone 4 F/10 transducer indicate that a sqrt pv of about 430 or smaller would achieve the 3 dB SNR. The pulse volume was calculated for zones 6a and 6b using the measured beam areas and pulse length.

The results of these measurements produced sqrt pv's of 500 for zone 6a and 476 for zone 6b, as shown in figure 27. Peak noise values were then measured on both the ETC calibration standard and the random defect billet (RDB). Physical complexities of the ETC standard that contains pilot holes and split lines limit the areas to measure noise, so the RDB was used to supplement noise data using a full gate and without artifact signals. These were then plotted against the predicted pulse volumes for the F/8 transducer, as shown in figure 28. The actual performance of the transducer using the smaller zones was in good agreement with earlier predictions of pulse volume capability. Inspection of zone 6a on the RDB and ETC calibration standards indicates that the #1 FBH sensitivity could be achieved if the shorter zone were used. The same evaluation using zone 6b fell short of the 3 dB peak noise requirement. The C-scan in figure 29 shows the results of 6a and 6b zoning and the five FBHs in the ETC standard.

Zone 6a
4.5″ deep hole 3.0-inch water path
Axial dia. = 0.115″
Cir. dia. = 0.047″ (5.4 deg)
Pulse width = 0.24 µsec. @ .244″/µsec = 0.059″
Square root pulse volume = **500**

Zone 6b
5.5″ deep hole 2.8-inch water path
Axial dia. = 0.067″
Cir. dia. = 0.073″ (8.4 deg)
Pulse width = 0.24 µsec. @ .244″/µsec = 0.059″
Square root pulse volume = **476**

FIGURE 27. PULSE VOLUME CALCULATIONS FOR THE ZONE 6 TRANSDUCER

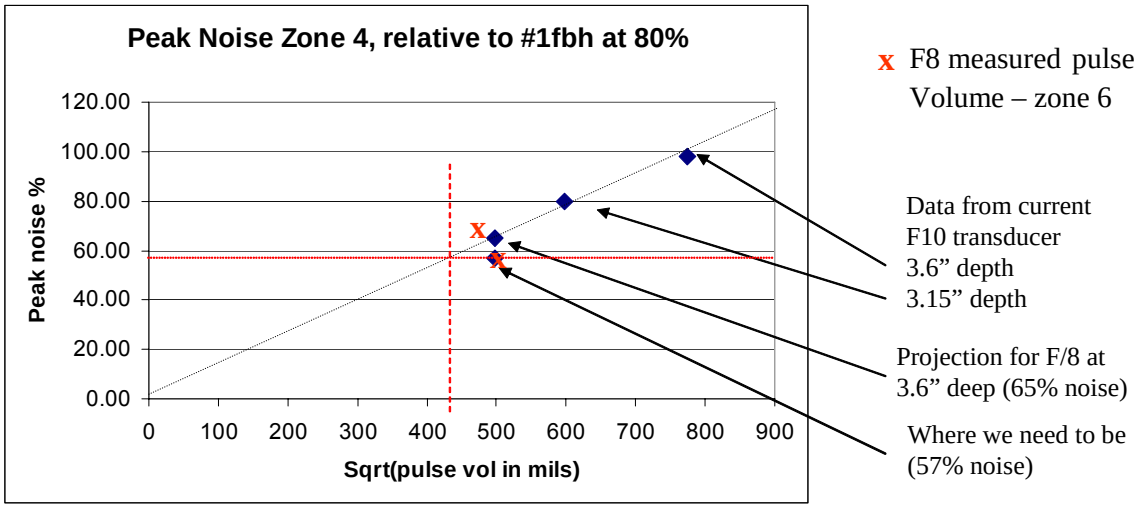

FIGURE 28. PERCENT NOISE PEAK VS THE SQRT PV ORIGINAL CURVE BASED ON F/10 ZONE 4 RESULTS

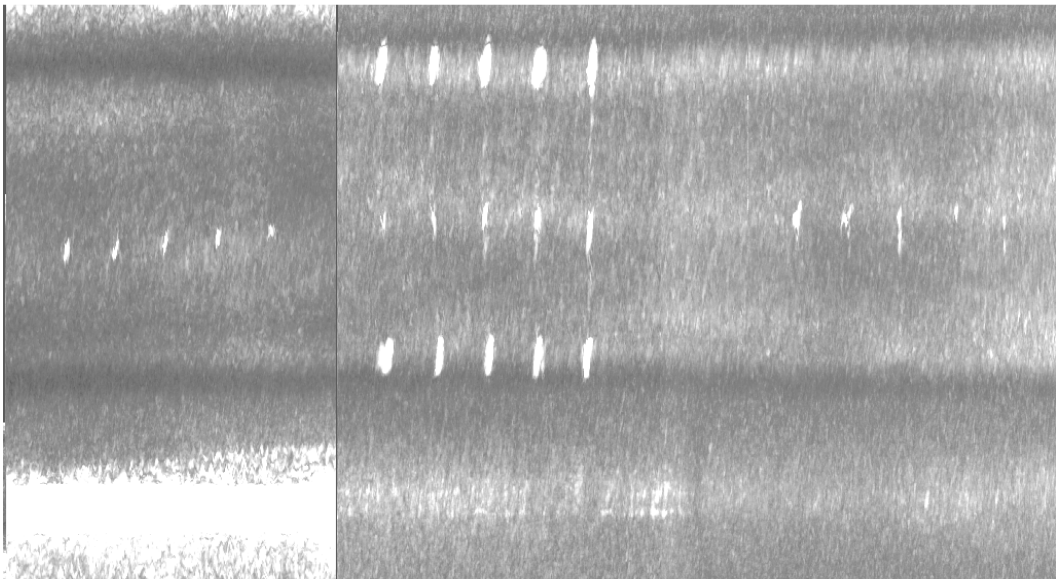

4.5 inches 5.0 inches 5.5 inches

FIGURE 29. C-SCAN OF ETC CALIBRATION STANDARD SHOWING THE FIVE FBHs FOR ZONES 6a AND 6b
(FBH sizes range in size from 0.4 to 0.8 mm (#1 to #2).)

3.3.6 Sensitivity Curves.

Two sensitivity curves were produced, one using the ETC 10″ diameter Ti standards (figure 30) and the second using the RDB (figure 31). There is some difference between the two due to different peak and mean noise values identified in the C-scans.

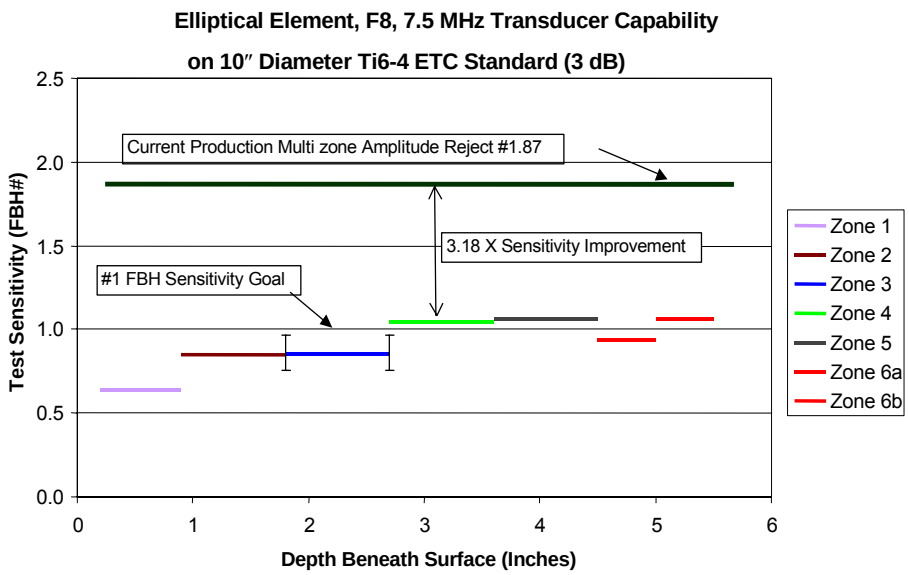

FIGURE 30. SENSITIVITY GRAPH USING THE ETC 10″ DIAMETER CALIBRATION STANDARDS

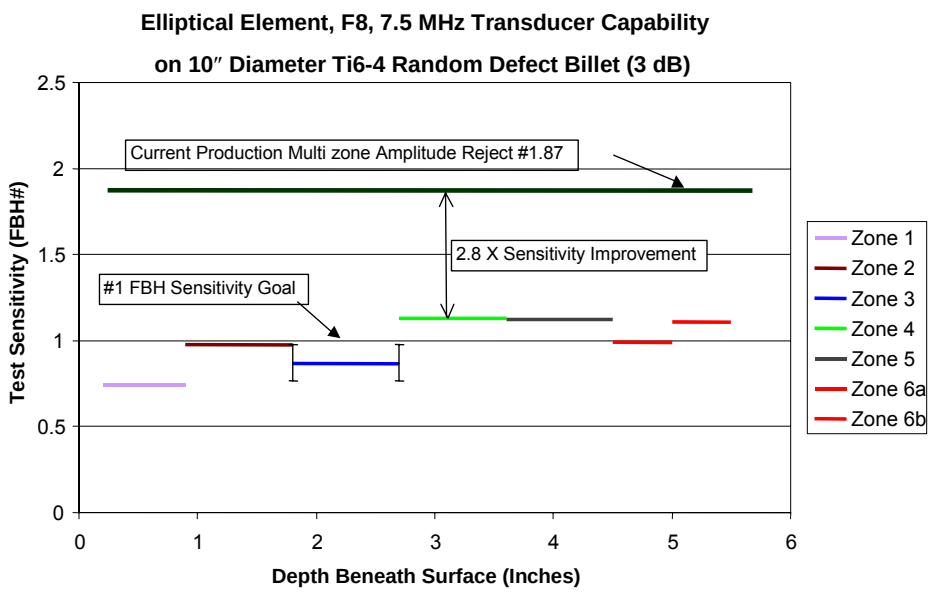

FIGURE 31. SENSITIVITY GRAPH USING THE RDB 10″ DIAMETER SPECIMEN

These sensitivity curves break the capability down on a zone-by-zone basis, and although the intent of the MZ inspection approach was to maintain the same pulse volumes in each zone, this was not always achieved. In addition, the microstructure characteristics from the outside diameter (OD) to the inside diameter (ID) of the billet change. Grain size is typically larger near the ID and will tend to create added noise. Although it might be possible to maintain the same pulse volume at each depth, the peak noise will change due to grain size and microstructure, resulting in a change in sensitivity. An examination of both curves shows the sensitivity decreasing with depth.

The values used in the graphs were obtained by taking the greatest noise value identified in each C-scan and determining the FBH number that would provide a response that is 3 dB greater than the noise. This is given by the expression:

$$FBH\# = [FBH\#_{\text{cal}}]\,[\sqrt{N_{pk+3\,dB} / S_{cal}}] \qquad (1)$$

Where $FBH\#_{cal}$ is the size of the calibration target in terms of FBH number, $N_{pk+3\,dB}$ is the peak noise value in the C-scan image at calibration plus 3 dB, and S_{cal} is the amplitude of the calibration signal (usually 80%). As an example, figure 32 shows the C-scan image for the first three zones. The maximum noise values were taken from these images for the ETC sensitivity graphs. As part of the study, the RDB was inspected at the sensitivity level achieved with the #1 FBH calibration. Zone 2 from the RDB is presented in figure 33.

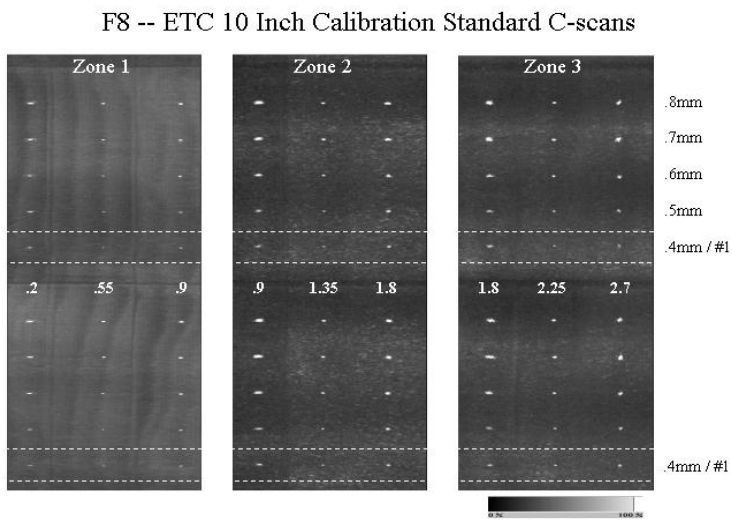

FIGURE 32. #1 FBH INSPECTION SENSITIVITY FOR ZONES 1-3 ON THE ETC CALIBRATION STANDARD

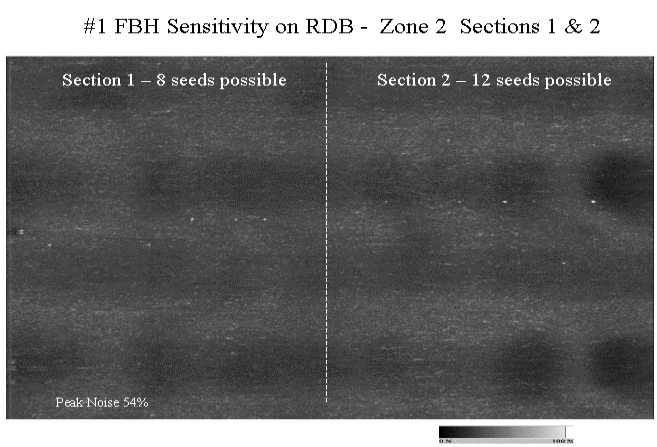

FIGURE 33. ZONE 2 #1 FBH SENSITIVITY ON THE RDB

3.4 SUMMARY OF LABORATORY EVALUATION FOR 10″ DIAMETER BILLET.

Current inspection of 10″ diameter Ti billet was to a #2 FBH sensitivity using six 5-MHz F/10 transducers and six zones. Moving to a #1 FBH or 3.5 times increase in sensitivity using fixed-focus transducers was demonstrated in a laboratory environment but would have some challenging obstacles ahead for practical implementation.

Maintaining transducer to billet orientation would be one critical factor. In conducting the laboratory evaluation, it became apparent that the response from the calibration targets was very sensitive to transducer alignment and water path. This is particularly true for deep zones 5 and 6. Very small changes in either transducer angle or water path produced large differences in target response. The surface finish of the billet would also have to be monitored more closely.

Achieving a sqrt pv of 450, particularly with the large element transducers, also presents difficulties for the transducer manufacturer. Although it might be possible to occasionally make a transducer that meets the specifications, consistently being able to reproduce and reliably manufacture sufficient quantities for industrial use is at issue.

The companion attenuation compensation study discussed below reveals the role this variable plays in achieving uniform inspection. Based on the location of the calibration targets, there will be an impact on inspection sensitivity. Efforts to produce more uniform billet microstructure and reduce this variability would lead to improved Ti billet inspection. Much of the difficulty in inspecting the Ti billet is the variation in the attenuation and noise associated with the billet conversion practices. Reducing this variation would simplify the UT inspection as would any effort to refine the grains near the billet center.

Figures 30 and 31 show that #1 FBH sensitivity at the 3 dB level was accomplished for three of the six zones. In the three deepest zones, the # 1 FBH target was missed by 10% or a sensitivity of #1.1 FBH. Based on the peak noise that was observed in both the ETC calibration standards and the RDB, a pulse volume of 202,500 $mils^3$ or a sqrt pv of 450 should achieve the required sensitivity for all zones. It was not clear whether transducer suppliers could successfully or consistently deliver on the required transducer specifications for the larger elements. One alternative approach would be to divide the length of zone 6 into two zones, as was done in this study. This would have the undesirable result of increasing either the number of transducers or the scan time. This would also necessitate the creation of new zoning schemes and redesign of the calibration standards from 1″ to 0.75″ or 0.5″ zones. Another alternative would be the development of phased array inspection practices.

3.5 ATTENUATION COMPENSATION PROCEDURES.

One goal of the ETC Phase II program was to critically examine existing methods for attenuation compensation during UT inspections of Ti alloy billets and, if necessary, to recommend improvements. This section documents those research efforts and resulting recommendations. As illustrated in figure 34, the billets to be inspected have a cylindrical geometry, with diameters ranging from 5″ to 14″ and lengths up to 20 ft. The inspection procedure is depicted schematically in figure 35. Two inspection methods are commonly used, CV and MZ,

respectively [17 and 18]. In the former, one cylindrically focused transducer with the focus located just below the billet surface is generally used to cover the depth range from the outer surface to just beyond the billet center, and a depth varying gain (or DAC) is applied so that the echo amplitudes from identical targets were independent of depth. For larger-diameter billets, a CV inspection may employ a second transducer focused deeper in the billet. For MZ inspections, a larger number of transducers were used, ranging from 4 to 7, depending on billet diameter, with each transducer designed to focus the sound beam within a given depth zone; the gain setting for each transducer is independently set, and DAC is generally not used within a given depth zone. Details of this method are provided in appendix B. For either method, the inspection procedure makes use of a calibration standard of the same diameter that contains FBH reflectors of a fixed size located at a series of depths (one FBH per depth). The MZ calibration standards containing the FBHs generally have a full-round geometry, with the holes themselves drilled into internal cavities. For CV inspections, the FBH reflectors are usually contained in chord blocks. For both types of inspections, an unaltered full-round section of the calibration billet material was available for back-wall signal acquisition. In this report, extensive use was made of a 6″ diameter, Ti-6-4 MZ calibration standard as illustrated in figure 36.

FIGURE 34. BILLETS AWAITING INSPECTION

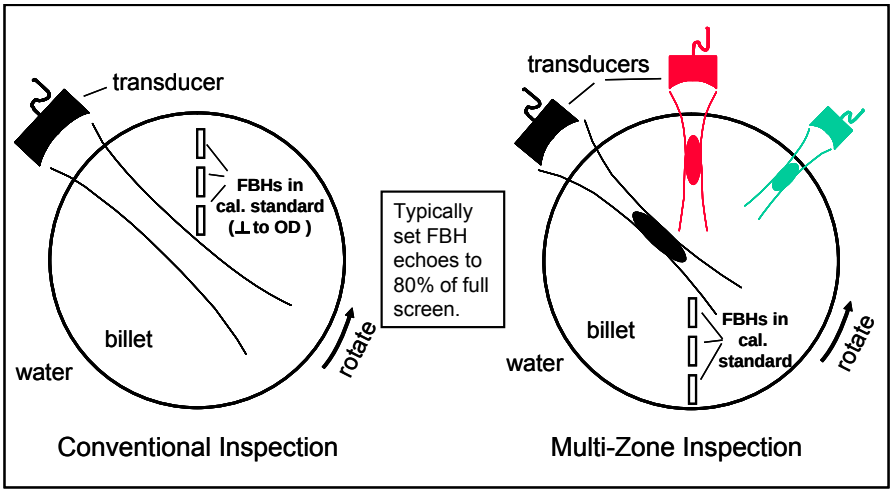

FIGURE 35. CONVENTIONAL AND MZ BILLET INSPECTIONS USE CALIBRATION STANDARDS CONTAINING FBH REFLECTORS

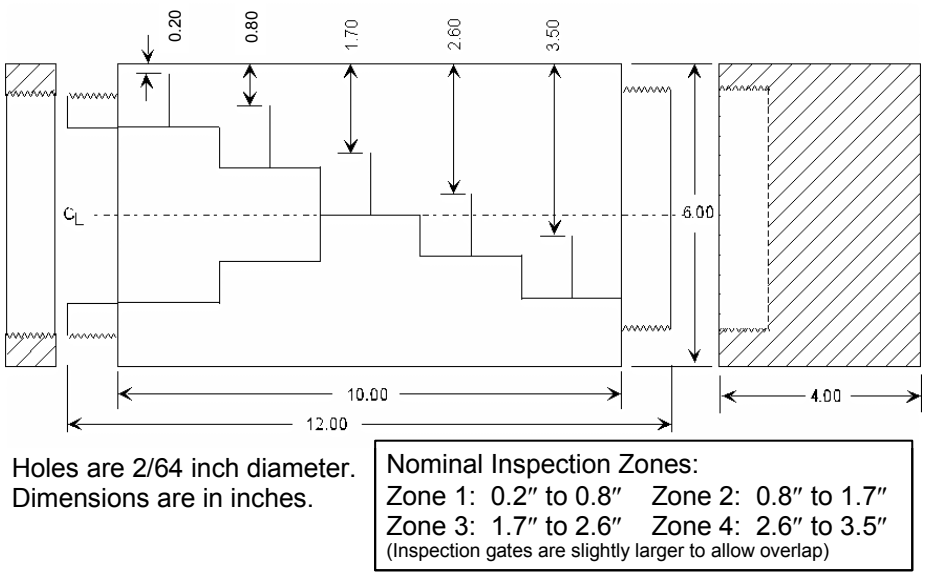

FIGURE 36. CALIBRATION STANDARD FOR AN MZ INSPECTION OF A 6″ DIAMETER BILLET

The basic inspection task is illustrated in figure 37. The calibration standard was first examined using the set of transducers. For either a MZ or CV billet inspection, the measurement system amplification (gain) was adjusted so that FBHs in the calibration standard produce sonic echoes of a specified amplitude, typically 80% FSH. It was desired that similarly sized FBH reflectors, if present in the billet to be inspected, would produce echoes of similar amplitude. In particular, as depicted in figure 37, if a reflector at depth z in the calibration standard produces an amplitude of 80% FSH, then similar reflectors in the test billet at the same depth but arbitrary axial and circumferential positions should all produce amplitudes greater than or near 80% FSH.

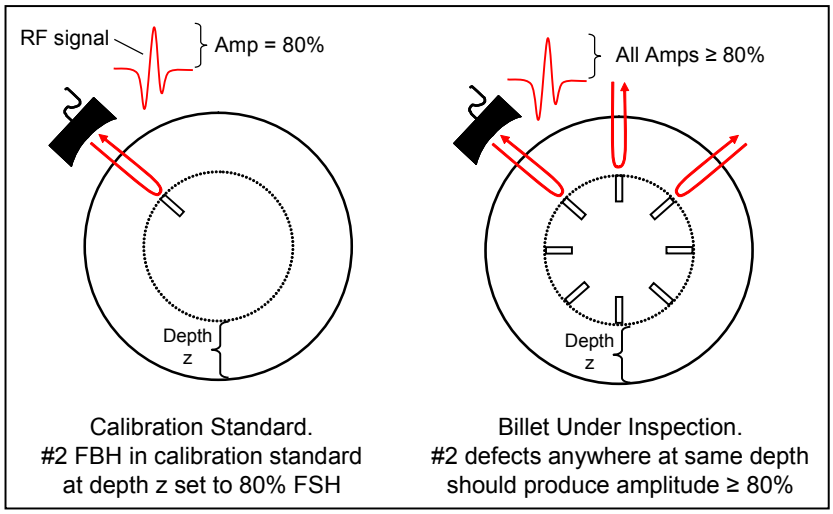

FIGURE 37. ULTRASONIC BILLET INSPECTION (IDEALIZED AT DEPTH Z)

The amplitudes of echoes seen in such pulse/echo inspections were determined in part by the UT attenuation of the billet material. Because the attenuations of the calibration standard and test billet may be different, the gain settings required for the test billet inspection may be different than those set using the calibration standard. The adjustment of inspection gain to account for attenuation differences is referred to as compensation.

In current practice, attenuation compensation values (when used) were generally determined by comparing the average amplitudes of back-wall echoes seen in the calibration standard and the test billet, respectively. This is shown in figure 38, with the back-wall data for both specimens gathered prior to the final inspection using the same transducer and same gain.

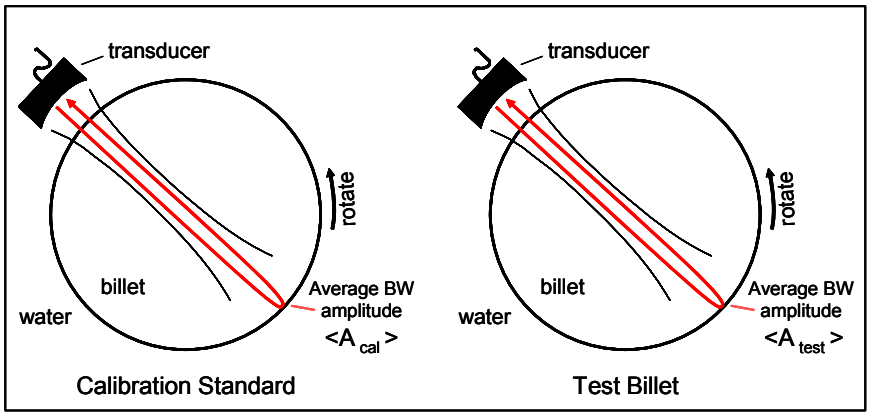

FIGURE 38. THE STANDARD METHOD FOR ATTENUATION COMPENSATION MAKES USE OF AVERAGE BACK-WALL AMPLITUDES

For MZ inspections, back-wall amplitudes were generally measured using the deep-zone transducer, which was focused near the billet center. For CV inspections employing more than one transducer, the deeper-zone probe was used to acquire back-wall echoes. The calibration standard typically contained a full-round segment without interior cavities or FBHs; this was used for back-wall echo acquisition. Since the test billet was also free of cavities, any representative portion of its length could be used for back-wall echo acquisition.

Let $<A_{cal}>$ and $<A_{test}>$ denote the average back-wall amplitudes seen in C-scans of the calibration standard and test billet, respectively. For the subsequent inspection of the test billet, the gain adjustment used to compensate for attenuation at depth z is generally taken to be

$$\textit{Gain adjustment (in dB) at depth } z = \left[20 \log_{10} \frac{< A_{cal} >}{< A_{test} >} \right] \frac{z}{D} \qquad (2)$$

where D is the billet diameter. For example, if the billet diameter is 10″ and the back-wall amplitude difference is 15 dB, the compensation value would be 1.5 dB/inch of depth in the test billet. The additional gain applied during the inspection of the test billet, as calculated using equation 2, would range from 0 dB at the OD to 7.5 dB at the billet center. Such compensations based on average back-wall amplitudes will be referred to as the standard method. The standard method, and several variations, will be discussed in section 3.6.6.

3.6 BANDING PHENOMENA AND UT PROPERTY VARIATIONS.

Before proceeding with the critique of the standard method, it is useful to recall several facts concerning Ti alloy billets. A typical billet begins as a cast ingot, which is worked by thermal/mechanical processing to reduce its cross-sectional area and to achieve a cylindrical geometry. The final microstructure can be quite complex, possessing identifiable features on several length scales ranging from centimeters for the large-scale macrostructure to microns or tens of microns for the individual metal grains, which are often clustered into colonies of intermediate size. Typical microstructures of Ti alloy billets were documented in the ETC Phase I report.

Although the billet shape has cylindrical symmetry, the billet microstructure and the associated UT properties were not cylindrically symmetric. This was because asymmetries were introduced by the mechanical working process, which usually involves rotating the billet through large angles between hammer strikes. The so-called banding patterns commonly seen in C-scan images of backscattered grain noise and back-wall amplitude were clear evidence of the deviation of billet microstructures from cylindrical symmetry. Typical examples of banding patterns are shown in figure 39. These images resulted from the inspection of a length of 14″ diameter Ti-6-4 billet intended for use in the fabrication of a calibration standard. The billet was inspected using a deep-zone MZ probe designed to focus near the billet center. The left-hand image in figure 39 shows backscattered grain noise amplitudes seen using an inspection gate extending from 6.4″-7.5″ deep in the billet. The right-hand image shows amplitudes of back-wall echoes when the inspection gate is narrowed and centered on the back wall. Both images have the same registration, meaning that corresponding points in the two images have the same axial and circumferential position on the billet surface. One sees that bands of low back-wall amplitude (high attenuation) match with bands of low backscattered noise, a common phenomenon for Ti alloy billets [19]. The banding patterns seen in figure 39 have an approximate four-fold rotational symmetry in the hoop direction. Four-fold or two-fold banding symmetries are often seen for Ti alloy billets. Note that throughout this report, C-scan images such as those in figure 39 always display rectified gated-peak amplitude versus scan position.

As might be expected on the basis of figure 39, different regions of a given Ti alloy billet can have significantly different UT properties. This was documented during Phase I of the ETC program [19]. One case study, using a 6″ diameter Ti-6-4 billet, is summarized in figure 40. Panel (a) displays the backscattered grain noise pattern that was seen when an axial-cylindrical scan of the specimen was made using a 5-MHz bicylindrically focused MZ transducer, and the resulting gated-peak noise amplitude was displayed as a function of scan position [19]. Prominent bands of high and low backscattered noise amplitude are seen. As shown in panel (b), two sets of rectangular coupons were cut from the billet for property measurements. Each set of three coupons was cut along a radius of the billet, one set from a region having a low-noise amplitude near the OD (at 1″ depth), and the other set having a high-noise amplitude near the OD. For sonic beam propagation in the radial direction, figure 40(c) shows measured longitudinal wave speeds, attenuations, and figure of merit (FOM) values for each coupon. The FOM is a measure of the noise generation capacity of the microstructure that (ideally) is a property of the microstructure alone and independent of the details of the measurement

procedure [19, 20, and 21]. One sees that the UT properties vary significantly throughout the billet, and that the differences are greatest near the OD.

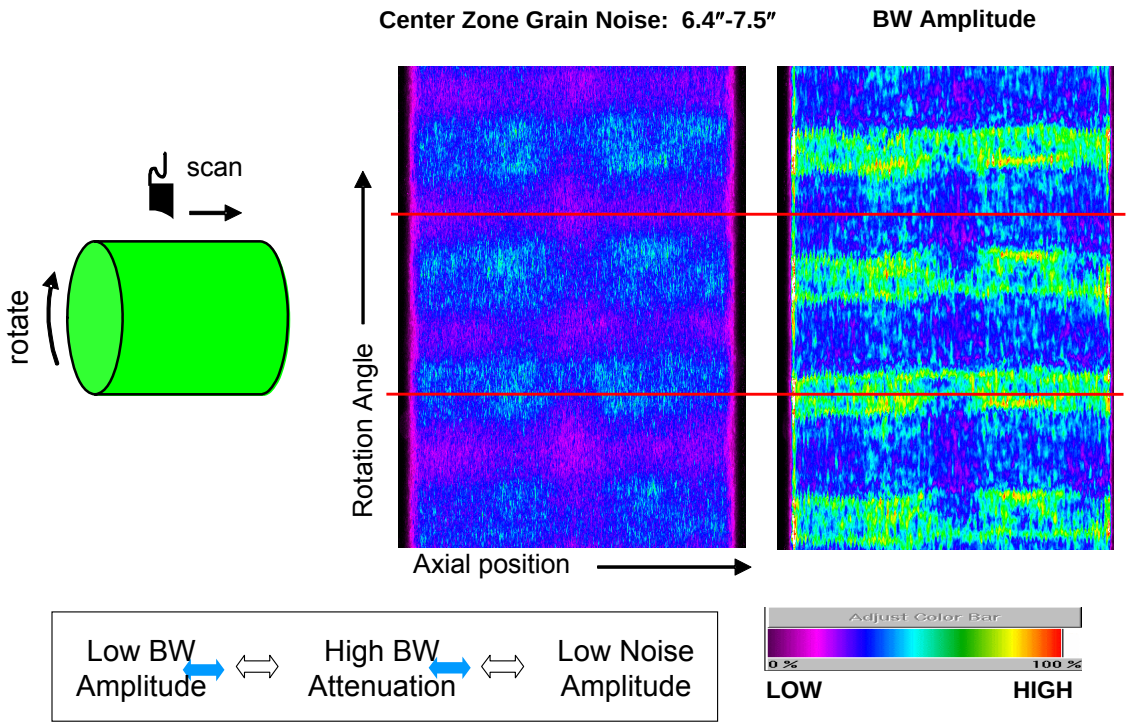

FIGURE 39. BANDING PATTERNS SEEN DURING THE INSPECTION OF A 14″ DIAMETER Ti-6-4 BILLET SPECIMEN

It is also important to note in figure 40 that changes in velocity and attenuation values are well correlated with changes in backscattered noise capacity. For Ti alloy billets, one generally finds an inverse relationship between backscattered noise and effective attenuation. This is shown in figure 41, which displays the results of measurements performed on the same set of six billet coupons shown in figure 40(b). For each coupon, measurements of UT attenuation and backscattered grain noise capacity were made in the radial, hoop, and axial directions [22]. The results at one frequency of interest (15 MHz) are displayed in figure 41, and the trend line through the data indicates that low values of grain noise are correlated with high values of attenuation. This inverse relationship is believed to be due to large-scale macrograins present in the cast Ti ingot, which become elongated in the axial direction during the working of the billet [22]. Knowledge of FOM variations is required to draw conclusions about attenuation levels from noise banding patterns.

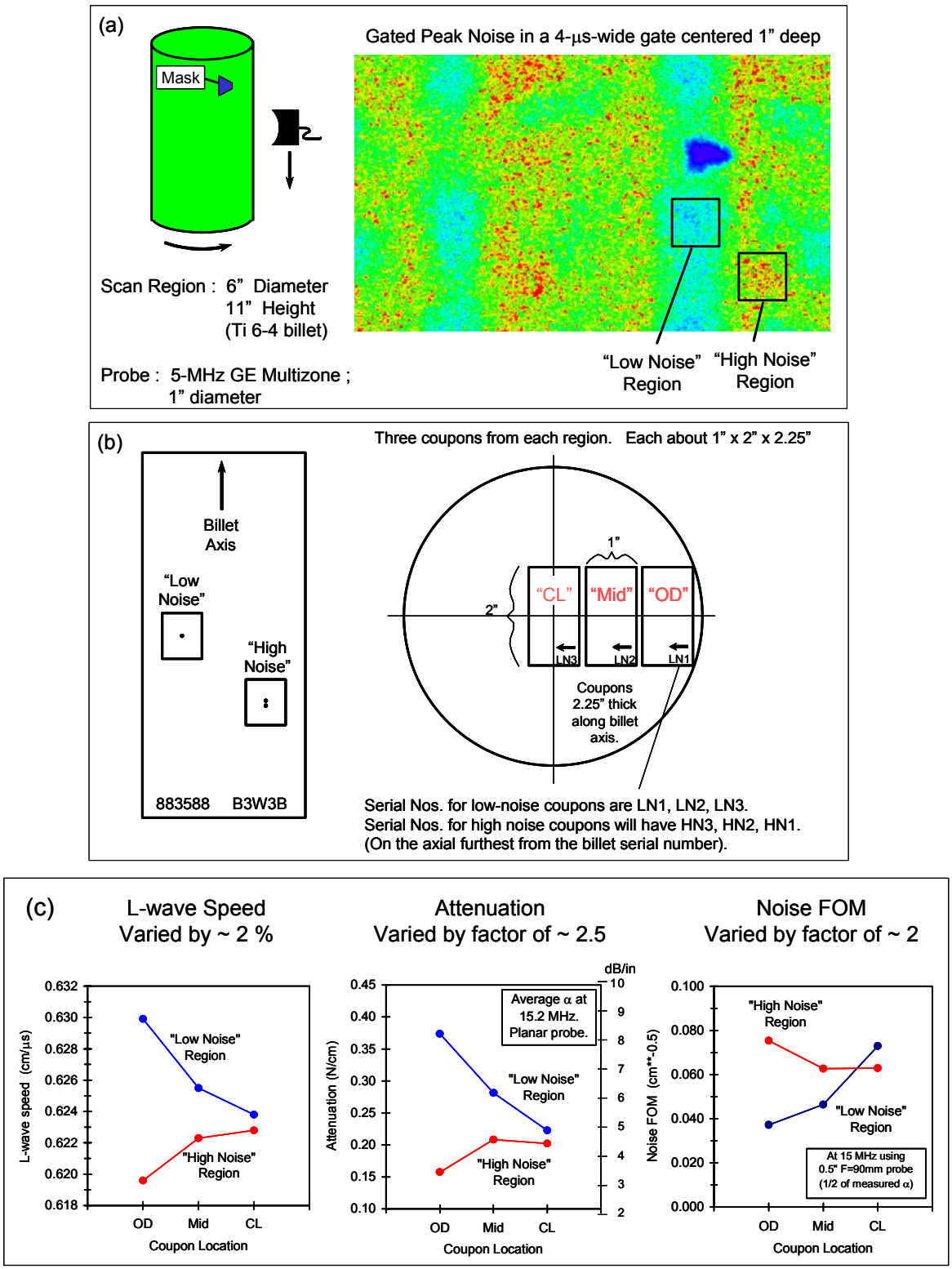

FIGURE 40. NOISE BANDING AND UT PROPERTY VARIATIONS SEEN IN A 6″ DIAMETER Ti-6-4 BILLET (a) NOISE BANDING PATTERN, (b) RECTANGULAR COUPON LOCATIONS, AND (c) UT PROPERTY VARIATIONS FOR RADIAL SOUND PROPAGATION

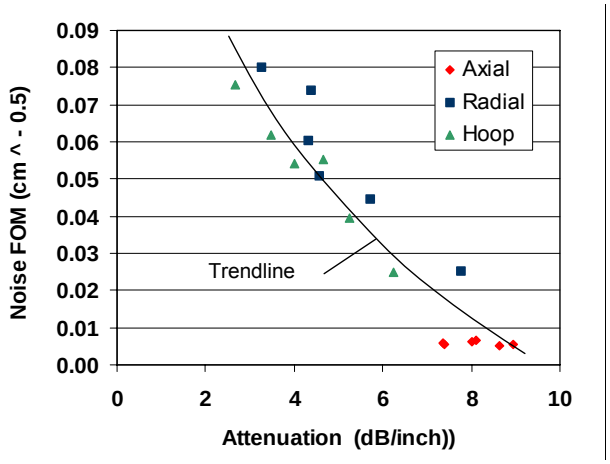

FIGURE 41. CORRELATION BETWEEN BACKSCATTERED NOISE FOM AND ATTENUATION FOR SIX COUPONS FROM A 6″ DIAMETER Ti-6-4 BILLET

In summary, the banding patterns visible in figures 39 and 40 resulted from variations in the billet microstructure, which led, in turn, to variations in ultrasonic velocity, attenuation, and grain noise capacity. Because the UT properties vary with position, one might suspect that identical reflectors located at different positions in a billet (but at the same depth) would give rise to different signal amplitudes upon inspection. This is indeed the case, and it has important implications for defect detection.

3.6.1 Attenuation Compensation Research Plan.

To investigate billet attenuation differences and to critique the standard compensation procedure, the ETC team developed a plan in accordance with that envisioned in the original ETC Phase II proposal:

> "The current attenuation compensation technique will be evaluated by applying it to several billet segments, then drilling a number of flat-bottomed or side-drilled holes into the sections, and comparing the measured amplitudes of those holes to those expected from the attenuation analysis. Improvements will focus on selection of a transducer which will minimize the effects of beam distortion (on the back-wall echo)…" [23]

As noted in section 3.5, the general goal of an attenuation compensation procedure was to determine how FBH amplitudes (or defect echo amplitudes) would vary with depth in a billet under inspection and to make appropriate gain adjustments to approximately equalize those amplitudes. The most direct way of doing this would be to place FBH or other reflectors at various depths into one portion of each billet under inspection (say near a butt end) and then use the echo amplitudes to set the inspection gains. Such a direct approach was impractical due to its expense. Instead, efforts to develop an alternative compensation procedure, which uses readily available echoes, such as those reflected by the billet back wall, were pursued. As demonstrated in figures 39 and 40, back-wall amplitudes in Ti alloy billets will vary with axial and circumferential position. These variations arise from two sources. First, large-scale systematic variations of UT properties with position, like those documented in figure 40(c), will naturally

lead to large-scale systematic variations in back-wall amplitude (banding). Second, on a smaller scale, say within a region of low back-wall amplitude, finer variations can be seen that are sometimes referred to as speckle. The speckle pattern results from distortions of the amplitude and phase profiles of the beam by the metal microstructure. Examples of such distortions are shown in references 24 and 25. Even if the microstructure is uniform on a large scale, the precise patterns of grain sizes and orientations will be different at different locations. These differences led to differing beam distortion effects at different positions and, hence, to different reflected amplitudes from identical defects or surfaces.

The effect of beam distortion on surface echoes can be very different from the effect on FBH echoes [26]. This is because surface echoes are quite sensitive to phase-front distortions (particularly when the beam is not focused on the reflecting surface), while FBH echoes are more sensitive to amplitude distortions. Consider focusing the beam first on an FBH at some depth and then on a back-wall surface at the same depth. In the limit where the diameter of the focused beam approaches the diameter of the FBH reflector, average attenuation values deduced from FBH and surface echoes would be identical if the modest back-wall curvature is neglected. Although this limit will not be reached in typical MZ billet inspections, moving toward it (by focusing the beam near the back wall) will likely improve the accuracy of compensation measurements. Also note that past experiments have shown that microstructure-induced signal fluctuations are smallest when the beam is focused on or near the reflector [27]. This is true for both FBH and surface echoes. Thus, the speckle component of the wide variations often seen in billet back-wall amplitude C-scans would likely be reduced if one were to focus on or near the back wall. These past findings motivated the investigation of different focusing schemes when obtaining back-wall amplitudes for attenuation compensation.

The detailed research plan eventually adopted by the ETC team had the following nine major steps.

1. Assemble a summary of the current billet compensation procedure, as practiced during MZ and CV inspections.

2. Locate a billet section that has a significantly lower average back-wall amplitude than the billet calibration standard of the same diameter. This test billet should also show appreciable back-wall banding.

3. Machine ≥10 FBH targets through the outside surface of the test billet, with the drilled holes only a few tenths of an inch deep, i.e., close to the back wall. Holes should be drilled into regions of high and low back-wall amplitude.

4. Make C-scan recordings of the back-wall echo and the FBH echo amplitudes and evaluate the results to see whether the amplitude variations for the two types of echoes are related. Investigate at least two focusing schemes: sound beam focused near the billet center and sound beam focused near the billet back wall.

5. In another portion of the test billet, drill other FBH targets (with long pilot holes) to be located near the billet center, i.e., near the deepest depth considered during a typical

inspection of a billet of that diameter. At least ten such holes should be drilled, distributed among regions of high and low back-wall amplitude.

6. Use the back-wall amplitude patterns of the test billet and calibration standard to calculate global attenuation compensation values. (In global compensation procedures, the same attenuation adjustment in dB/inch units is applied uniformly at all axial and circumferential positions.) In addition to the standard method based on comparing average back-wall amplitudes, consider alternative approaches using other attributes of the back-wall amplitude patterns.

7. Inspect the interior of the test billet (containing ≥10 FBH targets) in the usual manner, but with a fixed inspection gain. Postprocess the resulting C-scan data to determine the adjusted amplitudes of the FBH echoes that would result for each of the global compensation schemes considered in step 6. Compare the resulting FBH amplitudes to the ideal target level (80% FSH).

8. Investigate the use of local attenuation compensation procedures in which the gain adjustment (in dB/inch units) is different at different axial and circumferential positions. Use the variations seen in back-wall or backscattered grain noise C-scan images as the basis for the local adjustments. Apply each local compensation procedure considered to the FBH C-scan data acquired in step 7. Compare the adjusted FBH amplitudes to the 80% FSH target level.

9. Summarize the findings and make recommendations for improving inspections.

3.6.2 Current Billet Compensation Procedures.

Attenuation compensation during billet inspection, when performed, generally uses the standard method described earlier. Average back-wall amplitudes for the unaltered full-round segment of the calibration standard and a representative portion of the test billet are compared, and equation 1 was used to compute the gain adjustment. For either a CV or MZ inspection, the deepest focus transducer being used in the inspection of the billet interior was also used for back-wall echo acquisition. When gathering back-wall amplitude data from the test billet, the entire length of the test billet was not generally scanned. Rather, as illustrated in figure 42, it is common for local rotational/axial C-scans to be performed at several widely spaced locations along the billet, and the average back-wall amplitude is then determined from this collection of strip C-scans. If the average back-wall amplitude of the test billet is appreciably below that of the calibration standard, then gain adjustments computed using equation 1 are positive, and the amplification level for the inspection of the test billet must be boosted above that needed to adjust FBH amplitudes in the calibration standard to 80% FSH. Such positive gain boosts are generally implemented. If, on the other hand, the average back-wall amplitude of the test billet is above that of the calibration standard, a negative adjustment would be computed from equation 1. Such negative adjustments are usually not implemented, making the billet inspection somewhat more conservative than it would otherwise be.

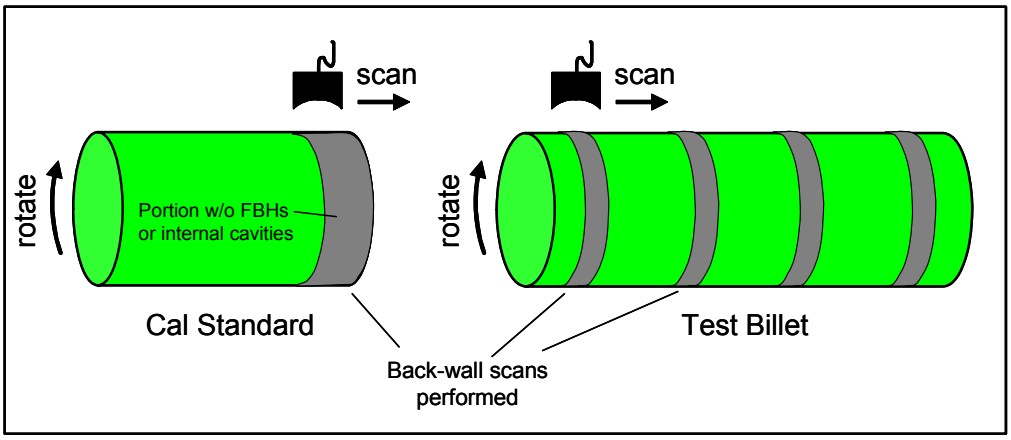

FIGURE 42. AREAS TYPICALLY SCANNED TO ACQUIRE BACK-WALL AMPLITUDE DATA FOR ATTENUATION COMPENSATION

3.6.3 Test Billet and Transducer Selection.

Steps 2-8 of the research plan outlined in section 3.6.1 could have been carried out using a test billet of any diameter for which a suitable calibration standard was available. One constraint was the need to perform measurements in which the sonic beam would be focused near the back wall. For any given billet diameter, it is possible to design an elliptical element, bicylindrically focused transducer that would focus the beam near the billet back wall. For 10″ diameter billet, such a transducer was in fact designed at GE Corporate Research and Development (CRD) using beam models developed at ISU. The 5-MHz probe was specifically designed to focus near the back wall (i.e., at 20″ depth) with a focal spot size near that achieved within each zone of a typical MZ inspection of 10″ diameter Ti alloy billet.

It was realized that existing MZ transducers could be used for back-wall focusing if the billet diameter was smaller. For example, the deep-zone (zone 7) transducer for 13″ diameter billet was designed to focus 6.5″ deep (in 13″ diameter billet) when operated at a water path of 3.5″. By increasing the water path to 6.6″, a beam spot of suitable area could be formed at the back wall of the 6″ diameter billet. Figure 43 shows the model calculations for two transducers, comparing the beam spot sizes at the back wall of the 6″ diameter billet. The results in the upper portion of the figure were used to select the 6.6″ water path subsequently used for the zone 7 transducer.

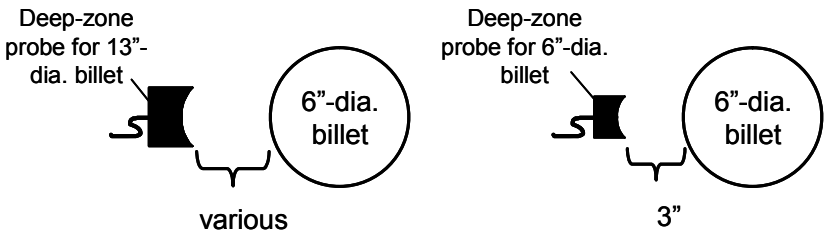

Beam Evaluations

Use of Zone 7 transducer of 13"Dia billet for 6"Dia billet backwall attenuation studies									
WP (in)	Focal Depth (in)	3dB DOF (in)	Z_left (in)	Z_right (in)	AMP @focus	6dB BD_ax @focus (in)	6dB BD_circ @focus (in)	6dB BD_ax @6"BW (in)	6dB BD_circ @6"BW (in)
7	4.4	2.35	3.25	5.6	0.0013023	0.165	0.293215309	0.17	0.408407038
6.8	4.55	2.1	3.55	5.65	0.0013805	0.155	0.292168112	0.17	0.387463087
6.7	4.5	2.05	3.6	5.65	0.0013806	0.15	0.287979322	0.17	0.387463087
6.6	4.5	2	3.65	5.65	0.0013617	0.15	0.282743334	0.165	0.397935063
6.5	4.5	1.95	3.7	5.65	0.0013212	0.145	0.282743334	0.165	0.397935063
6.4	4.65	1.9	3.75	5.65	0.0012554	0.14	0.299498495	0.165	0.408407038
6	4.75	1.85	3.9	5.75	0.0008331	0.13	0.378736441	0.165	0.555014693
5.5	4.95	1.85	4.15	6	0.0003454	0.13	1.041437947	0.15	1.235693089
Use of Zone 4 transducer of 6"Dia billet (w/ 3"WP) for 6"Dia billet backwall attenuation studies								0.595	0.303687285

Current method

Zone 7 transducer of 13" diameter billet
- Designed to focus at 6.5" depth in 13" billet
- with 3.5" water path
- Element diameter 2.35" (circular)
- Frequency 5MHz
- GFL(circumferential)=10.20", GFL(axial)=30.59"

(Lens velocity 0.1134 in/microsec;
Lens radii 14.87" ax, 4.96" circ)

Zone 4 transducer of 6" diameter billet
- Designed to focus at 3" depth in 6" billet
- with 3" water path
- Element diameter 1.75" (circular)
- Frequency 5MHz
- GFL(circumferential)=6.05", GFL(axial)=16.55"

FIGURE 43. MODEL CALCULATIONS OF BEAM PROPERTIES FOR TWO 5-MHz MZ TRANSDUCERS
(The rightmost two columns list beam diameters (-6 dB points for pressure squared) in the axial and circumferential directions at the back wall of 6″ diameter Ti-6-4 billet.)

Several lengths of 6″ diameter Ti-6-4 billet stock were located that had the desired features: large back-wall amplitude variations and a significantly larger mean attenuation than an available calibration standard of the same diameter. The material was part of the CBS heat that was purchased by the ETC during Phase I [7]. It was decided that this material would serve well for the attenuation compensation study. For measurements in which the beam was to be focused near the billet center, an MZ probe designed for the deep zone of 6″ diameter billet was used. For measurements in which the sonic beam was to be focused near the back wall, an MZ transducer designed for the deep zone of the 13″ diameter billet was used and operated at a 6.6″ water path. The characteristics of these two MZ probes are summarized in the bottom portion of figure 43. It was decided that these primary measurements would be supplemented by data acquired using a phased array transducer, operated to simulate a fixed-focus probe whose beam was focused either near the billet center or back wall. The 5-MHz phased array transducer in question was supplied to Honeywell (Phoenix) by R/D Tech and is described in figure 44. Although designed for 8″ diameter billet, the focusing scheme for the array could be altered to, approximately, focus the beam at the desired depths in 6″ diameter billet.

- 5 MHz 114 elements segmented elliptic probe designed for a nominal 8″ diameter billet and pre-focused at 4.5″. The layout of the elements is shown below.

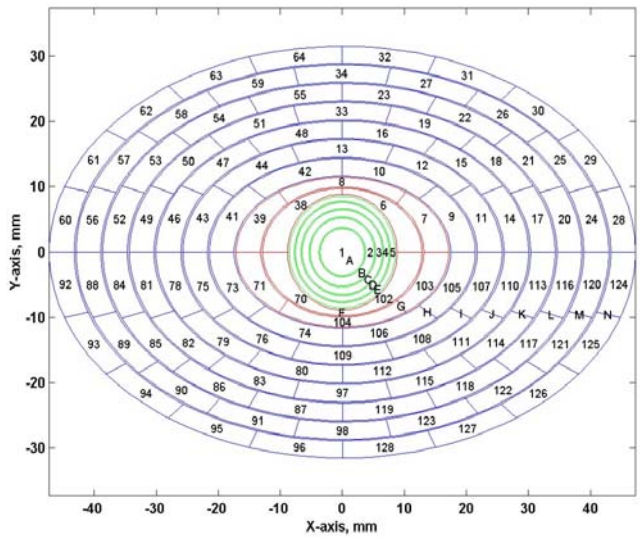

Standard Focusing

Standard focusing is a focusing method for which we apply the same group of delays to the elements in transmission and in reception to focus at a certain point. The result is a narrow beam at the focusing depth and a divergent beam at deeper depths.

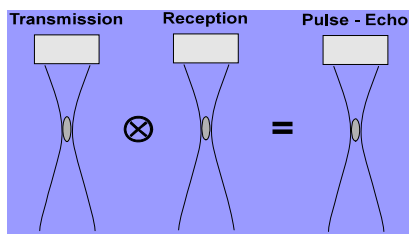

FIGURE 44. FIVE-MHz PHASED ARRAY TRANSDUCER, OPERATED IN STANDARD FOCUSING MODE TO SIMULATE INSPECTIONS WITH FIXED-FOCUS PROBES

3.6.4 Back-Wall Variations and Near-OD FBH Placements.

A 40″ long section of 6″ diameter CBS billet, denoted B2W1A, was selected for use in the initial investigations. Back-wall C-scans of this section acquired using the two MZ transducers are shown in figure 45. One sees that the overall pattern of high- and low-amplitude banding is similar for both transducers, indicating that the pattern results primarily from billet microstructure variations. The black rectangle in figure 45 locates a 15″ long subsection, which was subsequently cut from the larger piece and into which near-OD FBHs were later drilled. For all of the transducers used in the study, significant variations in back-wall amplitude were seen in the test billet. This is illustrated in figure 46, which shows an annotated back-wall C-scan of the 15″ length subsection acquired using one of the MZ transducers. Average and peak back-wall amplitudes are shown for four regions. The mean amplitudes of these regions differ by as much as a factor of 46/19=2.4 (or 7.7 dB), indicating mean attenuation differences as high as 1.1 dB/inch of billet depth.

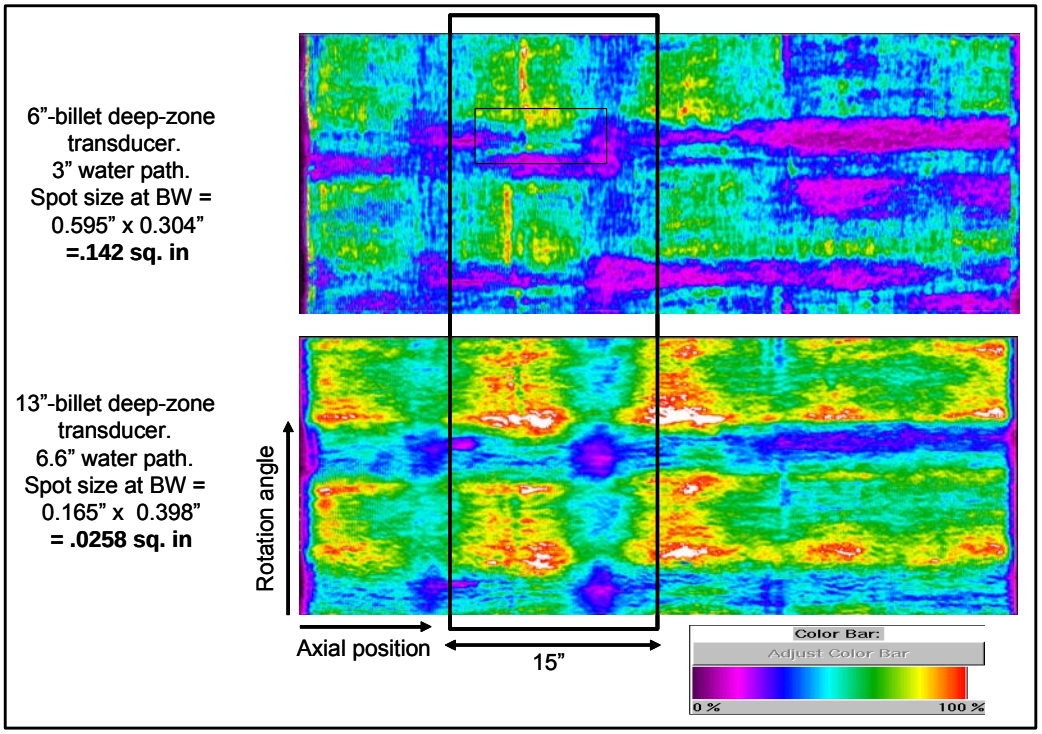

FIGURE 45. BACK-WALL C-SCAN IMAGES OF 6″ DIAMETER CBS BILLET (B2W1A) ACQUIRED USING TWO MZ TRANSDUCERS

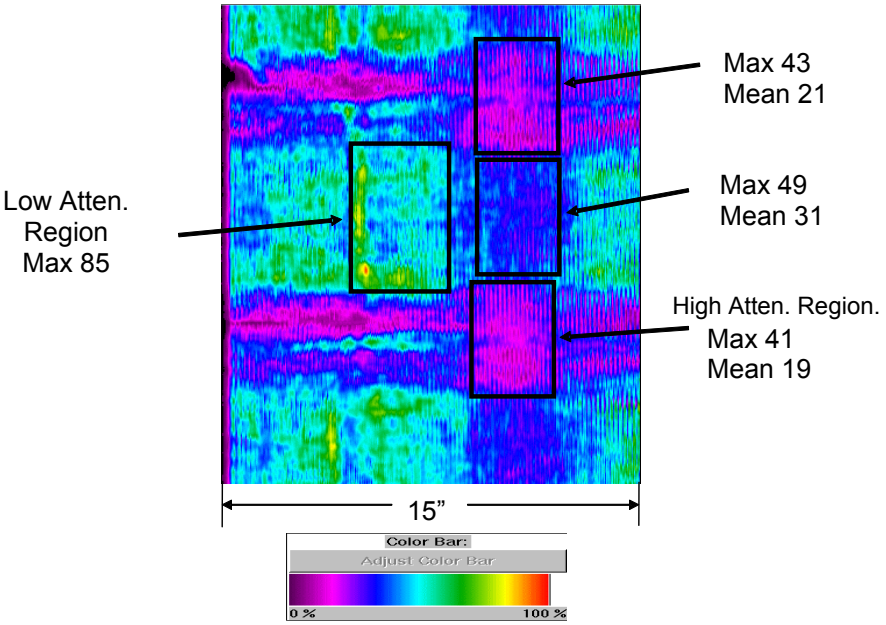

FIGURE 46. BACK-WALL AMPLITUDE STATISTICS FOR FOUR REGIONS OF THE 15″ LONG BILLET SECTION
(C-scan image acquired using the 6″ diameter billet, zone 4 transducer focused near the billet center.)

Figure 47 shows two schemes that were considered for drilling shallow FBHs into the back wall (OD) of the test billet. In this figure, the underlying back-wall C-scans were acquired using the phased array transducer with the beam focused near the back wall. Again, the pattern of high- and low-amplitude banding is similar to that shown in figure 46, although the color scheme and angular registration are different. The drilling scheme shown in the left-hand panel of figure 47 locates holes primarily in high- or low-amplitude regions and is expected to produce the maximum variation of FBH amplitudes if those amplitudes mirror the back-wall variations. The scheme shown in the right-hand panel uses a regular array of FBHs and would likely be more useful for a rigorous, statistical probability of detection (PoD) analysis. The regular array covers approximately 90º of circumferential arc and 6″ of axial length. Given the limited budget available for drilling holes, it was decided that achieving maximum variation in FBH amplitudes was of primary importance, and that this could be most effectively accomplished using the first drilling scheme.

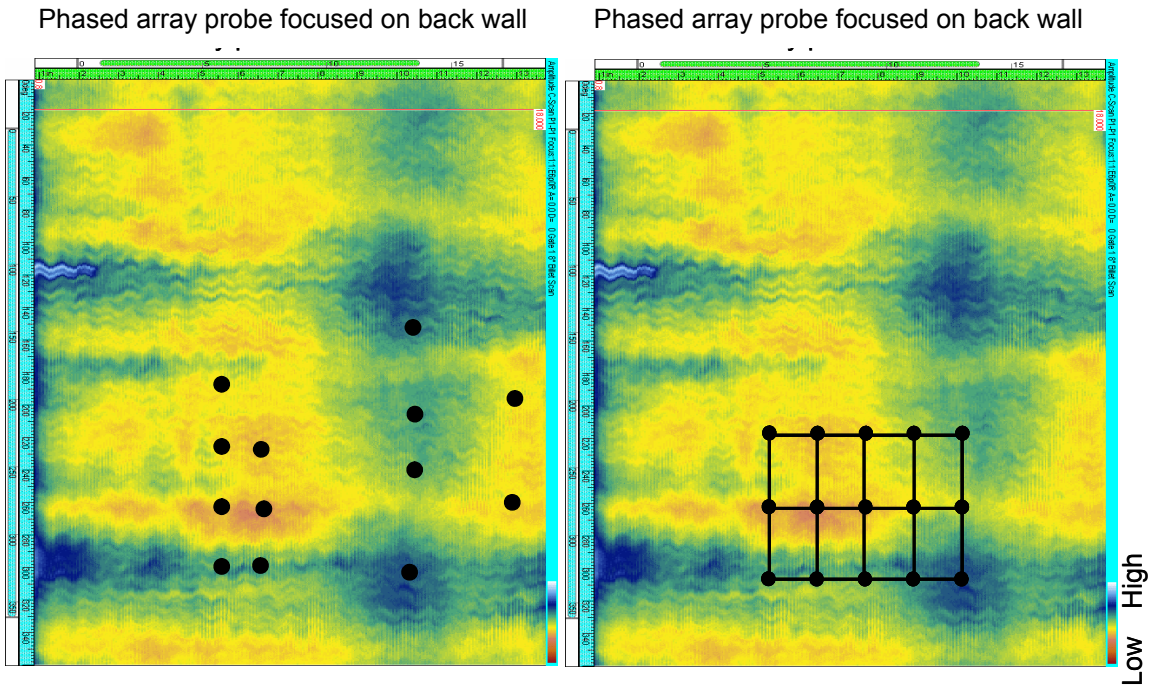

FIGURE 47. POSSIBLE SCHEMES FOR POSITIONING NEAR-OD FBHs RELATIVE TO THE BACK-WALL AMPLITUDE PATTERN

In accordance with the desire to compare back-wall echoes with those of nearby FBHs, certain conditions were imposed on the holes. The holes needed to be shallow, but drilled deeply enough to be easily resolved from the back-wall echo for all transducers used. The hole diameter needed to be as small as possible (#2 FBHs are used in the associated calibration standard), but large enough to be easily visible with all transducers. Finally, the holes needed to be drilled in such a manner that the inspecting beam did not have to pass through one hole on its way to a target hole on the opposite side. This latter requirement is most easily met by confining all holes to a region with less than 180° of circumferential arc.

A few FBHs having different diameters and depths were drilled near one end of the 15″ long test billet to examine resolvability issues. From C-scans of these holes, it was decided that #4 FBHs of 0.3″ depth would serve. Thirteen such holes were then drilled at the approximate locations shown in the left-hand panel of figure 47. For easy reference, the holes were numbered 1-13 from top-to-bottom and left-to-right as they appear in C-scan images. Figure 48 shows the finished test specimen and a C-scan image (gated at the FBH depth) of the specimen with the individual FBH images numbered.

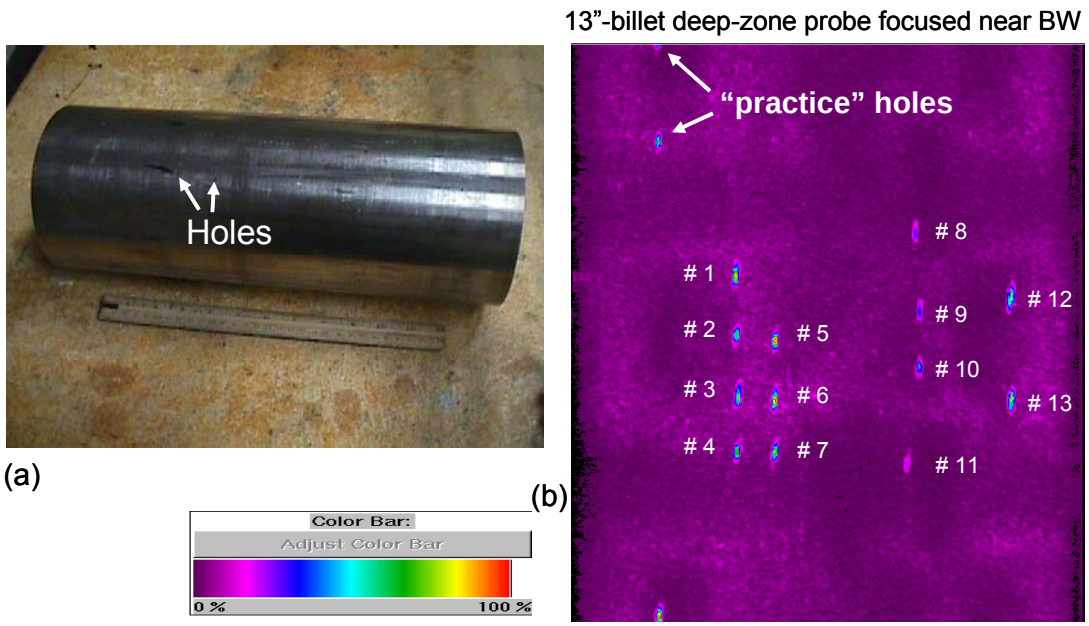

FIGURE 48. (a) 6″ DIAMETER Ti-6-4 TEST SPECIMEN CONTAINING NEAR-OD #4 FBHs AND (b) C-SCAN IMAGE SHOWING THE FBH ENUMERATION SCHEME

3.6.5 Correlation Between Back-Wall and Near-OD FBH Amplitude Variations.

The 15″ long section of 6″ diameter Ti-6-4 billet with its 13 shallow #4 FBHs was inspected using several focusing schemes having different beam sizes near the back wall. The objective was to determine the severity of the back wall and FBH fluctuations and to study the correlation between the two types of amplitudes at nearby locations. Six measurement trials were conducted using 5-MHz focused transducers:

1. Using an MZ probe designed for the deep zone of 6″ diameter billet (beam focused near center of test billet).

2. Using an MZ probe designed for the deep zone of 13″ diameter billet with the water path modified to approximately focus the beam at the back wall of test billet.

3. Using the 114-element phased array probe to approximately focus the beam near the center of the test billet.

4. Using the phased array probe to approximately focus the beam at the back wall of the test billet.

5. Like 3 above, but with an alternate phased array focusing algorithm.

6. Like 4 above, but with an alternate phased array focusing algorithm.

The alternate focusing algorithm for the phased array measurements was designed to better correct for small fabrication errors in the positioning of array elements along the transducer surface. For each trial, beam widths in the axial and circumferential direction at the -6 dB level were estimated from the FBH images.

The results of the six measurement trials are shown in figures 49 through 54. C-scan images resulting from the trials are shown in the upper panels of the figures. The upper left panel of each figure shows the rectified peak amplitude of the back-wall echo as a function of position for a full-round inspection of the 15″ long billet section. The upper right panel displays images of the FBHs, obtained by performing a second scan at increased gain, using a time gate that enclosed the FBH echoes but excluded the back-wall echoes. In all cases, the horizontal coordinate is parallel to the billet axis and the vertical coordinate is proportional to the billet rotation angle. Annotations on the upper panels list the peak FBH amplitudes and the average back-wall amplitudes in small regions centered about each FBH location. One expects the FBH to shadow the back wall immediately below it, thus altering the local back-wall amplitude. However, the back-wall echoes were very strong compared to the FBH echoes, and no significant effects of shadowing were seen. Thus, local back-wall amplitudes were measured in a simple fashion without regard to FBH shadows. In all cases, the listed amplitudes are the percentage of FSH. One notices in each figure that the back-wall and FBH amplitudes vary considerably, and that large (small) FBH amplitudes are usually associated with large (small) back-wall amplitudes at similar positions. The correlation between FBH and back-wall amplitudes is further illustrated in the lower panels of figures 49 through 54. For each of the four inspections, the absolute amplitudes of the back-wall and FBH signals have been adjusted to have a mean value of 50% FSH for the suite of FBH targets. These rescaled amplitudes are shown in the lower left panel, with the principal FBH targets numbered 1-13, as described in section 3.6.4. The lower right panels display correlation plots of the rescaled FBH amplitudes versus the rescaled back-wall amplitudes. If there were perfect correlation between the two types of echo amplitudes, the plotted points would all fall along a straight line passing through the origin and having a slope of unity. In each case, a best-fit line through the origin is shown, and its slope is seen to be close to the ideal value of 1 in each case.

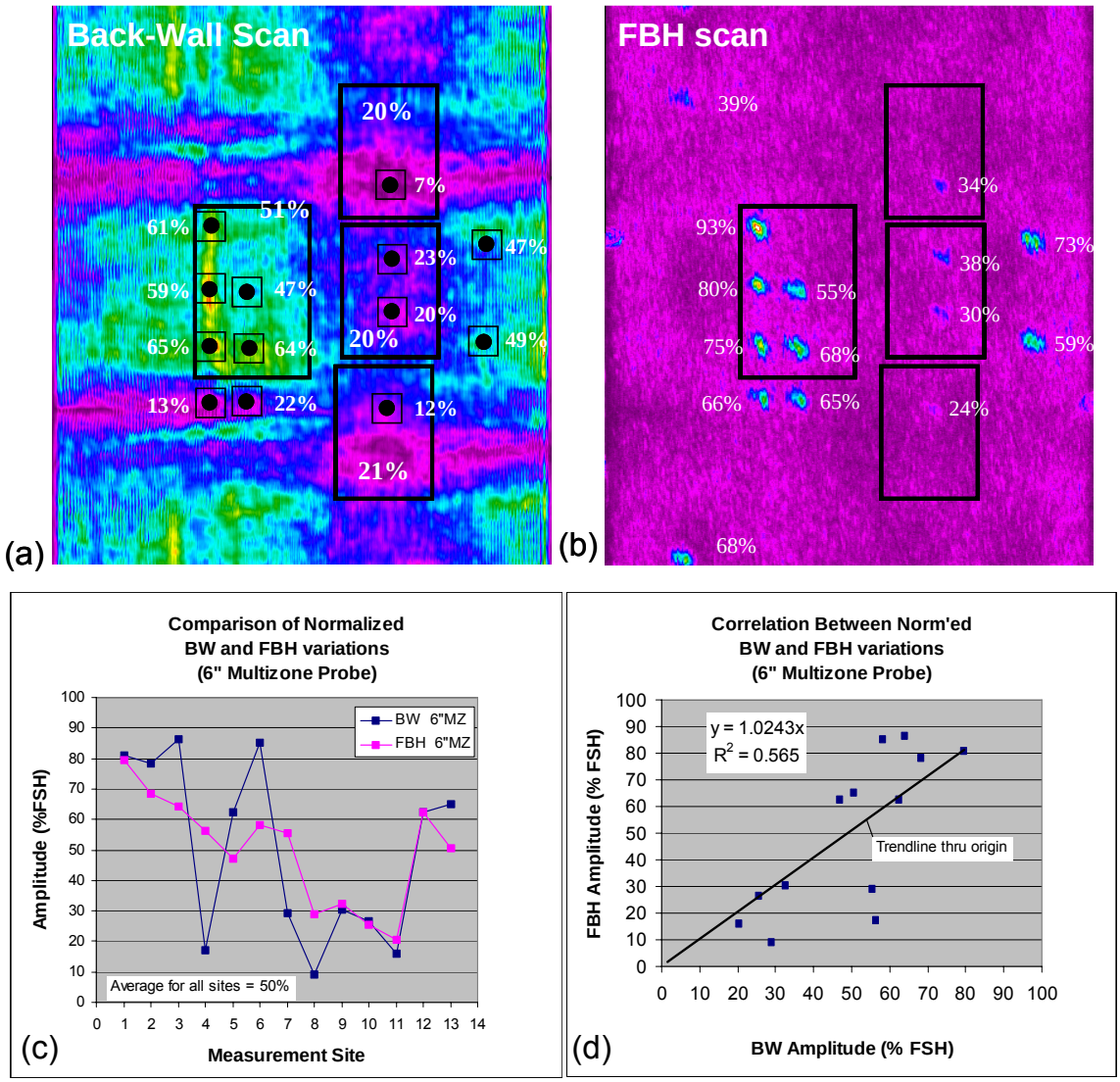

FIGURE 49. MEASUREMENTS ON A Ti-6-4 BILLET SEGMENT USING A 5-MHz, 6″ MZ PROBE FOCUSED NEAR THE BILLET CENTER (a) C-SCAN OF BACK-WALL AMPLITUDE, (b) C-SCAN GATED ON SHALLOW #4 FBH TARGETS DRILLED INTO THE BILLET OD, (c) SCALED BACK-WALL AND FBH AMPLITUDES, AND (d) CORRELATION BETWEEN BACK-WALL AND FBH AMPLITUDES
(Beam diameters (-6 dB) near the back wall are approximately 250 mils by 610 mils (axial by hoop).)

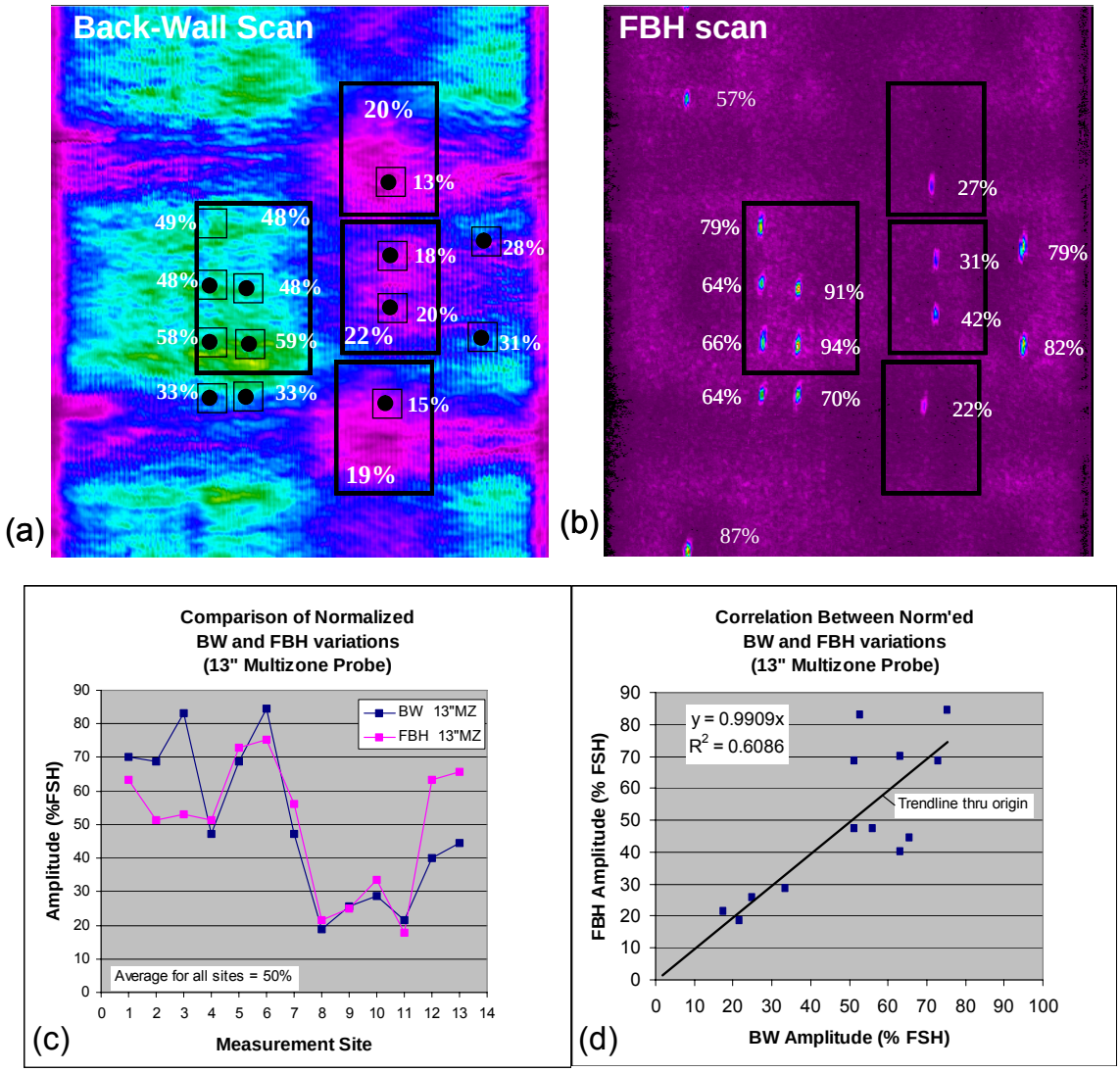

FIGURE 50. MEASUREMENTS ON A Ti-6-4 BILLET SEGMENT USING A 5-MHz, 13″ MZ PROBE FOCUSED NEAR THE BILLET BACK WALL
(Beam diameters (-6 dB) near the back wall are approximately 150 by 540 mils (axial by hoop).)

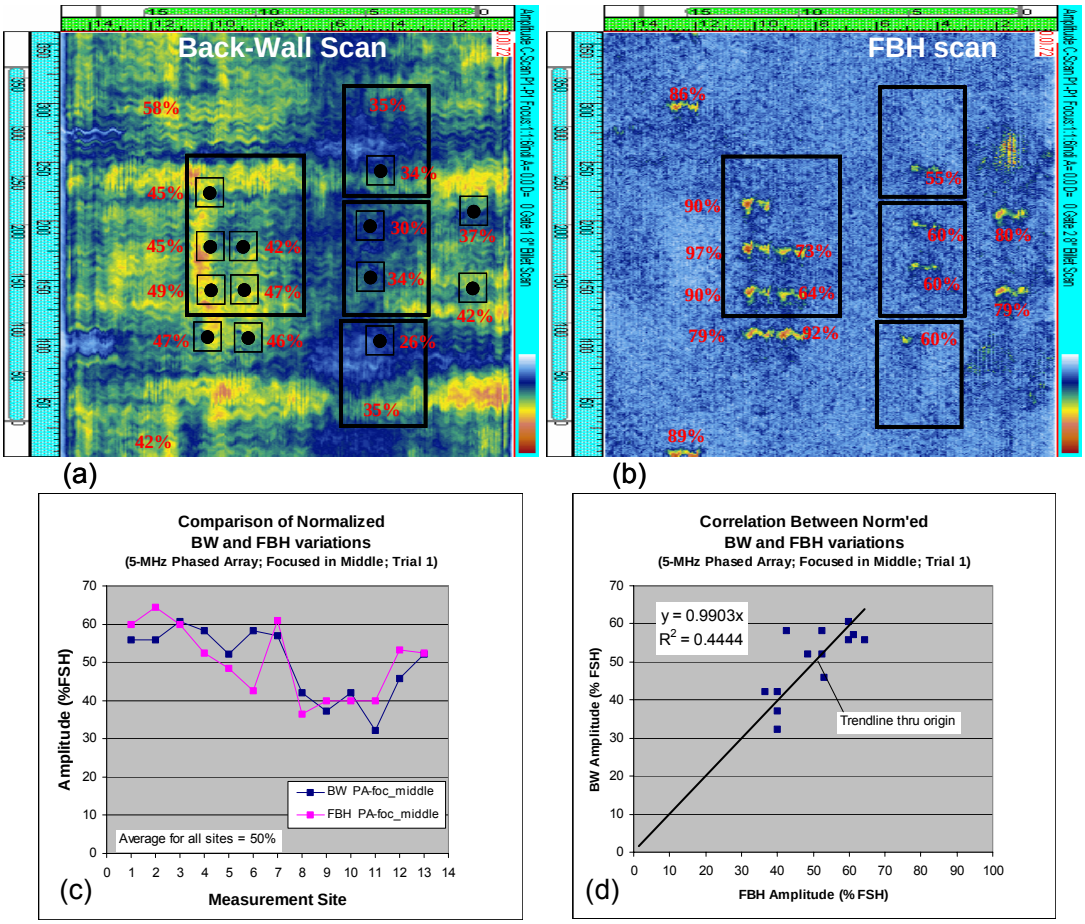

FIGURE 51. MEASUREMENTS ON A Ti-6-4 BILLET SEGMENT USING A 5-MHz PHASED ARRAY TRANSDUCER FOCUSED NEAR THE BILLET CENTER
(Beam diameters (-6 dB) near the back wall are approximately 400 by 600 mils (axial by hoop).)

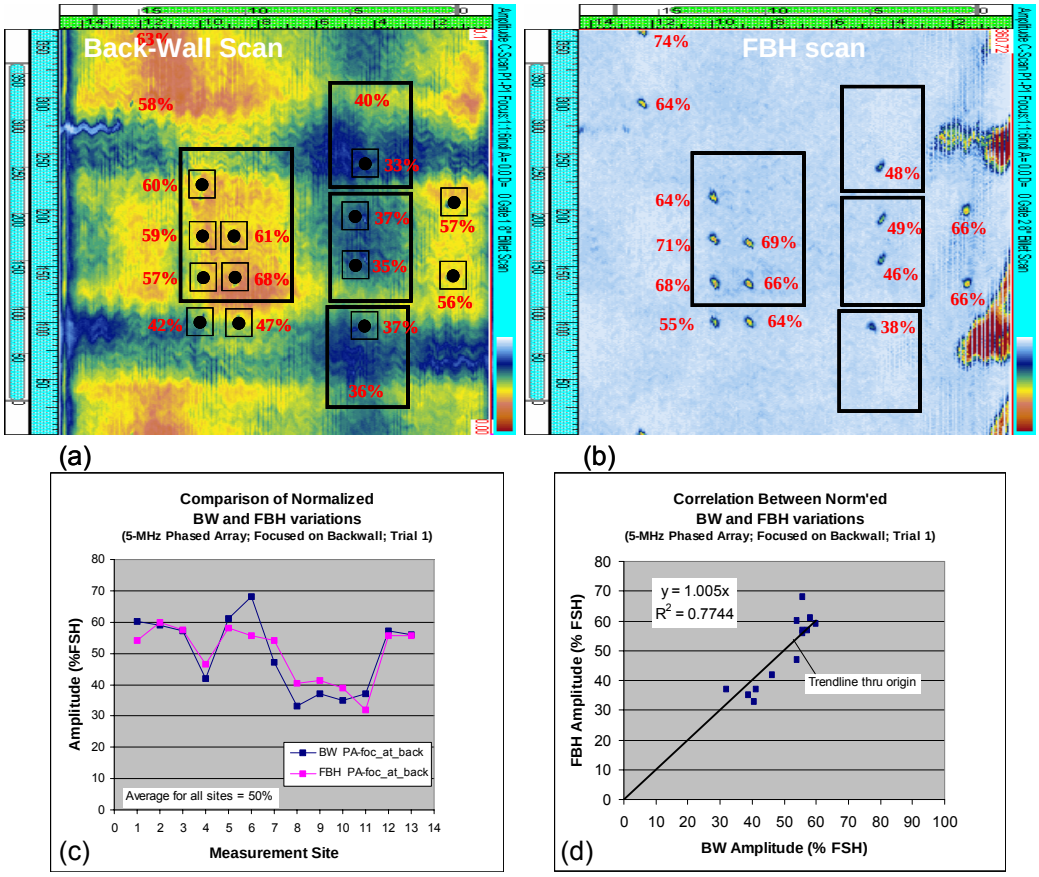

FIGURE 52. MEASUREMENTS ON A Ti-6-4 BILLET SEGMENT USING A 5-MHz PHASED ARRAY TRANSDUCER FOCUSED NEAR THE BILLET BACK WALL (Beam diameters (-6 dB) near the back wall are approximately 200 by 380 mils (axial by hoop).)

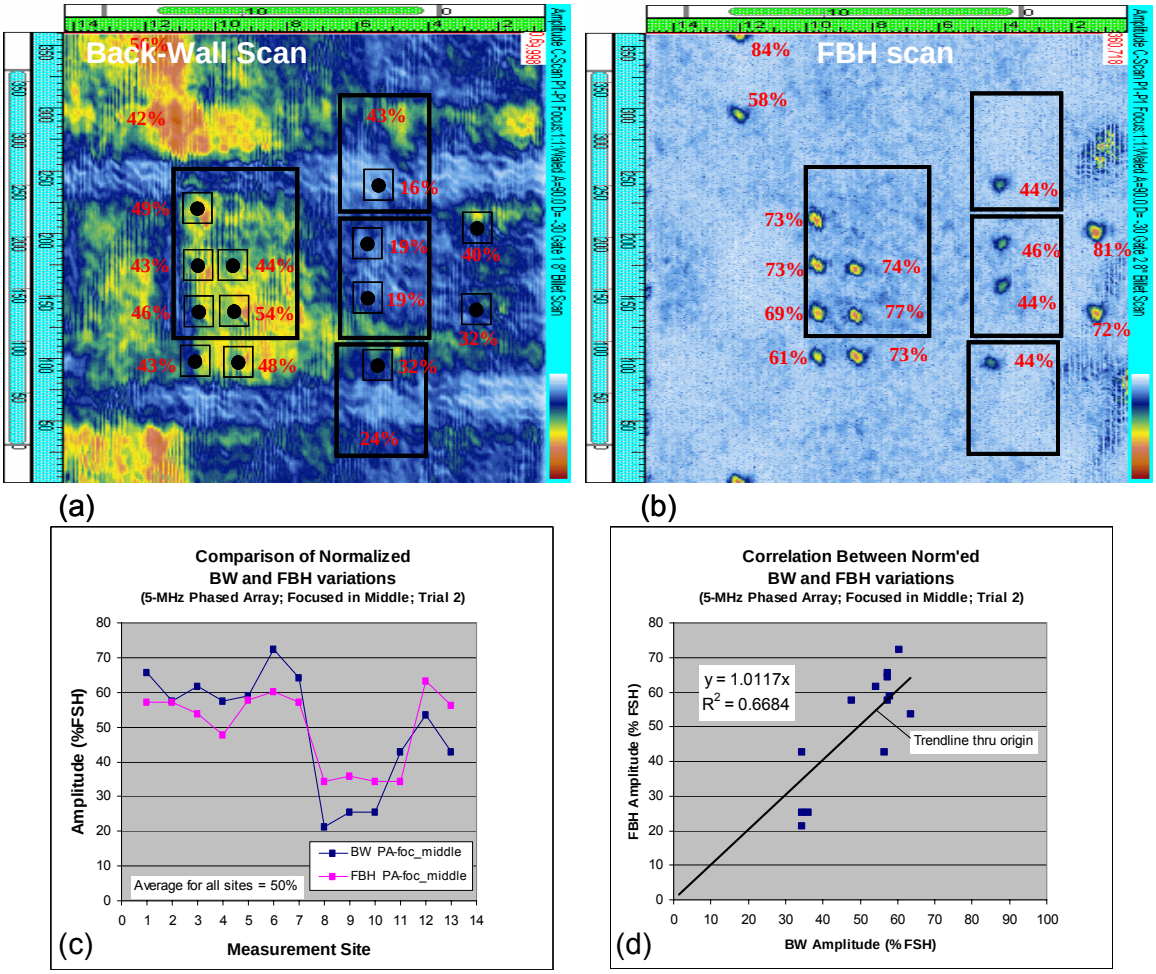

FIGURE 53. MEASUREMENTS ON A Ti-6-4 BILLET SEGMENT USING A PHASED ARRAY TRANSDUCER FOCUSED NEAR THE BILLET CENTER (ALTERNATE FOCUSING SCHEME)
(Beam diameters (-6 dB) near the back wall are approximately 400 by 600 mils (axial by hoop).)

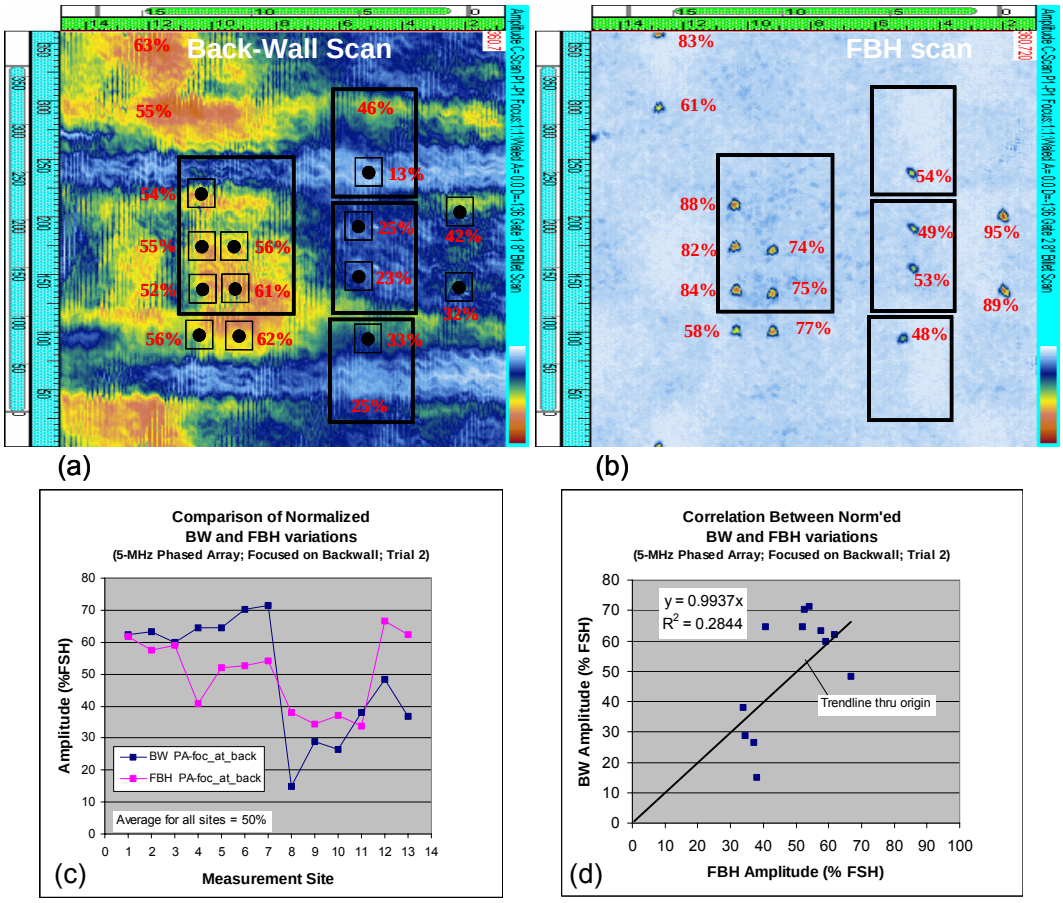

FIGURE 54. MEASUREMENTS ON A Ti-6-4 BILLET SEGMENT USING A PHASED ARRAY TRANSDUCER FOCUSED NEAR THE BILLET BACK WALL (ALTERNATE FOCUSING SCHEME)
(Beam diameters near the back wall are approximately 200 by 340 mils (axial by hoop).)

The following points summarize the results of the UT inspections conducted on the 15″ long Ti-6-4 billet specimen that contained 13 near-OD FBH targets.

- Both the FBH and nearby back-wall amplitudes varied significantly within the billet. For FBHs, the ratio of maximum/minimum amplitudes ranged from 2-4, depending on the inspection details. This FBH variability was large enough that it should be specifically accounted for during inspections via some sort of gain adjustment procedure.

- FBH and back-wall amplitudes tended to be fairly well correlated: sites with low (high) back-wall amplitudes tended to have low (high) FBH amplitudes as well. However, there were exceptions: e.g., sites where the local back-wall amplitude was smaller than average, while the nearby FBH amplitude was larger than average. Thus, it was wisest to use the back-wall fluctuation level as a general indicator of the level of fluctuations for

FBH signals, rather than inferring that a site with low (high) back-wall amplitude will necessarily have a low (high) FBH amplitude. It was also noted that the amplitude fluctuations from the mean tended to be higher for back-wall signals than for FBH signals. This indicated that using back-wall variations to estimate FBH variations would likely provide a conservative estimate of the latter.

- The fluctuation levels about the mean, and the degree of correlation between back-wall and FBH amplitudes, depend somewhat on the inspection setup. For the fixed-focus inspections, the back-wall and FBH fluctuation levels were more similar to one another (and the individual amplitudes more correlated) when the beam was focused near the back wall. The same was generally true for the phased array inspections, with the exception of trial 6.

The above points are further illustrated in figures 55 through 57. For all six measurements, figure 55 shows the 13 measured FBH amplitudes (left panel) and 13 associated (locally averaged) back-wall amplitudes at the same positions (right panel). As before, the amplitudes for each trial have been rescaled to have a mean value of 50% FSH for the collection of 13 measurement sites. One sees that sites with low (or high) back-wall or FBH amplitudes tend to have low (or high) amplitudes for all (or most) measurement setups. In addition, the back-wall amplitudes are fairly well correlated with the FBH amplitudes. For example, sites 8-11 that have lower than average back-wall amplitudes also have lower than average FBH amplitudes. However, the fluctuations about the mean are shown to be smaller, on average, for FBHs than for back-wall signals.

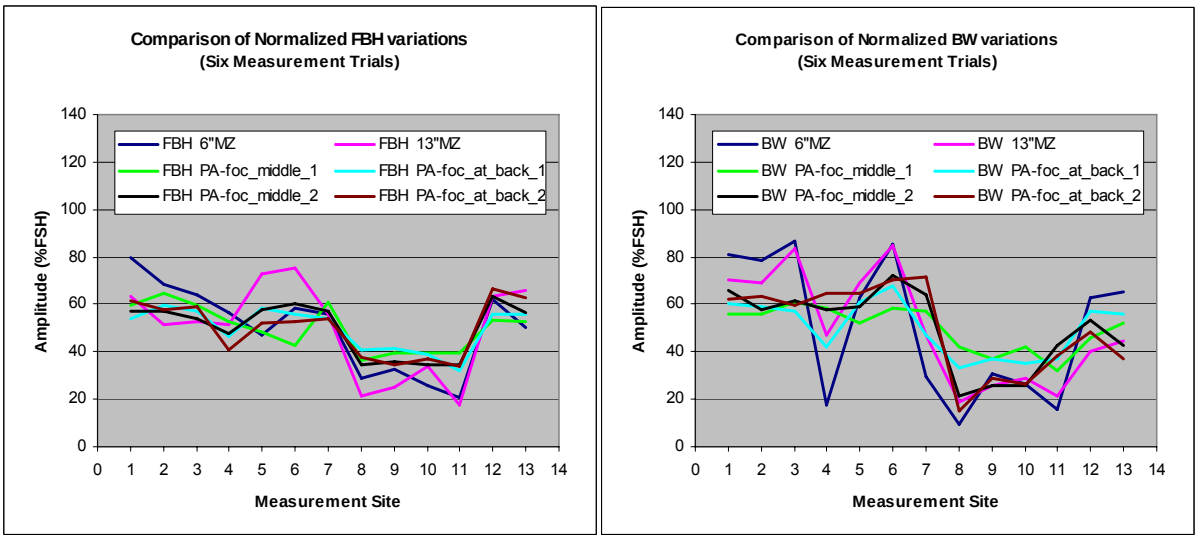

FIGURE 55. NORMALIZED FBH AMPLITUDES (LEFT) AND NEARBY BACK-WALL AMPLITUDES (RIGHT) SEEN IN THE SIX MEASUREMENT TRIALS
(Each curve has a mean of 50% FSH.)

The fact that the curves in figure 55 have similar overall shapes indicates that amplitude fluctuations are primarily due to actual differences in attenuation along different billet diameters.

The fact that the normalized curves are not identical indicates that the apparent attenuation along a given diameter depends, to some extent, on the transducer used in the measurement, a fact well established during Phase I [26].

Figure 56 shows two dimensionless measures of the amplitude fluctuations evident in figure 55. The first measure is simply the maximum amplitude divided by the minimum amplitude. The second is the standard deviation of the amplitudes divided by the mean amplitude. One sees that (1) the fluctuation level depends somewhat on the inspection setup; and (2) for a given setup, the fluctuation level tends to be smaller for FBHs than for back walls. Figure 57 shows the degree of correlation between the back-wall and FBH amplitudes as a function of the beam diameter at the FBH depth. The correlation measure used here is the correlation coefficient (R-squared) resulting from the linear fit to the FBH amplitude versus back-wall amplitude data, as illustrated in figures 49 through 54. Overall, the correlation between FBH and back-wall amplitude variations tended to improve when the beam diameter decreased. For the second phased array trial, however, focusing near the back-wall led to a lower R-squared value than focusing near the billet center. This may be partially due to the fact that the spread in back-wall amplitudes (about the mean value of 50% FSH) is significantly larger than the spread in FBH values for some cases (e.g., trial 6). This tends to lower the R-squared value for those cases. It is also likely that the precise values of FBH and back-wall amplitudes (and hence their correlation) is influenced by various inspection parameters such as the degree to which the incident beam is perpendicular to the billet specimen. There may have been some nonideality in the setup for trial 6, which explains the sizable difference in R-squared values for trials 4 and 6, both of which used the phased array probe with the beam focused near the billet back wall. The influence of setup parameters on back-wall and FBH amplitudes would no doubt be an illuminating topic for study, but it is beyond the scope of the present work.

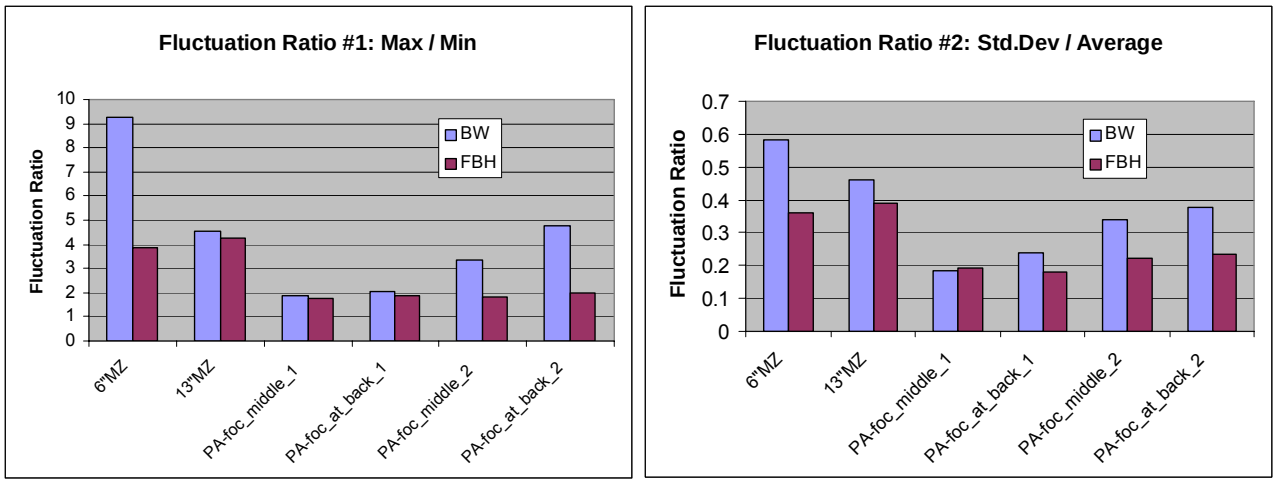

FIGURE 56. FLAT-BOTTOM HOLES AND (NEARBY) BACK-WALL AMPLITUDE FLUCTUATIONS SEEN IN SIX MEASUREMENT TRIALS USING A 15″ LONG Ti-6-4 BILLET CONTAINING 13 NEAR-OD FBHs

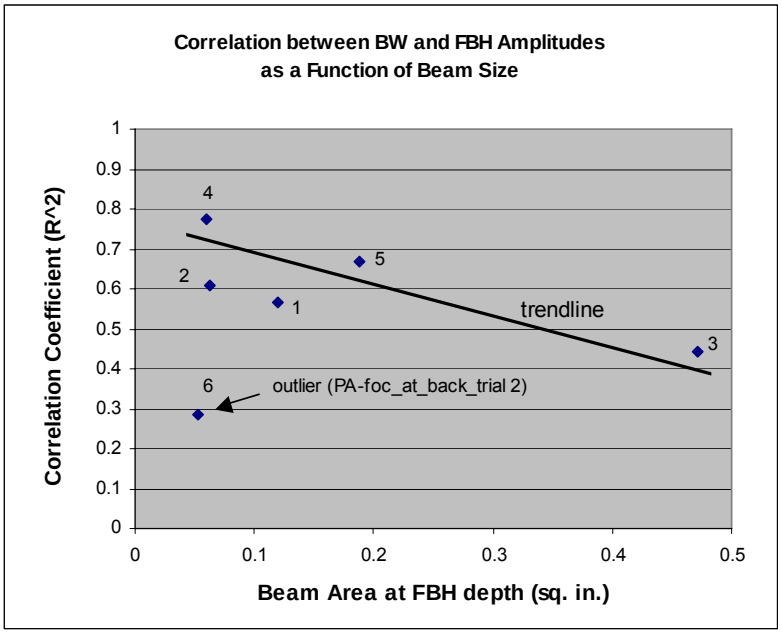

		(mils)	(mils)	(sq. in.)	
trial	probe	D-axial	D-hoop	Beam Area	Correl. Coeff.
1	6"MZ	250	610	0.1198	0.565
2	13"MZ	150	537	0.0633	0.609
3	PA-foc_middle_1	1000	600	0.4712	0.444
4	PA-foc_at_back_1	200	380	0.0597	0.774
5	PA-foc_middle_2	400	600	0.1885	0.668
6	PA-foc_at_back_2	200	340	0.0534	0.284

FIGURE 57. CORRELATION BETWEEN BACK-WALL AND FBH AMPLITUDES AS A FUNCTION OF BEAM SIZE AT THE FBH DEPTH (APPROXIMATELY 5.7″) (Measured beam diameters at the -6 dB level are listed beneath the graph for each of the six measurement trials.)

In summary, the above investigation (section 3.6) indicates that back-wall amplitude banding is associated with actual variations in the UT attenuation along different billet diameters. When identical FBHs are drilled a short distance into the billet OD, their echo amplitudes fluctuate in much the same manner as those of back-wall echoes at nearby positions. This suggests that back-wall echoes can be used to deduce attenuation differences that will also approximately describe the behavior of small-defect (e.g., FBH) amplitudes. When compensating for attenuation differences, one must be aware that identical reflectors at a given depth in either the calibration standard or the test billet can have significantly different amplitudes. For example, the amplitude of the reflected signal from a given calibration hole (used to set the preliminary inspection gain) will depend, to some extent, on whether that hole was drilled into a high- or low-attenuation band of the calibration standard. Thus, a robust compensation procedure will account not only for gross differences between the average attenuations of the calibration standard and test billet, but also for attenuation variations within both specimens.

3.6.6 Straw Man Procedures for Global Attenuation Compensation.

Recall that the adjective global was used to refer to attenuation compensation procedures in which a fixed gain adjustment in dB/inch units was applied uniformly at all axial and circumferential positions of the billet under inspection. Such adjustments are the simplest to implement in practical inspections, and the existing standard compensation procedure is of this nature. Based on the study of the 15″ long Ti-6-4 billet specimen, a basic global straw man compensation procedure having six variants, one being the standard approach, was proposed. Again, it was decided that 6″ diameter CBS billet material would be used to construct test specimens to test the variants.

3.6.7 Proposed Straw Man Global Attenuation Compensation Procedure.

1. Assume that the target inspection sensitivity is a #2 FBH. Also, assume that before any compensation adjustments are made, gains are adjusted to bring #2 FBHs in the calibration standard to 80% FSH.

2. Assume that the purpose of the compensation adjustments is to ensure (to some level of certainty) that a #2 FBH or equivalent reflector located anywhere within the billet to be inspected would generate an amplitude of 80% FSH or higher.

3. Using a suitable transducer, gather back-wall C-scan data from representative lengths of the calibration standard and billet to be inspected (BTBI) (two focusing schemes to be considered).

4. Calculate the amplitude difference in dB between some features of the back-wall C-scans of the calibration standard and BTBI (three combinations of features to be considered).

5. Divide the dB difference by the billet diameter to obtain an attenuation compensation value in dB/inch. Use this value to determine the gain adjustments needed for each inspection (depth) zone of the BTBI.

The choice of a suitable transducer in step 3 is open to interpretation. Back-wall fluctuations are likely to be more representative of FBH fluctuations if the transducer has a beam spot size on the back wall that is similar to the spot sizes of the transducers used in the actual inspection within their respective depth zones. However, a standard deep-zone MZ transducer (focused near the billet center) may work sufficiently well for surveying back-wall variations. It was proposed that both focusing schemes (focus near billet center; focus near billet back wall) be tested. As in the earlier measurements, the deep-zone MZ transducers designed for 6″ and 13″ diameter billet would be used to achieve the two proposed focusing conditions.

Different choices in step 4 of the back-wall C-scan features being compared will naturally lead to different dB/inch values. If it is known a priori that the FBHs in the calibration standard have been drilled into high- or low-attenuation bands, that information can be used when computing compensations. For existing calibration standards, it was believed that no consideration was given to attenuation banding when the holes were drilled. Moreover, the construction of the standards precludes viewing back-wall echoes from the billet OD in the vicinities of the

calibration holes. Each MZ calibration standard contains two parts, which abut one another in the axial direction: one is a full-round portion without alteration that is used to acquire back-wall echoes and the other contains the FBHs and internal cavities that allow the FBHs to be drilled. The two portions are screwed together but their original angular registration was generally not maintained. For CV inspections, the angular registration between the chord blocks and full-round specimen is also generally not known. For some individual calibration holes, it would likely be possible to estimate whether they were located in high- or low-attenuation bands by examining the local backscattered grain noise pattern or the local C-scan image of the echo from the associated cavity wall. In any given existing calibration standard, it was likely that some FBHs were drilled into high-attenuation bands and others into low-attenuation bands.

Rather than attempt to decipher and use detailed FBH location information, it was agreed that the location of any given FBH hole within the banding pattern of the calibration standard is unknown. Under this view, it was proposed that three back-wall amplitude feature combinations be considered in step 4, distinguished by how conservative one wishes to be in the compensation procedure:

- Standard: To deduce the attenuation difference, one compares average back-wall amplitudes in the calibration standard and the test billet. This corresponds to assuming that the calibration hole is located in an average attenuation region in the standard, and that the target flaw is located in an average attenuation region of the test billet. This may be regarded as the current standard practice for attenuation compensation.

- Semiconservative: Computes both the average and the standard deviation of the back-wall amplitude seen in the calibration standard and the test billet. One then compares the average plus one standard deviation in the calibration standard to the average minus one standard deviation) in the test billet. This corresponds to assuming that the calibration hole is in a somewhat low-attenuation region (one standard deviation above the average back-wall amplitude) of the calibration standard, and the target flaw is in a somewhat high-attenuation region of the test billet.

- Conservative: Compares the back-wall amplitude seen in the brightest region of the calibration standard C-scan to the back-wall amplitude in the dimmest region of the test billet C-scan. This corresponds to assuming that the calibration hole is in the lowest attenuation region of the standard and that the target hole is in the highest attenuation region of the test billet.

To test the six variations of the straw man compensation procedure, a suitable specimen had to be fabricated. It was desired that the test specimen contain numerous identical reflectors, all located at a depth where attenuation adjustments would be maximized. Since the 6″ diameter billet was routinely inspected over the depth range from 0″ to 3.5″, it was decided to place all reflectors (#2 FBHs) 3.5″ below the entry surface. A suitable calibration standard containing (among others) a #2 FBH located 3.5″ deep was available at GE.

As shown in figure 58, a candidate billet was to be located and cut into two sections with similar levels of back-wall amplitude variation. One section (B) would be used to fabricate the test

specimen (C) containing inferior FBHs. The other section (A) would be available for gathering back-wall amplitude data if the construction of specimen C precluded such measurements.

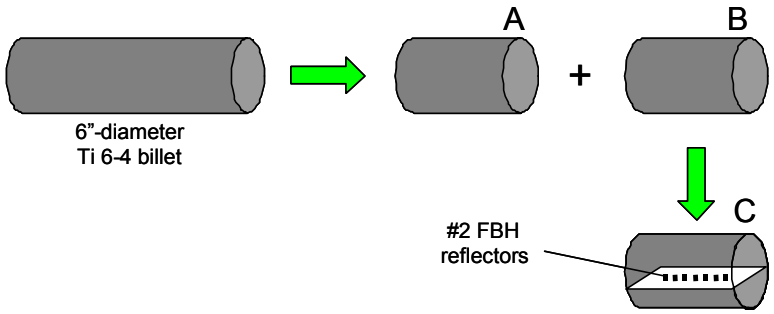

FIGURE 58. FABRICATION OF SPECIMENS TO TEST STRAW MAN PROCEDURES FOR ATTENUATION COMPENSATION

3.7 FABRICATION OF A TEST SPECIMEN CONTAINING NEAR-CENTER FBHS.

A suitable candidate billet section was located, namely, a 72″ long piece of 6″ diameter Ti-6-4 CBS stock bearing the designation B3W1BA. Back-wall amplitude C-scans made using the two deep-zone MZ transducers are shown in figure 59. The figure shows the upper scan using the zone 4 MZ transducer for 6″ diameter billet follows the current MZ practice for sampling attenuation differences. The lower scan using the zone 7 transducer for 13″ diameter billet and a 6.6″ water path produces a smaller focal spot on the back wall. Inspection gains were adjusted to yield similar average back-wall amplitudes. Note that the pattern of amplitude variations is very similar for both inspections. This similarity is further demonstrated in figures 60 and 61, where the average amplitudes within the small boxed regions of the C-scans are compared. In accordance with figure 58, two 18″ long sections were cut from one end of the 72″ piece, as indicated in figure 59, to serve as test specimens.

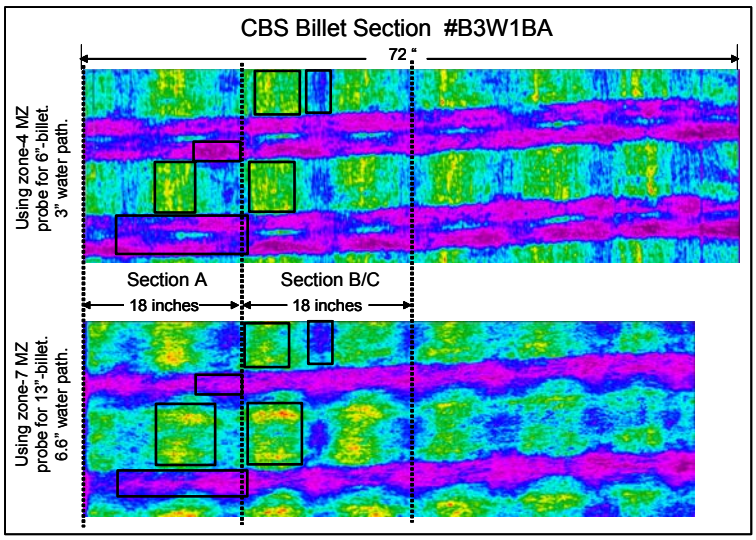

FIGURE 59. BACK-WALL C-SCANS OF THE CANDIDATE BILLET FOR THE STRAW MAN TEST

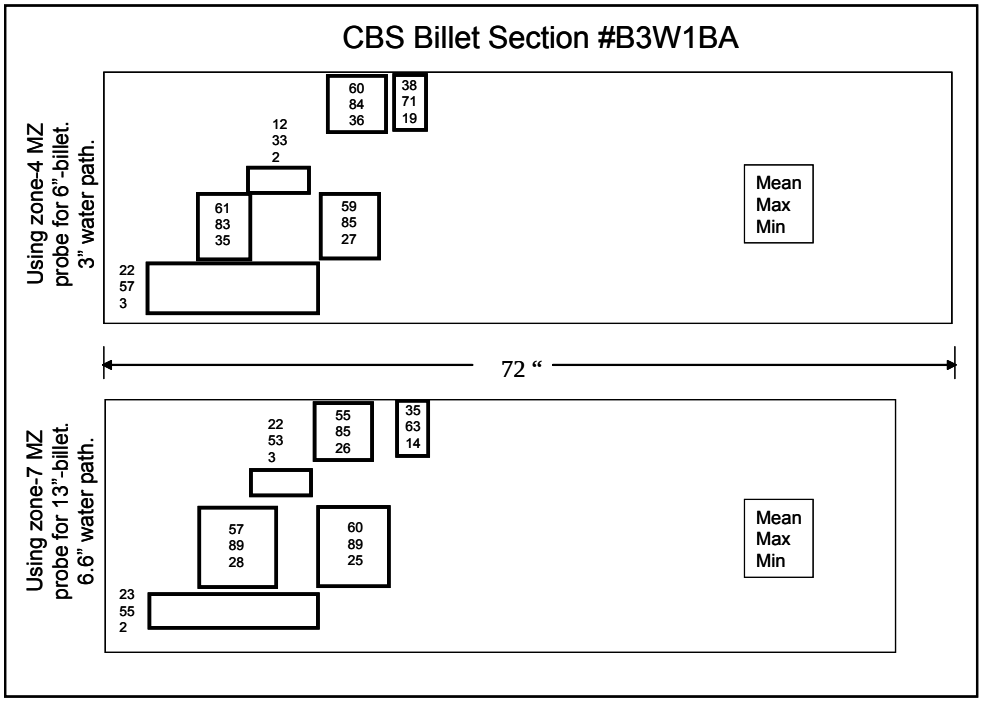

FIGURE 60. MEAN, MAXIMUM, AND MINIMUM BACK-WALL AMPLITUDES FOR VARIOUS REGIONS OF THE C-SCAN IMAGES SHOWN IN FIGURE 59
(Units are % FSH)

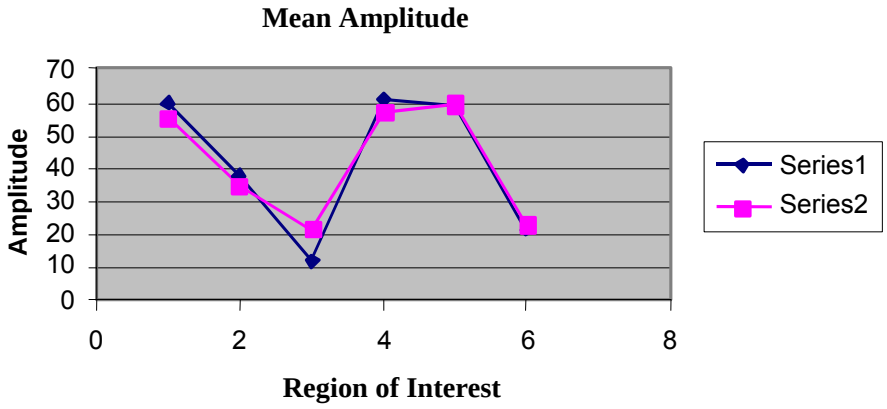

FIGURE 61. COMPARISON OF MEAN AMPLITUDES OF BACK-WALL ECHOES FOR THE SIX REGIONS INDICATED IN FIGURES 59 AND 60
(For series 1 (6″ diameter, zone 4 probe), the beam is focused near the billet center. For series 2 (13″ diameter, zone 7 probe), the beam is focused near the back wall.)

The manner in which #2 FBHs were drilled into the 18″ long test billet is illustrated in figure 62. Pilot holes of 205 mil diameter and 1.25″ length were first drilled, and 1.25″ length #2 FBHs (31.25 mil diameter) were then drilled into the bottoms of the pilot holes. In all, 17 #2 FBHs were placed at various axial and circumferential positions, with each hole located 3.5″ below the inspection entry surface on the opposite side of the billet. Eleven of the hole locations were

chosen using the back-wall amplitude patterns shown in figure 59, and six were chosen using the backscattered MZ noise pattern for the deepest zone. Locations were chosen to span the widest possible range of back-wall and noise amplitudes, with the presumption that this would lead to the widest possible variation of FBH amplitudes. Figure 63 shows the completed test specimen after the near-OD portion of each hole was plugged to prevent water infiltration.

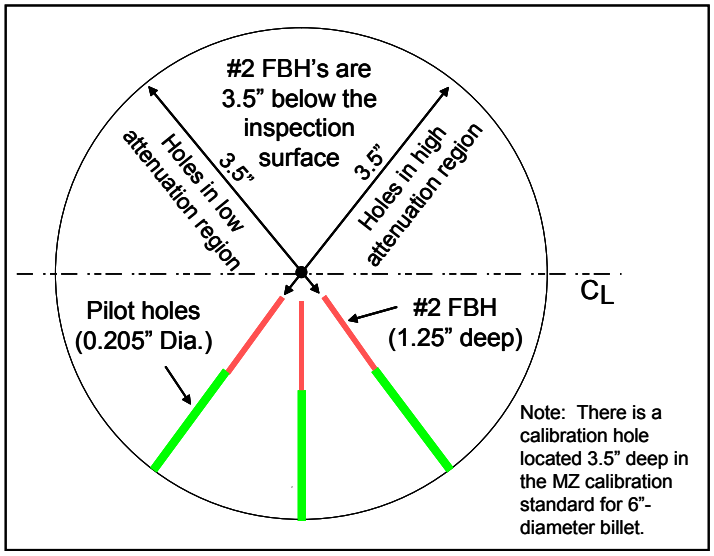

FIGURE 62. SIX-in.-DIAMETER, 18-in.-LONG Ti-6-4 TEST SPECIMEN SHOWING HOW #2 FBHs WERE DRILLED AT A DEPTH OF 3.5″ FROM THE INSPECTION SURFACE

FIGURE 63. SIX-in.-DIAMETER, 18-in.-LONG Ti-6-4 TEST BILLET SHOWING DRILLED AND PLUGGED HOLES

All C-scan images of back-wall and interior (noise + defect) echoes seen during inspections of the test billet have the same axial and circumferential registration and, hence, the locations of the FBH defects are the same for all images. These locations and their enumeration are shown in figure 64.

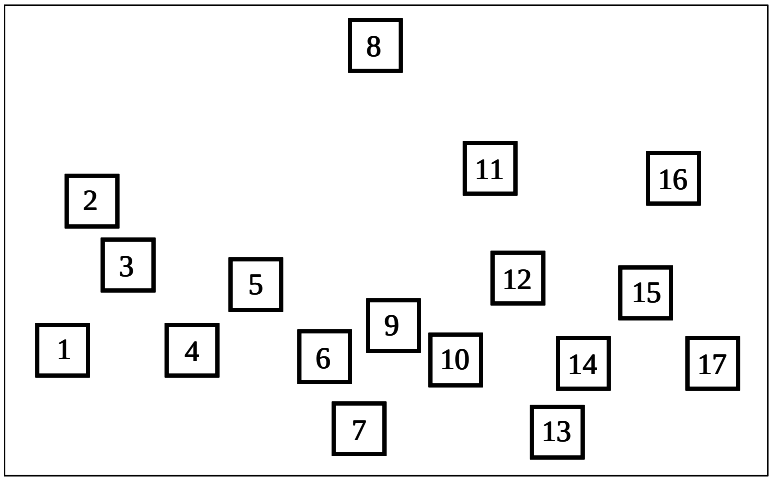

FIGURE 64. NUMBERING SCHEME FOR FBH LOCATIONS IN ALL C-SCANS OF THE 18″ LONG TEST BILLET

Echoes from the 17 #2 FBHs in the test billet will be compared with the echo from a #2 FBH at the same depth in the 6″ diameter MZ calibration standard. The design of the deep-zone portion of the calibration standard, containing #2 holes at depths of 2.6″ and 3.5″ is shown in figure 65(a). A typical C-scan of that portion of the standard is shown in figure 65(b).

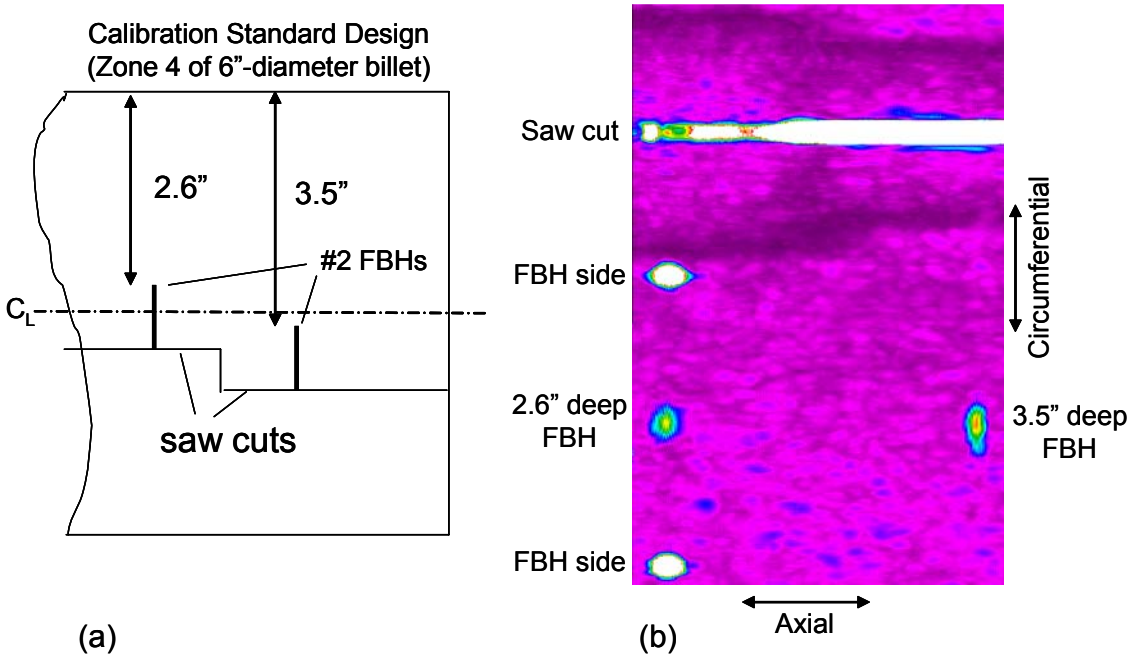

FIGURE 65. (a) LAYOUT OF THE DEEP-ZONE (ZONE 4) PORTION OF THE 6″ DIAMETER MZ CALIBRATION STANDARD AND (b) C-SCAN OF THE DEEP-ZONE REGION OF THE CALIBRATION STANDARD
(Beam focus near billet center)

3.7.1 Tests of the Global Attenuation Compensation Straw Man Procedure.

Back-wall C-scans of the test specimen and the full-round portion of the calibration standard were made to gather the data required to compute attenuation adjustments. In each case, as noted above, two transducers were used:

- Zone 4 MZ transducer for 6″ diameter billet at a 3″ water path (beam focused near billet center).
- Zone 7 MZ transducer for 13″ diameter billet at a 6.6″ water path (beam focused near billet back wall).

The resulting C-scans are shown in figures 66 and 67, respectively, along with annotations listing back-wall amplitude statistics within selected regions. As expected from the earlier scans of the 72″ long billet section, the patterns of back-wall amplitude variations in the test billet are similar for the two transducers. Also notice that shadows of the drilled holes in the 18″ long test specimen can be seen. These occur when the center of the sonic beam propagates along a drilled hole. For each drilled hole, two shadows are expected: one at the location shown in figure 64 and one on the opposite side of the billet (i.e., rotated by 180°). The appearance of the shadows was deemed to have little influence on the specific back-wall amplitude statistics listed in figures 66 and 67.

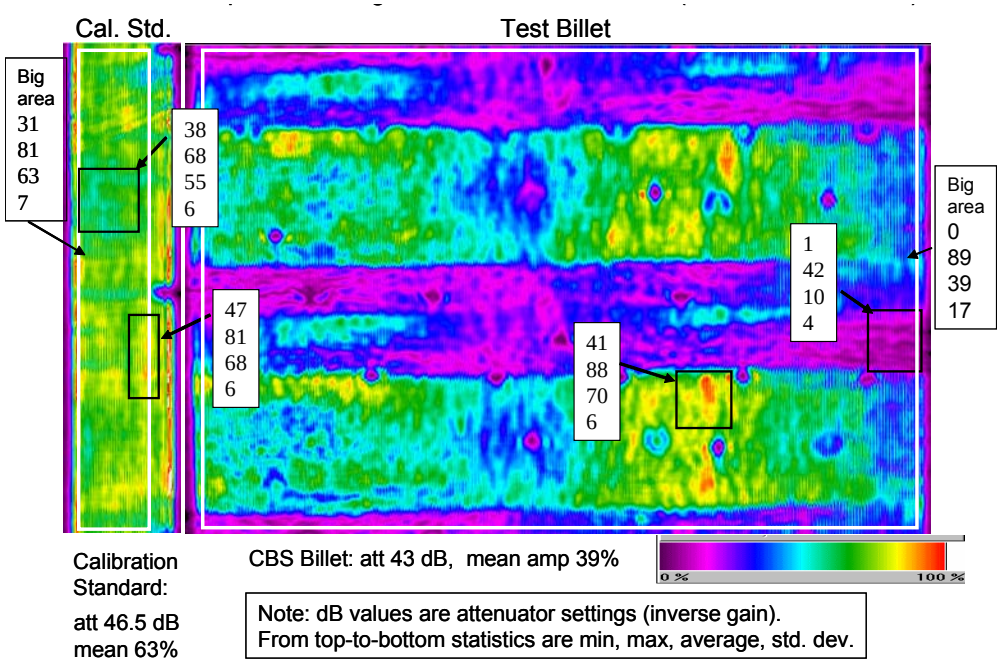

FIGURE 66. BACK-WALL C-SCANS OF THE CALIBRATION STANDARD (LEFT) AND TEST BILLET (RIGHT) ACQUIRED WITH THE BEAM FOCUSED NEAR THE 6″ DIAMETER BILLET CENTERLINE (ZONE 4)

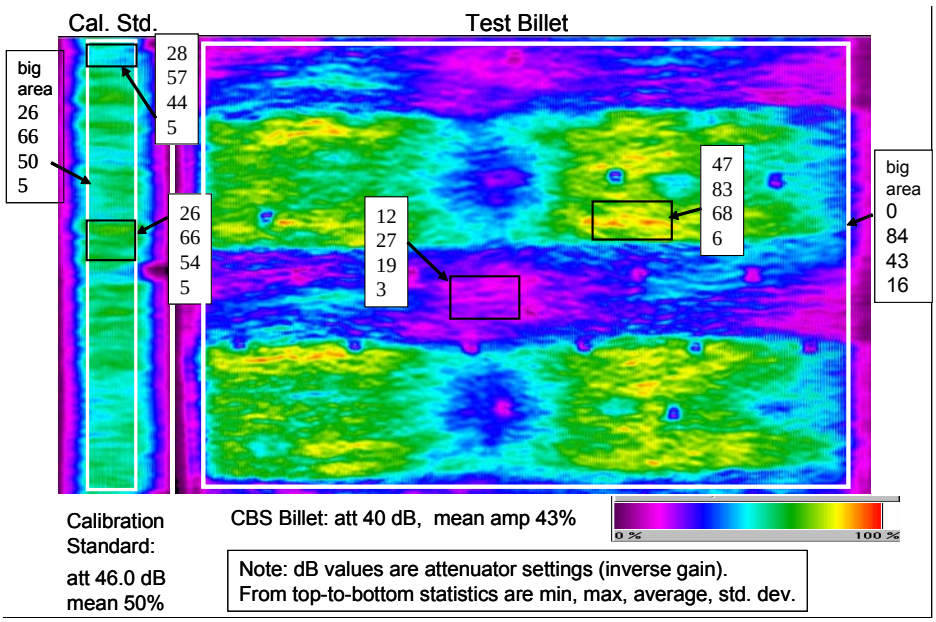

FIGURE 67. BACK-WALL C-SCANS OF THE CALIBRATION STANDARD (LEFT) AND TEST BILLET (RIGHT) ACQUIRED WITH THE BEAM FOCUSED NEAR THE 13″ DIAMETER BILLET BACK WALL (ZONE 7)

From the back-wall amplitude statistics listed in figures 66 and 67, attenuation compensation values for the six variations of the straw man procedure can be calculated using equation 2. An example of such a calculation is shown in figure 68 for the standard procedure, requiring a gain boost of 4.48 dB for a target located 3.5″ deep in the test billet.

"Standard" Attenuation Compensation Adjustment
(Using BW C-scan data acquired with beam focused near billet center)

Cal Std BW: attenuator setting = 46.5 dB; Mean amplitude = 63%

Test Billet BW: attenuator setting = 43.0 dB; Mean amplitude = 39%

Mean amplitudes at same gain: 63% and 26% @ 46.5 dB

dB difference between Std. and test billet = 20log[63/26] = 7.68 dB

Divide by billet diameter (6") ➡ 1.28 dB/in.

At 3.5 inch depth, amplitude adjustment is 4.48 dB or factor of 1.68

FIGURE 68. EXAMPLE ATTENUATION COMPENSATION CALCULATION

The resulting global attenuation adjustments for each of the six variations are listed in figure 68. These values must be multiplied by 3.5″ to obtain gain corrections (boosts) in dB for the FBHs in the test billet. The standard and semiconservative procedures use the back-wall amplitude average and standard deviation values listed in table 11. For the conservative procedure, the average back-wall amplitudes within a small high-amplitude region of the calibration standard and a small low-amplitude region of the CBS test billet was used. These extreme average amplitudes are estimated as (68=cal, 10=CBS) for centerline focusing and (60=cal, 19=CBS) for back-wall focusing, at the gains used for the raw back-wall C-scans shown in figures 66 and 67.

TABLE 11. COMPUTED ATTENUATION COMPENSATION VALUES IN dB/INCH OF DEPTH IN THE TEST BILLET

	Standard[a]	Semiconservative[b]	Conservative[c]
Focus at centerline	1.28	2.26	3.36
Focus at back wall	1.22	2.03	2.66

[a] Use average back-wall amplitudes for calibration standard and test billet.
[b] Use (average + σ) for calibration standard and (average - σ) for test billet.
[c] Use average of maximum amplitude zone for calibration standard and average of minimum amplitude zone for test billet.

After completing the back-wall measurements and analyses, the interior of the test billet was inspected. The usual procedure for an MZ inspection was followed; however, only the zone 4 inspection was performed. Zone 4 nominally extends from 2.6″-3.5″ deep, but a slightly larger acquisition gate is typically used so that there is some overlap between neighboring zones. The water path was set to 3″, and the calibration standard was scanned using the zone 4 transducer to locate the #2 FBH calibration holes at the ends of the zone. The gain was adjusted so that the amplitudes from both holes exceeded 80% FSH. The two echo amplitudes were sufficiently similar (1.6 dB difference) that water path adjustment was not necessary under standard inspection protocols. The calibration standard was then replaced by the test billet, and zone 4 was again scanned using a 3″ water path. A slightly higher gain setting (+2 dB) was used for the test billet inspection. After the measurements, the FBH amplitudes in the test billet were adjusted to compensate for attenuation differences. Since six variants of the straw man compensation procedure were being considered, it was most efficient to inspect the test billet once and then to make all gain adjustments during postprocessing. The results of the zone 4 inspections of the calibration standard and test billet are shown in figure 69. As expected, substantial variations were seen in the peak amplitudes of the 17 nominally identical reflectors in the test billet. The raw amplitudes varied from 38% to 96% FSH, or by about a factor of 2.5. The FBH amplitude variations are believed to be due to variations in the test billet microstructure and its associated attenuation.

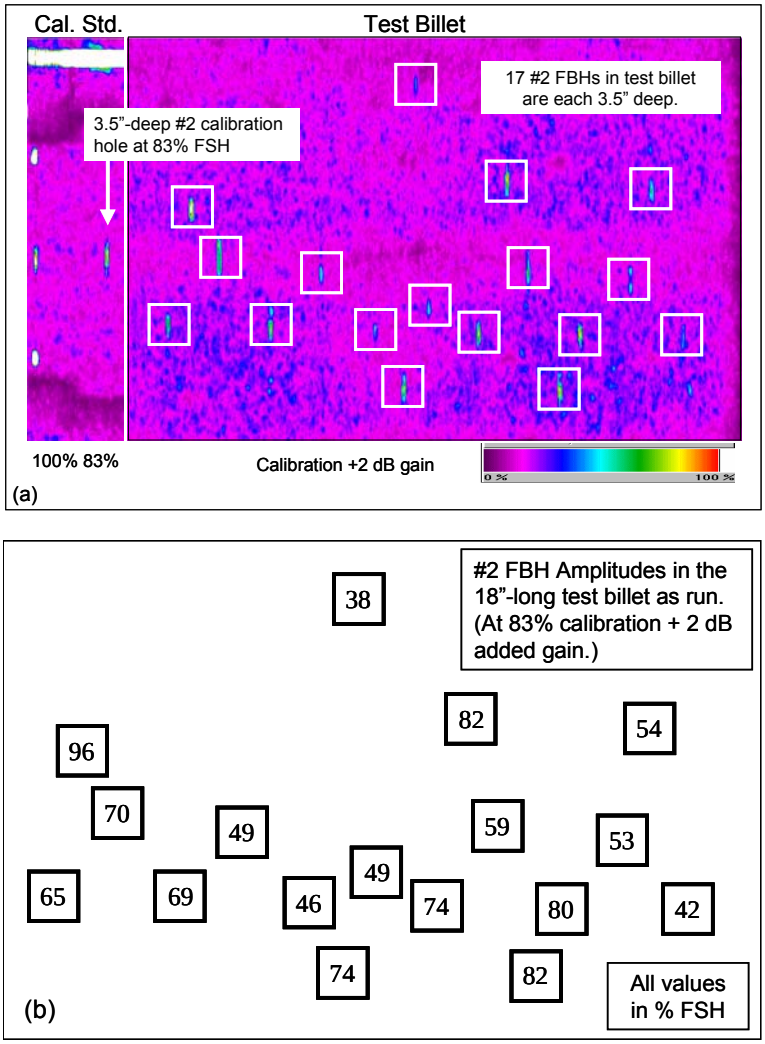

FIGURE 69. (a) C-SCAN IMAGES FROM ZONE 4 INSPECTIONS OF THE CALIBRATION STANDARD (LEFT) AND TEST BILLET (RIGHT) AND (b) RAW PEAK AMPLITUDES OF THE 17 #2 FBHs IN THE TEST BILLET

Figures 70 and 71 show the results of adjusting the FBH amplitudes in various ways to compensate for attenuation differences between the billet specimen and the 6″ diameter MZ calibration standard that was used as a reference. Figure 70 displays the amplitudes that result when no compensation is made, i.e., when the test billet is inspected at the same gain required to bring the 3.5″ deep #2 FBH in the calibration standard to 80% FSH. All 17 FBHs in the test billet are shown to have amplitudes below the 80% target threshold, with values ranging from 29%-74% FSH. Although none of the 17 defects would have been rejectable on the basis of peak amplitude ≥ 80% if no compensation were performed, several would have been rejected on the basis of a commonly used signal/noise (S/N) criterion, namely

$$\frac{S}{N} \equiv \frac{Flaw\ Signal\ Amplitude - Average\ Noise\ Amplitude}{Peak\ Noise\ Amplitude - Average\ Noise\ Amplitude} \geq 2.5 \qquad (3)$$

Automatic image analysis software developed by GEAE was applied to the as-run zone 4 C-scan of the test billet shown in figure 69(a). The software identified potential defects and calculated peak amplitudes and S/N for each, with the results shown in figure 71. Thirteen of the seventeen FBH defects were identified by the software, with one FBH (whose C-scan image had two lobes) being identified twice. Seven of the thirteen defects were determined to have S/N ≥ 2.5; these were the FBH defects having the seven highest amplitudes, namely, those enumerated 2, 3, 7, 10, 11, 13, and 14 in figure 64.

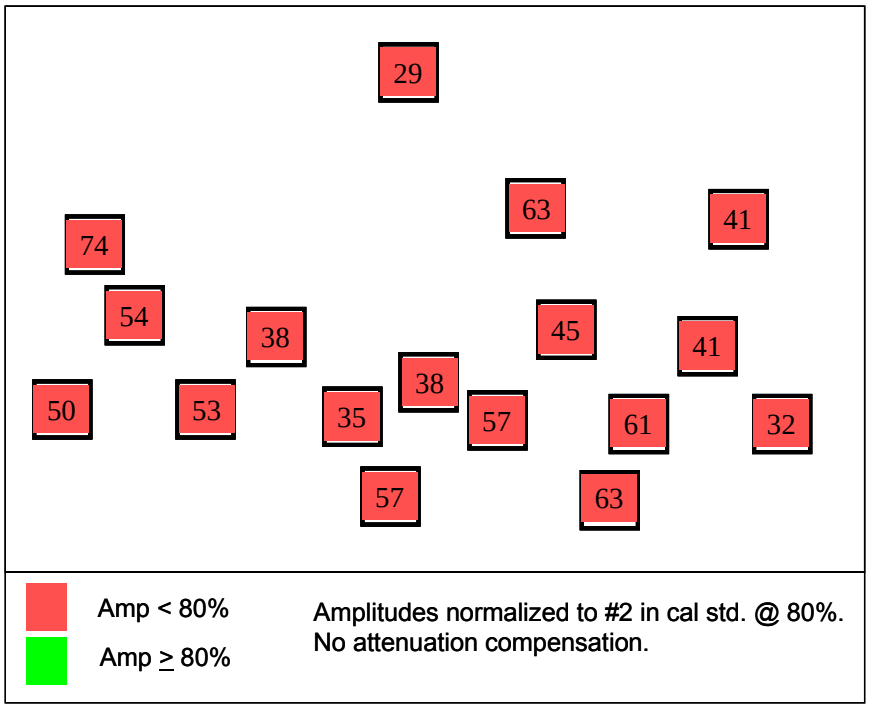

FIGURE 70. PEAK AMPLITUDES OF THE 17 #2 FBHs IN THE TEST BILLET WHEN NO ATTENUATION COMPENSATION IS USED (IN % FSH)

Figure 72 summarizes the results of applying the standard global compensation procedure to the test billet. The adjusted FBH amplitudes are shown for both focusing schemes used to acquire the back-wall C-scans on which the adjustments are based. If one assumes that the average back-wall amplitude is a good indicator of average FBH amplitude, then the standard compensation procedure is designed such that average amplitudes would be the same for FBHs in the calibration standard and test billet (if each specimen contained many identical reflectors at the same depth). Of course, the calibration standard contains only a single #2 FBH at 3.5″ depth. If one assumes that this particular calibration reflector is located near a region of average attenuation, then the average FBH amplitude in the test billet, after the standard compensation adjustment, should be near 80% FSH. This is seen in figure 72 to be approximately the case for either back-wall focusing method. Also, as might be expected, about half of the compensated amplitudes are above 80% and about half are below 80%. None of the FBHs having compensated amplitudes below 80% have S/N ≥ 2.5. Thus, none of these would have been rejected using the usual signal-to-noise criterion. Figure 72 indicates that when the standard compensation procedure is used, some regions of the test billet are being inspected to higher than

#2 FBH sensitivity, while other regions are being inspected to lower than #2 FBH sensitivity. To inspect the entire test billet to #2 FBH or better sensitivity (based on signal amplitude), the inspection gain must be boosted.

Heat No.: cbs Billet Id.: 6incbsz4 Zone : 4

Average Peak Noise Level: 34 %
Average Detection Level: 59 %

There were 14 indications found

	Indication	Axial	Rotary	Amplitude	SNR
	1	1.25	97	65%	1.89
	2	1.95	206	96%	4.02
	3	2.78	174	70%	2.70
	4	4.36	98	69%	2.17
	5	5.89	149	49%	1.83
	6	8.37	45	74%	2.73
	7	10.63	96	74%	2.51
	8	11.46	236	82%	3.46
	9	12.13	149	59%	2.31
	10	13.04	44	82%	2.71
	11	13.67	95	80%	2.59
The same FBH	12	15.18	136	53%	1.81
	13	15.20	151	50%	1.70
	14	15.80	221	54%	1.59

(a)

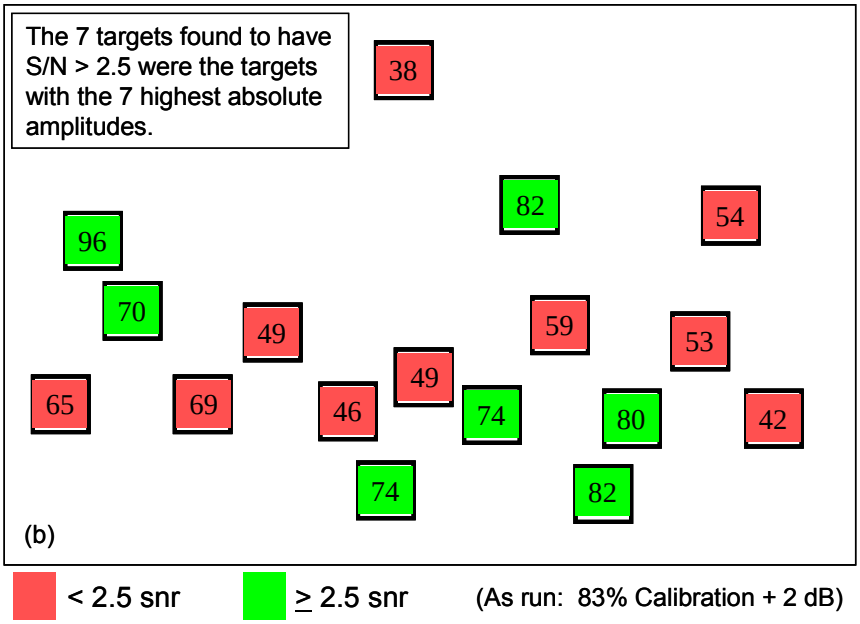

FIGURE 71. (a) OUTPUT GENERATED WHEN AUTOMATIC S/N SOFTWARE WAS APPLIED TO THE AS-RUN ZONE 4 C-SCAN OF THE TEST BILLET AND (b) AS-RUN PEAK AMPLITUDES OF THE 17 #2 FBH DEFECTS WITH S/N RANGES INDICATED

The results of applying the standard, semiconservative, and conservative compensation procedures to the test billet inspection are compared in figures 73 and 74. Adjustments made for figure 73 were based on back-wall C-scans acquired with the beam focused near the centerline, while those for figure 74 had the beam focused near the back wall for back-wall C-scan acquisition. The adjusted amplitudes of the individual FBHs shown in figure 74 are listed in table 12. Figure 75 then provides a brief comparison of the key results from the six variations of the basic global attenuation adjustment procedure. Note that as the compensation procedure becomes more conservative, the gain applied during the test billet inspection increases (see table 12) and the measured FBH amplitudes rise. For example, at 3.5″ depth where the FBHs are located, the semiconservative procedure in figure 73 applies 3.44 dB more gain than the standard procedure, and the conservative procedure applies an additional 3.84 dB of gain. As might be expected, all the FBHs in the test billet were found to have amplitudes greater than 80% FSH when the conservation compensation procedure was used. This was true for both of the focusing methods used to acquire back-wall C-scans; however, the focus at back-wall approach accomplished this at lower total inspection gain and, thus, is likely to lead to fewer false calls.

3.7.2 Local Attenuation Adjustments and Their Computation.

Thus far, only global compensation procedures have been discussed for which a fixed dB/inch adjustment is applied uniformly at all locations along the billet surface. Making the so-called local adjustments in which the applied gain (again in dB/inch units) varies with axial and circumferential position will now be considered. It is likely impractical at present to acquire raw UT data in which the gain varies with surface position. Thus, the local adjustment procedures to be discussed are intended to be used as postinspection tools, which can be used to adjust the amplitudes of suspected defect echoes to account for local variations in the attenuation of the test billet.

Several approaches for applying local adjustments were considered and tested using the back-wall C-scan pattern and the backscattered grain noise patterns in the various inspection zones as the basis for the adjustments. A number of methods were tested using different combinations of back-wall data and accumulated grain noise data for the inspection zones prior to and including the defects. In the end, it was found that the simplest methods, using back-wall data alone or backscattered noise data alone (from the center zone of the billet), worked as well as any, and the detailed discussions that follow will be confined to these. As before, measuring back-wall amplitudes using two different focusing schemes were considered. This led to a total of three local compensation procedures to be discussed based, respectively, on:

- Deep-zone backscattered gated-peak grain noise patterns acquired with the beam focused near the billet centerline.

- Back-wall gated-peak amplitude patterns acquired with the beam focused near the billet centerline.

- Back-wall gated-peak amplitude patterns acquired with the beam focused near the billet back wall.

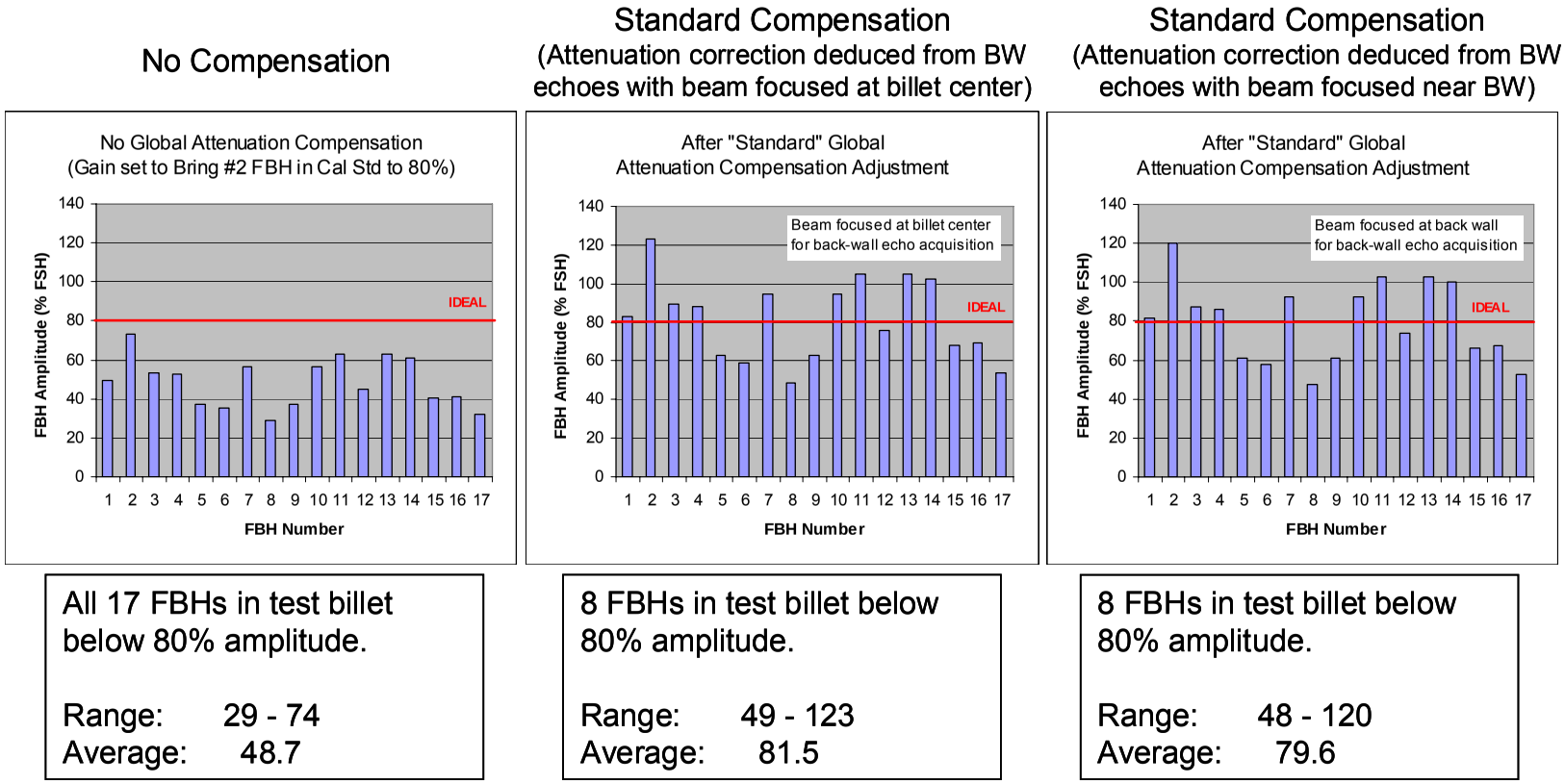

FIGURE 72. PEAK AMPLITUDES OF THE 17 #2 FBHs IN THE TEST BILLET USING THE STANDARD COMPENSATION PROCEDURE (RIGHTMOST TWO PANELS) AND NO ATTENUATION COMPENSATION (LEFTMOST PANEL)

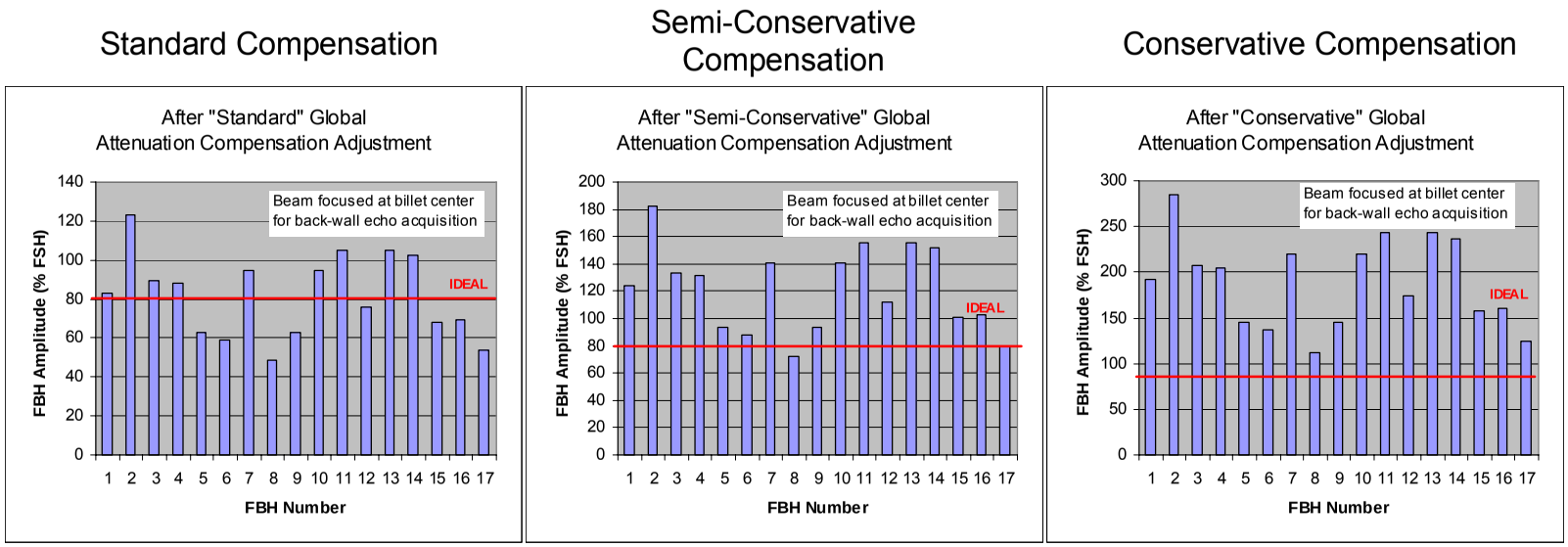

Standard Compensation	Semi-Conservative Compensation	Conservative Compensation
8 FBHs in test billet below 80% amplitude.	1 FBH in test billet below 80% amplitude.	0 FBHs in test billet below 80% amplitude.
Range: 49 - 123	Range: 72 - 183	Range: 113 - 284
Average: 81.5	Average: 121	Average: 189

FIGURE 73. RESULTS OF APPLYING THREE GLOBAL ATTENUATION COMPENSATION PROCEDURES TO THE TEST BILLET CONTAINING 17 #2 FBH DEFECTS, ZONE 4
(Back-wall C-scans on which the adjustments are based were acquired with the sonic beam focused near the centerline (zone 4 probe for 6″ diameter billet; 3″ water path).)

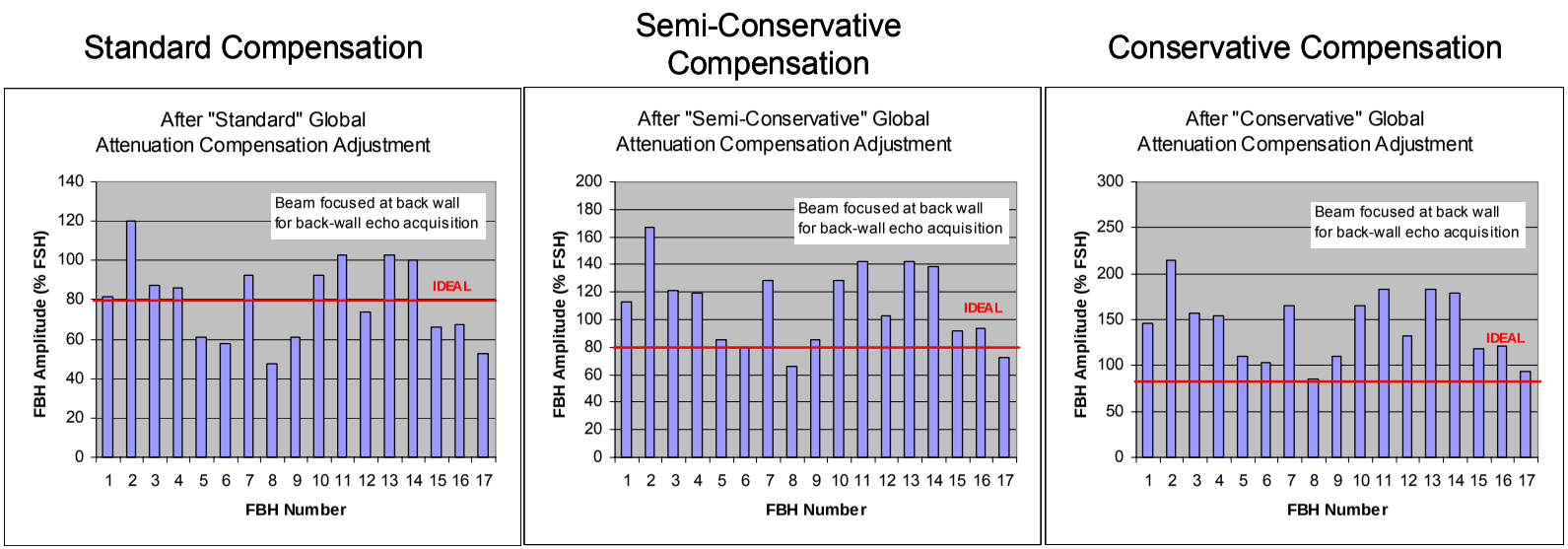

Standard Compensation	Semi-Conservative Compensation	Conservative Compensation
8 FBHs in test billet below 80% amplitude.	2 FBHs in test billet below 80% amplitude.	0 FBHs in test billet below 80% amplitude.
Range: 48 - 120	Range: 66 - 167	Range: 85 - 215
Average: 79.6	Average: 110	Average: 143

FIGURE 74. RESULTS OF APPLYING THREE GLOBAL ATTENUATION COMPENSATION PROCEDURES TO THE TEST BILLET CONTAINING 17 #2 FBH DEFECTS, ZONE 7
(Back-wall C-scans on which the adjustments are based were acquired with the sonic beam focused near the back wall (zone 7 probe for 13″ diameter billet; 6.6″ water path).)

TABLE 12. FLAT-BOTTOM HOLE AMPLITUDES FOR THE Ti-6-4 TEST BILLET AFTER ADJUSTMENT

FBH No.	FBH Amplitude As-Run	FBH Amplitude at Calculated Gain	Attenuation Compensated FBH Amplitudes					
			Centerline Focus Standard	Centerline Focus Semiconservative	Centerline Focus Conservative	Back-Wall Focus Standard	Back-Wall Focus Semiconservative	Back-Wall Focus Conservative
1	65	49.8	83.3	123.7	192.6	81.3	112.8	145.6
2	96	73.5	123.0	182.6	284.4	120.1	166.5	215.1
3	70	53.6	89.7	133.2	207.4	87.6	121.4	156.8
4	69	52.8	88.4	131.3	204.4	86.3	119.7	154.6
5	49	37.5	62.8	93.2	145.2	61.3	85.0	109.8
6	46	35.2	58.9	87.5	136.3	57.5	79.8	103.0
7	74	56.7	94.8	140.8	219.3	92.6	128.4	165.8
8	38	29.1	48.7	72.3	112.6	47.5	65.9	85.1
9	49	37.5	62.8	93.2	145.2	61.3	85.0	109.8
10	74	56.7	94.8	140.8	219.3	92.6	128.4	165.8
11	82	62.8	105.0	156.0	243.0	102.6	142.3	183.7
12	59	45.2	75.6	112.2	174.8	73.8	102.4	132.2
13	82	62.8	105.0	156.0	243.0	102.6	142.3	183.7
14	80	61.2	102.5	152.2	237.0	100.1	138.8	179.2
15	53	40.6	67.9	100.8	157.0	66.3	91.9	118.7
16	54	41.3	69.2	102.7	160.0	67.6	93.7	121.0
17	42	32.2	53.8	79.9	124.4	52.5	72.9	94.1
average =	63.6	48.7	81.5	121.1	188.6	79.6	110.4	142.6
minimum =	38	29.1	48.7	72.3	112.6	47.5	65.9	85.1
maximum =	96	73.5	123.0	182.6	284.4	120.1	166.5	215.1
Gain Adjustment in dB/inch:		0.00	1.28	2.26	3.36	1.22	2.03	2.66
Gain Adjustment at 3.5″ dB:		0.00	4.47	7.91	11.75	4.27	7.11	9.33
Amplitude multiple factor at 3.5″:		1.00	1.67	2.49	3.87	1.63	2.27	2.93

Results are listed for each of the six global compensation procedures.

Comparison of the Six "Global" Attenuation Compensation Schemes			
	Standard Compensation	**Semi- Conservative Compensation**	**Conservative Compensation**
Attenuation correction deduced from BW echoes with beam focused at billet center:	8 FBHs in test billet below 80% amplitude. Range: 49 - 123 Average: 81.5	1 FBH in test billet below 80% amplitude. Range: 72 - 183 Average: 121	0 FBHs in test billet below 80% amplitude. Range: 113 - 284 Average: 189
Attenuation correction deduced from BW echoes with beam focused at back wall:	8 FBHs in test billet below 80% amplitude. Range: 48 - 120 Average: 79.6	2 FBHs in test billet below 80% amplitude. Range: 66 - 167 Average: 110	0 FBHs in test billet below 80% amplitude. Range: 85 - 215 Average: 143

FIGURE 75. SUMMARY OF FBH AMPLITUDE STATISTICS FOR THE SIX GLOBAL COMPENSATION PROCEDURES

As before, for 6″ diameter test billets, the zone 4 transducer for the 6″ diameter billet was used to gather noise or back-wall data for the scenario where the beam was focused near the centerline, and the zone 7 transducer for the 13″ diameter billet was used to gather back-wall data with the beam focused near the back wall.

It was agreed that local adjustments will likely be made after global compensation adjustments have already been applied. The global adjustment (if any) will have determined the fixed inspection gain at a given depth and, hence, determined the average amplitude for a collection of (many) reflectors (defects) located at that depth. Under this view, a local gain adjustment is computed relative to a billet-wide average, and describes the extra gain at a given position above and beyond that required for the average location for that depth.

The basic approach to making local adjustments is straightforward. When analyzing either the noise or back-wall amplitude pattern, it was assumed that the amplitude variations seen are due solely to attenuation variations. Let $A(x,\theta, z_A)$ denote the measured amplitude (in % FSH units) in the test billet at axial position x, circumferential position θ, and one-way depth z_A. In particular, $A(x,\theta, z_A)$ here will represent either a back-wall amplitude (z_A=billet diameter) or backscattered noise amplitude measured from an inspection zone centered near the billet centerline (z_A=billet radius). Also, let $<A(z_A))>$ denote the billet-wide average of $A(x,\theta, z_A)$ over all axial and hoop positions. Within the test billet, the difference between the local attenuation along the billet diameter at position (x,θ) and the billet-wide average (in dB/inch-of-depth units) is written as

$$\Delta\alpha = \alpha(x,\theta) - <\alpha> = 20\log[A(x,\theta,z_A)/<A(z_A)>]/z_A \quad [dB/inch] \tag{4}$$

In a similar manner, FBH(x,θ,z) denotes the amplitude from a FBH located at position (x,θ,z) in the test billet, and <FBH(z)> denotes a billet-wide average amplitude for a large population of identical reflectors at the same depth. To estimate the amplitude difference between an FBH at location (x,θ,z) and the average FBH at the same depth, the attenuation difference calculated from equation 4 is used.

$$FBH(x,\theta,z)/<FBH(z)> = 10^{\Delta\alpha \bullet z/20} = [A(x,\theta,z_A)/<A(z_A)>]^{z/z_A} \qquad (5)$$

In this manner, the effect of local attenuation variations within the test billet can be estimated from measured back-wall or grain noise data.

Note that the backscattered noise level observed at a given depth depends on both the average attenuation to that depth and the backscattering capacity (FOM value) of the local microstructure. Thus, in writing equation 4 for the noise case, it is tacitly assumed that the grain noise capacity of the microstructure (i.e., the FOM value) is approximately uniform along the centerline and independent of the approach angle there. This approximation is supported by measurements summarized in figure 39, where billet properties near the centerline are similar to one another whether the centerline is approached through a high- or low-noise band. Thus, differences in backscattered noise levels from the billet center are assumed to be primarily due to differences in average attenuation values along different billet radii. Note, however, that for backscattered noise from a depth other than the billet centerline, the FOM value is expected to vary with surface position and, hence, equation 4 cannot be readily justified.

It is reiterated that the approach being taken here must be regarded as an approximation because it is tacitly assumed that the attenuation is uniform along a given radius or diameter specified by (x,θ). For example, when using back-wall amplitudes to make the adjustments, it is assumed that the average attenuation in dB/inch computed along a full diameter is equal to the average attenuation computed, say, over the first 2 inches of depth. But it was found in earlier studies (e.g., figure 39) that billet attenuation varies with depth. Thus, this approach is likely more accurate for deeply positioned defects than for those located near the OD, since the path lengths z_A and z will be more similar. Also, when using noise amplitudes to make the adjustments, the analysis assumes that the effective attenuation for noise is the same as that for FBH echoes. It may be that attenuation for noise (due to energy loss alone) is lower than that for FBHs (due to combined energy loss + beam distortion). Some evidence of this was seen in billet property measurements carried out during ETC Phase I [25]. Thus, an adjustable scaling factor > 1 could be added when translating from noise attenuation to FBH attenuation. However, such fine tuning was not attempted for the present analysis.

Finally, note that the presence of the defect itself influences the noise or back-wall amplitude pattern used to compute the local adjustment. For this reason, when measuring the local amplitude $A(x,\theta,z_A)$, the noise or back-wall amplitude is averaged over a small area centered on the defect coordinates, and a smaller region in the immediate shadow of the defect is excluded.

Although only the deep-zone (zone 4) noise C-scan was eventually used for local attenuation adjustments, a full four-zone MZ inspection was carried out on the test billet to obtain noise data. The resulting C-scan for one of the zones is shown in figure 76 together with boxes marking the axial and hoop locations of the (deeper) 17 FBH defects. A similar C-scan for zone 4 was shown in figure 69. Within each box, noise statistics were calculated (minimum, maximum, mean, and standard deviation) and their values are listed in figure 77 for each inspection zone. For zone 4, the images of the FBHs also appear in the C-scan and must be excluded when calculating noise statistics. This was done using software designed by GE for calculating SNRs. The software determined mean and peak noise levels in the vicinity of each defect, and these values are listed in figure 77.

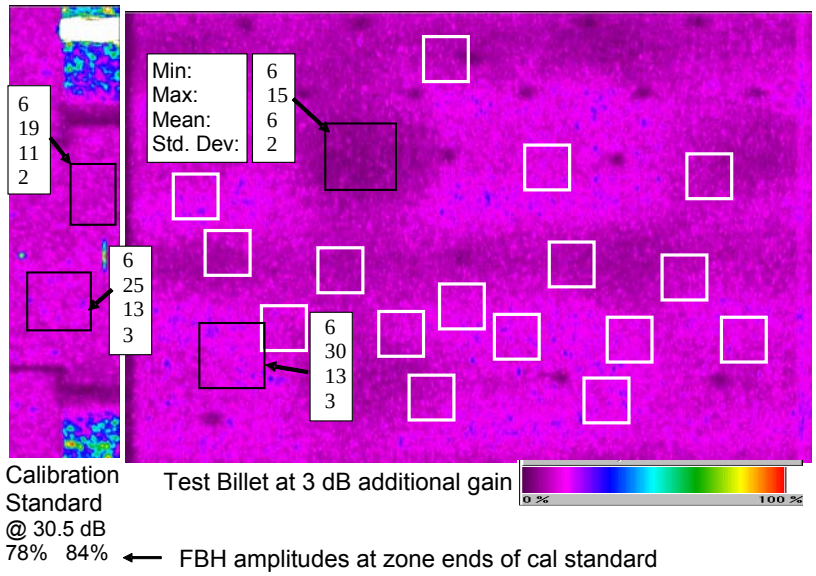

FIGURE 76. ZONE 3 C-SCAN OF THE 18″ LONG TEST BILLET SHOWING ANALYSIS BOXES FOR THE COMPUTATION OF NOISE STATISTICS

The noise amplitudes at corresponding axial and hoop positions in different zones are somewhat correlated. This is indicated by figure 78 where the measured mean noise amplitudes at the 17 locations of interest are displayed. Noise amplitudes within each zone are normalized to an average value of 100 for the set of 17 measurements and generally range between 70 and 130. Discounting zone 1, which shows relatively little variation, normalized noise values for the other three zones tend to rise or fall together as the axial and hoop position is varied. Only the local mean noise amplitudes for zone 4 are used to make local attenuation adjustments. When using equations 3 and 4, the local noise mean, $A(x,\theta, z_A)$, as listed in figure 77, is compared to the full-scan average noise amplitude estimated to be $<A(z_A)>=17$ on the same (raw) scale.

Raw Backscattered Noise Statistics for the 6"-diameter 18"-long Ti 6-4 Test Billet (gated-peak noise amplitudes in % FSH)

	Zone 1				Zone 2				Zone 3				Zone 4	
Location	Mean	Min	Max	Std.Dev	Mean	Min	Max	Std.Dev	Mean	Min	Max	Std.Dev	Mean	Max
1	15	12	26	2	13	5	28	4	14	7	24	3	19	33
2	20	29	11	3	15	5	31	4	14	6	24	3	19	34
3	20	13	34	3	9	4	18	2	9	4	19	2	15	28
4	20	11	30	3	11	4	25	3	11	5	22	2	18	30
5	15	12	26	2	10	5	18	2	8	4	15	2	14	25
6	18	11	28	2	13	4	35	4	10	4	20	3	14	24
7	18	11	28	2	15	5	35	5	10	4	19	2	16	32
8	17	9	28	3	11	2	27	3	9	3	20	2	12	25
9	19	9	29	3	16	7	38	4	13	7	25	3	16	29
10	19	9	28	3	13	4	34	5	13	7	24	3	18	30
11	19	12	31	3	13	6	24	3	13	6	24	2	19	36
12	18	12	26	2	10	4	20	2	9	4	20	2	14	28
13	19	11	30	3	16	11	30	3	14	8	26	3	21	38
14	19	11	30	3	17	7	35	4	13	7	29	3	19	35
15	18	11	27	2	15	7	30	4	12	6	21	2	16	31
16	20	13	100	3	13	5	33	3	9	4	18	2	18	32
17	16	11	24	2	12	4	28	3	11	4	25	3	17	37

For Zone 4, the full-area mean noise amplitude is 17% FSH

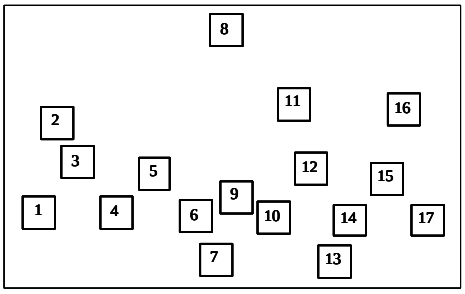

Locations in scans

Depths of Inspection Zones		
Zon	Start	End
1	0.2	0.8
2	0.8	1.7
3	1.7	2.6
4	2.6	3.5

FIGURE 77. NOISE STATISTICS AT THE AXIAL AND HOOP LOCATIONS OF THE 17 FBH DEFECTS

Raw Average Noise Levels

Location	Zone 1	Zone 2	Zone 3	Zone 4
1	15	13	14	19
2	20	15	14	19
3	20	9	9	15
4	20	11	11	18
5	15	10	8	14
6	18	13	10	14
7	18	15	10	16
8	17	11	9	12
9	19	16	13	16
10	19	13	13	18
11	19	13	13	19
12	18	10	9	14
13	19	16	14	21
14	19	17	13	19
15	18	15	12	16
16	20	13	9	18
17	16	12	11	17
Ave =	18.24	13.06	11.29	16.76
To normalize such that average = 100 in each zone multiply the above values by:				
	Zone 1	Zone 2	Zone 3	Zone 4
	5.484	7.658	8.854	5.965

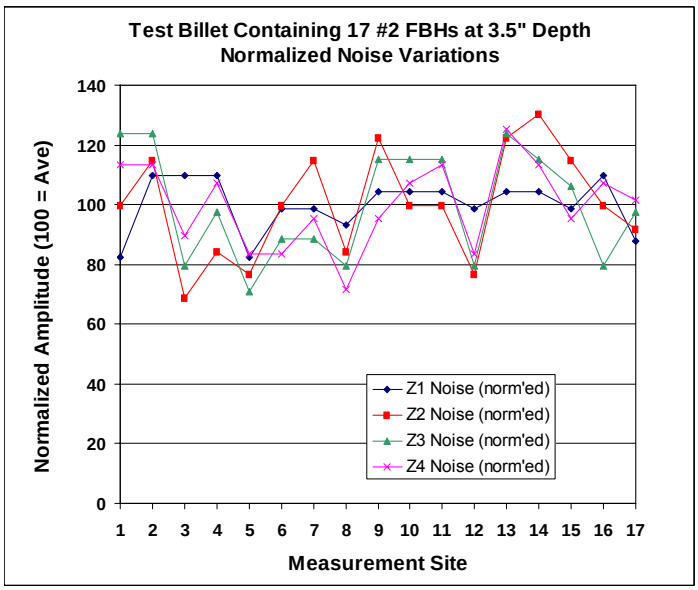

FIGURE 78. RAW AND NORMALIZED AVERAGE GATED-PEAK NOISE AMPLITUDES SEEN IN THE MZ INSPECTION OF THE Ti-6-4 TEST BILLET

The back-wall C-scans used to make local attenuation adjustments are shown in figures 66 and 67, respectively, for the two focusing schemes. For each C-scan, average back-wall amplitudes in the (axial and hoop) vicinity of the defects were measured using the two methods illustrated in figure 79(a). In the first method, amplitudes at each site were computed for an area consisting of a rectangle with a smaller centered rectangle removed, the center being large enough to fully cover the shadow cast by the defect. Special image analysis software was written for this purpose. To test the software, back-wall amplitude statistics were also computed using a second method in which the area used in the analysis was the union of two rectangles located on either side of the defect shadow. As shown in figure 80, the two methods yielded similar estimates of the local average back-wall amplitude in the vicinity of each defect. For the later local attenuation adjustments, method 1 values were used.

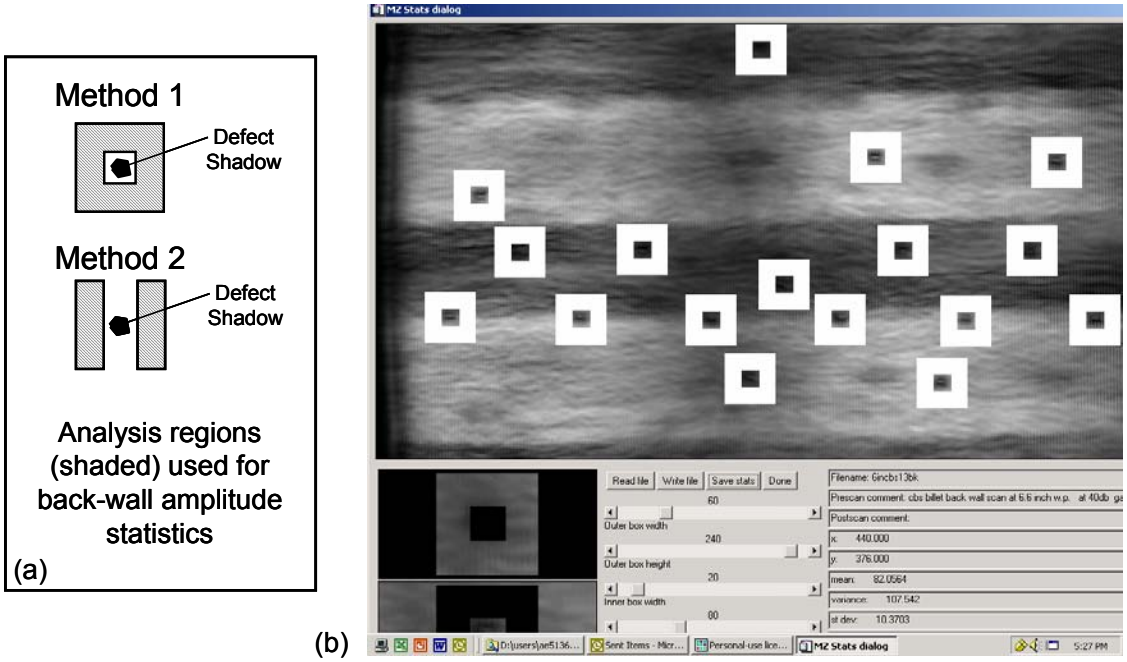

FIGURE 79. (a) METHODS OF CHOOSING THE ANALYSIS REGION USED TO COMPUTE THE AVERAGE BACK-WALL AMPLITUDE IN THE VICINITY OF EACH DEFECT AND (b) ANALYSIS REGIONS (WHITE/BLACK SQUARES) FOR THE BACK-WALL C-SCAN OF THE TEST BILLET MADE WITH THE BEAM FOCUSED NEAR THE BILLET BACK-WALL (USING METHOD 1)

	Focus at CL	
Location	Method 1	Method 2
1	48.0	52.0
2	50.7	55.5
3	22.6	14.0
4	46.6	55.0
5	22.5	21.0
6	30.1	40.0
7	36.7	37.0
8	19.7	23.0
9	21.1	20.5
10	43.4	57.0
11	62.3	63.5
12	26.7	25.5
13	64.4	67.0
14	47.8	62.5
15	29.6	33.0
16	48.5	52.0
17	28.4	36.5
ave =	38.2	42.1

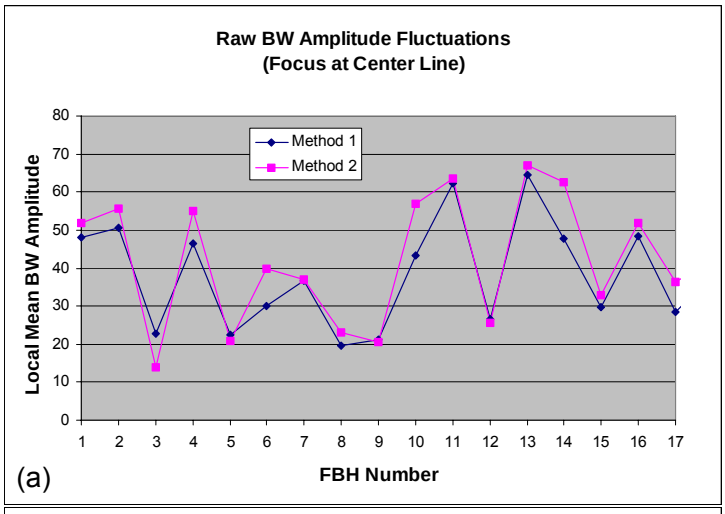

	Focus at BW	
Location	Method 1	Method 2
1	51.9	62.5
2	61.4	62.5
3	29.9	23.5
4	51.4	62.0
5	27.9	27.0
6	32.1	40.0
7	32.1	31.5
8	19.9	20.0
9	21.8	19.5
10	46.2	54.5
11	66.7	66.5
12	31.1	32.0
13	61.2	62.0
14	53.9	63.5
15	33.1	35.5
16	49.3	47.5
17	33.9	42.0
ave =	41.4	44.2

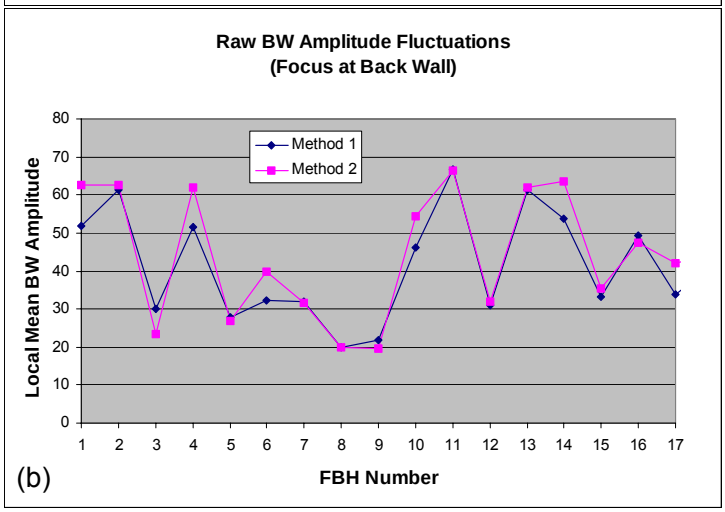

FIGURE 80. RAW AVERAGE BACK-WALL AMPLITUDES IN THE VICINITIES OF THE 17 FBH DEFECTS IN THE TEST BILLET (a) BEAM FOCUSED NEAR BILLET CENTERLINE AND (b) BEAM FOCUSED NEAR BILLET BACK WALL

From the measured local zone 4 noise or back-wall amplitudes, local attenuation adjustment factors can be computed using equation 4. The results are listed in table 13. The first three columns list the (raw) mean noise and back-wall amplitudes at each measurement site [$A(x, \theta, z_A)$] and the full-scan average [$<A\ (z_A)>$]. The last three columns evaluate the rightmost term in equation 4, which is the predicted ratio of the local FBH amplitude at position (x, θ, z) to the full-scan average (assuming many identical FBH defects at depth z). In applying equation 4, one takes $z = 3.5''$ as the depth of the defects, used $z_A = 6''$ for back-wall amplitudes, and $z_A = 3''$ for noise amplitudes. The latter value was chosen because grain noise versus depth curves acquired without DAC tend to peak near the focal depth, which was nominally 3″ for the zone 4 C-scan used to gather the noise data in question. For a gated-peak noise C-scan, the peak noise voltage observed at a given pixel location could occur at any depth within the inspection gate; however, the peak voltages tend to be clustered near the focal depth.

TABLE 13. LOCAL ATTENUATION ADJUSTMENT FACTORS AT THE 17 FBH SITES DETERMINED FROM LOCAL BACK-WALL AND GRAIN NOISE AMPLITUDES

	Raw Amplitudes Used to Compute Adjustments			Computed Local Adjustment Factors at 3.5″ Depth		
Location	Back Wall (Focus at CL)	Back Wall (Focus at CL)	Zone 4 Noise (Focus at CL)	Back Wall (Focus at CL)	Back Wall (Focus at CL)	Zone 4 Noise (Focus at CL)
1	48.0	51.9	19	1.13	1.12	1.14
2	50.7	61.4	19	1.17	1.23	1.14
3	22.6	29.9	15	0.73	0.81	0.86
4	46.6	51.4	18	1.11	1.11	1.07
5	22.5	27.9	14	0.73	0.78	0.80
6	30.1	32.1	14	0.86	0.84	0.80
7	36.7	32.1	16	0.97	0.84	0.93
8	19.7	1909	12	0.67	0.64	0.67
9	21.1	21.8	16	0.70	0.67	00.93
10	43.4	46.2	18	1.07	1.04	1.07
11	62.3	66.7	19	1.31	1.29	1.14
12	26.7	31.1	14	0.80	0.83	0.80
13	64.4	61.2	21	1.34	1.23	1.28
14	47.8	53.9	19	1.13	1.14	1.14
15	29.6	33.1	16	0.85	0.86	0.93
16	48.5	49.3	18	1.14	1.08	1.07
17	28.4	33.9	17	0.83	0.87	1.00
Full C-Scan						
Average:	39	43	17			

Notes:

CL = centerline

A factor of 1.13, for example, indicates that the FBH amplitude at that location is expected to be 13% larger than the billet-wide average due to lower than average attenuation.

Predicted FBH amplitude fluctuations are compared with measured fluctuations in figure 81. Recall that equation 4 predicts the amplitude of a defect at a specific location relative to that of a (hypothetical) billet-wide average amplitude for many similar defects at the same depth. Of course, one does not have a full billet-wide population of #2 FBHs at 3.5″ depth, but rather 17 specific members of that population. To construct figure 81, a value of 100 was assigned to the billet-wide defect amplitude when making the predictions. To get an average value of 100, the measured amplitudes of the 17 real defects were normalized. The average of the 17 predicted amplitudes for each local adjustment procedure is typically a few percent below 100, perhaps suggesting that the 17 chosen locations tend to be in preferentially low-amplitude zones. As figure 81 shows, the predicted pattern of amplitude fluctuations is very similar for the three local adjustment procedures. Each predicted fluctuation pattern is also fairly similar to the measured pattern, but there are a few noteworthy exceptions: for defects 2 and 3, the measured amplitudes are significantly above the predictions, and for defects 16 and 17, the measured amplitudes are significantly lower than predicted.

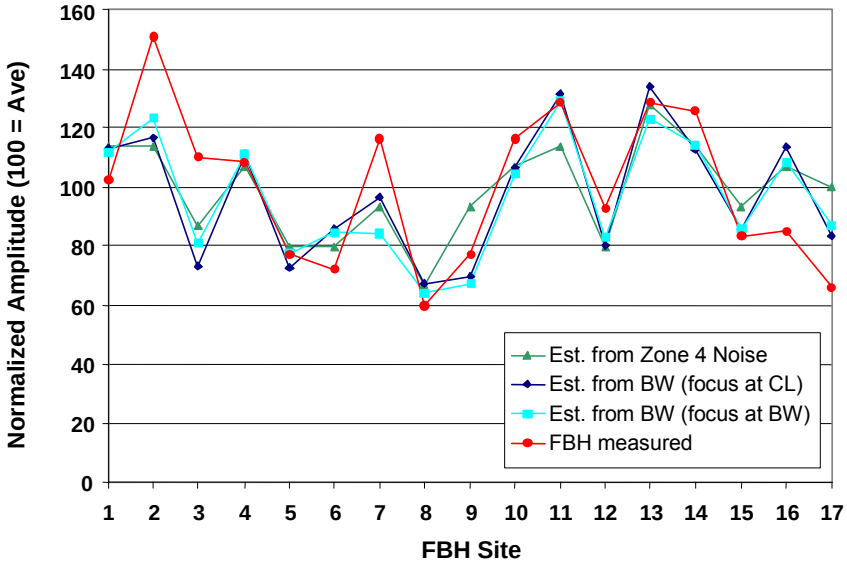

FIGURE 81. COMPARISON OF MEASURED AND PREDICTED FBH AMPLITUDES OF THE 17 #2 FBH DEFECTS IN THE TEST BILLET (NORMALIZED TO AN AVERAGE OF 100)

The relationship between the measured and predicted FBH amplitudes at the 17 sites in the test billet is further explored in figure 82. There, the data shown in figure 81 have been replotted in a different way. For each of the three procedures used to estimate local FBH amplitudes, the measured amplitude of each defect has been plotted against the predicted amplitude. Again, the 17 measured amplitudes have been normalized to an average of 100, and the predictions assume an average of 100 for a large (billet-wide) population of defects. If there were a perfect correspondence between the measured and predicted amplitudes, the plotted points would lie along a straight line of unit slope and the correlation parameter R^2 for the best-fit line would equal 1. For each of the three local estimation procedures, similar levels of scatter about the best-fit line are seen. R^2 values are somewhat larger (better correlation) for estimates made from back-wall amplitudes as opposed to backscattered noise. Also, for estimates made from back-wall amplitudes, the correlation is best when back-wall amplitudes are measured with the beam focused near the back wall.

If one estimates, on the basis of back-wall or grain noise C-scans, that a defect at a specific axial and hoop location will have an amplitude above or below average due to local attenuation variation, then the inspection gain used at that specific location can, in principle, be adjusted. The aim of such local gain adjustments is to equalize the echo amplitudes of identical defects located at the same depth but different lateral positions in the billet. The gain multiplication factor required to equalize amplitudes (in linear rather than dB units) is the inverse of the term on the far right-hand side of equation 4. At the sites of the 17 #2 FBHs in the test billet, the required gain factors for the three local adjustment procedures under consideration are, thus, the inverses of the numbers listed in the last three columns of table 13.

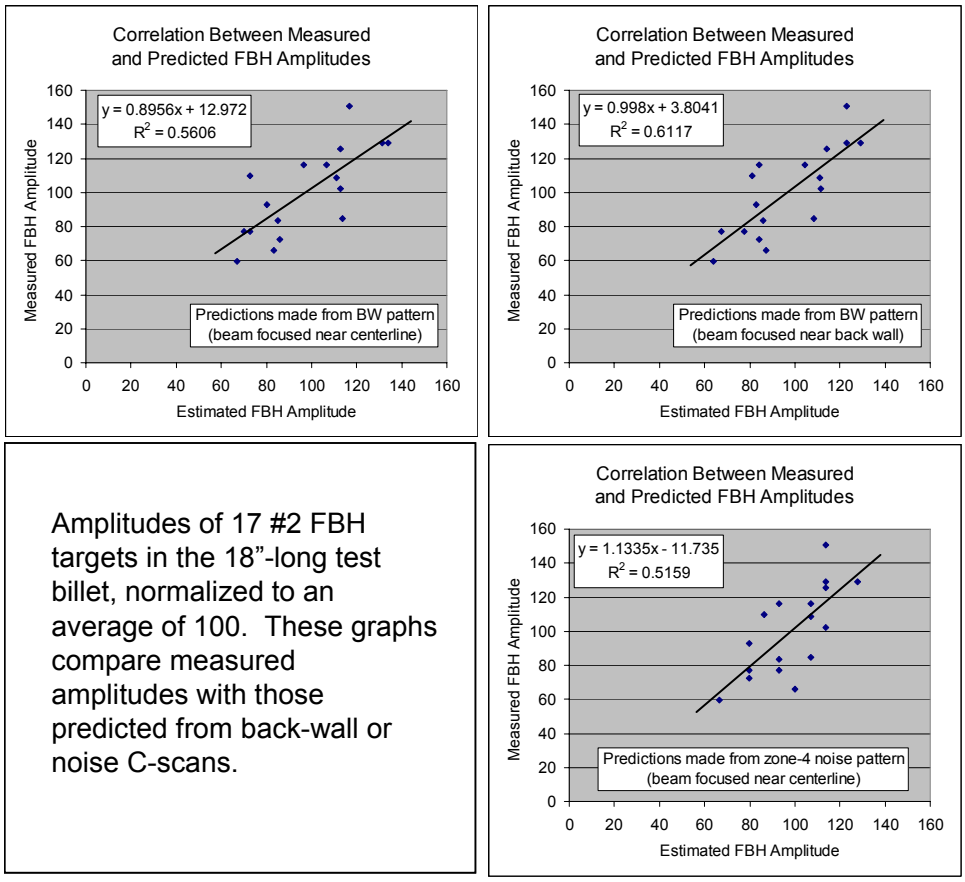

FIGURE 82. CORRELATION BETWEEN PREDICTED AND MEASURED FBH AMPLITUDES IN THE Ti-6-4 TEST BILLET

Local attenuation adjustments can be made either on their own or in combination with one of the global compensation procedures discussed earlier. The data resulting from the MZ inspection of the Ti-6-4 test billet has been postprocessed to show how the amplitudes of the 17 defects would appear if (1) local compensation was used alone, (2) local compensation was applied following the standard global compensation procedure; or (3) local compensation was applied following the semiconservative global compensation procedure. For each of the three combinations there are several cases, depending on whether local compensation made use of grain noise or back-wall amplitudes and on the choice of focusing method used to gather back-wall C-scans. The results are shown in figures 83 through 85. In a given figure, a single global adjustment procedure has been applied, e.g., the standard procedure for figure 84. For the upper three panels of each figure, the global adjustment (which is always based on back-wall amplitudes) has been made using data acquired with the beam focused near the centerline. For the lower three panels, the global adjustment is based on back-wall data with the beam focused on the back wall. From left to right in each figure, the result of ignoring local adjustments or applying local adjustments based on back-wall or noise amplitudes are displayed, respectively. For cases in which both the global and local adjustments are based on back-wall data, the same focusing scheme is assumed to have been used when acquiring that back-wall data.

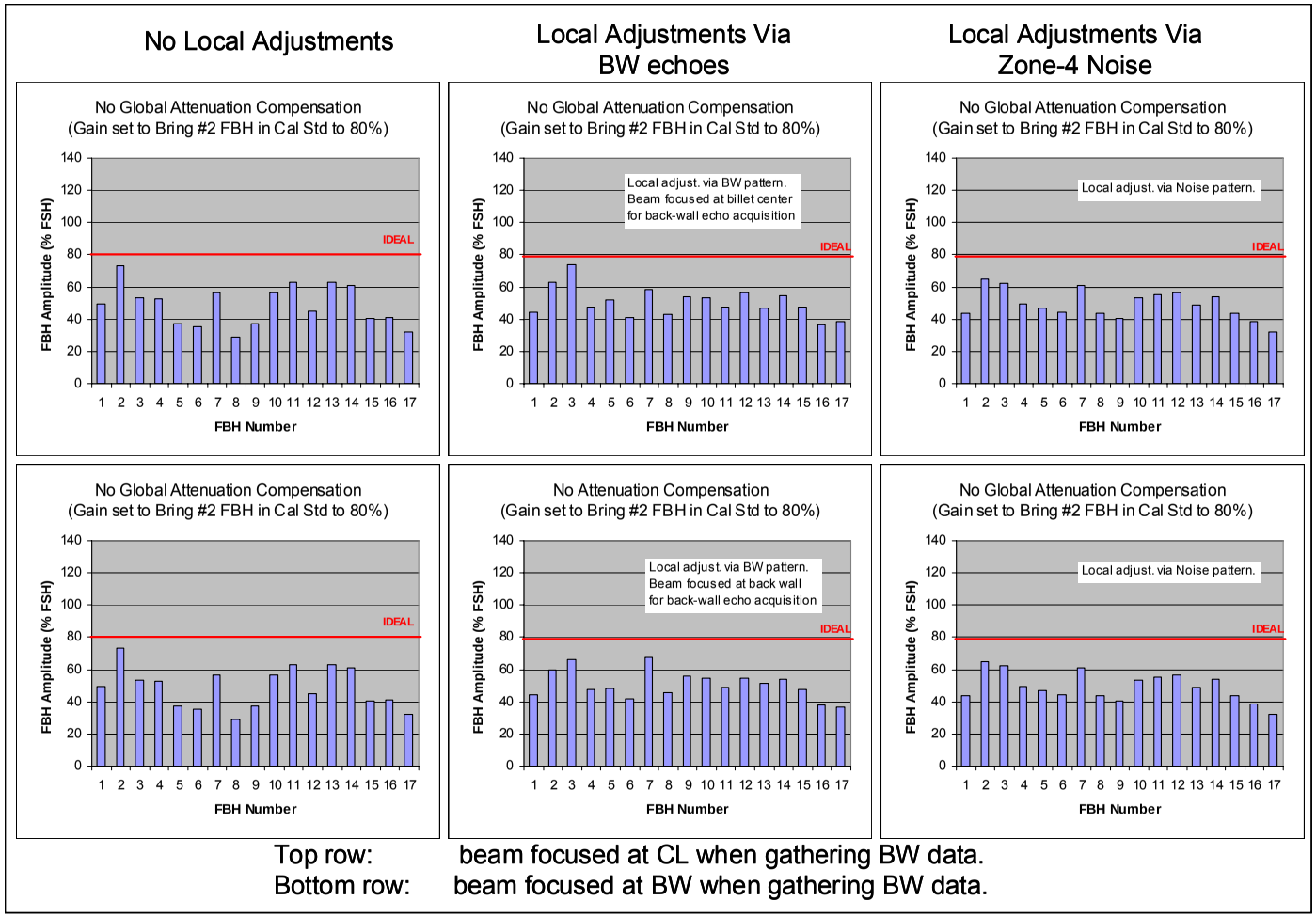

FIGURE 83. RESULTS OF APPLYING LOCAL ATTENUATION COMPENSATION PROCEDURES TO FBH AMPLITUDES IN THE Ti-6-4 TEST BILLET
(No global compensation has been used.)

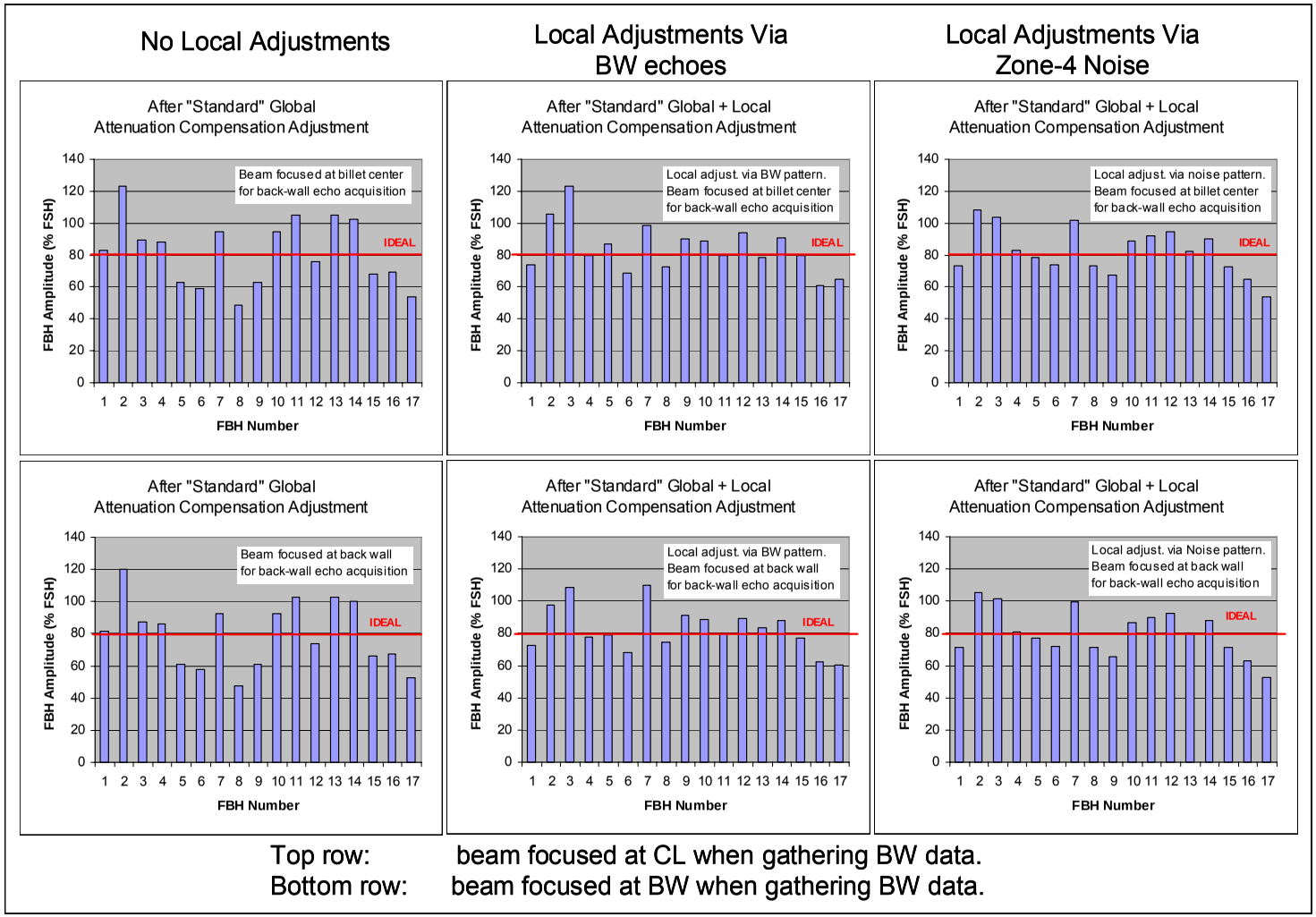

FIGURE 84. RESULTS OF APPLYING LOCAL ATTENUATION COMPENSATION PROCEDURES TO FBH AMPLITUDES IN THE Ti-6-4 TEST BILLET, STANDARD GLOBAL COMPENSATION
(Here, local compensation is used in combination with the standard global compensation procedure.)

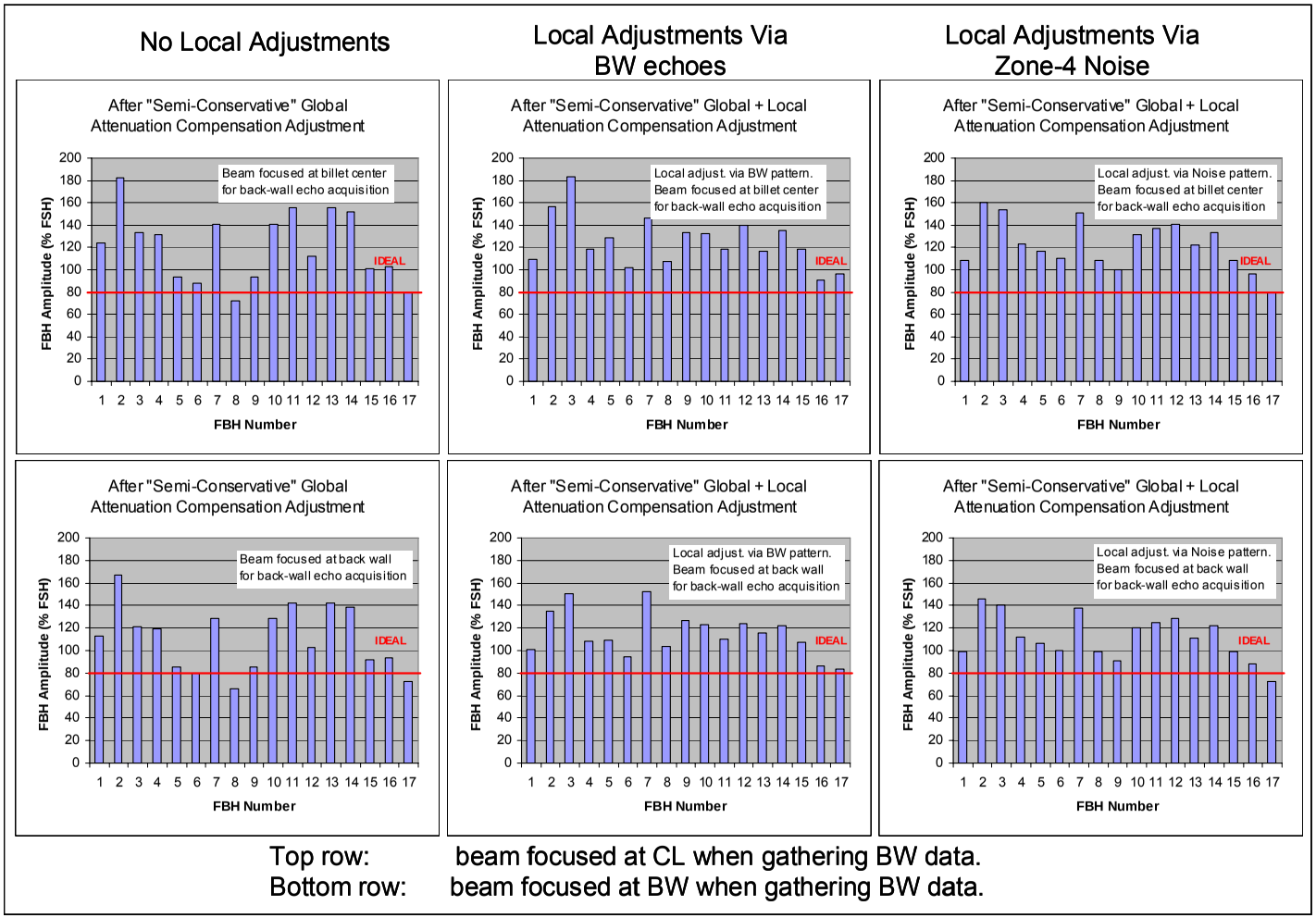

FIGURE 85. RESULTS OF APPLYING LOCAL ATTENUATION COMPENSATION PROCEDURES TO FBH AMPLITUDES IN THE Ti-6-4 TEST BILLET, SEMICONSERVATIVE—GLOBAL COMPENSATION
(Here, local compensation is used in combination with the semiconservative global compensation procedure.)

The various combinations of global + local attenuation adjustments considered in figures 83 through 85 are summarized in figure 86, and key statistics of the adjusted FBH amplitudes are listed in table 14. The tabulated statistics include the range of FBH amplitudes, the mean amplitude, the minimum and maximum amplitudes, the ratio of the standard deviation to the mean (which serves as a measure of the severity of the fluctuations), and the number of amplitudes below the target level of 80% FSH. A study of figures 83 through 85 and table 14 reveals that local adjustments based on equations 3 and 4 tend to reduce the fluctuations of the FBH amplitudes about their mean without a significant change in the mean amplitude. The standard deviation of the fluctuations is reduced by about 40% for local adjustments based either on back-wall amplitudes or center zone grain noise. When the standard global procedure is combined with the different local adjustment methods, about half of the FBH amplitudes remain below 80% FSH. However, when local adjustments are combined with the semiconservative global procedure, all adjusted FBH amplitudes (with one exception) were greater than 80% FSH. That one exception occurred for FBH #17 (see figure 64 for FBH #17 location) when backscattered noise from zone 4 was used to make the local adjustments. In the zone 4 C-scan image, just below and right of FBH #17 (see figure 69), heightened noise amplitudes are seen, which may actually result from a defect in that vicinity. These heightened signals boost the assigned mean noise level near FBH #17 when the automatic analysis software is used. The larger mean noise amplitude then results in a smaller local attenuation adjustment than would otherwise be the case. Thus, the fact that the adjusted amplitude for FBH #17 is slightly below 80% (using the semiconservative global + noise-based local procedures) may in fact be due to the presence of defects. Hard alpha defects are known to exist in the CBS billet heat from which the test specimen was fabricated [7].

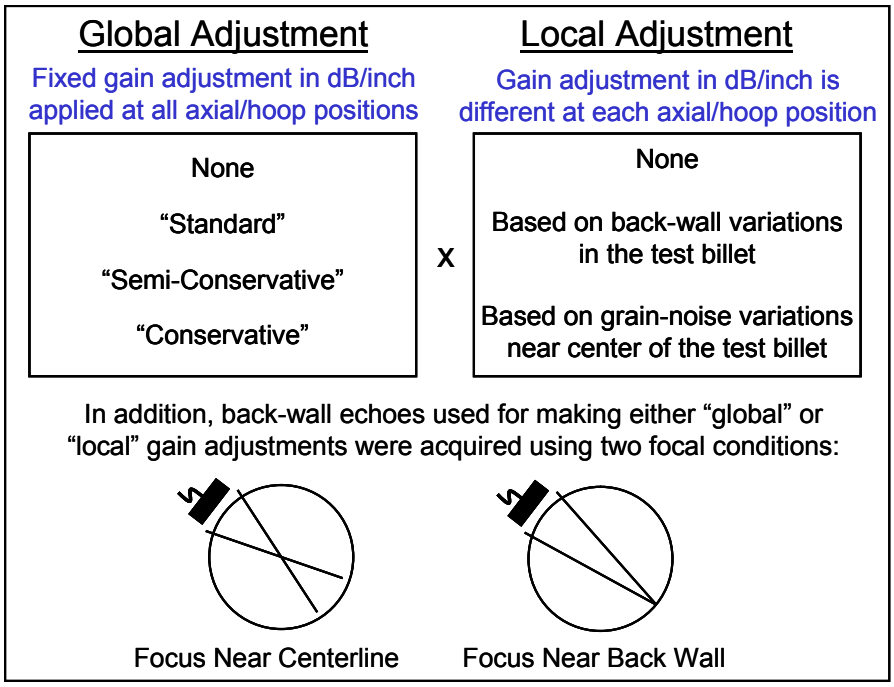

FIGURE 86. COMBINATIONS OF GLOBAL AND LOCAL ATTENUATION COMPENSATION PROCEDURES CONSIDERED IN THIS REPORT

TABLE 14. STATISTICS OF ADJUSTED FBH AMPLITUDE VARIATIONS IN THE 18″ LONG TEST BILLET FOR EACH OF THE ATTENUATION COMPENSATION PROCEDURES CONSIDERED

Attenuation Compensation Method Details			Statistics of 17 Adjusted FBH Amplitudes in the Test Billet				
Global Procedure	Local Procedure	Beam Focus for Back Wall C-Scan	Average (% FSH)	Range (% FSH)	Max/Min	Std. Dev./Avg.	Number Below 80%
None	None	N/A	48.7	29-74	2.53	0.26	17
None	Via back wall C-scan	At billet centerline	50.5	36-74	2.02	0.18	17
None	Via back wall C-scan	At billet back wall	50.7	37-67	1.82	0.17	17
None	Via zone 4 noise	N/A	49.3	32-65	2.01	0.18	17
Standard	None	At billet centerline	81.5	49-123	2.53	0.26	8
Standard	None	At billet back wall	79.6	48-120	2.53	0.26	8
Standard	Via back wall C-scan	At billet centerline	84.4	61-123	2.02	0.18	6
Standard	Via back wall C-scan	At billet back wall	82.8	60-110	1.82	0.17	9
Standard	Via zone 4 noise	At billet centerline	82.4	54-108	2.01	0.18	8
Standard	Via zone 4 noise	At billet back wall	80.5	53-106	2.01	0.18	8
Semiconservative	None	At billet centerline	121.1	72-183	2.53	0.26	1
Semiconservative	None	At billet back wall	110.4	66-167	2.53	0.26	2
Semiconservative	Via back wall C-Scan	At billet centerline	125.4	91-183	2.02	0.18	0
Semiconservative	Via back wall C-scan	At billet back wall	114.8	84-152	1.82	0.17	0
Semiconservative	Via zone 4 Noise	At billet centerline	122.5	80-160	2.01	0.18	0
Semiconservative	Via zone 4 Noise	At billet back wall	111.7	73-146	2.01	0.18	1
Conservative	None	At billet centerline	188.6	113-284	2.53	0.26	0
Conservative	None	At billet back wall	142.6	85-215	2.53	0.26	0
Conservative	Via back wall C-scan	At billet centerline	195.3	141-284	2.02	0.18	0
Conservative	Via back wall C-scan	At billet back wall	148.2	108-197	1.82	0.17	0
Conservative	Via zone 4 noise	At billet centerline	190.7	124-250	2.01	0.18	0
Conservative	Via zone 4 noise	At billet centerline	144.2	94-189	2.01	0.18	0

In general, local attenuation adjustments based on back-wall amplitudes were found to be slightly superior to those based on backscattered noise, and when back-wall amplitudes were used, adjustments computed with the beam focused on the back wall were slightly superior to those computed with the beam focused at the billet centerline.

3.8 SUMMARY AND RECOMMENDATIONS FOR ATTENUATION COMPENSATION.

Cylindrical billets of Ti alloy are ultrasonically inspected prior to use in fabricating rotating jet engine components. Although each billet has a cylindrical geometry, its UT properties are not cylindrically symmetric due to asymmetries in the process used to produce the billet from the cast ingot. In the inspection process, a calibration standard of the same diameter containing FBH reflectors is used to set the initial inspection gain (i.e., the signal amplification level). If the UT attenuation of the billet to be inspected differs significantly from that of the calibration standard, or if attenuation varies significantly with position within either the standard or test billet, then the inspection gain should be adjusted to achieve the desired defect detection sensitivity. Implementing such gain adjustments is referred to as attenuation compensation. Several procedures for determining attenuation-compensated gains were investigated and tested using 6″ diameter Ti-6Al-4V billet into which many FBH were drilled.

Two billet specimens were fabricated for the study. The first, 15″ long, contained 13 shallow #4 FBHs drilled 0.3″ into the billet OD at various locations spanning a wide range of back-wall amplitudes. The purpose of this specimen was to determine whether the large back-wall amplitude variations evident in C-scan images implied that echoes from a collection of small, identical defects (FBH reflectors) would display similar large variations. FBH amplitudes and back-wall amplitudes at nearby locations were measured using both fixed-focus and phased array transducers. Two basic focal procedures (local and global) were investigated, having the sonic beam focused near the billet centerline and back wall, respectively. Six measurement trials were conducted, and for each trial, the FBH and back-wall amplitudes were found to vary significantly within the billet. These amplitude variations were believed to result from variations of the local UT attenuation within the test billet. For FBHs, the ratio of maximum-to-minimum amplitudes ranged from 2-4, depending on the inspection details. This FBH variability was large enough that it should be specifically accounted for during inspections via some type of compensation procedure. FBH and back-wall amplitudes in the first test specimen were found to be fairly well correlated: sites with low (high) back-wall amplitudes tended to have low (high) FBH amplitudes as well. The fluctuation levels about the mean, and the degree of correlation between back-wall and FBH amplitudes, depended somewhat on the inspection setup. The back-wall and FBH fluctuation levels were more similar to one another (and the individual amplitudes more correlated) when the beam was focused near the back wall. Although nearby FBH and back-wall amplitudes were reasonably well correlated, a few exceptional cases were seen, i.e., sites at which the local back-wall amplitude was smaller than average while the nearby FBH amplitude was larger than average. Thus, it is wisest to use the back-wall fluctuation level as a general indicator of the level of expected FBH fluctuations, rather than inferring that a site with a low (high) back-wall amplitude will necessarily have a low (high) FBH amplitude as well.

The measurements on the first test specimen indicated that back-wall echo variations can be used to monitor attenuation variations within a billet, i.e., that defect amplitudes (in this case FBH

amplitudes) vary with lateral position in a similar manner to back-wall amplitudes. The measurements also indicated that attenuation compensation procedures should ideally account for both (1) the average attenuation difference between the calibration standard and test billet and (2) local attenuation variations within either the standard or the test billet.

To test various procedures for using back-wall amplitudes to compensate for attenuation, the second test specimen was fabricated. This 18″ long specimen contained 17 #2 FBHs located 3.5″ deep, i.e., at the far end of the depth range considered in either an MZ or CV inspection of 6″ diameter billet. The FBH sites were chosen on the basis of the back-wall and backscattered noise C-scan patterns to span the widest possible amplitude range. A standard MZ inspection of the second test specimen was carried out without attenuation compensation, and the amplitudes of the 17 FBH targets were measured relative to that of a similarly sized FBH located 3.5″ deep in the calibration standard. The data was then postprocessed to determine the effect of applying various attenuation compensation procedures. In the simulated inspections, the amplitude of the 3.5″ deep #2 FBH in the calibration standard was set to 80% FSH; and it was desired that all of the #2 FBHs in the test billet produce adjusted amplitudes of 80% FSH or higher and, hence, be identified as rejectable defects.

The gain adjustments considered fall into two broad categories:

- Global attenuation compensation procedures in which a fixed gain adjustment (in dB/inch units) is applied at all axial and hoop locations in the test billet. These adjustments are based on the back-wall C-scan patterns of the calibration standard and the test billet. Current inspection practice uses only global procedures.

- Local attenuation compensation procedures in which the gain adjustment varies with axial and hoop location in the test billet. These adjustments are based on C-scan patterns of back-wall amplitude or backscattered grain noise in the test billet.

Three global compensation procedures were considered distinguished by how conservative one wishes to be in the adjustment procedure. These procedures are referred to as

- Standard: To deduce the attenuation difference, one compares average back-wall amplitudes in the calibration standard and the test billet. This corresponds to assuming that the calibration hole is located in an average attenuation region in the standard and that the target flaw is located in an average attenuation region of the test billet. This may be regarded as the current standard practice for attenuation compensation.

- Semiconservative: One compares (avg. + std. dev. of back wall) in the calibration standard to (avg.-std. dev. of back wall) in the test billet. This corresponds to assuming that the calibration hole is located in a somewhat low-attenuation region (one standard deviation above the average back-wall amplitude) of the calibration standard and that the target flaw is located in a somewhat high-attenuation region of the test billet.

- Conservative: One compares the back-wall amplitude seen in the brightest region of the calibration standard C-scan to the back-wall amplitude in the dimmest region of the test

billet C-scan. This corresponds to assuming that the calibration hole is located in the lowest attenuation region of the standard and that the target hole is in the highest-attenuation region of the test billet.

Two fixed-focus transducers were used to acquire the back-wall C-scans on which the global (and some local) adjustments were based, one with the beam focused near the billet centerline and one with the beam focused near the billet back wall. Various combinations of global and local adjustments were considered in the study, as indicated in figure 86, and the results of applying each combination are summarized in table 14.

The first step consisted of global adjustments alone. It was found that the standard global attenuation compensation procedure accounts well for the overall attenuation difference between the calibration standard and the test billet (as it is designed to do), but does not treat local attenuation variations in either the standard or the test billet. When the standard compensation procedure was used, only about half of the target defects in the test billet were rejectable based on having a reflected amplitude exceeding the 80% target threshold. Moreover, those FBH defects having low amplitudes were not rejectable based on either amplitude or a commonly used signal-to-noise criterion (S/N > 2.5). The standard procedure was judged to be inadequate for either focusing method used to acquire back-wall echoes for attenuation compensation. The standard compensation procedure essentially overinspects low-attenuation bands in the test billet while underinspecting high-attenuation bands.

The semiconservative and conservative global compensation procedures apply higher inspection gains and consequently cause a larger number of the test defect amplitudes to exceed the 80% FSH threshold and, hence, be identified as rejectable. The additional gain (above that required by the standard procedure) was approximately 1 dB/inch for the semiconservative procedure and 2 dB/inch for the conservative scheme. Only one or two of the target FBHs had amplitudes below 80% FSH when the semiconservative adjustment procedure was used, depending on the focusing method used to acquire back-wall C-scan data. For the conservative procedure, all adjusted amplitudes were greater than 80%; however, the focus at back-wall approach accomplished this at lower inspection gain and, thus, is likely to lead to fewer false calls in noisy billets.

Although global attenuation compensation is easiest to accomplish at the inspection facility, local compensation procedures were also studied. The local compensation approach is regarded as a possible postprocessing tool to adjust amplitudes of candidate defects identified in the primary inspection that uses global compensation. Local compensation, as defined here, does not change the average amplitude of a large collection of defects distributed throughout the test billet, but does boost the amplitudes of defects located in high-attenuation regions and reduce the amplitudes of defects located in low-attenuation regions. Regions of low (high) attenuation are identified by higher (lower) than average back-wall amplitude or center zone grain noise. Local adjustments based on earlier equations 4 and 5 were found to reduce the fluctuations of FBH amplitudes in the test billet without a significant change in the mean amplitude. The standard deviation of the fluctuations was reduced by about 40% for local adjustments based either on back-wall amplitudes or center zone grain noise. When the standard global procedure is combined with the different local adjustment methods, about half of the FBH amplitudes still

remained below the 80% FSH target level. This results in an average sensitivity equal to a #2 FBH, with about 50% of FBH detected and 50% undetected. However, when local adjustments are combined with the semiconservative global procedure, virtually all adjusted FBH amplitudes were greater than 80% FSH. Local attenuation adjustments based on back-wall amplitudes were found to be slightly superior to those based on backscattered noise, and when back-wall amplitudes were used, local adjustments computed with the beam focused on the back-wall were slightly superior to those computed with the beam focused at the centerline.

Based on the above findings, several tentative recommendations can be made to improve inspection practice. It was noted in the test billet that FBH amplitudes at a given depth varied significantly with axial and hoop position, due to local attenuation variations. These variations will cause echo amplitudes from some defects (i.e., those located in high-attenuation bands) to be significantly below expected values, and such low-amplitude defects will not necessarily be rejected based on typical S/N criteria. Similar amplitude variations are also expected within the calibration standards themselves. Such variations would likely be obvious if the calibration standards contained several identical FBHs at a given depth, rather than the single hole typically used. If it is known that the FBHs in a given calibration standard have been drilled into high- or low-attenuation bands, that information can be used during attenuation compensation. Unfortunately, calibration holes in existing standards were drilled in random positions relative to attenuation banding patterns, and internal cavities within the standards usually preclude the measurement of back-wall echoes from the OD or backscattered grain noise from the centerline region. Thus, when using existing standards, it would be safest to adopt the conservative approach, i.e., to assume that FBHs in the calibration standard could have been drilled into low-attenuation bands, and that flaws in the billet may exist in high-attenuation bands. This will require the inspection gain to be boosted beyond that used for the standard compensation procedure currently being used for many inspections. Such gain boosts will necessarily increase absolute grain noise levels, particularly near the billet centerline, and may result in the deep zone regions of some billets being deemed uninspectable. Alternatively, the semiconservative adjustment approach could be used if combined with local compensation based on either back-wall amplitudes or centerline grain noise. However, attenuation compensation procedures based on global + local combinations may be too complicated at the present time for practical application at the factory.

When new calibration standards are made, the luxury exists of placing the FBH reflectors at axial and hoop locations of the owner's choosing. It is recommended that for new standards (1) FBHs should be drilled into high-attenuation bands, and (2) when these calibration standards are used in the inspection of other billets, one should compare zones of low back-wall amplitude in both the calibration standard and the test billet when deducing global attenuation adjustments. This will be equivalent to the conservative global compensation procedure. The adjustment procedure will be very similar to that currently being used at the factory; the only change is using low back-wall amplitudes rather than average back-wall amplitudes to compute gain adjustments. Again, inspection gains will effectively be boosted by both the increased gain needed to set these weaker FBH echoes in the calibration standard to 80%, and by the increased gain associated with computing adjustments using low-amplitude back-wall bands in the test billet. The recommended approach of drilling calibration holes into high-noise bands has been followed for

the fabrication of a new 14″ diameter Ti-6-4 billet standard constructed as part of the ETC Phase II program.

Finally, note that this study was based on specimens constructed from a single heat of Ti-6-4 billet produced several years ago, and that billet fabrication procedures evolved over time. Although the inspection procedure followed the MZ approach, it is believed that the basic findings would apply to CV inspections as well, since the findings follow from an inherent characteristic of the billets themselves, namely, the variation or banding of UT properties. The gain differences that separate the standard, semiconservative, and conservative attenuation compensation procedures depend on the severity of the banding. Anecdotal evidence indicates that some billet fabricators have been adjusting production procedures to limit noise banding, and this should serve to limit attenuation variations as well. As billet properties become more rotationally symmetric, the gain adjustment needed to implement the conservative compensation procedure will approach that of the current standard procedure. Increasing the inspection gain to implement a more conservative inspection will necessarily increase backscattered noise levels from the deeper zones where the gain adjustments are largest. In some cases, the increased noise levels may lead to undesirable false-call levels. For a given billet, the effect of such a change on peak and average noise levels can be readily calculated if back-wall and interior C-scan data are available. Those OEMs who have access to such archival data should use them to assess the effect on interior noise levels of adopting the recommended compensation procedures. If archival data is not available, attempts should be made to gather and store back-wall C-scan and interior noise data for current and future inspections. Such data will enable banding severity to be assessed and allow the effects of proposed modifications in inspection procedures to be determined.

3.9 ASSESSMENT OF LARGE-DIAMETER BILLET.

One of the goals of the program was to assess the sensitivity of MZ inspection for large (>10″) diameter Ti billets. The largest billet diameter used to make rotating parts of jet engines is 14″. Before the start of the program, 13″ was the largest billet diameter for which MZ transducers had been manufactured. Since an MZ transducer set did not exist for 14″ diameter billets, the approach was to concentrate exclusively on the inspectability of the region near the centerline of the billet. This was believed to be the most difficult region to inspect because of long metal travel and potential billet microstructure differences that could exist from the OD to centerline. This section describes the design and evaluation of the performance of transducers intended for the inspection of the region near the centerline of 14″ Ti billets.

The zoning scheme for MZ inspection of 14″ diameter billets is given in table 15. It is based on guidance in Aerospace Material Specification (AMS) 2628. The number of zones is dictated by the number of available channels of an MZ production system, which has a total of eight channels. One channel is reserved for monitoring the back-wall signal. Thus, the number of available channels for inspection is seven. The zone size for all zones, except the first two, is 1.1″. In this study, the concentration was on the inspection of the center zone of the billet, which is referred to as zone 7 in table 15. It spans from 6.4″ to 7.5″ and covers the centerline of the billet.

TABLE 15. ZONING SCHEME FOR MZ INSPECTION OF 14″ DIAMETER BILLETS

Zoning Scheme for 14″ Diameter Billets			
Zone	Start	End	Center
1	0.2	1.0	0.60
2	1.0	2.0	1.50
3	2.0	3.1	2.55
4	3.1	4.2	3.65
5	4.2	5.3	4.75
6	5.3	6.4	5.85
7	6.4	7.5	6.95

3.9.1 Chord Block Fabrication.

A chord block was designed to assess inspection sensitivity for zone 7 using both CV and MZ inspections. A schematic of the block is shown in figure 87.

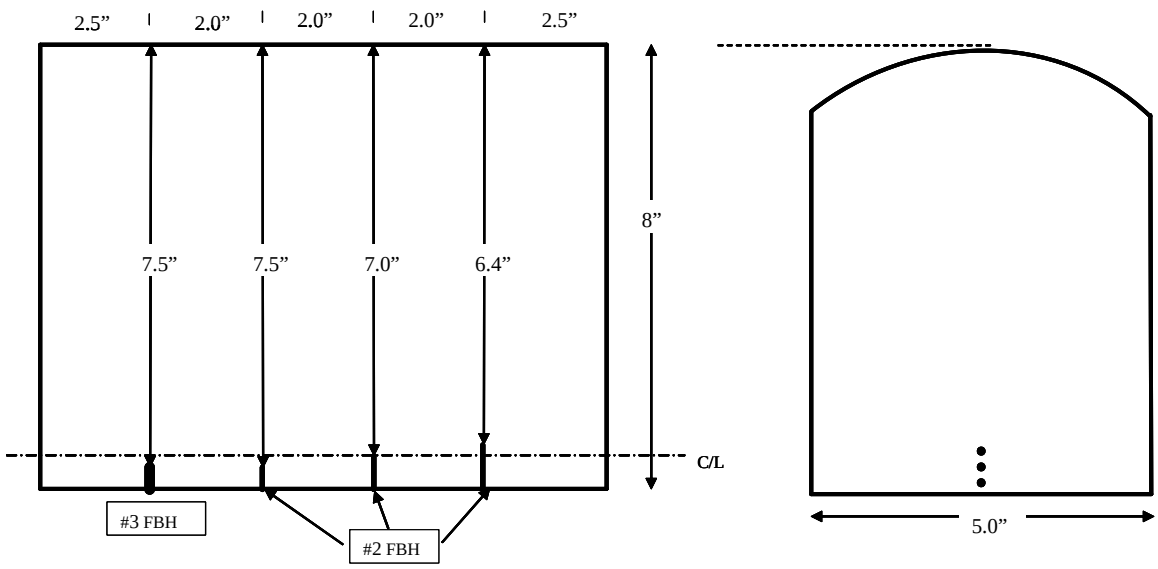

FIGURE 87. CHORD BLOCK SCHEMATIC

A 27″ long piece of 14″ diameter Ti-6-4 billet was acquired to make the chord block. The intent was to select a high-noise region from which to cut the chord block. To identify high-noise regions, the billet was scanned using a bicyclindrically focused transducer designed for the inspection of the central zone of 13″ diameter billet. The zone position for the noise scan is from 6″ to 7″. Calibration was performed using #3 FBH at 6″ and 7″ of a 13″ diameter Ti-6-4 calibration standard. The minimum of the two FBH responses was set to 80% FSH and an additional 7.5 dB was added to the gain to increase noise content of the C-scan image. The resulting C-scan of the billet is shown in figure 88 and reveals that noise is nonuniform through

the billet. The chord block was cut from the high-noise location marked with a black box. The final block has three #2 FBHs (0.03125″ diameter) at 6.4″, 7.0″ and 7.5″ depths and a #3 FBH (0.0469″ diameter) at 7.5″. The holes are spaced 2″ apart. The length of the block in the axial direction is 11″; the width of the block is 5″. Note that the noise is nonuniform within the sample. Higher noise is exhibited towards the right end of the billet. The shallower holes were placed in this region. In Ti billets, higher noise is associated with lower attenuation. Thus, the attenuation is lower towards the end of the chord block where the 6.4″ deep hole is placed.

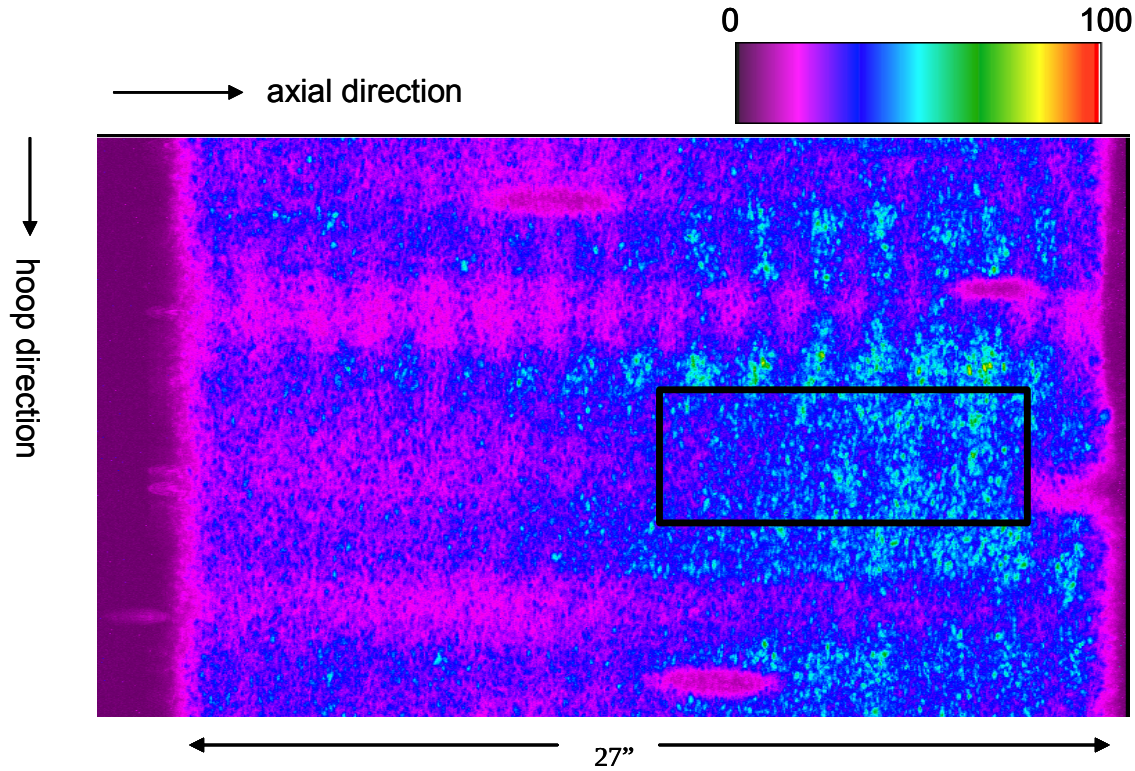

FIGURE 88. NOISE SCAN OF THE BILLET FROM WHICH CHORD BLOCK WAS MADE (Transducer used for inspection of central zone of 13″ diameter billet was used, gate: 6.0″-7.0″. Setup: Ti #3 FBH 80% + 7.5 dB. The location of chord block is marked with a black box.)

In addition to the chord block, a 10″ long, full-round piece was cut for attenuation compensation measurements. The purpose of this piece was to compare attenuation between the material of the chord block and the material of the billet to be inspected.

3.9.2 Baseline CV Inspection.

First, the chord block was scanned with a transducer used in CV inspection. The transducer was made available by a billet supplier. This was a 5-MHz, cylindrically focused transducer with focal length of 7″. The transducer had a rectangular element with a length of 0.75″ in the axial direction of the billet and 1.0″ in the circumferential direction. The entire chord block was scanned with a 2.2″ water path. The resulting C-scan image is shown in figure 89(a). One can see that only the #3 FBH is detectable in this case. After that, the area containing #3 FBH was rescanned with a water path of 3.0″. This water path is used in the production inspections with

this transducer by a supplier. Figure 89(b) shows the resulting image. Although the amplitude reflected from #3 FBH signal was reduced, the SNR stayed approximately the same. SNR was calculated using the formula used by the MZ inspection system:

$$SNR = \frac{P_s - \mu_n}{P_n - \mu_n} \quad SNR = \frac{P_s - \mu_n}{P_n - \mu_n}$$

where P_s is the peak signal from the defect of interest, P_n is the peak noise, and μ_n is the mean noise in the surrounding area. In both scans, the SNR was approximately 1.5. Note, that this is a conservative way to evaluate inspection sensitivity, because the scans were collected with constant gain, selected such that #3 FBH at 7.5″ depth gives a signal with amplitude equal to 80% of FSH. In actual measurements, DAC is used and such a high gain is only applied to the 7.5″ deep FBH signal. The conclusion is that the CV inspection, which uses a single transducer to inspect the entire volume of 14″ diameter Ti billet, can resolve #3 FBH near the center of the billet but cannot resolve #2 FBHs. Also, SNR ratio for #3 FBH is low. But because of the large beam footprint, this inspection is not highly sensitive to transducer misalignment and billet geometry imperfections.

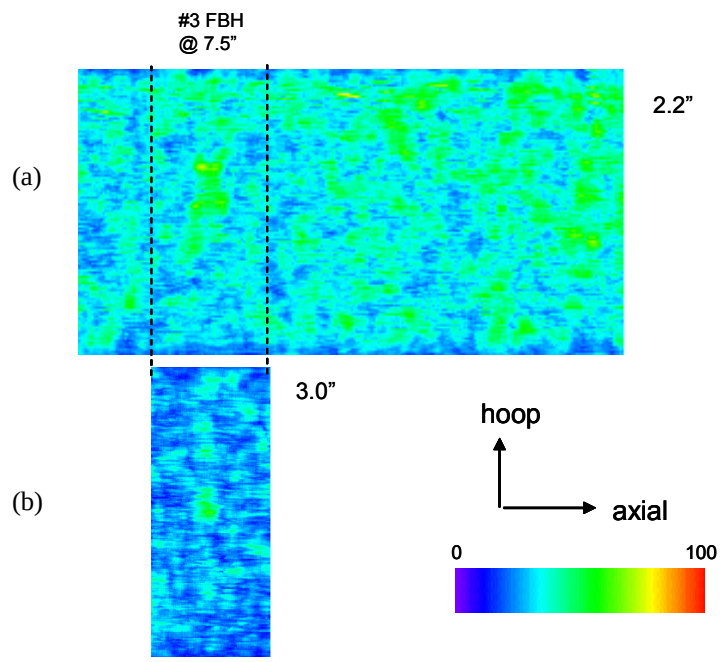

FIGURE 89. SCANS OF THE CHORD BLOCK WITH A TRANSDUCER USED IN A CV INSPECTION (a) WATER PATH = 2.2″ AND (b) WATER PATH = 3.0″
(The location of #3 FBH is marked with a rectangle.)

After completion of the CV inspection, an MZ transducer originally designed to inspect the center zone (6″-7″) of 13″ diameter billet was used to scan the chord block. This transducer is a master standard used for internal GE activities for the production inspection of 13″ diameter billets with a 3″ water path. It has a circular element of 2.35″ diameter. Its focus in the hoop

direction is 10.0″ and in the axial direction is 30.6″. The chord block was scanned with 3″ water path, generating the image shown in figure 90(a). In addition to the #3 FBH, it was also possible to resolve #2 FBHs at 6.4″ and 7.0″ depths. Only the #2 FBH at 7.5″ depth remained undetectable. An attempt was made to focus deeper by shortening the water path to 2.5″. But the #2 FBH at 7.5″ depth still remained undetectable. The resulting C-scan image is shown in figure 90(b). As expected, the MZ transducer provided better sensitivity than the conventional transducer. The expectation was to achieve further sensitivity improvement by designing a transducer that specifically targets the inspection of the central zone (6.4″-7.5″) of 14″ diameter billet.

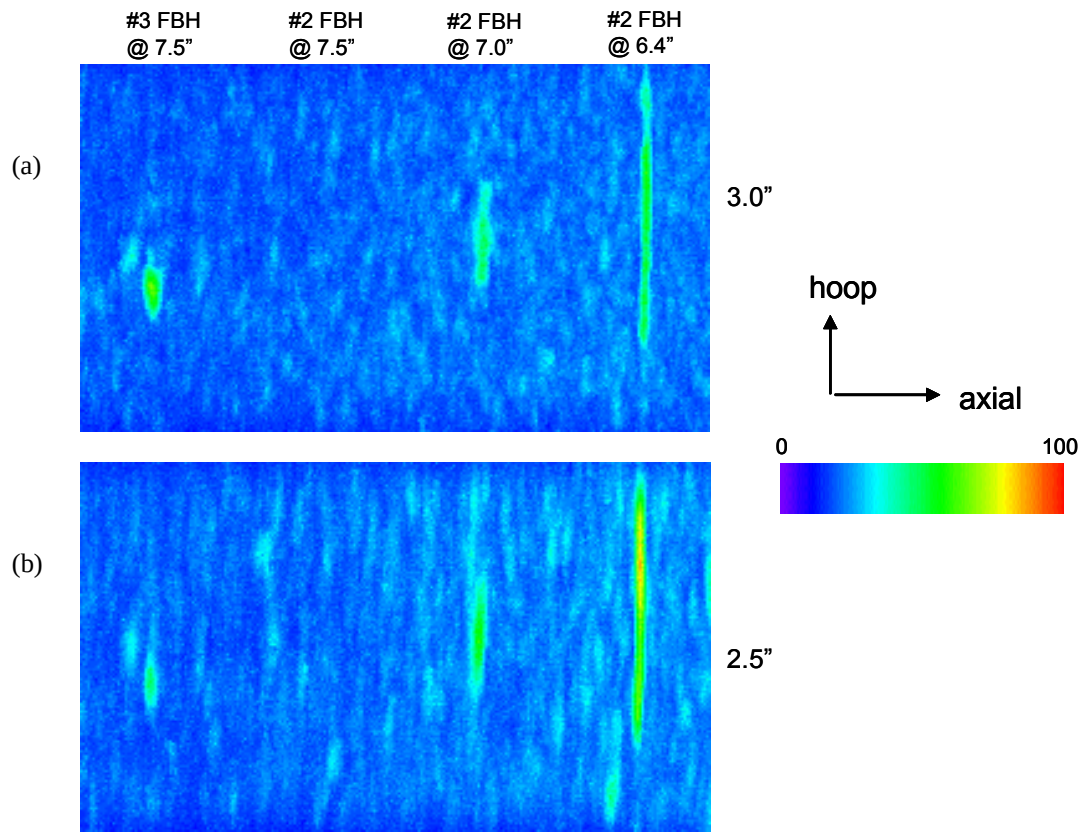

FIGURE 90. SCANS OF THE CHORD BLOCK WITH AN MZ TRANSDUCER DESIGNED FOR THE INSPECTION OF THE CENTRAL ZONE OF 13″ DIAMETER BILLET (5 MHz, 2.35″, FOCUS 6.45″ IN 13″ BILLET) (a) WATER PATH = 3.0″ AND (b) WATER PATH = 2.5″

3.9.3 Transducer Design.

It was assumed that the desired transducer has an elliptical element and bicyclindrical focus and its center frequency is 5 MHz and bandwidth is 60%. Such a transducer is characterized by four parameters, as shown in figure 91 and discussed in section 3.2.2. There are two dimensions: diameter in circumferential direction (D_x) and diameter in axial direction (D_y), and two geometrical focal lengths: circumeferential (F_x) and axial (F_y).

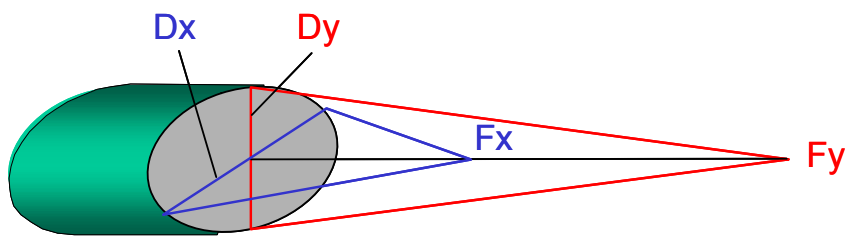

FIGURE 91. SCHEMATIC OF AN ELLIPTICAL ELEMENT, BICYLINDRICALLY FOCUSED TRANSDUCER

Ray-tracing calculations were performed. Assume that one wants to design a bycylindrically focused transducer that focuses at depth, F_1, in a billet of radius, R, made of material with longitudinal wave speed, V_1.

Geometrical focal lengths are defined by the following formulae:

$$F_x = wp + F_1 \frac{V_1}{V_0}$$

$$F_y = wp + \frac{F_1}{\frac{F_1}{R} - \frac{V_0}{V_1}\left(1 - \frac{F_1}{R}\right)}$$

where wp is the desired water path and V_0 is the wave speed in water. Transducer dimensions are given by the formulae below:

$$D_x = 2\theta_1\left(wp\frac{V_0}{V_1} + F_1\right)$$

$$D_y = 2\theta_1\left[wp\left(\frac{F_1}{R} + \frac{V_1}{V_0}\left(1 - \frac{F_1}{R}\right)\right) + F_1\right]$$

where

$$\theta_1 = \tan^{-1}\left(\frac{0.5}{\frac{F}{D}\frac{V_0}{V_1}}\right)$$

$\frac{F}{D}$ is called the F number of the transducer. It defines the size of the beam at focus as well as the depth of the field as follows:

$$Beam\ Diameter = 1.03\frac{F}{D}\frac{V_0}{f}$$
$$Depth\ of\ field = 4\frac{V_0}{f}\left(\frac{F}{D}\frac{V_0}{V_1}\right)$$

Performing this calculation for the focus at the center (F_1 = 7″) of the 14″ diameter billet (R = 7″) for $\frac{F}{D} = 10$ and $\frac{F}{D} = 8$ one obtains the F/8 and F/10 (transducer #1) transducer designs in table 16. For optimal transducer performance, it is desirable to maximize the SNR. SNR is inversely proportional to the square root of pulse volume. Pulse volume is equal to the product of pulse duration and beam diameter. It was assumed that the transducer would have a central frequency of 5 MHz and, thus, pulse duration is fixed. In this case, in order to maximize SNR, one needs to minimize the beam diameter through the zone of interest. To determine beam diameter of a bicyclindrical transducer at a given depth, the UT model developed by ISU was used. To obtain the optimal transducer design, the beam size within the zone was minimized:

$$\min_{Fx,Fy,Dx,Dy} \left[Maximum\ beam\ diamter\ within\ the\ zone\ from\ 6.4'' \text{ to } 7.5''\right]$$

The direct search complex algorithm [28] was used to perform this minimization. The resulting transducer design is given in table 16 as optimal (transducer 2). As one can see, the transducer designed using this approach has an F value equal to 7.

Thus, there were three candidate designs: F/10 and F/8 that were obtained using the ray-tracing approach and the optimal design that was obtained by minimizing the beam diameter over the zone of interest. The next step was to model the performance of each of the designs and select which transducers to order. Figure 92 shows the comparison of on-axis profiles within the zone of interest for the above mentioned designs as well as for the central zone of the 13″ diameter billet transducer. Figure 93 shows beam diameters for the same four designs. As expected, the optimal design has the smallest beam diameter within the zone, but it has more variation in the responses from the middle and ends of the zone and would require the use of the DAC.

TABLE 16. SPECIFICATIONS OF TRANSDUCERS 1 (F/10) AND 2 (F/7) INTENDED FOR THE INSPECTION OF THE CENTRAL ZONE OF 14″ DIAMETER Ti BILLET AS WELL AS F/8 DESIGN AND EXISTING TRANSDUCER INTENDED FOR INSPECTION OF CENTER ZONE OF 13″ DIAMETER BILLET

F/8								
Zone	Zone Start	Zone End	Approximate Focus Depth	Aperture	Diameter X	Diameter Y	Radius of Curvature X	Radius of Curvature Y
Center	6.4″	7.5″	6.9″	F/8	5.10″	3.93″	10.04″	32.85″
F/10 (Transducer 1)								
Zone	Zone Start	Zone End	Approximate Focus Depth	Aperture	Diameter X	Diameter Y	Radius of Curvature X	Radius of Curvature Y
Center	64″	7.5″	6.9″	F/10	4.12″	3.18″	10.06″	33.29″
Optimal (Transducer 2)								
Zone	Zone Start	Zone End	Approximate Focus Depth	Aperture	Diameter X	Diameter Y	Radius of Curvature X	Radius of Curvature Y
Center	6.4″	7.5″	6.9″	F/7	6.08″	4.65	10.00″	32.24″
Center Zone Transducer of 13″ Diameter Billet								
Zone	Zone Start	Zone End	Approximate Focus Depth	Aperture	Diameter X	Diameter Y	Radius of Curvature X	Radius of Curvature Y
Center	6.0″	7.0″	6.5″	F/10	2.35″	2.35″	10.12″	33.15″

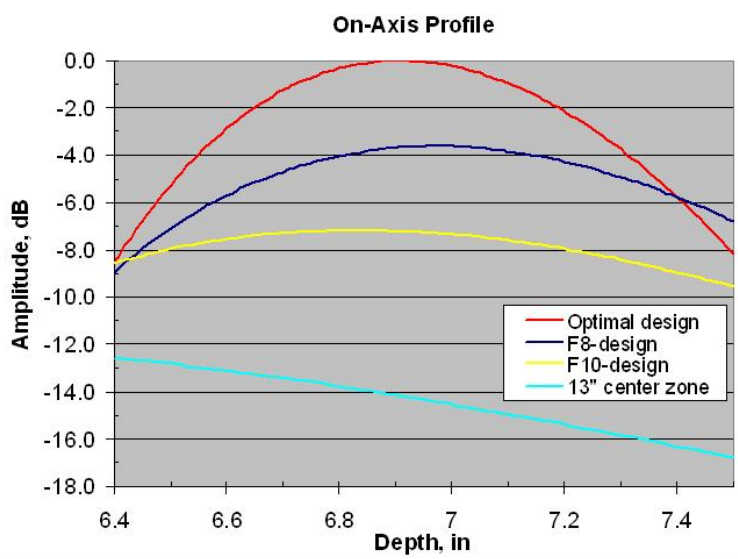

FIGURE 92. MODEL-PREDICTED ON-AXIS (RADIAL DIRECTION) RESPONSE WITHIN CENTER ZONE OF 14″ DIAMETER Ti BILLET FOR VARIOUS TRANSDUCER DESIGNS

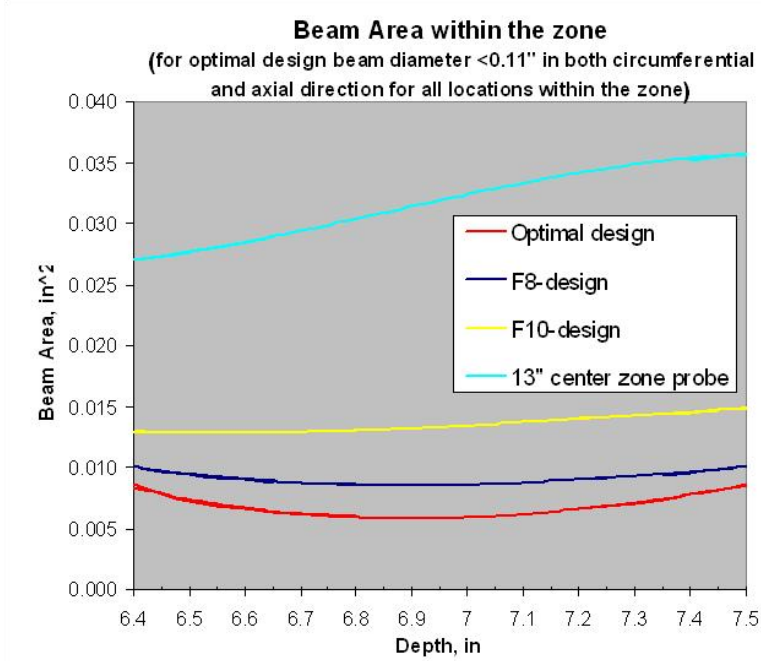

FIGURE 93. MODEL-PREDICTED BEAM SIZE WITHIN CENTER ZONE OF 14″ DIAMETER Ti BILLET FOR VARIOUS TRANSDUCER DESIGNS

The program included design and manufacture of two MZ transducers for the inspection of the zone around the centerline of 14″ diameter billet. The transducers were used to evaluate the chord block described above. The team selected two different designs: F/10 and the optimal design, which happened to be F/7. The F/10 transducer will be referenced as transducer 1 and the optimal design transducer as transducer 2. The transducers had the following requested specifications:

- Center frequency: 5.0 ±0.5 MHz
- Bandwidth: ≥ 60%
- Element material: Piezo-composite
- Focusing method: Curved element
- Excitation pulse: 300V exponential pulse with half-amplitude pulse width approximately 100 nsec
- Impedance matching: 50 ohms
- Receiver bandwidth: 25 MHz
- Operating water path: 3.0″

- Element profile is a bicylindrical surface (surface of a toroid), defined by two principal radii of curvature

- Element size and focal parameters are provided in table 16 with the following definitions:

  – x direction perpendicular to billet axis
  – y direction along billet axis

The two transducers were delivered as curved element transducers made of piezo-composite material. For curved element transducers, radii of curvatures are very close to geometrical focal lengths (GFL), which are used in the transducer modeling. Essentially, specifying the radii of curvatures was equivalent to specifying GFLs. Figure 94 shows the modeled beam area of these two transducers within the zone of interest. Figure 95 shows transducer 2.

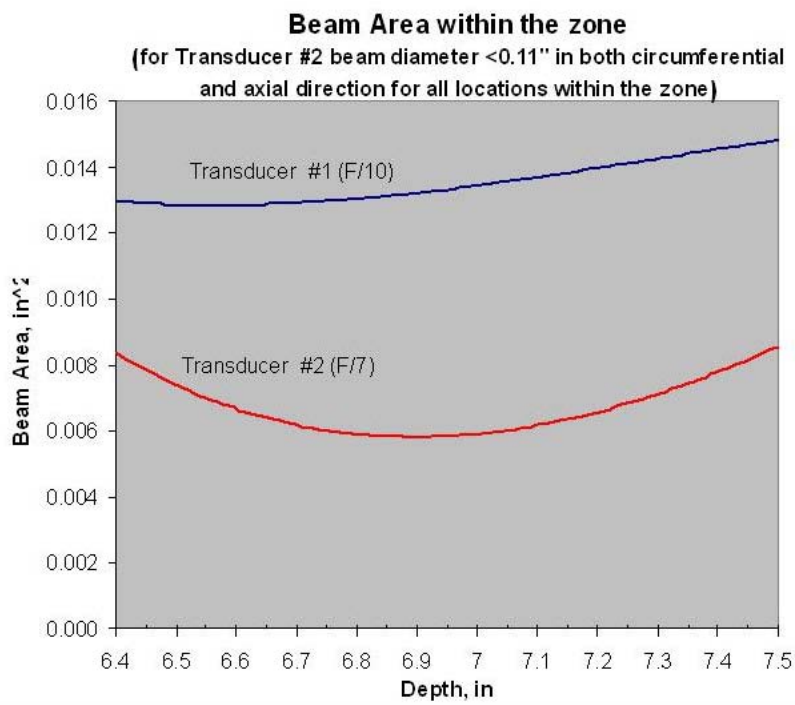

FIGURE 94. PREDICTED BEAM AREA WITHIN THE CENTRAL ZONE OF 14″ DIAMETER BILLET FOR TRANSDUCERS 1 AND 2

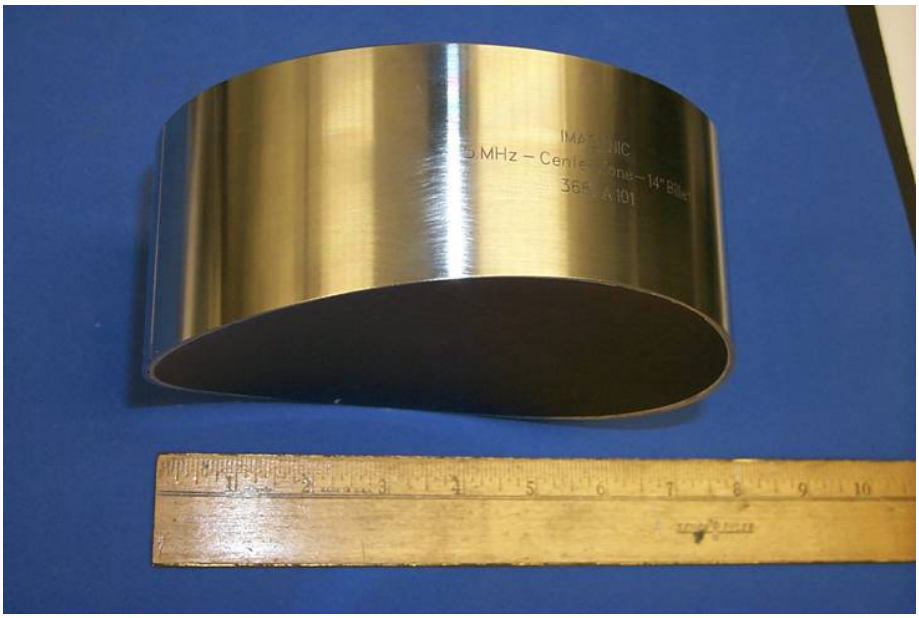

FIGURE 95. TRANSDUCER 2

3.9.4 Transducer Characterization.

Several steps have been performed to characterize the transducers. First, the transducer focal parameters were determined using the V(z) method [14] discussed in section 3.2.2. Second, a ball target in water was scanned using different water paths to assess the symmetry of the sound field. Third, measurements on the chord block were performed to assess the potential inspection sensitivity. The results are discussed with more details below.

The intent of the V(z) method for bicyclindrical transducers is to determine GFLs of the manufactured probe and to conclude if the transducer meets the specifications. This transducer characterization uses only a flat reflector and, thus, does not require calibration blocks. As discussed in section 3.2.2, it could potentially be done by the transducer manufacturer. An aluminum plate that was designed to be aligned with the UT tank rails was used as a reflector in these measurements. The water path was varied from 8″ to 36″ with 0.2″ step increments. The general setup arrangement for V(z) measurements is shown at figure 96. A front wall waveform was acquired at each position with 0.02 μsec resolution. Figure 97 shows acquired waveforms for several water paths for transducer 1.

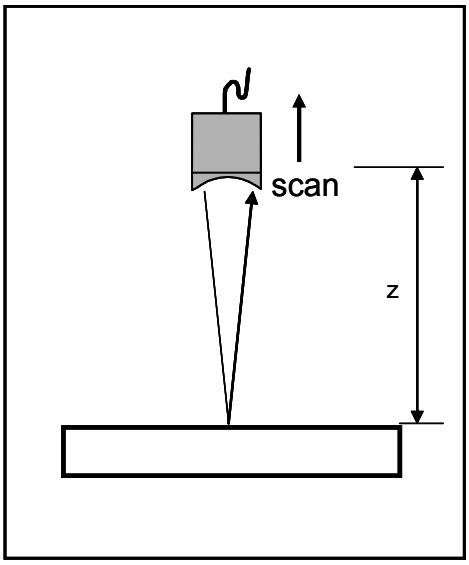

FIGURE 96. V(z) METHOD FOR TRANSDUCER CHARACTERIZATION

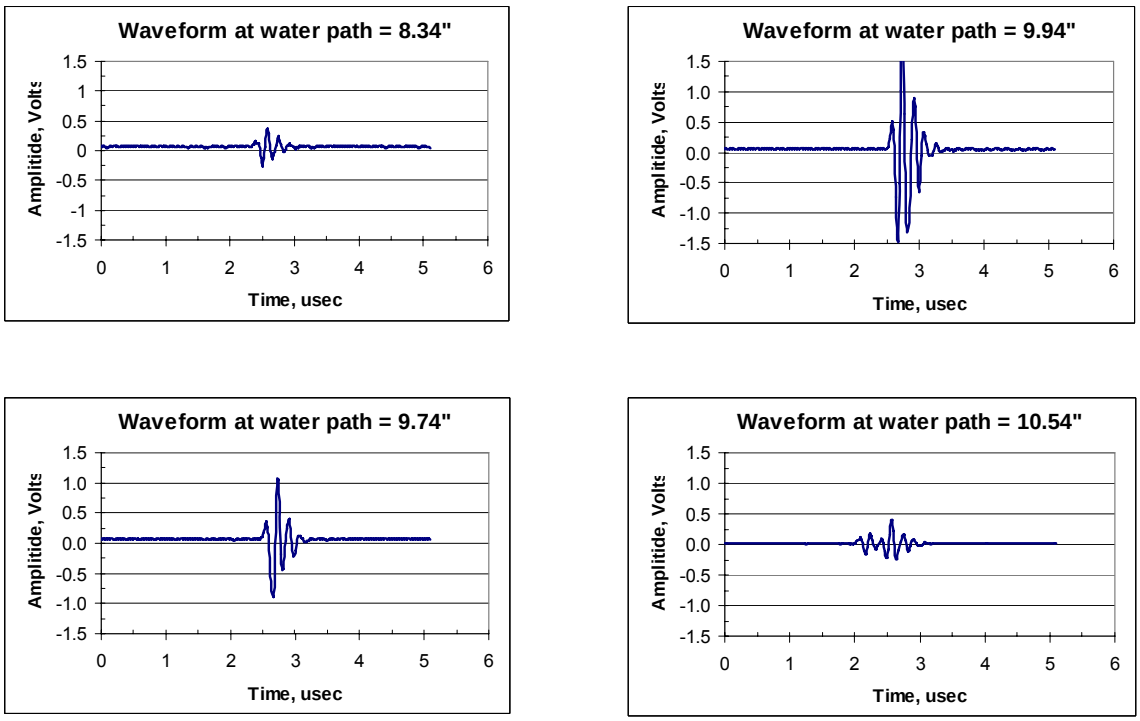

FIGURE 97. WAVEFORMS AROUND THE FIRST FOCUS OF TRANSDUCER 1

Spectral components of acquired waveforms are shown in figures 98 (transducer 1) and 99 (transducer 2) with circles for frequencies 4.69 and 6.08 MHz. One can see that there is a sharp peak at around the 10″ water path, which corresponds to circumferential focus and a smaller and wider peak at around 32″, corresponding to the axial focus. Given these results, it was assumed that actual element diameters are close to the designed values.

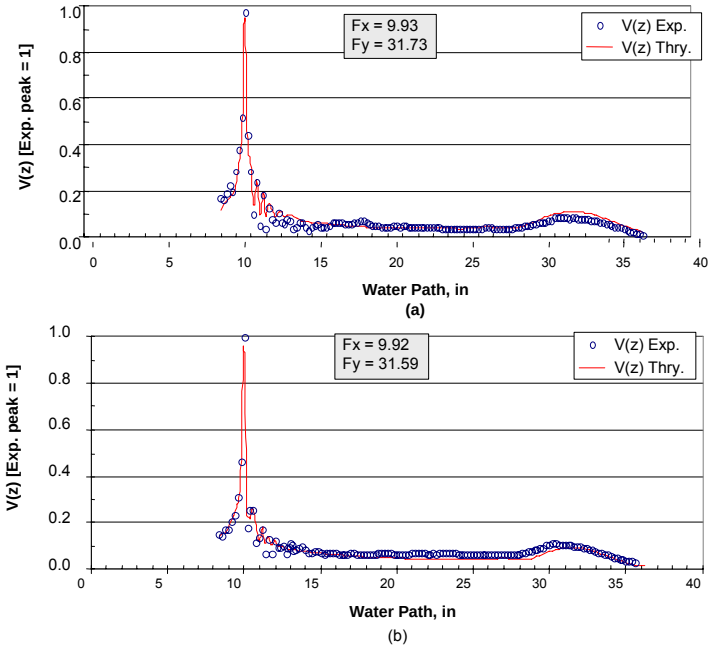

FIGURE 98. V(z) AT (a) 4.69 MHz AND (b) 6.08 MHz FOR TRANSDUCER 1 (Spectrum range used in reconstruction: 3.5-7 MHz. Reconstructed values for F_x and F_y are given.)

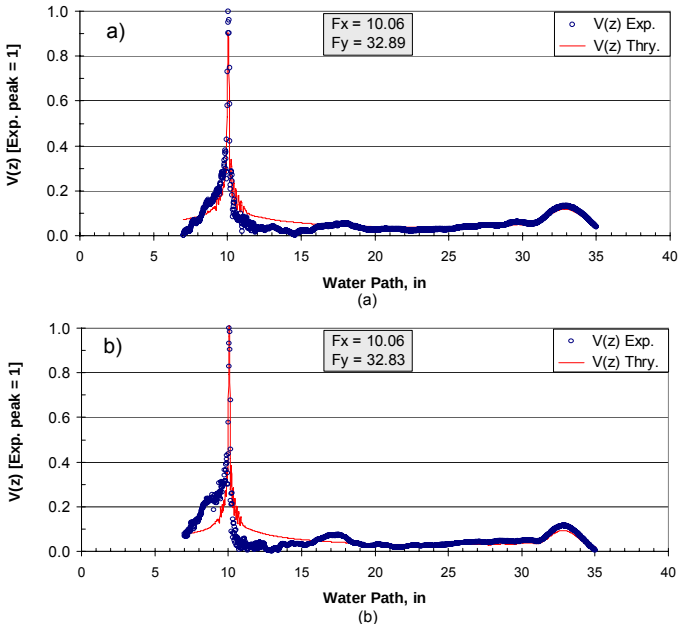

FIGURE 99. V(z) AT (a) 4.69 MHz AND (b) 6.08 MHz FOR TRANSDUCER 2 (Spectrum range used in reconstruction: 3.5-7 MHz. Reconstructed values for F_x and F_y are given.)

The two parameters determined by the inversion procedure, which minimizes the difference between measured and calculated V(z) curves, were GFLs in circumferential (F_x) and axial (F_y) directions. The reconstruction is performed for each frequency in the 3.5-7.0 MHz range. The solid line in figures 98 and 99 show the best fit for the theoretical prediction. At 4.69 MHz, the reconstructed value for F_x and F_y are 9.93″ and 31.73″, respectively. At 6.08 MHz, F_x = 9.92″ and F_y = 31.59″. Figure 100 shows the reconstructed values of F_x and F_y as a function of frequency.

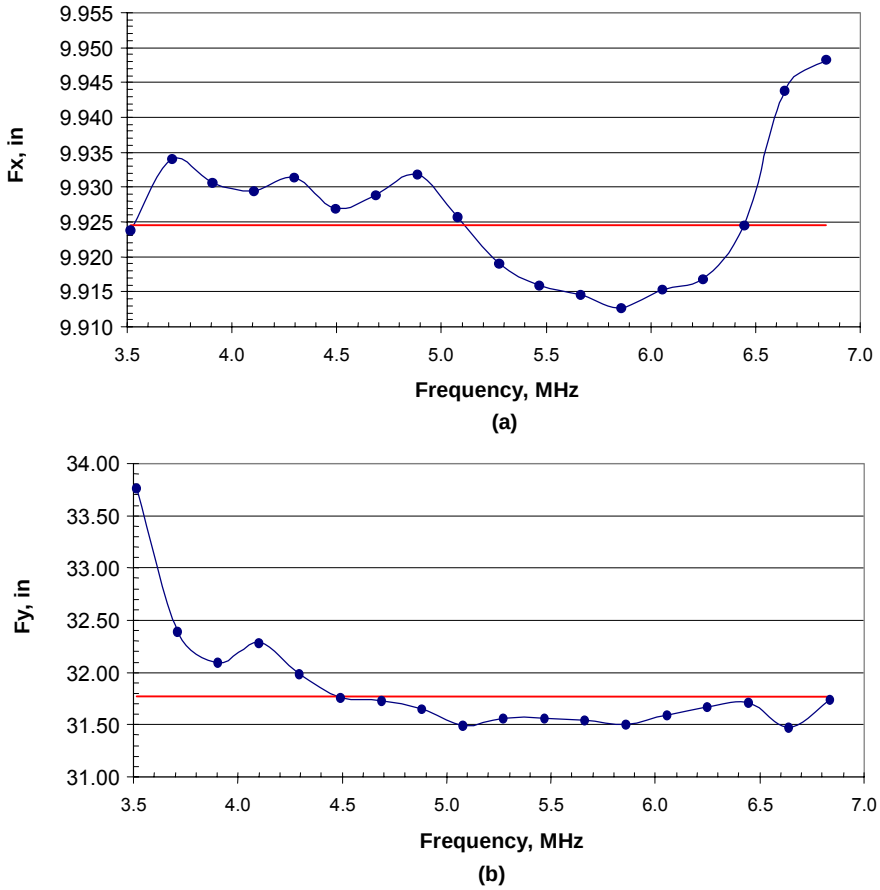

FIGURE 100. RECONSTRUCTION RESULTS FOR GFL IN (a) CIRCUMFERENTIAL, F_x, AND (b) AXIAL, F_y, DIRECTIONS AT VARIOUS FREQUENCIES FOR TRANSDUCER 1 (Spectrum range used in reconstruction: 3.5-7 MHz.)

The average reconstructed value for F_x = 9.93″ and for F_y = 31.41″. They are very close to the nominal values of F_x = 10.06″ and F_y = 33.29″. The second set of V(z) measurements was performed with 0.02″ water path increments. The reconstructed values of F_x = 9.92″ and F_y = 31.80″ were obtained form this data. One can see that reducing the step increment by a factor of 10 (0.02″ versus 0.2″) gave a very similar result. This indicated that the coarser step increment of 0.2″ was adequate. Figure 101 shows similar results for transducer 2. The reconstructed values versus nominal values for both transducers are given in table 17. One can see that the reconstructed values are close to the nominal ones.

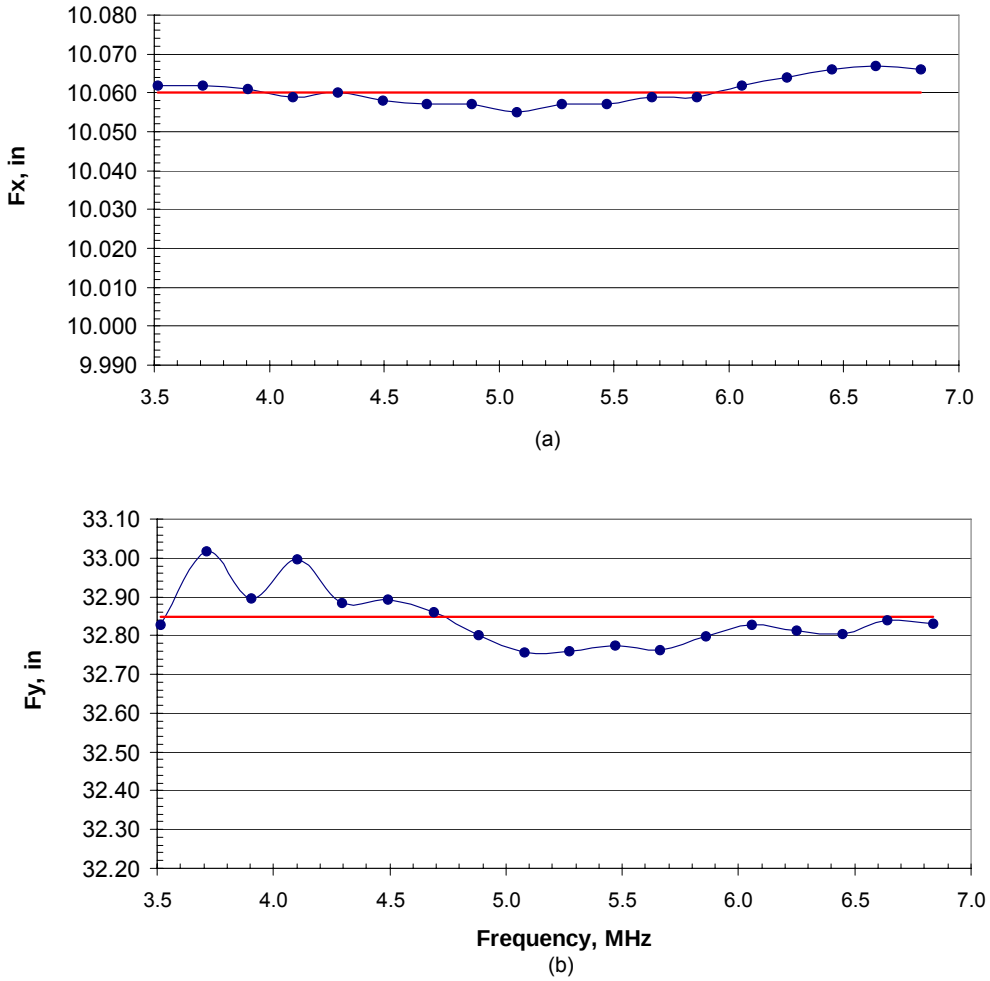

FIGURE 101. RECONSTRUCTION RESULTS FOR GFL IN (a) CIRCUMFERENTIAL, F_x, AND (b) AXIAL, F_y, DIRECTIONS AT VARIOUS FREQUENCIES FOR TRANSDUCER 2 (Spectrum range used in reconstruction: 3.5-7 MHz.)

TABLE 17. RESULTS OF V(z) RECONSTRUCTION FOR TRANSDUCERS 1 AND 2

	Transducer 1 (F/10)		Transducer 2 (F/7)	
	F_x (in.)	F_y (in.)	F_x (in.)	F_y (in.)
Nominal	10.06	33.29	10.00	32.24
Reconstructed	9.92	31.80	10.06	32.85

F_x, F_y reconstructed from V(z) curves.

To complete transducer characterization, the efficiency factor of the two transducers needed to be calculated. This was done by acquiring a reference waveform from 1″ deep #1 FBH in an IN100 calibration block with a water path of 5.15″. The water path was selected such that the transducer focused on the hole. To check for beam symmetry, a 5/16″ diameter steel ball target was scanned in water. Scans with different water paths were performed. Figure 102 shows the

comparison between measured and modeled scans for water paths of 9.91″, 11″, and 12″ for transducer 1. One can see that the transducer produces a symmetrical field and the model predicts well the empirical patterns. Similar results for transducer 2 are shown in figure 103.

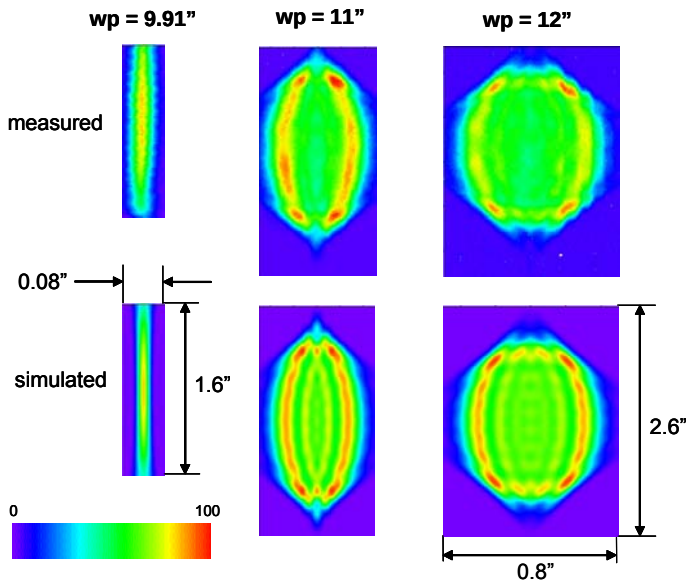

FIGURE 102. MEASURED AND SIMULATED C-SCANS OF 5/16″ DIAMETER STEEL BALL TARGET IN WATER FOR TRANSDUCER 1
(Ball target is near first focus of the transducer.)

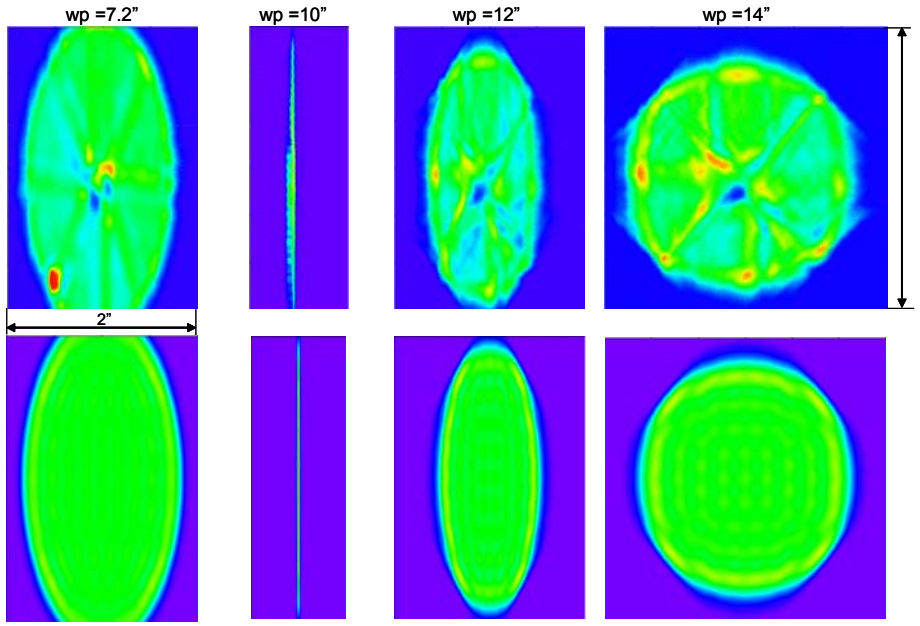

FIGURE 103. MEASURED AND SIMULATED C-SCANS OF 5/16″ DIAMETER STEEL BALL TARGET IN WATER FOR TRANSDUCER 2
(Ball target is near first focus of the transducer.)

From the described results, it was concluded that the transducers are well-behaved, i.e., they have frequency, bandwidth, and focal characteristics close to the desired parameters and generate a symmetrical beam pattern.

3.9.5 Chord Block Measurements.

Measurements on the chord block were performed with results for Transducer 1. The water path was selected to achieve the optimal zone balance. A water path of 2.5″ produces the zone balance of 1 dB (response from the #2 FBH at 6.4″ is equal to 50% FSH and from the #2 FBH response at 7.5″ equals 56% FSH). The chord block was scanned with this water path, and figure 104(a) shows the resulting C-scan. The locations of different FBHs are marked at the top of the image.

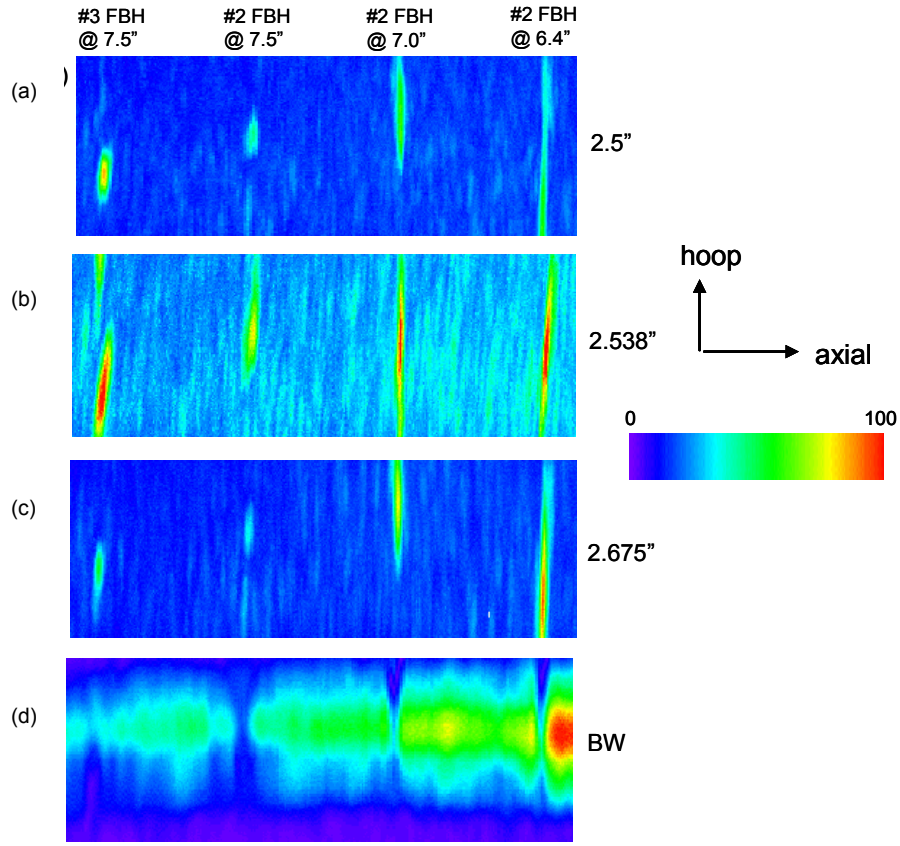

FIGURE 104. SCANS OF THE CHORD BLOCK WITH DIFFERENT WATER PATHS (a) WATER PATH = 2.5″; (b) WATER PATH = 2.538″, FOCUS AT 7.5″ DEEP #2 FBH; (c) WATER PATH = 2.675″, FOCUS AT 7.0″ DEEP #2 FBH; AND (d) BACK-WALL SCAN

To use the automatic SNR calculation feature of the GE-MZ software, the data was converted into MZ format. The results of SNR analysis using the GE-MZ software are shown in figure 105. For all #2 FBHs at 6.4″, 7.0″, and 7.5″, the SNR is greater than 2. Significant distortion of spatial response from the #2 FBH at 6.4″ was observed and is likely due to the microstructure

variations. The water path was adjusted by focusing at the 7.5″ deep #2 FBH and then at the 7.0″ deep #2 FBH. The resulting water paths, were 2.538″ and 2.675″, respectively. The chord block was rescanned with the new water paths, and figures 104(b) and 104(c) show the resulting C-scans for 2.538″ and 2.675″ water paths, respectively. From figure 104(c), one can see that focusing at the center of the zone (7.0″) does not produce the acceptable 3 dB zone balance. The reason for this can be explained by looking at attenuation changes in the axial direction. The back wall of the chord blocks was monitored to assess attenuation variability, and figure 104(d) shows the back-wall C-scan. One can see that the attenuation increases from right to left of the image, i.e., from shallower to deeper hole positions. The same behavior can be observed by looking at the noise in the billet from which the chord block was cut, as shown in figure 88. Noise is higher towards the right end of the box. It was demonstrated before that in Ti billet material, high noise and low attenuation are correlated [29]. Since it appears that attenuation is higher at the location of deeper holes, one needs to focus deeper to achieve the zone balance. Essentially, the focus needs to be even deeper than the 7.5″ deep hole to ensure the zone balance.

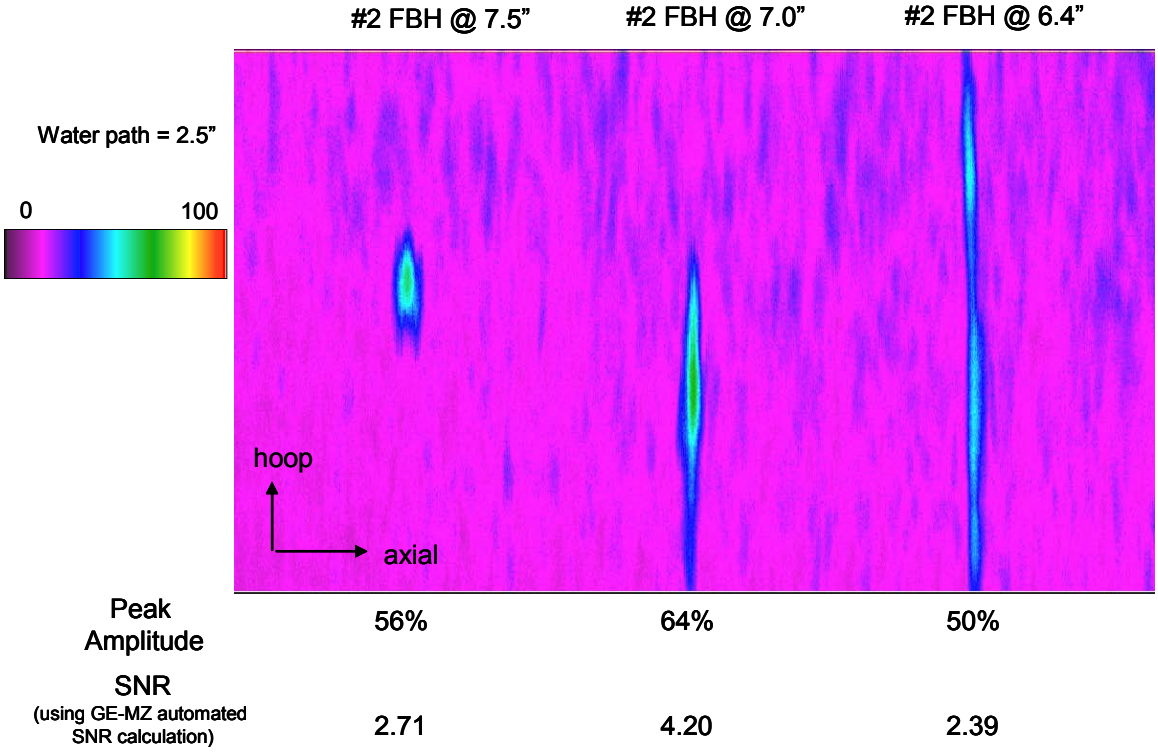

FIGURE 105. ANALYSIS OF ONE OF THE CHORD BLOCK SCANS (WATER PATH = 2.5″) USING AUTOMATIC SNR CALCULATION FEATURE OF GE-MULTIZONE SOFTWARE

Transducer 2 was also evaluated on the chord block. Zone balance was achieved at the 2.7″ water path. Figure 105 shows the C-scan from 6.4″, 7.0″, and 7.5″ deep #2 FBHs.

It was found that the amplitude of the signals from FBHs was extremely sensitive to alignment. The change in angular orientation of the probe in axial-radial plane of the billet of 0.2 degree

resulted in a 6 dB drop in the signal. It was also determined that when one tries to perform the alignment on the back side of the chord block, the amplitudes from FBHs were not maximized. These effects made the scanning of the block with transducer 2 very challenging. Figures 106(a) and 106(b) show two attempts to scan the block with a 2.7″ water path. Figures 106(c) shows the chord block scan with water path = 2.92″.

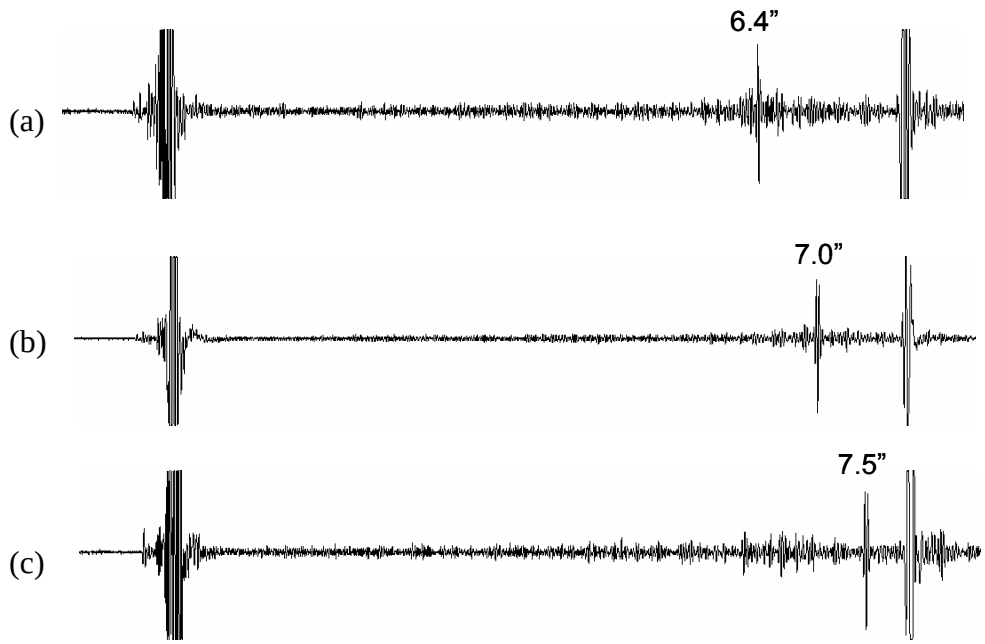

FIGURE 106. WAVEFORMS WITH RESPONSES FROM #2 FBHs IN CHORD BLOCK WATER PATH = 2.7″
(The only difference is axial position and gain. Gain is the same for 6.4″ and 7.5″ deep holes, and for a 7.0″ deep hole, the gain is 5 dB lower.)

With extreme care to arrive at alignment, it was possible to resolve #2 FBHs with SNR >2. For back-to-back comparison between transducers 1 and 2 performances, a more precise motion control system is required. If this transducer is to be used in actual inspections, there should be strict requirements on the geometry of the billet and the accuracy of alignment; otherwise, there is significant concern of creating blind zones since the beam size is very small. Based on these observations, transducer 2 does not seem to be practical for production inspections. However, it could be used to verify or achieve higher resolution in the area of a suspected indication, which was detected using the lower resolution inspection.

3.10 SUMMARY OF 14″ CHORD BLOCK EVALUATION.

It was demonstrated that #2 FBH sensitivity was achieved in the MZ inspection of the central zone of this 14″ diameter billet with at least 2:1 SNR, for this chord block material. Evaluation of a CV transducer indicated that a # 3 FBH sensitivity was achieved at 1.122 to 1 SNR. A considerable amount of effort was required to align the transducer for these measurements. The level of difficulty required to achieve the response indicates that reliable production inspection of

14″ diameter product would require additional assessment and potential development activities. Note that these measurements were made on a chord block, which limited the scanning motion. The results for a dynamic billet inspection, i.e., a billet rotation inspection, are not available and would require a full-round sample. While the results are encouraging, a considerable effort may be required prior to implementation of a new inspection.

4. SUMMARY AND CONCLUSIONS.

The focus of this program was on improvement to inspection sensitivity for Ti billet. Considerable effort went into the design and characterization of transducers, laboratory evaluation of transducer performance, understanding the effect of attenuation on detectability, and a limited feasibility study for large-diameter billet. The following are the primary conclusions:

- Computer-based transducer design models were developed in the Engine Titanium Consortium (ETC) Phase I program and further validated in the Phase II program. The models were successfully used in design of transducers for 10″ and 14″ diameter billet.

- Several transducer characterization methods were compared. Factors included the ability of the characterization method to adequately indicate performance of the probe, the measurement of parameters used in model calculations, and the ease of use in making the characterization measurement. Ease of use is important because it is desirable for the transducer vendors to be able to characterize a transducer prior to shipment and without the requirement for special samples. A method, known as V(z), was developed for use by vendors for future use in characterizing transducers. It was also demonstrated to provide necessary performance and model input information.

- Evaluation of F/10 and F/8 transducers in two of the zones (zones 2 and 4) showed that the F/10 transducer did not have sufficient signal-to-noise performance for the desired #1 flat-bottom hole (FBH) sensitivity.

- A full set of F/8 transducers was used to measure sensitivity to #1 FBH throughout the depth of the 10″ diameter billet. On average, the #1 FBH sensitivity target was met. However, it was necessary to divide zone 6 into two subzones to meet the desired sensitivity.

- Concerns exist with the current manufacture of large element transducers, particularly the ability to consistently deliver desired bandwidth and frequency repeatably.

- Measurements of back-wall echo variation were correlated with attenuation variations within a billet. It was found that back-wall amplitudes can be used to account for attenuation differences between the calibration standard and the test billet.

- Attenuation is a significant factor in billet inspection. Using existing setup procedures, the response from identical FBHs was found to vary from 24% to 93% when the expected response for all holes was 80%. Three different attenuation compensation procedures were evaluated. Both local and global compensation were included with the global

method deemed easiest to accomplish in a production inspection facility. Consideration should be given to false calls and accept/reject criteria when selecting the attenuation compensation procedure.

- It is recommended that the attenuation properties of the billet be taken into account in the design of calibration standards, particularly placement of FBHs.

- Two multizone (MZ) transducers, F/10 and F/7, were designed and fabricated for evaluation of a 14″ diameter chord block. The two curved element, piezo-composite transducers were evaluated on #2 and #3 FBHs at depths of 6.4″, 7.0″, and 7.5″. They were also characterized using the V(z) method. From the transducer characterization results, it was determined that the transducers had the desired frequency, bandwidth, and focal properties.

- The evaluation of the MZ transducers indicated that #2 FBH could be detected with a signal-to-noise ratio (SNR) of (>2:1). Amplitude of the signals was sensitive alignment. Based on limited work with the chord block, reliable MZ production inspection requires a full-round 14″ calibration standard.

- The evaluation of conventional 5 MHz transducer on a 14″ diameter chord block indicated that #3 FBH was achieved at a 1.122:1 SNR.

5. REFERENCES.

1. Keller, M., Patton, T., Degtyar, A., Umbach, J., Hassan, W., Kinney, A., Roberts, R., Margetan, F., and Brasche, L., "Inspection Development for Nickel Billet—Engine Titanium Consortium Phase II," FAA report DOT/FAA/AR-05/29, 2005.

2. Costa, J.R., Gonzalez, R.E., Guyotte, R.E., Salvano, D.P., Swift, T., and Koenig, R.J. (chair), "Titanium Rotating Components Review Team Report," Federal Aviation Administration, Aircraft Certification Service, Engine and Propeller Directorate, Boston, MA, December 14, 1990.

3. Adams, J., Murphy, T., and Provenzano, N., "Update on Rotor Integrity Subcommittee Initiatives," 2nd Annual FAA/AF Workshop of the Application of Probabilistic Methods to Gas Turbine Engines, November 1996.

4. FAA Advisory Circular 33.14-1, "Damage Tolerance for High Energy Turbine Engine Rotors."

5. Copley, D., "ETC Multizone Update," *Proceedings of the Open Forum*, May 1996.

6. Mucciardi, T. and Raulerson, D., "Phased Array Inspection of Titanium Billet," *Proceedings of the Open Forum*, May 1996.

7. Brasche, L., Chiou, T., Thompson, R.B., Smith, K., Meeker, B., Margetan, F., Panetta, P., Chenail, R., Galli, F., Umbach, J., Raulerson, D., Degtyar, A., Bartos, J., Copley, D., McElligott, B., Howard, P., and Bashyam, M., "Contaminated Billet Study," FAA report DOT/FAA/AR-05/16, 2005.

8. Thompson, R.B., Chiou, C.-P., Gray, T., Margetan, F., and Roberts, R., "Use of UT Models in Titanium Inspection Development," *Proceedings of the Open Forum*, May 1996.

9. Margetan, F.J., Han, K.Y., Yalda, I., Goettsch, S., and Thompson, R.B., "The Practical Application of Grain Noise Models in Titanium Billets and Forgings," *Review of Progress in QNDE*, 14B, D.O. Thompson and D.E. Chimenti, eds., Plenum Press, NY, 1995, pp. 2129-2136.

10. Howard, P., Copley, D., and Gilmore, R., "Transducer Design for High Sensitivity Ultrasonic Inspection of Titanium," *Review of Progress in QNDE*, Vol. 16, 1996, p. 893.

11. Roberts, R., "Phased Array Beam Modeling Using a Discretely Orthogonal Gaussian Aperture Basis," in *Review of Progress in QNDE*, Vol. 23, D.O. Thompson and D.E. Chimenti, eds., 2004.

12. Howard, P., Copley, D., Young, J., Neiters, E., and Gilmore, R., "An Improved Methodology for the Inspection of Titanium Alloys," *Proceedings of the 1996 IEEE Ultrasonics Symposium,* Vol. 1, M. Levy, S. Schneider, and B. McAvoy, eds., IEEE Press, 1996, pp. 727-730.

13. Dumas, P., Poguet, J., and Fleury, G., "New Piezocomposite Transducers for Improvement of Ultrasonic Inspections," in *Review of Progress in QNDE*, Vol. 22A, D.O. Thompson and D.E. Chimenti, eds., American Institute of Physics, Melville, NY, 2003.

14. Margetan, F.J., Roberts, R., Chiou, C.-P., and Thompson, R.B., "Determination of the Effective Focal Characteristics of Bicylindrically-Focused Ultrasonic Transducers," *Review of Progress in QNDE*, Vol. 21A, D.O. Thompson and D.E. Chimenti, eds., American Institute of Physics, Melville, NY, 2002, pp. 791-798.

15. Margetan, F.J., Brasche, L., Chiou, T., Keller, M., Degtyar, A., Umbach, J., Hassan, W., Patton, T., and Smith, K., "Fundamental Studies of Nickel Billet Materials—Engine Titanium Consortium Phase II," FAA report DOT/FAA/AR-05/17, June 2005.

16. Minachi, A., Margetan, F.J., and Thompson, R.B., "Reconstruction of a Piston Transducer Beam Using Multi-Gaussian Beams (MGB) and its Applications," in *Review of Progress in QNDE*, Vol. 17A, D.O. Thompson and D.E. Chimenti, eds., Plenum Press, NY, 1996, pp. 907-914.

17. Copley, D. and Howard, P., "Operational Performance of a Multizone Billet Inspection System," in *Review of Progress in QNDE*, Vol. 14, D.O. Thompson and D.E. Chimenti, eds., Plenum Press, NY, 1995, pp. 2145-2151.

18. Nieters, E., Gilmore, R., Copley, D., and Howard, P. in *Review of Progress in QNDE*, Vol. 14, D.O. Thompson and D.E. Chimenti, eds., Plenum Press, NY, 1996, pp. 1495-1502.

19. Margetan, F.J., Thompson, R.B., and Yalda-Mooshabad, I., "Backscattered Microstructural Noise in Ultrasonic Toneburst Inspections," *Journal of Nondestructive Evaluation*, Vol. 13, 1994, pp. 111-136.

20. Margetan, F.J., Thompson, R.B., Yalda-Mooshabad, I., and Han, Y.K., "Detectability of Small Flaws in Advanced Engine Alloys," ISU Center for NDE, July 1993.

21. Margetan, F.J., Thompson, R.B., and Yalda-Mooshabad, I., "Modeling Ultrasonic Microstructural Noise in Titanium Alloys," in *Review of Progress in QNDE*, Vol. 12B, D.O. Thompson and D.E. Chimenti, eds., Plenum Press, NY, 1993, pp. 1735-1742.

22. Panetta, P.D., Thompson, R.B., and Margetan, F.J., "Use of Electron Backscatter Diffraction in Understanding Texture and the Mechanisms of Backscattered Noise Generation in Titanium Alloys," in *Review of Progress in QNDE*, Vol. 17A, D.O. Thompson and D.E. Chimenti, eds., Plenum Press, NY, 1998, pp. 89-96.

23. Brasche, L., Duffy, T., Bartos, J., and Smith, K., "Engine Titanium Consortium Phase II Technical Proposal Volume I," July 1998.

24. Margetan, F.J., Gigliotti, M., Brasche, L., and Leach, W., "Fundamental Studies: Inspection Properties for Engine Titanium Alloys," FAA Report DOT/FAA/AR-02/114, December 2002.

25. Panetta, P.D., Margetan, F.J., Yalda, I., and Thompson, R.B., "Observation and Interpretation of Microstructurally Induced Fluctuations of Back-Surface Signals and Ultrasonic Attenuation in Titanium Alloys," in *Review of Progress in QNDE*, Vol. 16B, D.O. Thompson and D.E. Chimenti, eds., Plenum Press, NY, 1997, pp. 1547-1554.

26. Margetan, F.J., Panetta, P.D., and Thompson, R.B., "Ultrasonic Signal Attenuation in Engine Titanium Alloys," in *Review of Progress in QNDE*, Vol. 17B, D.O. Thompson and D.E. Chimenti, eds., Plenum Press, NY, 1998, pp. 1469-1476.

27. Margetan, F.J., Hassan, W., and Thompson, R.B., "An Experimental Study of Microstructure-Induced Ultrasonic Signal Fluctuations in Jet-Engine Titanium Alloys," in *Review of Progress in QNDE*, Vol. 19, D.O. Thompson and D.E. Chimenti, eds., Plenum Press, NY, 2000, pp. 1433-1440.

28. Gill, P.E., Murray, W., and Wright, M., “Practical Optimization,” Academic Press, NY, 1981.

29. Margetan, F.J., Gigliotti, M., Brasche, L., and Leach, W., “Fundamental Studies: Inspection Properties for Engine Titanium Alloys,” FAA Report DOT/FAA/AR-02/114, December 2002.

APPENDIX A—MAJOR ACCOMPLISHMENTS OF THE ETC PHASE I PROGRAM

- Fabrication of samples necessary for fundamental studies and for development and validation of inspection techniques. Samples included various flat-bottom hole (FBH) samples, synthetic hard alpha samples, chord blocks, development standards, and actual notched or cracked hardware, all of which will be catalogued in the Airworthiness Assurance Nondestructive Inspection Validation Center Sample Database.

- Transducer design models for cylindrical geometry, fixed-focus and phased array transducers, which allow the user to optimize a transducer for a given inspection scenario. Software was delivered to the original equipment manufacturers (OEM) for use in transducer design and procurement. The models were used in selection of a series of transducers for both flat part and curved surface inspection as part of optimization studies completed in Engine Titanium Consortium (ETC) Phase I. Those results will guide ETC Phase II inspection efforts.

- Demonstrations of multizone and phased array systems to OEMs, the Federal Aviation Administration, and billet and forging suppliers were held as part of the Phase I program in cooperation with RMI Titanium of Niles, Ohio. The purpose of the demonstrations was to demonstrate the capabilities of zoned inspection systems in a factory environment and determine the users perspective of ETC technologies. Updates were also provided at each of the three open forums, including a summary of hard alpha detections.

- Using the contaminated billet, the detectability of multizone inspection using discrete fixed-focus transducers and of the phased array annular transducer were demonstrated to be similar.

- An industrywide specification for titanium (Ti) billet inspection was issued as Aerospace Material Specification (AMS) 2628 through the auspices of SAE Committee K.

- Fundamental changes are now being realized in the approach taken to in-service eddy-current inspection through the development of a suite of ETC tools that enable disciplined, reproducible digital data using equipment that is low in acquisition cost and generic across all engine models such that every engine shop in the world can afford to acquire tools. The tools are also robust and intuitive for the community to use improving the reliability and sensitivity of inspections performed during the service life of aircraft engines.

- Development and commercialization of the portable eddy-current scanner and data acquisition system that enables acquisition of disciplined digital data and provides a platform for processing that data. The system was designed to be marketed for $50 thousand or less, weigh less than 40 lb to enable use by a single inspector, and provide the majority of the capabilities of the large, expensive fixed-base scanners typical of military applications, meeting all of the original program goals. The development process was accomplished with input from the OEMs and airlines through various visits, design reviews, and Air Transport Association (ATA) demonstrations and meetings.

- Initial application of the scanner was in the Hamilton Standard regional propeller recovery effort in the wake of the Carrolton, Georgia, crash. Initial use of the ETC scanner led to detection of a crack in a blade shank that had previously been accepted with another technique. This led Hamilton Standard to invest in a scanner of their own for use in the recovery effort. The scanner was successfully used during the refurbishment of propeller shanks with 100 propeller shanks inspected, four shanks rejected, and one additional crack found. By providing a more sensitive inspection, additional existing shanks could be used in the refurbishment effort, thereby allowing the closing action to be achieved on schedule without the mandatory grounding of aircraft. By avoiding groundings, not only was inconvenience to the traveling public avoided, but several regional carriers were able to stay in business with an estimated $15 million savings to the industry.

- Beta site testing of the portable scanner allowed introduction of the technology to the air carriers and encouraged end user feedback in future developments. The first beta site was at United Airlines and involved the assessment of JT9D-7R4 14/15 stage HPC bores. This inspection is performed primarily with the engine in a semiassembled condition using fabricated tooling such that the scanner could be mounted to the engine while in the horizontal build fixture and the inspection performed through the HPC shaft with the high pressure turbine (HPT) installed if desired. The scanner was in place at United Airlines for 3 months, enabling inspection of four engines. Data was acquired during the beta site tests that allowed for comparison of the system to existing manual requirements in the Alert Service Bulletin for this hardware. Cracking was successfully found with both techniques. However, the portable scanner system allowed additional margin in detecting smaller cracks.

- Additional applications were defined and developed by AlliedSignal, including the TFE 731 fan disk blade slots, a significant accomplishment given the extreme slash angle and depth of the slot. AlliedSignal invested significant internal funds to address probe and technique development as part of the introduction process. AlliedSignal has made a significant commitment to the use of semiautomated inspection to address overhaul inspection with the purchase of two production units and further utilization expected through third-party overhaul shop implementation.

- American Airlines requested beta site test application of the portable scanner to the fan hub of the small fan versions of the JT8D, i.e., straight 8s or baby 8s. The inspection areas included the blade slots, bore (face, corner, and inner diameter), and the web to rim transition radius. At this time, three engines have been inspected with the results matching those required by the Airworthiness Directive (AD). An American Airlines nondestructive testing (NDT) engineer was provided training, which enabled him to train other inspectors on the use of scanner. Data is being collected such that a request for an alternate means of compliance with the existing AD will be granted. As the existing technique is manual, no difficulty is anticipated in achieving an alternate means of compliance. Plans are to pursue the alternate means in 1998. A full demonstration of the scanner was provided to the airlines in April 1998.

- A specification was generated by the ETC to encompass the needs of the industry for future generation eddy-current instruments. The specification included input from the OEM development and applications groups and major air carrier engine shops as well as the instrument manufacturers. The intent of the specification is to create a basis for and direction to the industry in the development of future instrumentation with elements of the specification already appearing in newer eddy-current instruments.

- Flexible substrate technology used in array probes developed by General Electric (GE) was adapted to form a single element probe and applied to engine applications. The technology is now available commercially.

- A boundary element model formulation was used to develop a tool for predicting field vectors emanating from eddy-current probes. This parameter is key in predicting the sensitivity of the probes to particular crack orientations in various geometries and was used extensively in the development of wire wound wide area probes. Using the model enabled a larger number of design iterations to be explored than were possible if probes were built to assess each design. The tool and further derivations of the tool are being used at Pratt & Whitney on an ongoing basis to design and build probes to address engine applications. One of the probes developed by Pratt & Whitney is being evaluated for application to JT8D fan hub inspection.

- A low-pressure (LP) rotor rotator was designed and built to provide controlled rotation of the LP rotor while installed in the engine. It is generic in that it will work on all high by-pass ratio engines (no inlet guide vanes) and facilitates the collection of disciplined eddy-current data for on-wing inspection of fan and LP compressor disks, and LP turbine hardware. A demonstration was performed on a JT9D engine. Borescope manufacturers have shown an interest in the device as a way of assisting in the inspection of LP turbine hardware.

- A probability of detection (PoD) methodology was developed, which allows the determination of the PoD of internal flaws in Ti for use in the validation of inspection systems. The approach differs from previous work in two important ways. First, it is based on statistical detection theory, requiring the determination of the distributions of signal and noise. These distributions are assumed to be controlled by three sources of variability associated with material microstructure, details of the measurement process such as scan plan, and flaw morphology. In contrast to existent methodologies, the statistical detection approach allows one to make a direct determination of the probability of false alarms as well as PoD, information that is valuable in a variety of contexts, including assessing the economic penalties of achieving a desired PoD by lowering the threshold too low. These consequences are taken into account by the OEMs in setting threshold levels, and thus influence the PoD that can be realized for a given inspection. Second, the methodology makes explicit use of mathematical models, which describe the physics of the inspection process. Because of the limited number of naturally occurring hard alpha inclusions that occur in Ti and the fact that billet disposition time pressures limit the amount of metallurgical information that can be obtained regarding the true size, shape, and composition of the inclusions, the utility of traditional empirical approaches for PoD determination is limited. Using physical models of the inspection process allows

the maximum amount of information to be extracted from limited experimental observations. In addition, it allows one to predict the effects of changes to the inspections setup (e.g., probe properties and scan increments). The methodology has been exercised to generate PoD curves for FBHs and synthetic hard alphas. Validation using Contaminated Billet Study (CBS) indications is under way with the initial results being quite positive. Phase II will complete further validation and transition the research-grade code to a useable tool for the OEMs.

- Quantitative PoD information has been made available to life management groups, including input to Advisory Circular 33.14-1, "Damage Tolerance for High Energy Turbine Engine Rotors." At the request of the Rotor Integrity Steering Committee, default PoD curves have been provided using previous methodologies. Based on the data assembled by the Jet Engine Titanium Quality Committee, PoD estimates have been made for naturally occurring hard alpha inclusions. However, these are not as comprehensive as would be desired because of

  – a limited number of hard alpha inclusions actually found in production,

  – the size of many of these defects has not been properly determined metallographically due to the need to make a rapid disposition of the billet, and

  – much of the ultrasonic data was saturated.

  These determinations of the PoD of naturally occurring hard alpha inclusions will be improved in Phase II, based on the results of the CBS. The experimental data will be obtained in Phase I, with analysis to be completed in Phase II. Finally, members of the life management community have indicated that the ability to predict the effects of inspection and defect parameters on PoD, as discussed above, should play an important role in future risk and life management studies.

APPENDIX B—DESCRIPTION OF MULTIZONE INSPECTION FOR BILLET

The multizone system is a real-time, personal computer (PC)-based platform that employs custom-built, analog, electronics using up to eight parallel (nonmultiplexed) channels, each with a remote pulser/receiver matched to the ultrasonic transducer. Scanned helically, the billet is divided into concentric zones with a focused transducer used to acquire peak-detected C-scan image data for each zone. The depth of each zone is established by the depth of focus of that transducer. C-scan image data from all channels are displayed simultaneously on a 1024 x 1280 cathode-ray tube (CRT) and scroll as the inspection advances along the billet length. The data are written to optical storage upon completion of the inspection.

Custom postscan analysis software was developed to detect flaws using signal-to-noise-based algorithms. This software provides more reproducible results than conventional systems and greatly reduces operator fatigue and the chance for error.

B.1 SYSTEM.

Prior to the multizone system, the conventional test methods were limited in sensitivity due to material noise and lack of transducer focusing. In addition, there was no digital data acquisition or storage. To correct this situation, a system was designed that would use focused transducers to overcome material noise and, therefore, improve detection. However, multiple compound focused transducers were required to inspect the billet volume to uniform sensitivity. The transducers are fitted with dual curvature lenses to produce a diffraction-limited, symmetrical focus. This configuration provides more uniform sensitivity versus depth for a given scan rate. Inspection zones are determined by the transducer focal zone parameters, i.e., diameter, d, and focal length, F. Each transducer inspects a depth of material roughly equal to the –3 dB depth of field, ε_z, and at a spatial sampling rate at least half the –6 dB beam diameter, ε_x. (See equations B-1 and B-2.)

$$\varepsilon_z = 3.6\lambda[\mathrm{F/d}]^2\, c_1/c_2 \qquad \text{(B-1)}$$

$$\varepsilon_x = 1.03\, \lambda[\mathrm{F/d}] \qquad \text{(B-2)}$$

The value, c_1, is the sound velocity in water (0.058 in./μsec), c_2 is the sound velocity in titanium (Ti) (0.243 in/μsec) and λ is the wavelength (0.049 in. in Ti at 5 MHz). A typical multizone transducer produces 5-MHz, F/8.0 beams that are approximately 0.1″ diameter and 0.8″ depth of field for Ti. At deeper depths, larger F numbers are used due to the manufacturability limitation in element diameters produced by commercial vendors. By increasing the transducer size and depth in the material of its focal zone, overlapping foci are produced to uniformly inspect the billet volume, see figure B-1.

The ultrasonic instrument uses custom analog electronics with up to eight parallel, nonmultiplexed channels based on the NIM architecture. The parallel, nonmultiplexed architecture was used to eliminate any unattenuated sound, which might interfere with a given channel's signal. A multiplexed solution also introduces possible speed limitations. Each transducer has its own remote pulser/receiver, which is matched to that specific transducer. The

user can set various parameters for each channel such as attenuation, signal gate delay and width, and triggering rate. The data generated for each channel or zone is an analog, peak-to-peak C-scan voltage ranging from 0 to 10 volts, which is sent to the computer for display and storage.

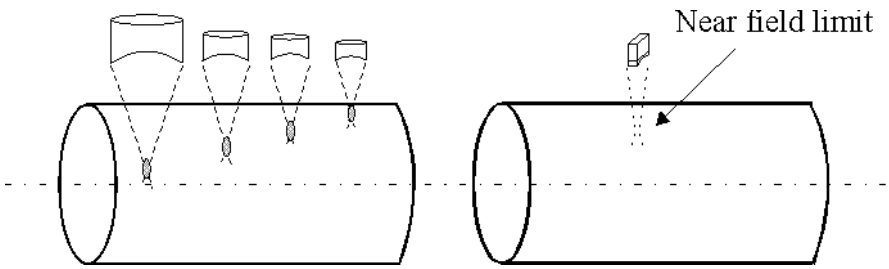

FIGURE B-1. MULTIZONE INSPECTION VS TYPICAL INDUSTRIAL INSPECTION

The computer is an Intel-based PC (e.g., 486, Pentium, etc.) with a large amount of random-access memory (RAM) (64 MB or larger is recommended) running MSDOS and Windows®. The RAM permits storage of data from all eight channels in memory as it is acquired. This eliminates time-consuming disk accesses during acquisition. Standard data acquisition boards are used for digital handshaking signals between the computer and the electronics and for digitization of the analog C-scan data. A 21″ 1280 x 1024 resolution color monitor allows all eight channels to be displayed simultaneously during acquisition. The archival storage requirement was achieved using a write-once-read-many (WORM) optical disk for archiving the image data. Report generation is accomplished using a high-quality color PostScript printer. Figure B-2 shows the complete system diagram.

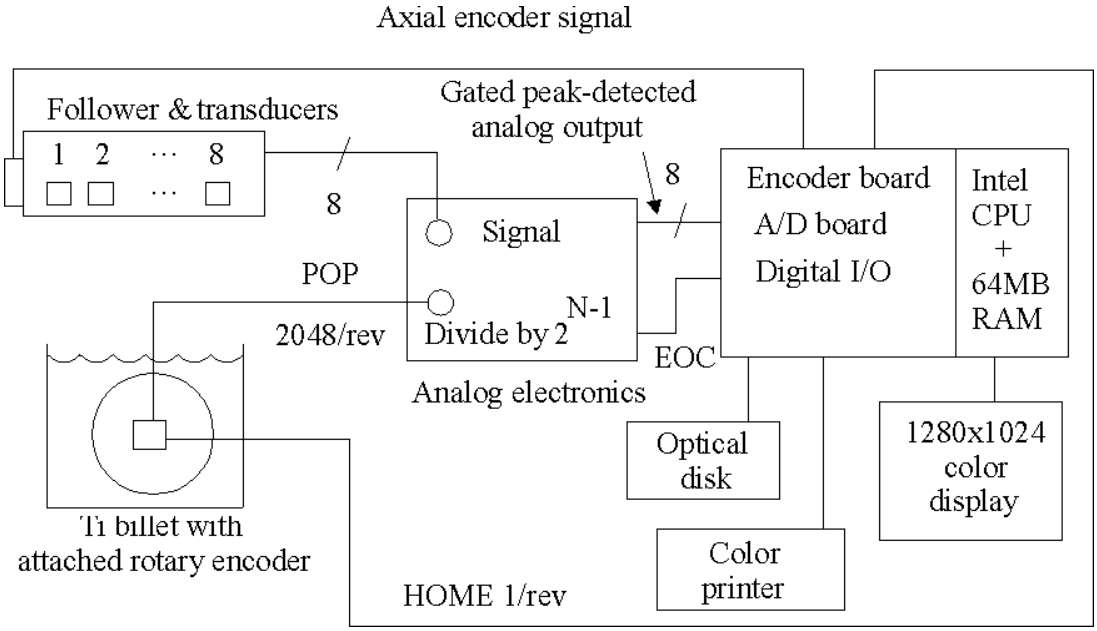

FIGURE B-2. MULTIZONE SYSTEM BLOCK DIAGRAM

B.2 SYSTEM OPERATION.

For inspection, the billet is immersed in a water tank and rotated about its axis. The maximum billet rotation speed is approximately 30 RPM. The transducers, aligned normal to the billet surface, are mounted on a stage or follower that rides on a track over the tank. As the billet rotates, the follower moves axially along the billet length and the material is inspected in a helical pattern.

An axial encoder is mounted on the follower and is used to report axial position of the transducers during the scan. A rotary encoder is coupled to an adapter, which is attached to the end of the billet using double-sided adhesive tape. This encoder generates a once-per-revolution index or home pulse, which is used by the computer acquisition software to determine the 0° location on the billet. The rotary encoder also generates a 2048 pulse-per-revolution signal. This signal provides a position-dependent trigger for the ultrasonic transducers known as a pulse-on-position or POP pulse. The POP signal is used by the electronics to synchronize the triggering of the transducers for all eight channels to the billet rotation. Each channel will divide down the 2048 master POP to the sample rate required to inspect the particular zone.

Outer zones with larger radii require more samples than inner zones to fully inspect the material. The sample count for a given zone is a function of the zone circumference and the beam diameter, $\varepsilon_{x,}$ of the transducer. While transducers covering the larger radii zones fire more often than their smaller radii counterparts, all transducers fire simultaneously when they do trigger. This greatly minimizes the possibility of any unattenuated sound from any channel interfering with the signal from any other channel.

Prior to inspection, the user must start the acquisition software on the computer. Based on the billet material and diameter, the operator is instructed on how to configure the electronics. Parameters such as attenuation, signal gate delay and width, and POP rate are set using thumbwheel switches on the electronics for the required number of channels. Information such as operator ID, billet length, and identification numbers must be entered into the software as well. Once the electronics are configured and the acquisition software is running, the rotary encoder begins triggering the electronics. The electronics fire the transducers and produce analog C-scan data values. These analog signals, along with axial position information, are sent to the PC acquisition software for storage in RAM and display. Upon scan completion, the user is given the opportunity to enter any comments about the scan. Data is then transferred from computer memory to disk and later archived to a WORM optical disk for permanent storage.

B.3 POSTSCAN ANALYSIS.

The implementation of digital data acquisition allows postscan analysis, which is not possible with any current billet inspection systems. A typical multizone inspection on a single billet can generate 30 MB or more of ultrasonic image data. These data can include flaw signals obscured by an acoustic noise level that varies both circumferentially and axially along the billet. An image analysis software package was developed to aid the operators in finding indications. This package, which runs on the system PC, provides a Microsoft Windows-based graphical user interface for displaying and manipulating the inspection results. Using data analysis tools such

as maximum value, axial cross sections, and image magnification, the operator is able to locate signals that are above the local acoustic noise and display them at high resolution The operator can then isolate potential rejectable signals and a surrounding area of homogeneous noise for each indication. Using those two regions of interest (ROI), the operator can calculate the signal-to-noise ratio (SNR) for each indication where SNR is defined as

$$SNR = \frac{P_s - \mu_n}{P_n - \mu_n}$$

where P_s is the maximum value of the signal ROI, P_n is the third highest (to exclude electrical noise spikes) value in the noise ROI, and m_n is the mean of noise ROI. Material acceptance criterion based on both peak amplitude and SNR are applied to the indication to make the accept/reject decision. The PC can quickly review 30+ MB of data, allowing the task to be completed before the billet is removed from the tank. Since the scan positional information is stored along with the image data, the operator can return the transducer to the location on the billet where an indication exists to verify its location and mark the billet for sectioning to remove the material surrounding the indication.

B.4 TRANSDUCERS.

The transducers in use for the majority of production multizone testing are ceramic element designs focused with loaded epoxy lenses and of nominal 5 MHz frequency. Diameters vary from 0.625″ to 2.35″. The objective of the transducer design was to provide an equal response from flat-bottom hole targets at the near and far ends of the inspection zone (within a 3 dB tolerance) and to minimize the sound beam area throughout the focal zone.

System specification for operation of multiple fixed focus transducers (multizone).

MECHANICAL	
Capacity	Billet diameter 4.5″ to 15.0″ Billet length 12.0″ to 240.0″ Maximum weight 6000 pounds
Rotation speed	1 to 60 rpm Maintain constant rotation speed within ±10% of setting
Indexing	Helical (constant speed) or step indexing Index range 0.010″ to 0.100″ per revolution Index distance accuracy ±0.003″
Bar follower/manipulators	Capacity: 8 transducers Maximum transducer diameter 3.0″, case length 3.0″ Transducer face to billet distance 2.0″ to 5.0″ Transducer alignment adjustment about axis x (parallel to billet axis), y (across bridge, perpendicular to billet axis) and c (about transducer axis). Locking pin to engage slot in transducer housing to fix c-axis alignment. Manipulator and follower to maintain transducer normal to billet surface within ±0.5 degrees.
Transducers:	
Reference	Reference AMS 2628 Annex B for details of transducers
Frequency	5 MHz
Bandwidth	45% to 65%
Diameter	0.625″ to 2.35″
Construction	Stainless steel housing with alignment slot to engage locking pin in manipulator
Instrumentation:	
Encoders	Submersible billet rotation encoder coupled to billet via adapter plate and flexible coupling, generating 2048 pulses per revolution Index axis encoded to 0.001″ resolution
Architecture	8-channel parallel architecture Based on NIM standard
Pulsers	Remote pulsers matched to transducer capacitance (150 to 3500 pF)
Instrument	Repetition rate synchronized to internal clock or rotary encoder Pulse-on-position pulse rates of 128, 256, 512, 1024, 2048 pulses per revolution, selectable for each channel Linear amplifier, bandwidth Attenuator range 0-59.5 dB One gate per channel Gate synchronized to initial pulse or interface echo Gate delay Gate width range Gate output one analog channel per gate, 0 to 10 volts, proportional to maximum peak-to-peak range in gated region

	Oscilloscope display (typical Tektronix TDS 420)
Data Acquisition Hardware:	
CPU	133 MHz Pentium, Industrial rack mount 64 MB RAM 500 MB SCSI Hard Disk 3.5″ Diskette Drive
Monitor	21″, 1280 x 1024 x 256 resolution
Video Board	Number Nine GXI-TC (DOS Software) 120 x 1024 x 256 (Windows NT Software)
Archival Storage	Preferred: ISO 9660 CD-ROM Acceptable: Pioneer Type “A” WORM Magneto-Optical Disk with Instar Optical Disk Software
Printer	Postscript Color printer (typical Tektronix Phaser 200I)
Analog-to-Digital Conv.	8 parallel channels using simultaneous sample-and-hold 8-bits over the range of 0-10 volts (Data Translations DT2829)
Encoder Input	Quadrature Encoder Board (Technology 80 Model 5312)
Data Acquisition Mode	Pulse-on-position
Software:	
Data Acquisition	GE-developed software running under MSDOS v5.0 or higher (Currently undergoing upgrade to run under Windows NT v3.51)Real-time scrolling display of eight channels
Data Analysis	GE-developed software running under Windows 3.11, Windows 95, or Windows NT with IDL v4.0.1b from Research Systems Incorporated
Data File Format	network Common Data Format (netCDF)